

CRANFIELD UNIVERSITY

AYODELE JAMES OYELEKE

VENTILATION AND THERMAL PERFORMANCE OF AN
INTEGRATED SYSTEM FOR USE IN HERITAGE BUILDINGS

SCHOOL OF WATER, ENERGY AND ENVIRONMENT
PhD in Energy

PhD
Academic Year: 2017 - 2018

Supervisor: Dr Patrick Verdin
January 2018

CRANFIELD UNIVERSITY

SCHOOL OF WATER, ENERGY AND ENVIRONMENT
PhD in Energy

PhD

Academic Year 2017 - 2018

AYODELE JAMES OYELEKE

Ventilation and Thermal Performance of an Integrated System for
use in Heritage Buildings

Supervisor: Dr Patrick Verdin
January 2018

© Cranfield University 2018. All rights reserved. No part of this
publication may be reproduced without the written permission of the
copyright owner.

ABSTRACT

Providing modern mechanical heat recovery ventilation for heritage dwellings poses the challenge of invasive duct-work and unwanted modifications to the building fabric. A retrofitted ventilation system will be more desirable if it is inconspicuous and hidden within the building fabric.

The author's original contribution to knowledge encompasses the original proposal and development from first principles of a novel natural ventilation heat recovery system utilizing disused chimneys in heritage dwellings. The system consists of an omnidirectional flue-like windcatcher integrated with a plate heat exchanger. This research provided new information on functional design of geometry, operational characteristics, and feasibility in terms of ventilation and heat recovery performance of counter-current natural air flow in the system.

Two commercial CFD programs, namely Autodesk CFD 2013 and Ansys Fluent v14 were employed to perform RANS simulation of 3D models of the system. A comparison of flow results gotten from these packages showed a maximum difference of 10%. This proved the corresponding accuracy of the simpler and more user-friendly Autodesk CFD when compared with the more established Ansys Fluent software package.

The air flow and thermal performance of the system's two main parts were investigated at steady state wind speeds of 0.5m/s, 1.5m/s, 2.5m/s, 3.5m/s and 4.5m/s incident on the windcatcher at 90 degrees. Results were evaluated for a $27m^3$ design room ventilated at 0.7ach.

At all wind speeds, the final windcatcher prototype exhibited the desired flow pattern with no short-circuit and provided more than the minimum required air change rate at all incident wind speeds above 1 m/s.

When the windcatcher is integrated with the heat exchanger, the system's ventilation performance was 0.3ach at 0.5m/s incident wind speed. This increased to 4.5ach at 4.5m/s incident wind speed. Thermal effectiveness of the system peaked at 46% at 0.5m/s wind speed and decreased to 22% at 4.5m/s

wind speed. When compared with the heat exchanger solitary performance, thermal effectiveness was reduced by an average of 27% at all incident wind speeds. This performance reduction is due to the non-uniform pattern of supply air flow through the system.

Further work is required to provide experimental data on the performance of the system and investigate the effect of unsteady air flow incident at different angles on the windcatcher. Proposals for these are included. Further work is also required to incorporate features that will minimize fouling in operation and improve heat recovery effectiveness.

Keywords:

Windcatcher, Plate heat exchanger, Heat Recovery Ventilation, Natural Ventilation, Passive Ventilation, Heritage dwellings, Badgir, Disused Chimney, Cowl, Low Reynolds Flow Heat Exchanger.

ACKNOWLEDGEMENTS

I would like to express my gratitude to my supervisors; Dr Patrick Verdin, Professor Gioia Falcone, and Professor Sai Gu for their kind advice and support during this research work.

Dr Athanasios Kolios's intervention and effort in transitioning between supervisors and bringing this work to fruition is also gratefully acknowledged.

A word of appreciation is also due to Dr Hosein Torabmostaedi for his kind support in carrying out the simulations in the research.

Lastly, my heartfelt thanks go to my parents Chief Joseph Oyeleke and Mrs Lydia Oyeleke for their unflinching moral and financial support during this research.

TABLE OF CONTENTS

ABSTRACT	i
ACKNOWLEDGEMENTS.....	v
LIST OF FIGURES.....	ix
LIST OF TABLES	xiii
NOMENCLATURE	xiv
1 INTRODUCTION.....	1
1.1 Design Selection.....	7
2 LITERATURE REVIEW	11
2.1 Energy Loss in Heritage Dwellings	12
2.1.1 Fabric Heat Loss	12
2.1.2 Ventilation Heat Loss	14
2.2 Energy Recovery Techniques in Ventilation Systems.....	16
2.2.1 Mechanical Ventilation Heat Recovery System (MVHR)	19
2.2.2 Natural Ventilation; Windcatcher and Modelling Techniques	26
2.3 Influence of Previous Works on Proposed Design	30
3 AIMS AND OBJECTIVES.....	37
4 METHODOLOGY	39
4.1 3D CAD.....	39
4.2 Computational Fluid Dynamics - CFD.....	39
4.2.1 Assumptions.....	41
4.2.2 CFD Theory.....	41
4.2.3 Turbulence Modelling	43
4.2.4 Near Wall Treatment	48
4.2.5 Meshing.....	51
4.2.6 Discretization.....	54
4.2.7 Solver Settings	56
4.2.8 Convergence	58
4.2.9 Post Processing	59
4.2.10 Validation	60
5 WINDCATCHER DEVELOPMENT	63
5.1 Theory and Concept	63
5.2 Analysis and Results.....	68
5.2.1 Air Flow Rate Analysis	68
5.2.2 Extract Flow Analysis	104
5.2.3 Short Circuit Flow Analysis.....	107
5.2.4 Final Prototype	117
5.2.5 Autodesk CFD Results Comparison.....	126
6 HEAT EXCHANGER DEVELOPMENT	129
6.1 Design Considerations.....	129
6.1.1 Heat Transfer Process in Heat Exchangers	130

6.1.2 Heat Exchanger Construction	131
6.1.3 Heat Exchanger Compactness.....	135
6.1.4 Heat Exchanger Flow Patterns.....	136
6.2 Modelling Heat Exchanger Performance	137
6.2.1 Capacity Ratio.....	138
6.2.2 Heat Exchanger Effectiveness	138
6.2.3 Logarithmic Mean Temperature Differential	139
6.2.4 Heat Transfer Units	140
6.3 Theory.....	141
6.3.1 Heat Transfer over Flat Plates	141
6.3.2 Heat Transfer Coefficient in Heat Exchangers	144
6.3.3 Heat Transfer Surfaces	146
6.4 Heat Exchanger Concept.....	147
6.4.1 Problem Specification.....	148
6.4.2 Pressure Drop	152
6.4.3 Heat Duty	154
6.4.4 Sizing	155
6.5 Analysis and Results.....	161
6.5.1 Heat Transfer Optimization	161
6.5.2 Final Prototype	161
7 DESIGN OF VALIDATION EXPERIMENTS.....	189
7.1 Thermal Comfort Study.....	190
7.2 Wind Tunnel Testing of Windcatcher.	191
7.2.1 Test Model	191
7.2.2 The Wind Tunnel.....	196
7.2.3 Air Flow Measurement	198
7.2.4 Fluid Motion Visualization.....	205
7.2.5 Experimental Setup.....	206
7.2.6 Experimental Error Sources	207
7.3 Large Scale Testing	210
8 CONCLUSION AND RECOMMENDATIONS.....	211
8.1 Conclusion	211
8.1.1 Windcatcher	213
8.1.2 Heat Exchanger	216
8.1.3 Whole System	219
8.2 Recommendations for Future Work	219
REFERENCES.....	223
APPENDICES	265
Appendix A Windcatcher Initial Concepts	265

LIST OF FIGURES

Figure 1-1: Proposed Ventilation System	6
Figure 2-1: Timeline of Mean SAP Ratings by Dwelling Age [56].....	12
Figure 2-2 Space Heating System by Dwelling Construction Date [58].....	13
Figure 2-3: Heat Loss Trend in Average Dwellings [19]	15
Figure 5-1 System Flow Structure	67
Figure 5-2: Windcatcher Base Model	68
Figure 5-3: Simulation Model Domain	71
Figure 5-4: Autodesk CFD Mesh (Wake region to the left).....	81
Figure 5-5: Autodesk CFD Adapted Mesh.....	82
Figure 5-6: Model 1 (Base Model)	83
Figure 5-7: Model 1 Velocity Vector Plots	84
Figure 5-8: Model 1 Flow Short-Circuiting at 1.5m/s to 4.5m/s.....	85
Figure 5-9: Model 1 Annular Inlet Channel Flow Path	87
Figure 5-10: Model 1 Annular Inlet Flow Path at 0.5m/s Wind Speed (Zoomed)	87
Figure 5-11: Model 1 (Base Model) Supply Air Volume Flow Rate.....	88
Figure 5-12: Incident Wind By-Passing Windcatcher	89
Figure 5-13: Model 1 Central Outlet Flow Rate	90
Figure 5-14: Model 2	91
Figure 5-15: Supply Air Flow Rates for Models 1 and 2	92
Figure 5-16: Model 2 Supply Air Short- Circuit Flow Path	93
Figure 5-17: Model 2 Extract Air Flow Vector Plot.....	93
Figure 5-18: Pressure Variation over Extract Channel Surface	94
Figure 5-19: Model 3	95
Figure 5-20: Inlet Air Flow Rates for Models 1, 2 and 3	96
Figure 5-21: Model 3 Extract Air Flow Vector Plot.....	96
Figure 5-22: Model 3 Flow Ratios through Windward Dome Sections	97
Figure 5-23: Model 3 Pressure Variation Over Outlet Channel Surface	98

Figure 5-24: Model	99
Figure 5-25: Supply Air Flow Rates for Models 1, 2, 3 and 4	100
Figure 5-26: Model 5	102
Figure 5-27: Supply Air Flow Rates for Models 1, 2, 3, 4 and 5	102
Figure 5-28: Ratio of Supply and Short-Circuit Flows for Model 4 and 5	103
Figure 5-29: Extract Flow Rates for Models 1 and 5	104
Figure 5-30: Extraction Sections	105
Figure 5-31: Model 1 Dome Sections Flow Rates	106
Figure 5-32: Model 1 Extract Channel Velocity Vector Plot.....	107
Figure 5-33: Short Circuit Flow.....	107
Figure 5-34: Percentage Short Circuit Flow at 4.5m/s Incident Wind Speed..	108
Figure 5-35: Percentage Short Circuit Flow at 0.5m/s Incident Wind Speed..	108
Figure 5-36: Actual Short Circuit flow at 4.5m/s Incident Wind Speed	109
Figure 5-37: Actual Short Circuit flow at 0.5m/s Incident Wind Speed	109
Figure 5-38: Incident Wind Direction	110
Figure 5-39: Model 1 Reference.....	111
Figure 5-40: Model 1 Supply Channels Pressures At 4.5m/s Incident Wind Speed	112
Figure 5-41: Model 1 Supply Channels Pressures At 0.5m/s Incident Wind Speed	112
Figure 5-42: Model 2 & 3 Reference	113
Figure 5-43: Models 2&3 Supply Channels Pressures at 4.5m/s Incident Wind Speed	114
Figure 5-44: Models 2&3 Supply Channels Pressures at 0.5m/s Incident Wind Speed	114
Figure 5-45: Models 4&5 Reference.....	115
Figure 5-46: Models 4&5 Supply Channels Pressures at 4.5m/s Incident Wind Speed	116
Figure 5-47: Models 4&5 Supply Channels Pressures at 0.5m/s Incident Wind Speed	116
Figure 5-48 Valve at Rest Position	118
Figure 5-49 Valve Action against Outflow	118

Figure 5-50 Valve in Closed Position Preventing Further Outflow	119
Figure 5-51 Three-Gate Valve Arrangement	120
Figure 5-52: Final Prototype with Non-Return Valve (units in mm).....	121
Figure 5-53: Simulation Model.....	122
Figure 5-54: Ansys Windcatcher Mesh.....	123
Figure 5-55: Windcatcher Channel Velocities.....	125
Figure 5-56: Windcatcher Flow Performance	125
Figure 5-57 Autodesk CFD Windcatcher Velocity Vectors at 0.5m/s Wind	127
Figure 5-58 Autodesk CFD Windcatcher Velocity Vectors at 4.5m/s Wind	127
Figure 5-59 Comparison of Predicted Channel Velocities	128
Figure 6-1: Typical Fouling Resistances [263].....	145
Figure 6-2: Heat Exchanger and End Caps.....	149
Figure 6-3: Supply and Extract Flow Paths Through End Caps	150
Figure 6-4: Heat Exchanger Channel	152
Figure 6-5: Heat Exchanger Pressure vs Heat Transfer Rate Graph	156
Figure 6-6: Heat Exchanger Pressure Drop vs Channel Breadth Graph	157
Figure 6-7: Heat Exchanger Channel Length vs Heat Transfer Rate Graph ..	158
Figure 6-8: Heat Exchanger Channel Length vs Channel Breadth Graph	159
Figure 6-9: Heat Exchanger Design Point Graph	160
Figure 6-10: Final Prototype	162
Figure 6-11: Simulation Model (Rings not shown).....	164
Figure 6-12: Ansys Mesh Settings.....	166
Figure 6-13: Supply and Extract Flow Temperature Change	168
Figure 6-14: Heat Exchanger Effectiveness	169
Figure 6-15: Annular Supply Flow Temperature Contour	170
Figure 6-16: Centre Extract Flow Temperature Contour	171
Figure 6-17: Velocity Contour of Centre Channel Flow through Heat Exchanger	171
Figure 6-18: Heat Flux on Heat Transfer Surfaces of Heat Exchanger	172
Figure 6-19: Turbulence Intensity Through Heat Exchanger Channel.....	173

Figure 6-20: Heat Exchanger Pressure Drop	174
Figure 6-21: Contour of Pressure Distribution at 2.5m/s Incident Wind Speed	174
Figure 6-22 Whole System Simulation Domain	176
Figure 6-23 Symmetry through Heat Exchanger	176
Figure 6-24 System Windcatcher Velocity Vector at 0.5m/s Wind Speed	179
Figure 6-25 System Heat Exchanger Extract Velocity Vector t 0.5 m/s Wind Speed	179
Figure 6-26 System Channel Velocities	180
Figure 6-27 System Ventilation Performance	181
Figure 6-28 System vs Windcatcher Ventilation Performance.....	182
Figure 6-29 Velocity Contour 4.5m/s Wind Speed.....	183
Figure 6-30 System Channel Flow Temperature Change	184
Figure 6-31 System vs Heat Exchanger Effectiveness.....	185
Figure 6-32 Temperature Contour at 0.5m/s Wind Speed.....	186
Figure 6-33 System Temperature Contour at 4.5m/s Wind Speed.....	186
Figure 6-34 Temperature Contour- Zoomed.....	187
Figure 6-35 Windcatcher Temperature Contour at 0.5m/s Wind Speed	187
Figure 6-36 System vs Heat Exchanger Pressure Drop	188
Figure 7-1: Test Model	195
Figure 7-2: Wind Tunnel.....	197
Figure 7-3: Pitot - Static Tube in Wind Tunnel.....	201
Figure 7-4: Kimo cp302 Manometer	203
Figure 7-5: Ultrasonic Flow Meter Set-Up [310]	205
Figure 7-6: Experimental Set-Up	207

LIST OF TABLES

Table 5-1: Simulated Models for Windcatcher Supply and Extract Flow Rate Optimization.....	72
Table 5-2: Mesh Independence Test results	124
Table 6-1: Mesh Independence Test results	167
Table 6-2 Equivalent Channel Velocities at Wind Speeds.....	168
Table 6-3 Whole System Mesh Independence Study.....	178

NOMENCLATURE

A	Area (m^2)
C_p	Pressure coefficient
E	Heat exchanger effectiveness
F	Empirical correction factor
Fr	Froude number
Gr	Grashof number
K	Turbulent kinetic energy (J/kg)
L	Thickness of solid medium (m)
Nu	Nusselt number
P	Fin perimeter (m)
Q	Heat transfer rate in Watts (W)
R	Heat transfer resistance (K/W)
T	Temperature in Kelvins (K)
U	Mean velocity (m/s)
$U, V \text{ and } W$	Components of velocity (m/s)
V	Volume (m^3)
c_v	Volumetric heat capacity ($J \cdot m^{-3}K^{-1}$)
h	Heat transfer Coefficient ($W \cdot m^{-2}K^{-1}$)
c	Specific heat capacity ($J \cdot kg^{-1}K^{-1}$)
f	Friction factor
g	Acceleration due to gravity ($m \cdot s^{-1}$)

k	Thermal conductivity ($W/m.K$)
l	Characteristic length (m)
n	Efficiency
q	Heat flux ($W.m^{-2}$)
ν	Kinematic viscosity (m^2/s)
Δ	Difference
α	Thermal diffusivity (m^2/s)
β	Compactness or heat transfer surface area density (m^2/m^3)
δ	Distance from Wall (m)
ε	Turbulent energy dissipation ($\frac{m^2}{s^3}$)
θ	Temperature difference (K)
μ	Dynamic viscosity ($kg/(m.s)$)
ρ	Density ($kg.m^{-3}$)
σ	Prandtl number
ω	Specific dissipation rate ($1/s$)
\bar{h}	Average heat transfer coefficient (W/m^2K)
h_c	Convective heat transfer coefficient (W/m^2K)
C_C	Coefficient of adaptation
C_M	Coefficient of differential probe
C_T	Coefficient of Temperature Compensation
C_p	Specific heat capacity at constant pressure ($J.kg^{-1}K^{-1}$)

C_μ	Empirical constant
D_h	Hydraulic diameter (m)
P_S	Static pressure (Pa)
P_T	Total pressure (Pa)
Q_v	Volume flow rate (m^3/s)
T_0	Surface temperature (K)
T_∞	Fluid Temperature (K)
T_i	Initial Body Temperature (K)
U_o	Free stream velocity (m/s)
U_t	Overall heat transfer coefficient (W/m^2K)
Y_k	Turbulent dissipation of k
Y_ω	Turbulent dissipation of ω
c_p	Air specific heat capacity at constant pressure in ($J.kg^{-1}K^{-1}$)
\dot{m}	Mass flow rate (kg/s)
Γ_k	Diffusivity of k ($1/s$)
Γ_ω	Diffusivity of ω ($1/s$)
δ_s	Length scale (m)
σ_K and σ_ϵ	Turbulent Schmidt numbers
σ_t	Turbulent Prandtl number
τ_w	Wall shear stress (Pa)
U^+	Velocity Tangent to wall (m/s)

1 INTRODUCTION

Paragraph 3.8 of Approved document Part L1B [1] defines Heritage buildings as 'buildings which are of local architectural or historical interest and which are referred to as a material consideration in a local authority's development plan'. However, P. Malpass [2] made a distinction between 'Heritage' and 'heritage'; 'Heritage' representing particular buildings designated as being of architectural or cultural importance and 'heritage' as the entire stock inherited from the past. He made a point of all housing being a form of 'heritage' to be valued as they convey the entire embodiment of the cultural state within which they were built. In this context, the UK is rich in heritage buildings and of interest to this research are traditional dwellings of the type constructed during the Victorian and Edwardian era into the early 20th century. This period spans 1837-1945 and the dwellings constructed constitute around a quarter of the total housing stock in the UK [3]; [4]; [5].

1837–1919 saw the emergence of Victorian and Edwardian architecture. It was an era of boom in housing construction; around 7.6 million dwellings were built with most surviving till date. Characteristic of these buildings are solid masonry walls, raised timber floors, single-glazed timber frame sash windows, roofs usually clad in slates, and open fires in chimneys to maintain indoor comfort in winter. Into the 20th century, the method of construction changed with introduction of the cavity wall in 1919 [6]. However, the chimney open fire method of maintaining indoor comfort largely stayed the same till around 1945 when the uptake of central heating started slowly, aided by the great smog of 1952 which led to the introduction of the clean air act of 1956 [6]. The act which sought to encourage the use of clean fuel in homes, eventually led to a decline in the use of open fires in chimneys [7]. Now almost a century after they were built, Victorian and Edwardian era dwellings still make up 20% of the total dwellings for England [8], 20% for Scotland [9], 17% for Wales [10] and 10.6% of those in Northern Ireland [5]. Additionally, in Northern Ireland dwellings constructed between 1919 and 1940 are 7.4% of the total [5]. In Scotland those built between 1919 and 1944 make up about 12% [9], in Wales 33% [10] and in England an additional 16% [8].

In addition to chimneys for providing heat in winter, ventilation was also an important feature of these dwellings because of its necessity for the correct functioning of the building components and indoor cooling during summer months. Many problems can occur from water entrapped within the building materials of heritage dwellings. Hence, discrete openings were intentionally created during their construction to allow uncontrolled air infiltration [6]. Ventilation through the floor was maintained by timber floors built on joists over the plinth on ground floors. The void created is then vented by grilles at the sides to get rid of moisture and infiltrate gaps in the flooring. Traditional sash windows were without seals and leaky, and rooms like kitchens where high moisture levels are expected were fitted with roof vents. The stairwells were designed as ventilation stacks to aid air movement and were often open at the top and fitted with adjustable ventilators. Venting strategies were also incorporated into the roofing. Gaps known as 'penny gaps' were maintained between sarking boards to provide trickle ventilation for the wooden rafts [11].

The presence of these fixed ventilation features meant most habitable rooms had fire places with chimneys [6]. The open fires provided radiant heat to people around them making comfort possible in the low air temperatures brought about by excessive air infiltration in winter [7]. Techniques for circulating combustion air for the fireplaces were also incorporated into dwellings. Spaces and perforations made in doors allowed top floor fireplaces to draw warm air from lower levels, and grilles around the fire place on the floors allowed the air to be drawn also from the adjacent space below to reduce draught through the doors [11].

Nowadays, these heritage dwellings are mostly retrofitted with modern heating systems where possible, and they consume large quantities of energy to make them habitable. This is primarily because the energy is readily lost to the environment and must be replenished at high rates to maintain indoor comfort [12]. Research shows that these dwellings are replaced at a low rate of about 1% a year [13], and the profiles of existing ones show that many have very poor energy efficiency [12]. This situation has brought to the forefront the impact of this heritage dwelling stock on building energy consumption in the UK.

There is a general interest in conserving heritage buildings [14]; [15]; [16]. History, memory and continuing management of heritage are some of the reasons that give rise to this interest. Heritage dwellings form the distinctive character of many urban centres, providing a visual cultural reference, and creating continuity with the past [17]. However, issues of climate change and conservation of non-renewable resources make upgrading them very important. As stated in the British Standard [18], “the continued use of heritage buildings with improvements in their energy use efficiency is a global priority as simply replacing them is costly in economic terms and from an energy perspective, ineffective, as new builds require a significant amount of embodied energy from non-renewable sources – typically equivalent to five to ten years’ worth of the energy to light, heat and condition the existing build. In global environmental terms, the balance of advantage strongly favours the retention of existing building stock, particularly when performance in terms of energy consumption in use can be improved”.

To achieve this improvement, it is essential to tackle the means through which energy is lost in these dwellings. One significant means, is through ventilation [12]; [19]. Studies have shown ventilation heat loss accounts for between 20% to 53% of total heat loss in these dwellings [19] [12] [20] [21] [22]. It is helpful to recognize the difference between ‘ventilated’ and ‘vented’ air spaces. A ventilated space is intended to facilitate the flow of air through it for human comfort. In contrast, a vented space has openings to the outside air that allow water vapour to breathe out for the preservation of building material. The Chartered Institution of Building Services Engineers (CIBSE) is the prime source of expertise in the UK Building Services industry. Their current recommendations for heritage dwelling ventilation is between 0.5-1ach [23]. Nowadays, in carrying out energy efficiency upgrades to heritage dwellings, improvements are being made to fabric airtightness of ventilated spaces and controlled ventilation provided to the recommended levels without impeding the function of vented spaces. The principle of “build tight, ventilate right” being promoted for new builds is increasingly recognized as the basis for energy efficient ventilation in buildings, and generally extended to heritage dwellings with special considerations for their fabric materials.

Many manufacturers of ventilation systems have developed products aimed at providing controlled ventilation in dwellings. A readily available solution is the installation of a whole house mechanical ventilation system with heat recovery (MVHR). With MVHR systems, fans are used to extract air from rooms via ducts and passed through a heat exchanger located in a central unit before being exhausted outside. Concurrently, fresh incoming air is preheated via the heat exchanger and ducted to the living space. Providing modern MVHR systems for heritage dwellings comes with numerous challenges [31]; the initial costs are high, duct-work is invasive and there are inherent complexities in installation and commissioning. The energy saving potential of this system is also highly contentious with many scientific investigations negating standalone claims of energy savings [32]; [33]; [34]. Furthermore, compared to purpose built modern dwellings, accommodation for modern ventilation systems are not ready-made or easily created in heritage dwellings.

An alternative is natural ventilation with heat recovery. There is a dearth of natural ventilation systems with heat recovery aimed at heritage dwellings. Extensive literature search and market research by the author only revealed bespoke MVHR systems modified for use in heritage dwellings [17] and one discontinued natural ventilation product [24] in the UK market. Thus, owners of these dwellings are largely limited to MVHR systems and large scale installations of this system in refurbishment are common [25]; [26]; [27]; [28]; [29]; [30]. Hence, there is a present challenge in providing a fit-for-purpose ventilation heat recovery system for heritage dwellings.

Retrofitted ventilation systems must respect the aesthetic and historic value of a dwelling. The answers to questions of users expectations, space requirement, age and past, present and future uses of the structure [31] is an important determinant. A sound solution is thus limited in size, type, cost, complexity and location. A retrofitted ventilation system will generally be more desirable if it is inconspicuous, and hidden within the building fabric without causing extensive invasive modifications [31]. This is easier to achieve in more recent purpose-built homes, but in many heritage dwellings, availability of vertical and horizontal

distribution space is a problem [31]. The skill of inserting new heat recovery ventilation systems into an heritage dwelling requires a combination of lateral thinking with an imaginative and innovative use of technology, while taking advantage of the opportunities offered by the building in question so as to make the building do its practical duty well and be graceful and pleasing in doing it [31].

A common feature of heritage dwellings are disused chimneys. Chimneys are open to the atmosphere and present a leakage path for indoor air. During energy efficiency upgrades, disused chimneys, along with other leakage paths, are usually sealed off to improve air-tightness. However, ventilation heat recovery can be achieved passively by utilizing windcatcher techniques to deliver fresh air at low level through the chimney opening and extract air through the same chimney via diffusers at high level on the chimney breast. A counter flow heat exchanger in the flow path will recover the heat from the extract air flow to preheat the supply air. This way, only a single ducting and a terminal diffuser are required. This is an attractive solution not only for cutting energy usage and cost, but for the minimalistic installation and modification required. This proposal can be achieved by the development of two main parts that will make up a system employing this method:

- A windcatcher to capture incident wind for passive ventilation air supply and extraction through the same chimney.
- A low resistance thermally efficient energy/heat exchanger to recover otherwise lost heat contained in the outgoing ventilation air flow.

The author's representation of the proposed system is shown in Figure 1-1.

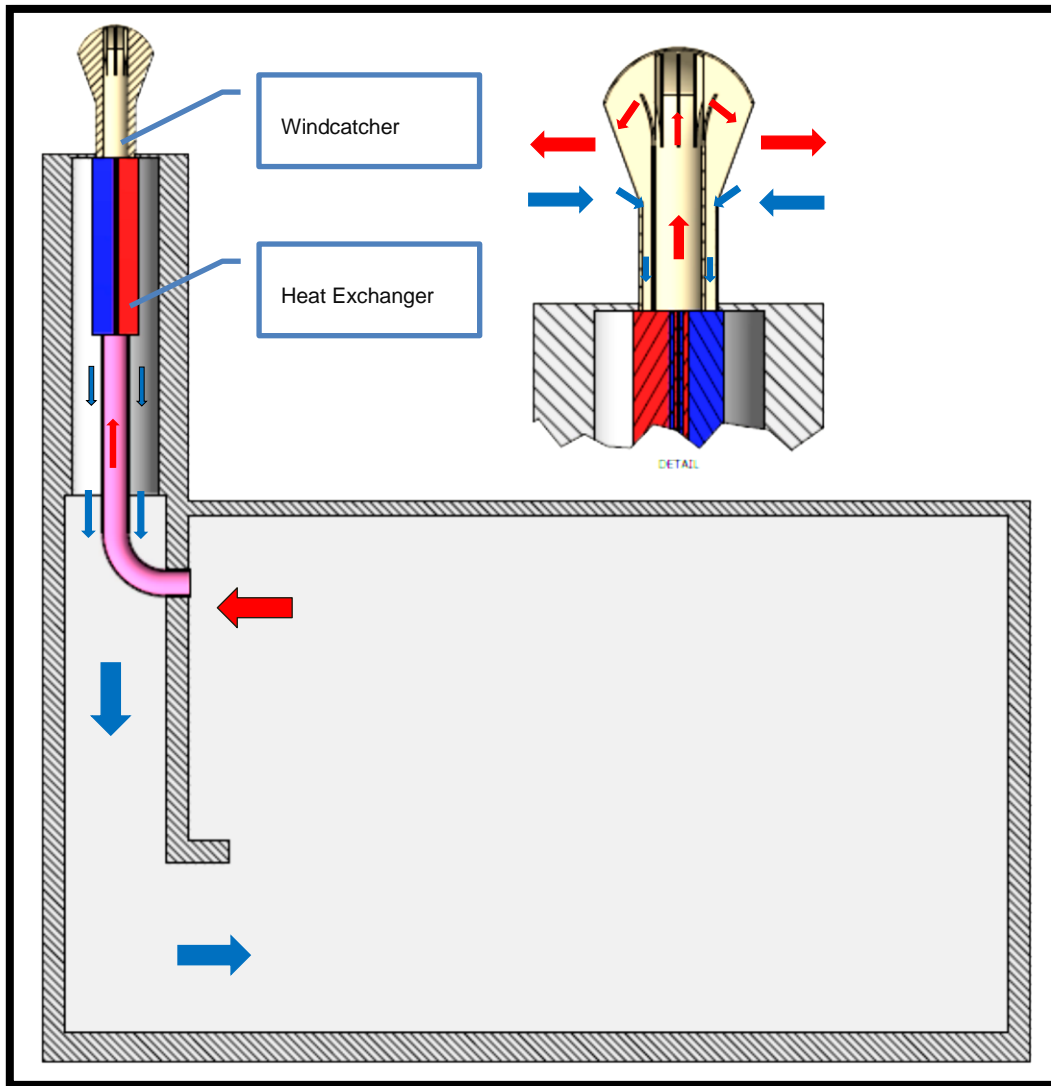


Figure 1-1: Proposed Ventilation System

The system require no fan to drive air flow. The windcatcher is a cylindrical multi-directional fixed part that mimics the form of a traditional chimney cowl. This is fixed atop an existing chimney to replace the cowl. It consists of two concentric cylinders of different heights with a dome cap. The longer central cylinder is an outlet terminal for air flow exiting the living space driven by buoyancy and extractive pressure created by the cowl geometry. The annular opening created between these cylinders forms an omnidirectional air inlet for atmospheric wind into the system. The windcatcher is attached to a heat exchanger at its base which fits into the chimney. The heat exchanger is also cylindrical, with distinctive

counter-flow air paths through it to extract heat from the outgoing air flow and pre-warm the incoming supply air. The supply and extract air paths through the entire system is mainly concentric. The central air path acts as the extract and consists of a duct running from the heat exchanger base to terminate in a vent at high level within the living space. The chimney void itself acts as the air supply channel with the disused fireplace as its terminal. Multi-storey heritage dwellings usually have multiple fireplaces with multiple flues where individual units of this system can be installed for a whole building application.

1.1 Design Selection

Many works in literature works have explored the concept of windcatchers to implement natural ventilation in buildings [35]; [36]; [37]; [38]. Many of these rely on the low pressure created on the leeward end of a fixed windcatcher to drive extract air flow [36]; [35]. These windcatchers are usually aligned along the direction of the prevailing wind in the area they are installed. However, in operation, constantly changing incident wind directions make the channels alternate between supply and extract modes, and this makes it hard to incorporate heat exchangers into these designs. Some designs have incorporated vane-like features to rotate the windcatchers so the air supply channel always faces the prevailing wind direction [37]; [38]. While this may seem to overcome the wind direction problem, the resulting geometry and constant rotation makes them aesthetically unsuited to heritage dwellings. The system proposed in this research overcomes these deficiencies by providing fixed supply and extract air flow channels in every incident wind direction while remaining aesthetically suited to heritage dwellings without necessitating unwanted modifications to the building.

A cylindrical overall form factor is appropriate for the windcatcher because it mimics the common form of chimney cowls, and offers the possibility of harnessing incident wind from any direction. This is divided into multiple sections to provide support for a concentric central tube that serves as the central outlet. The divisions also provide narrowing channels for flow acceleration over the central channel surface.

Windcatchers generally depend on forces of the incident wind and indoor air buoyancy to drive air flow [39]. The central outlet is intended to harness these two forces to drive extract flow. Indoor air buoyancy due to temperature stratification will naturally drive air upwards towards an extract vent located at high level in the living space. Outdoors at the windcatcher, the acceleration of incident air over the surface of the extract channel will serve to induce low pressure over the extract surface and drive extraction by the venturi effect.

The choice of a dome cap over other designs was informed by two advantages that this form offers; the dome further mimics the form of traditional chimney cowls. In addition, it offers a streamlined cavity over the extract channel which will align air flow, and also experience low pressure when atmospheric wind is incident on its external surface. These will aid extraction.

While design inspirations can be taken from the pros and cons of existing types of heat exchangers, to effectively cater to the retrofit needs common to heritage dwellings, the heat exchanger part needed to be accommodated within the building fabric without necessitating conspicuous modification to the dwelling. Heat exchangers accommodated within operational chimneys for reclaiming flue gas heat are commonplace as the chimney provides a good location to house heat exchangers without affecting the dwelling's character. However, because of its hard accessibility, and limited width, the chimney limits the size and complexity of heat exchangers that can be housed within it. Thus, a recuperative counter-flow plate heat exchanger was selected. Plate heat exchangers are relatively simple and flexible. Common types can be easily taken apart for cleaning or expanded with more plates to enhance their capacity. In forced flows, the turbulent moving fluids readily attach and detach from the heat exchange surfaces and fouling is seldom a problem [40]; [41]. Also, due to their high heat transfer rates, other forms of recuperative heat exchangers with comparable performance are usually 6 times larger in size [42]. The thermal efficiency of a counter-flow configuration is also relatively high because it provides a nearly constant temperature differential along the heat exchange surface. However, they may require bigger sizes because of the small temperature difference

between the fluid streams [43]; [44]; [45]. The long length of chimneys presents a good space to extend the heat exchanger along the flow direction for performance optimization.

A similar system to that proposed is the ventive [24] system. The particular ventive product referenced is now discontinued, and there is no performance data available for it in published scientific literature. However, investigation conducted in this research shows that, while the geometry employed in the product does intend an omnidirectional supply channel, it suffers from severe flow short-circuiting within the windcatcher, and this vastly reduces its ventilation and heat exchange effectiveness. The extract air flow path is not fixed, and air also exits the system from the supply channels. Short-circuiting has the undesired effect of directly routing the supply air flow back into the extract channel without mixing properly with the room air. In simulations carried out in this research, fixed geometry employing the ventive design only supplied 2% of its captured air flow at room level. This is detailed in sections 5.2.1.1, 5.2.1.3.1 and 5.2.3.

The system proposed in this research aims to overcome all these deficiencies and more by investigating performance characteristics of air-flow and heat exchange in the proposed system and incorporating geometric features to facilitate desired operation and optimize performance.

The following chapter presents a review of scientific literature to provide insight into the energy consumption of UK heritage building stock and numerous developments in energy efficient ventilation. This is followed by a chapter detailing the aims and objectives of this research and areas where new knowledge will be provided on the performance mechanisms and properties of the proposed system. An explanation of the numerical techniques to be applied is presented under the next chapter titled "Methodology". Following this, two chapters are respectively dedicated to the windcatcher and heat exchanger development, analysis and discussion of results. An iterative approach was employed for these tasks. The initial models were developed by the author and presented with their required performance characteristics. Major deficiencies in

performance were then investigated and a final prototype is presented which fulfils the defined requirements.

Proposals for experimental investigation of the system is included in subsequent sections before recommendations and conclusions.

2 LITERATURE REVIEW

Numerous scientific investigations into ventilation in heritage dwellings have presented innovative solutions and useful information over time on the subject of ventilation heat recovery in heritage dwellings. Under this section, many of these are reviewed and references have been made to the relevant ones building up to the solution proposed in this research work.

Common and novel technologies applied in ventilating heritage dwellings are reviewed and broadly classified under mechanical and natural ventilation. Recent developments as well as established forms were reviewed. These revealed the different debates in the scientific community on the perceived advantages and disadvantages of each technique.

Lots of literature agree on ventilation heat recovery as a means of limiting ventilation energy loss in heritage dwellings but express reservations on gains claimed when it is achieved by consuming other forms of energy such as fossil fuel derived electricity [33]; [46]; [47]; [48]; [49]; [50]; [51]. Hence, recent developments have been in trying to achieve ventilation heat recovery with zero energy consumption in operation [52]; [53]. In developing the proposed system, analytical and experimental works available in literature on technologies that bear similar characteristics to the operation of the system were looked at. Since windcatchers rely on wind driven ventilation and passive stack effects [35]; [54]; [55], various investigations into wind driven ventilation in dwellings were also reviewed.

For the heat exchanger component of the proposed system, different heat exchanger technologies were reviewed under recuperative and regenerative classifications. Much focus was on recuperative technologies. Particularly, that of plate heat exchangers because of their relative simplicity and compactness compared to other technologies. Common and novel materials and configurations were examined as well as parameters used for quantifying performance. Experimental and analytical studies into performance enhancement of heat

exchangers in the areas of heat recovery efficiency and pressure drop were also looked at.

2.1 Energy Loss in Heritage Dwellings

Scientific understanding of energy use in building has identified the two-major means through which energy is lost in dwellings as the building fabric and ventilation [32]. Recent trend has been to make heritage dwellings energy efficient by making them air-tight, insulating the fabric, and providing sufficient controlled ventilation. The current state of heritage dwellings with regards to these measures is discussed below.

2.1.1 Fabric Heat Loss

The two areas of provision of energy efficient heating systems and fabric insulation have been the focus of UK government incentives on reducing energy consumption in UK heritage dwellings. Results have been encouraging as yearly values from 1991 shows an upward trend which is largely due to increasing uptake of energy efficient measures (Figure 2-1).

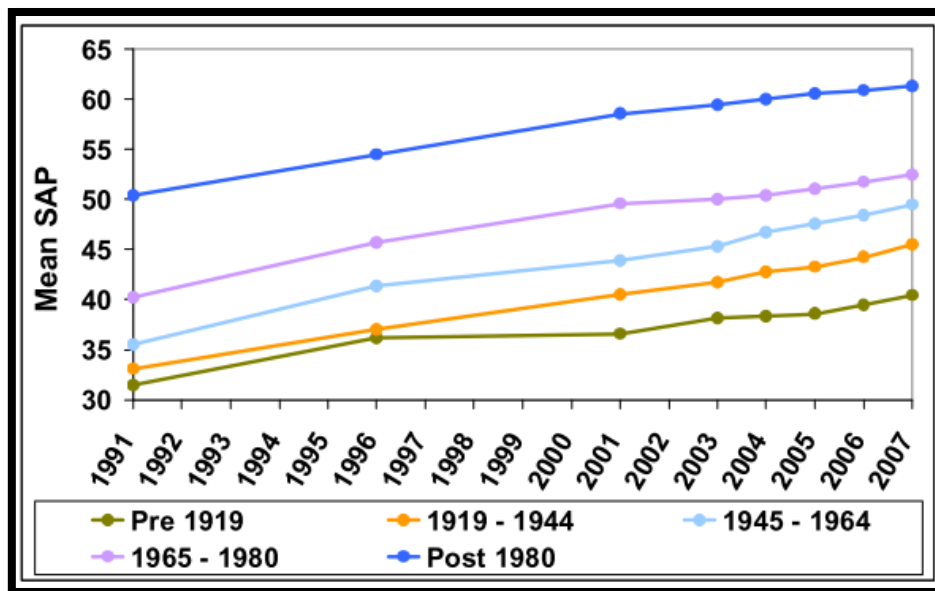


Figure 2-1: Timeline of Mean SAP Ratings by Dwelling Age [56]

Insulating building fabric against heat loss has mainly consisted of filling the cavity between the two leaves of walls with rock wool, glass wool, cellulose and foams. With older heritage dwellings, fabric insulation has not caught on considerably, largely due to the absence of cavity walls. Only 16% of pre-1919 have cavity walls and considerably less than half of those figures have wall insulation [57]. Loft insulation is also relatively poor compared to post-1945 stock with a highest proportion of uninsulated lofts occurring in pre 1919 dwellings [57]. As refurbishment works on the heritage dwelling stock have been relatively recent, a higher percentage of them have modern highly efficient condensing boilers when compared to post 1990 dwellings [58] (Figure 2-2). However, this has not translated into overall lower energy consumption. The main mechanism of energy loss in dwellings is through heat loss across the building fabric and openings in the fabric as opposed to boiler inefficiency [32].

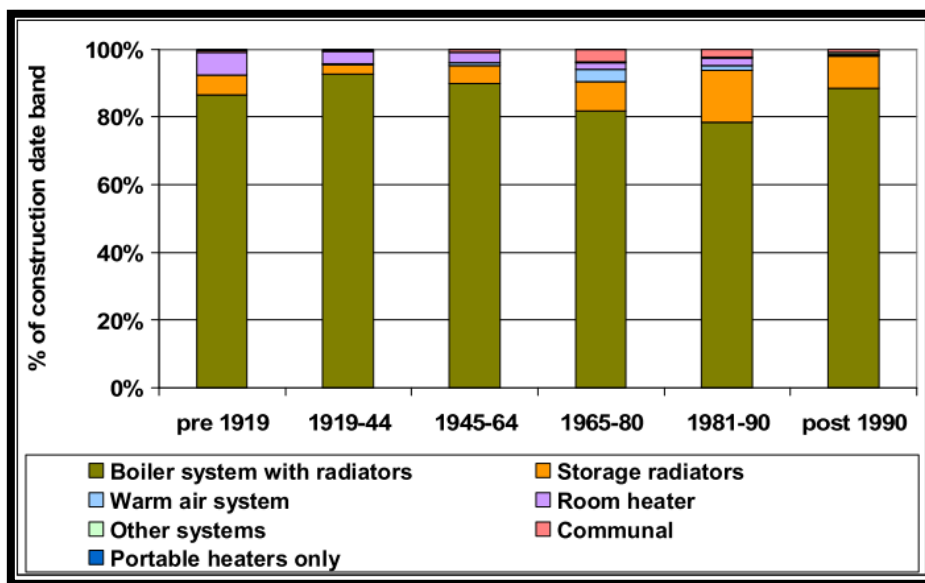


Figure 2-2 Space Heating System by Dwelling Construction Date [58]

Another popular measure for addressing energy loss through the fabric sections occupied by windows is the installation of multiple glazed windows which work by utilizing the insulating properties of air or vacuum between two or more window panes. Multiple glazing is standard in modern new builds and refurbished

dwellings. Studies by the Building Research Establishment (BRE) [58] on dwellings in England revealed that less than 30% of pre 1919 buildings and only 9% of pre 1945 dwellings have no double glazing. Compared with fabric insulation, the impact of this on energy consumption in heritage dwellings has been nominal because windows constitute relatively small areas compared to walls [57].

All of these measures have resulted in the average SAP rating of pre 1919 dwellings rising to 40 while that of dwellings constructed between 1919 and 1945 is around 45.5 [56].

(The “Standard Assessment Procedure”-SAP is the official method of assessing the energy efficiency of dwellings in the UK. The methodology uses a scale of 1 -100 to represent a dwelling’s energy efficiency with a higher SAP rating indicating better performance.)

2.1.2 Ventilation Heat Loss

A study by J. Utley et al [19] on the average UK dwelling revealed the trend year on year from 1970, the means through which heat loss occurs in dwellings. The results showed that ventilation is a significant means, accounting for an average of 20% of the total heat loss (Figure 2-3).

The change from open fires to central convective systems is contributory to the level of heat loss now observed through ventilation. In the 19th century, open fires provided radiant heat which does not heat up the air, thus comfort was possible in the low air temperatures caused by excessive infiltration [6]. In contrast, modern convective heating systems heat up indoor air to provide the same effect. This volume of heated air is readily lost during ventilation and infiltration.

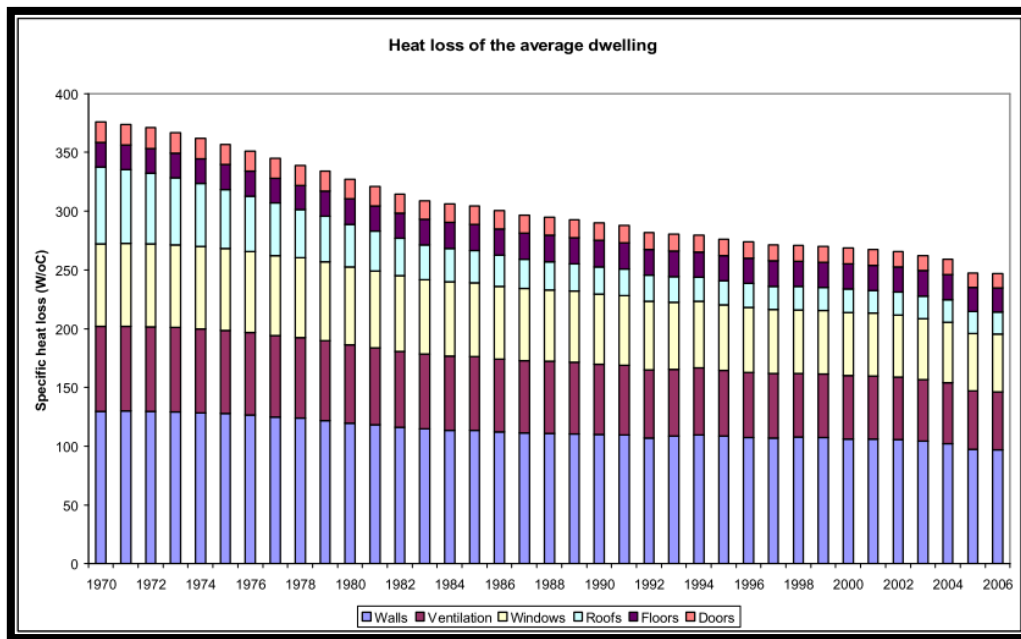


Figure 2-3: Heat Loss Trend in Average Dwellings [19]

As much as this suggests this problem can be overcome by simply replacing of convective systems with radiant heating systems, H. Hanibuchi et al [59], when they investigated the thermal performance of a radiant heating system concluded that approximately 50% of the heat transfer mechanism was by convection. Thus, considerable amounts of energy will still be readily lost through ventilation if radiant systems are employed.

The impact of ventilation heat loss on total energy consumption in dwellings is well documented. In his investigation on 46 historic dwellings of varying sizes across the UK, J. Beedell et al [12] discovered that energy consumption is quite significant and uncontrolled ventilation was pointed out to be a significant contributor with infiltration rates through sash windows alone contributing up to 3 air changes per hour. In total, ventilation contributed 30% of the total heat loss in these buildings. M. Liddament et al [20] described different methods for estimating the mass flow rate of ventilation air out of a building and the enthalpy difference between incoming and outgoing air. In their work, ventilation heat loss energy implication for buildings in the UK was found to be approximately 36%. H.

Awbi [21] placed this value between 30-60% percent and noted ventilation as the most prominent energy loss process in existing buildings. As high as 53% was estimated by M. Orme [22] for heat losses in 13 industrialised nations. In his work, D. Colliver [60] quantified this energy when he collected hourly weather data and calculated the energy required to maintain a constant mass flow rate of 1kg/h air at 18 degree set point as 87.8MJ.h/kg for the Heathrow area in London.

Currently, in refurbishing heritage dwellings for the future, fabric are made airtight and controlled ventilation provided for comfort, removing air pollutants and moisture control in building materials. However, improvements in required air quality standards has continually pushed up this controlled ventilation rate to abate the many problems caused by poor indoor air quality [33]. Consequently, heat loss through this means is still very important.

2.2 Energy Recovery Techniques in Ventilation Systems

A common way of reducing energy lost through controlled ventilation is by utilizing energy recovery techniques. This involves the recovery of energy, mainly in the form of sensible heat or total enthalpy from the outgoing exhaust air and preconditioning incoming air with it. It has the advantage of providing the required level of ventilation to maintain the required level of indoor air quality without the associated energy loss. In an early research into residential ventilation heat recovery W. Fisk et al [51] discovered that average dwellings (volume of $340m^3$ and height of 2.5 m) with energy recovery will potentially use between 5.3Gj to 18Gj less energy for heating during the heating season compared to ones without. In process industries, application of energy recovery have resulted in massive savings usually with payback periods of under two years because of the higher temperature gradients between fluid stream [61]. In buildings applications however, the smaller temperature gradients amplify the effect of other parameters on the energy recovery efficiency and economic performance.

Energy recovery systems can be broadly classified based on flow characteristics. A broad classification divides them into counter flow, cross-flow and parallel flow systems. In parallel flow types, the fluid streams travel in the same direction as

they flow through an energy exchanger while in counter flow the directions are opposite. Cross flow configuration brings the fluid streams to flow across each other [62]. The thermal performance of these configurations differs because of the temperature difference pattern along the fluid path. The parallel flow type brings the most energy dense portion of one fluid stream together with the least energy dense portion of the other. This causes a large energy differential and transfer at the heat exchanger entrance. However, this difference gradually diminishes, and the energy concentrations approach one another asymptotically along the length of the exchanger. Consequently, only a limited thermal efficiency can be achieved by using a parallel flow configuration in energy exchangers. In a counter flow configuration, the most energy dense portions of both fluid streams contacts at one end, and the least energy dense portions at the other end. This provides a nearly constant energy differential between the two streams over the length of the exchanger, resulting in relatively higher efficiencies [63]. Cross flow configurations are more difficult to analyse as many different configurations are possible. Typically, the energy differential along the exchanger is similar to that of cross flow exchangers [62].

Energy recovery systems can also be classified into recuperators and regenerators. In regenerators, the extracted energy from one stream is transported by a medium to be regenerated at another location. Applications in ventilation such as heat pipes and rotating drum regenerators fall into this category. In recuperative energy exchange, the streams of fluid exchange energy continuously and are usually separated by walls. A ventilation supply and extract air stream on opposite sides of a conductive plate typify what recuperative energy recovery is in building ventilation. As the air streams move, they continuously exchange energy across the plate that separates them without mixing. The construction of plate energy exchangers is usually of many of this kind of passages with different streams arranged side to side to form a single unit. Different configurations exist to enhance the energy transfer properties, and depending on the material used for the plate, the energy exchanged maybe purely sensible heat or total enthalpy consisting of sensible and latent heat parts [64].

Metals have been used extensively for sensible heat recovery in plate exchangers, but due to surface fouling and freezing which can drastically reduce the heat exchanger's effectiveness, numerous new materials are being investigated for building ventilation applications. Polymer plates are promising and have been reported to give satisfactory sensible heat exchange properties [65]; [66]; [67]. For total enthalpy recovery, lot of investigations have been done on utilizing membrane materials in ventilation applications [34]; [68]; [69]; [70]; [71]; [72]; [73]; [74]; [75]. Membranes are permeable materials that allow the exchange of moisture and heat between air streams but are impermeable to some gases. Some of the materials that have been experimented with includes cellulose based compounds, cellophane, Nafion, polyether-polyurethane, polystyrene-sulfonate, and polyvinylidene fluoride [76].

Latent heat composition of ventilation extract air in dwellings can be significant and in theory, its recovery can significantly increase the efficiency of any ventilation system. M Nasif et al [77] investigated the effects of latent heat recovery in air conditioning systems using mathematical methods. In their comparison of conventional systems that mix extract and supply air to deliver air at a set point, and fresh air delivery systems incorporating enthalpy recovery, they reported an 8% reduction in energy consumption with enthalpy recovery. The enthalpy gradient between air streams in ventilation applications puts a limit on the effectiveness of membranes in latent heat recovery. It reduces as supply air humidity approaches the indoor air humidity set point. Conversely a high differential in the air stream humidity levels can lead to substantial energy savings [76]; [78]. L. Zhang et al [78] investigated a hydrophilic membrane based energy recovery ventilator in Hong Kong weather where 81% of ventilation air treatment energy is used to bring down relative humidity levels, and proved it to be highly beneficial in reducing energy consumption.

Contrary to expectations, total enthalpy recovery does not out rightly surpass sensible heat recovery as a better solution in most ventilation applications. The total efficiency of total enthalpy recovery systems was characterized in an equation by J Liu et al [79] as enthalpy efficiency which consists of sensible and

latent parts. The weighted coefficient of these parts was proposed to be used in determining the appropriate application of energy recovery devices. As such, a climate with low humidity difference between supply and extract air will have a higher weighted coefficient of sensible heat efficiency in the enthalpy efficiency equation and will benefit more from a sensible heat recovery system as opposed to a total heat recovery one. Notably, H. Han et al [80], when they tested an Enthalpy Recovery Ventilation (ERV) system between two opposite chambers to simulate outdoor and indoor conditions, observed that the humidity efficiencies of ERV are less than temperature efficiencies irrespective of season. Thus, total enthalpy recovery can be of similar or even lower performance than sensible heat recovery depending on climate.

In building ventilation applications, the energy recovery techniques discussed above are implemented in broadly two kinds of systems i.e. mechanical and natural ventilation heat recovery systems. Mechanical heat recovery ventilation units are very popular in the UK and have become the de facto standard technology in ventilation heat recovery. Natural ventilation heat recovery is a relatively newer concept and various investigations are still ongoing on the subject [52]; [81]; [82]; [83]; [84]; [85]; [86].

2.2.1 Mechanical Ventilation Heat Recovery System (MVHR)

MVHR systems consist of a fan and heat recovery module inside a central unit connected to air supply and extract ducts. The central unit is usually made to fit in existing ceiling voids. Extract ducts from rooms where high levels of moisture are produced, such as the bathroom and kitchen, are connected to the central unit and air supply from the central unit are ducted to other living rooms in the dwelling. The outside air intake and exhaust terminals are usually located on adjacent sides of a building and ducted to the central unit to minimise cross-contamination. Within the central unit, energy is recovered from the outgoing exhaust air and used to preheat the supply air into the living space by an energy exchanger without mixing the air streams. Air movement through the entire system is done by the fan which works against the system's flow resistances and

filters that remove intake air debris, pollen and dust from the supply air. Thus, system air flow performance is guaranteed and can be finely controlled.

During the times heritage dwellings were built, natural ventilation was the mode of choice for providing thermal comfort. Integration of MVHR in heritage dwellings is particularly difficult because they were not designed or built to be ventilated by mechanical means. Thus, many retrofit ventilation systems for heritage dwellings must be bespoke and this adds to costs and complexity.

Members of the 3ENCULT project [87] develop passive and active solutions for conservation and energy efficient retrofit of heritage buildings in European urban areas. In evaluating the question of MVHR in heritage dwellings; how to deal with these buildings and if it makes sense to integrate these systems into heritage buildings. They make a point of occupant and building ventilation needs being contradictory in some cases where controlled ventilation is supplied. However, studies have shown that humans exhibit more thermal tolerance when natural ventilation is employed [88], which makes a case for natural ventilation when these contradictions occur and can be met by natural ventilation. They advocated for an air permeability level of 1/hr for MVHR retrofits to be financially viable. Different methods were also proffered for the integration of MVHR systems into heritage dwellings.

Cascade ventilation has been prescribed as one way to reduce the problem of duct distribution. In this method, the building is divided into air supply zones, air extract zones and air transfer zones like corridors through which overflow air is transferred between the first two. This reduces the need to install ducts in multiple rooms for ventilation. A modification of this method is the active overflow method where MVHR is installed close to the extract zones and extracts directly outdoors. A single duct is employed to supply fresh pre-heated air directly into distribution zones and small fans are employed to circulate the air in and out of adjoining rooms. Ventilation efficiency is low with this method as the air mixes in the distribution zone.

The energy consumption of fans in MVHR systems quickly raises questions about its energy saving potential. As such, the financial and energy saving advantage

of MVHR in heritage and dwellings in general is a subject of much research and has been found to depend on a number of factors some of which vary are highly variable such as human factors [89]. Some of these factors are discussed below.

2.2.1.1 Utilization

In view of the high capital outlay on most of residential MVHR units, the payback period can be long if the system is hardly utilised. Factors such as local climatic conditions influence utilization, and can affect potential energy and cost savings achievable with MVHR systems. J. Liu et al [79] simulated MVHR performance using climate data from five locations and found marked difference in performance and consequently, energy saved. The technical advantage increases as the enthalpy difference between the exhaust and incoming air increases. When only sensible heat recovery is employed, as common in most systems, climates with higher Heating Degree Days (HDD) are more susceptible to benefit due to a longer possible duration of use. By assuming an indoor temperature set point, the area bounded by the graph of the set point and outside air temperature variation on a 'Temperature vs Duration' graph for a location can give an indication of the recoverable sensible energy for any climate in a season.

A study by M. Drost [47] on utilization patterns of heat recovery ventilation systems in 38 dwellings revealed that theoretical savings are an over-estimation, as usage patterns revealed an average utilization period of 7 hours a day. Lai et al [90] reached a similar conclusion of 7.2 hours per day which further reduces the energy savings due to the system and makes the payback period prohibitively long. Y. El Fouih et al [33] studied the primary energy consumption of MVHR systems in different types of buildings and concluded that they don't offer significant gain when mostly utilized during the day time, as fabric and indoor heat gains ultimately lowers heating demand. However, applications with high prescribed ventilation rates such as in schools, have been found to shorten payback periods by M. Rasouli et al [48].

Schibuola et al [91] investigated the effect of ventilation system refurbishment in heritage apartments and observed a 43% yearly reduction in fan energy consumption when the installed mechanical heat recovery system was demand

controlled based on occupancy. They concluded that demand-controlled ventilation could improve the performance of mechanical heat recovery ventilation in dwellings with high variability in occupancy.

In a report by Tim Sharpe et al [92] into MVHR systems in 237 dwellings, they found that half of occupants in dwellings with MVHR disabled the system out of concern for operating cost and lack of understanding on utilization. Same was observed by McGill et al [93] when they compared two dwellings with natural and mechanical ventilation with heat recovery. They concluded that knowledge on use of the system was significantly lacking in the home with MVHR. In social housing in the UK, Gupta et al [94] observed the same, as occupants switched off their MVHR systems because they perceived them to be costly to operate. These studies revealed that sole utilization of the system was hard to achieve and occupants vented through windows which significantly reduced the amount of energy saved by the system.

2.2.1.2 Indoor Heat Gains and Fabric Composition

Indoor energy gains should also be factored into any decision to install an MHRV system. Kindinis et al [95] in the study of the thermal and energy behaviour of a 1906 heritage dwelling, observed that the difference in internal heat gains between an unoccupied and eight person occupancy scenario is quite high at about 20 kWh/m² over a 6 months period. Homod et al [96] conducted an investigation into the use of natural ventilation to reduce mechanical ventilation energy consumption in a dwelling and observed that significant reduction in ventilation energy consumption can be realized in dwellings utilizing mechanical system when thermal mass and indoor gains are factored into the control of the mechanical system. M. Rasouli et al [48] emphasized the effects of indoor gains when they showed that uncertainties in indoor gains significantly increase uncertainty in the payback period of MVHR systems.

The passive thermal properties of many heritage dwellings was emphasized by Omar et al [97] when they investigated the indoor environment of a heritage dwelling and concluded that it self-regulates without the need for mechanical ventilation. The higher heights of rooms in older dwellings was suggested as a

contributory factor to thermal performance. Rubio-Bellido et al [98] studied an urban conglomerate of heritage dwellings to analyse the passive design strategies that were applied in designing the dwellings. They observed that the heritage dwellings were designed to adapt to their environment without the need for mechanical ventilation, and indoor heat gains significantly contributed to this, and dampening of indoor temperature variations.

The benefit of employing energy recovery with the associated cost, compared to other means of ventilation was investigated by C. Simonson [99]. His comparison of primary energy consumption revealed that for the appropriate construction method in cold weather, ventilation heat recovery during the heating season can be comparable to a natural ventilation system. B. Yassine et al [100] further revealed the impact the fabric composition of buildings can have on the potential energy savings of ventilation systems when they investigated the optimal wall configuration to achieve comfort indoor conditions by developing a numerical model to predict and control indoor temperature when mechanical ventilation without energy recovery is employed. They came up with an optimal fabric composition that made simple extract-only mechanical ventilation feasible.

Zhou et al [101] developed a heat balance model coupling different factors that affect indoor temperature in a naturally ventilated building. They were able to predict the optimum configuration of fabric and internal thermal mass to maintain comfort internal temperature. Hence, a good knowledge of the thermal properties of a buildings fabric is essential in determining the feasibility of adding MVHR systems. In an investigation concluded in September 2013 by Calebre; the low-energy technology research project [102], it was discovered that implementing MVHR in typical existing homes without extensive modifications to the building fabric increases energy cost for the occupant.

E. Juodis [49] stated the significance of the heat gain/heat loss ratio for a building and defined a thermal balance point as the outdoor temperature where indoor heat gains compensates for heat loss through ventilation. In the presence of sufficient heat gains and controlled ventilation, the practical efficiency of MVHR

systems may be reduced by up to 20%, and their suitability should be established with a knowledge of indoor gains and weather conditions [49].

2.2.1.3 Air Tightness and Installation

Another important factor affecting MVHR systems' performance is the dwelling's fabric air tightness. A. Dadoo et al [103] reported a high dependency of energy savings possible with MHRV's on a dwelling's air tightness. Dwellings with several air leakage paths will not guarantee air passage through the equipment and recovered heat will be readily lost. C. Roulet et al [50] discovered the effect of this combined with internal leakage in MVHR systems to reduce heat recovery efficiencies to between 5% and 69%.

Banfill et al [104] conducted model tests on a 1930s solid wall dwelling to determine the point when improvements in dwelling air tightness saves enough energy to offset that consumed by using MVHR in the dwelling. They concluded that MVHR only provides an overall reduction in energy consumption when the dwelling's air permeability has been reduced to $3\text{m}^3/\text{m}^2\cdot\text{h}$ at 50Pa. The difficulty and complications in achieving this level of air tightness was highlighted. Natural ventilation delivered the same level of energy savings at permeability values around $10\text{m}^3/\text{m}^2\cdot\text{h}$ which is more easily achieved in performing air tightness retrofits in heritage dwellings. In their measurements taken from real life installations of MVHR systems, C. Roulet et al [50] showed negative energy savings in some installations. A conclusion of 'hard to recommend' was reached on small residential units studied and the main inhibitor to energy savings was identified as the fans, duct work and filter resistance of the system. Performance in cooling mode was also discussed and the role the fans play in increasing cooling loads in summer was highlighted.

When MVHRs are not installed, commissioned or maintained properly, imbalance in supply and extract air flow pressurizes the dwelling and worsen ventilation heat loss. White et al [89] tested the in situ performance of a MVHR system in a 1930s house and observed that it is problematic to install such systems into old dwellings. The complications inherent in installing and commissioning the systems lead to poor performance of the unit if not carried out to a high-quality.

They concluded that manufacturer stated efficiencies can differ significantly from in situ values due to this.

When positive or negative pressure is created in a dwelling, some volume of air enters passes through leaks in the dwelling rather than via the MVHR system. The installation of MVHRs operating in an unbalanced state in heritage dwellings can be detrimental to the building fabric. When warm humid air is driven through leaks in the building fabric, condensation can occur at cold points leading to moisture accumulation that may lead to progressive structural damage. This is moreso important in heritage dwellings where it can be difficult to make air tight compared to purpose built new dwellings. A heat recovery system should always operate in balanced way that do not pressurize the dwelling. When this is achieved, the level of airtightness at which savings can be made by utilizing ventilation heat recovery decreases significantly and the costs to achieve it accordingly [89].

In the report by Tim Sharpe et al [92] into MVHR systems in 237 domestic projects, only 16% of the homes analysed had their MVHR systems properly commissioned. In installing MVHR systems in dwellings, flexible ducting is usually employed to provide flexibility in the installation. The study found that between 40%-44% of MVHR systems utilizing flexible ducts had air flow performance as designed. They concluded that realizing energy savings from MVHR installation is a challenge for industry and the most prevalent problem is imbalance between supply and extract flows which leads to ventilation heat loss.

2.2.1.4 Air Quality

The main advantage identified for mechanical heat recovery units on which there has been a consensus is “good air quality” because filters are always incorporated in the system and air supply can be regulated. Air quality, though being of utmost health concern, is highly occupant dependent. In a study by T. Maier et al [105] to analyse occupant’s perception of thermal comfort according to the type of ventilation system installed, occupants scored the natural, extract only and MVHR systems equally on air quality. Existing real-life installations where MVHR have been applied in heritage dwellings and investigated have

continually revealed occupant's concerns that give no credit to improved air quality. The national social housing provider, Affinity Sutton, under their FutureFit programme in July 2013 [26] reported 78 issues related to ventilation in 55 properties when they retrofitted 150 dwellings with MVHRs. The issues ranged from noise to energy consumption, insufficient ventilation and damp.

In terms of primary energy, carbon emission and final cost to consumer, there's no clear advantage presented by MVHR systems over natural ventilation [106]. Additionally, the installation of these systems with the associated ductwork presents invasive modifications which are detrimental to the character of heritage dwellings.

2.2.2 Natural Ventilation; Windcatcher and Modelling Techniques

Natural ventilation is the provision of fresh replacement air to a room via natural air movement through the space. This is due to wind generated pressure differences, buoyancy stack flows, or a combination of both acting on openings in the building fabric. The variability of these factors makes natural ventilation more complicated and trickier to control. However, humans are more thermally tolerant in naturally ventilated spaces [88]. In a study by Ealiwa et al, 54% of occupants reported claimed to be satisfied and thermally neutral in naturally ventilated buildings compared to 15% in air-conditioned buildings [107].

During the times heritage dwellings were built, natural ventilation was the mode of choice for providing thermal comfort. With the advent of mechanical means of ventilation, development of this technique continued to decline. However, there has been a resurgence of interest in natural ventilation techniques, mainly due to environmental concerns and depletion of natural resources. The motivation to save cost is also clear. The operational energy consumed in naturally ventilating a dwelling is zero compared than that of a mechanical system. Heritage dwellings are particularly affected because they were not designed or built to be ventilated by mechanical means. Thus, many retrofit ventilation systems for heritage dwellings must be bespoke and this adds to costs and complexity.

Wind catchers are traditionally towers built into a building to capture and/or expel air at high altitudes. They have existed in their traditional form for years; especially in the middle east where they have been in use for summer cooling and ventilation of dwellings for around for 3000 years [108]. In its modern form, commercially available windcatchers are external roof-mounted units that supply and extract air from the attached space usually through short lengths of ducts. Many of these are largely unfit for heritage dwellings purposes because they do not preserve the character of the dwelling [109]; [110]. In terms of air flow arrangement, existing windcatchers are either air supply-only units, supply & extract units or rotating supply & extract units.

Supply-only unit as the name implies, only captures incident air flow at high altitude and directs it into the living space. The stale air extraction point is usually through windows or other openings built into the building fabric. In winter, to recover heat from outgoing air flow to pre-heat cold incoming air will necessitate the use of regenerative heat exchangers that transport the recovered heat from the supply point to the extraction point. This is quite complex and too obstructive to be a desired solution in heritage dwellings.

Supply and extract units have multiple air flow channels. If the channels are divided into 2 along a plane perpendicular to the direction of the prevailing wind, it effectively separates the channels into the air supply half facing the prevailing wind and the extract half facing the opposite direction. Air extraction occurs partly due to the low pressure generated in the wake region of the incident wind. At any instance, each half is connected to the living space; sometimes at different ends of the room to allow for proper air circulation and mixing before extraction. However, wind direction often changes, and each channel constantly alternate between being in supply and extract mode. This makes it problematic for integrated heat recovery. To address this problem, in some modern windcatchers, sails, such as can be found on wind vanes, have been incorporated into the design to constantly rotate the whole external part of windcatcher so the supply channel always faces the direction of the prevailing wind. BedZed [109] is

such a system. These designs are big, complex and unfit for use in heritage dwellings.

The techniques used in modelling and investigating natural ventilation systems like windcatchers can be broadly divided into three, namely Analytical and empirical methods, computational simulation and experimental methods.

Analytical and empirical methods are usually applied to simple geometries. Analytical models develop fundamental equations of fluid flow and heat exchange to build mathematical models for predicting performance in similar scenarios. Empirical models improve on this by incorporating measured values derived from experimentation. The simplification and approximations made in the development of many analytical and empirical largely restricts their applicability to other scenarios and can lead to large margins of error. In comparing experimental and empirical models for single sided natural ventilation for a room, Larsen et al [111] stated an uncertainty of 23% which represented an improvement on earlier expressions for air flow driven by thermal buoyancy and wind. In another simplified case of natural ventilation in a room with two openings on the same wall, the experimental and model-predicted values observed by Chu et al [112] differed by 13% on the average. When applied to more complex scenarios which are representative of real applications, the simplified interaction between temperatures, pressure variation from gusts, wind direction and intrinsic flow properties like turbulence become more prominent and can render these models totally inapplicable. Ai et al [113] observed this when they applied different analytical and empirical models to the prediction of ventilation rates for a multi-storey building, and made comparisons with CFD modelling. They concluded that none of the empirical models is applicable, mainly because they do not account for the difference in ventilation characteristics between different rooms in the same building.

The computational simulation techniques of natural ventilation system design mainly utilize Computational Fluid Dynamics (CFD) simulations. The validity of the CFD technique has been proven in many studies [114]; [115]; [116]; [117] with the main disadvantage being time consumed and computational resources

required. CFD investigations are usually coupled with experiments to validate the CFD model, then the model is used to study different scenarios that would have proven difficult or expensive to study experimentally. The accuracy of CFD in predicting natural ventilation flow is largely dependent on the resolution of flow scales, boundary conditions and assumptions made in the CFD model [118]. A. Fouquier et al [119] in 2013 reported an increase in the number of CFD applications in building ventilation development and described it as the most complete approach in building ventilation systems simulation.

Experimentation in natural ventilation system design can either be carried out on full or reduced scale basis. Full scale experimentation is mostly carried out on test buildings on site or in large climate chambers. The use of tracer gas techniques in this regard is well known [120]. Ventilation performance is assessed by measuring tracer gas concentration levels over time. Other measurements such as air velocity and direction are measured by anemometers and visual means like smoke and silk threads [120]. As imagined, in-situ experimentation can be difficult and expensive. Data resolution is also a problem, as it might be impractical to take measurements at many points within a large building. It is also impossible to control external factors and useful data always require experimentation over an extensive period. Many examples of full scale experiments exist in literature; Stathopoulou et al [121] conducted a full scale experiment to investigate air quality in two large athletic halls with different ventilation systems (natural and mechanical) in relation to outdoor pollution and meteorological conditions. Lee et al [122] also employed a similar technique to investigate air quality in 14 public places with mechanical ventilation systems in Hong Kong over 5 months. Assimakopoulos et al [123], Zhu et al [124], Halios et al [125], and Guo et al [126], all conducted full scaled experiments to investigate ventilation systems. Data obtained from full scale experiments, while not free from errors paint a very realistic picture of actual air flow and thermal interactions in a building, and are very useful for the validation of CFD models for further analysis of different scenarios during an investigation [127].

Small scale experiments are economical and controllable ways to carry out ventilation system investigations. This technique uses reduced scale versions of larger models to predict real life ventilation performance. Wind tunnel testing has seen wide application in this regard [115]; [128]; [129]; [130]; [131]; [132]; [133]; [134]; [135]; [136], and has been confirmed as a robust technique in natural ventilation system development; H. Montazeri et al [95], M. Esfeh et al [96] and others have used this method in the investigation of windcatchers. The ability of measurements taken from reduced scale models in a wind tunnel to predict flow characteristics in a full-size model is highly dependent on being able to replicate aspects of the real flow in the scaled experiment. Scaled models must be dynamically similar to the full-size model for it to properly replicate the fluid flow properties of a full-size model. Dynamic similarity can be established if the relationship between physical properties like the Reynolds number of both systems is the same. When other properties of the fluid play an important role in the fluid motion, other non-dimensional parameters like Grashof number, Prandtl number, etc. must also be matched in the scaled model.

2.3 Influence of Previous Works on Proposed Design

Natural ventilation excludes the electricity driven operation of MVHR. In many instances, implementing heat recovery for natural ventilation involves recovering heat from natural passive stack flows [137]. Different concepts have been investigated for this purpose in existing scientific literature.

In its simplest form, heat is recovered from passive stack extract flow with a recuperative plate heat exchanger and used to pre-heat the wind driven supply air. A. Mardiana et al [138] investigated this when they combined a 20-channels plate exchanger with a commercial windcatcher and tested it a laboratory. Recorded temperature change between air streams was up to $5.1^{\circ}C$ for incident air velocity of 3.1m/s. The pressure drop and consequent ventilation air flow performance across the entire system was not investigated. Practical problems with this kind of system include excessive pressure drop across the heat exchanger, and failure of the system due to the cooling down of extract air through the heat exchanger and the consequent loss of buoyancy [139]. M.

Simonetti et al [86] offered a solution to this issue when they developed and tested a low-pressure heat exchanger aimed at natural ventilation systems. They recorded heat exchanger effectiveness up to ~45%. They also observed a decreased thermal performance with increased channel size caused by thin thermal boundary layer unaffected by flow in the cross-sectional core. There is a dearth of research around plate heat exchangers in windcatcher applications; also noted by M. Simonetti et al [86]. A review of heat recovery ventilation systems by D. O'Connor et al [53] in 2016 listed only one.

Other scientists have investigated the use of decentralized regenerative heat exchanger arrangements [140]. An example is when the heat in the extract air is recovered in an air-to-liquid heat exchanger, and the liquid is pumped to open areas of the building facade to preheat the incoming ventilation air. K. Mahmud et al [141] investigated this technique in a novel system utilizing a pumped desiccant solution and recorded efficiencies up to 50%. C. Hviid et al [142] used water and recorded efficiencies of up to 75%. A. Haghghi et al [143] also investigated a windcatcher integrated with a solar adsorption system for summer applications and concluded that air temperature change of up to $20^{\circ}C$ is achievable. In practical applications, these arrangements are unsuitable for use in applications which require little or no intrusive modifications to buildings [60].

Centralized regenerative heat exchange in unitary windcatcher systems have also been investigated many times. Thermal wheel in a windcatcher was investigated by D. O'Connor et al [144]; [84] and found to be unsuitable for significant heat exchange between air streams.

Because many attempts at natural ventilation heat recovery in buildings depend on buoyancy forces being strong enough to overcome the heat exchanger resistance, heat pipes have found extensive application as a method of heat recovery [145]; [146]; [52]; [147]; [148]; [149]; [150]; [151]. J.K Calautit et al [128] observed up to 17% percent drop in air flow rate when they used CFD to simulate ventilation heat recovery using heat pipes in a windcatcher. Their results showed a 15k increase in air temperature. L. Shao et al [139]; [152] investigated different configurations of heat pipes for heat recovery in a passive stack and reported

heat exchange efficiencies of up to 50%. In their experiments, values of pressure loss were about 1Pa and pressure loss coefficient decreased with increasing air flow velocity, eventually staying constant above a critical Reynolds number while total pressure loss increased. S.B Riffat et al [153] emphasized the effect of velocity on the heat recovery effectiveness of heat pipes and observed that heat recovery effectiveness decreased with increasing air velocity. It was also unaffected by the heat pipe pattern of arrangement, and staggered heat pipe arrangement along the air flow path did not give better overall performance than straight in-line ones. This was further confirmed by B. Hughes et al [83] when they numerically studied the spacing between heat pipes in a ventilation heat recovery system and recorded no significant difference in heat transfer rates. S. Riffat et al [153] recommended a low velocity flow to recover more heat in these systems but also pointed out the effect of heavier cold outdoor air above the heat exchanger which can retard the flow and cause back-draughting. In a solar assisted chimney, G. Gan et al [154] observed a 60% drop in ventilation rate when they used heat pipes in heat recovery. Given that typical buoyancy flows in air ducts with heat pipes have velocities of between 0.5m/s - 1m/s, they recommended that wind forces should be harnessed to drive air extract flow.

Other studies in scientific literature have provided knowledge that can be combined in developing a fit for purpose natural ventilation system with heat recovery for heritage dwellings.

Mahmoudi Zarandi [155] analysed the thermal behaviour of 53 windcatcher designs to determine the optimum geometry for dwellings in Yazd, Iran. This provided much knowledge on the function of windcatchers. Khnai et al [156] in their experimental study into the air flow and thermal performance of windcatchers, observed that they are capable of generating air flow in the attached space at zero ambient wind velocity when humidity is introduced.

Troi et al [87] highlighted the many spatial issues associated with integrating ventilation systems in heritage dwellings and suggested the use of disused chimneys as ventilation shafts. Etheridge [157] also investigated the use of long ducts to temper the effect of wind pressure variation on flow performance in

natural ventilation systems. They concluded that the inertia offered by air contained in long chimney ducts of ventilation systems utilizing this technique can tolerate gust strength increases of 50%. The utilization of long duct-like channels as supply and exhaust terminals in natural ventilation systems was shown to be beneficial in the maintenance of flow configuration.

Sibille et al [158] suggested a means to utilize chimney ducts for the proposed system when they developed a coaxial duct for use in MVHR system to enable space saving installation in dwellings. This allowed for extract and supply air flow in an attached ventilation system to use minimal fabric modification during installation. They were able to come up with a geometry that allows for counter current coaxial air supply and extract flow with negligible short circuit.

The system proposed in this research, also incorporates features intended to create a venturi effect to drive extract flow from incident wind. Van Hoof et al [134] studied the venturi effect for driving natural ventilation extract flow and confirmed the feasibility of this technique with a recommendation to minimize guide vanes to reduce flow resistance. Y.Kim et al [38] investigated a ventilator utilising venturi principles and recorded ventilation flow rates which increased with increasing intake area.

H. Montazeri et al [36]; [159]; [160] conducted three studies on the properties of different number of openings in windcatchers. In their experimental study of the performance of a cylindrical wind catcher with different numbers of flow channels, they concluded that the induced air flow rate decreases by increasing the number of channels but sensitivity to incident wind angle decreased which makes the geometry with higher number of openings ideal for an omnidirectional application. Dehghani-sanij et al [161] also described cylindrical windcatchers as the most advanced with better performance than square ones when they developed a multi-directional retractable windcatcher. Other studies [162]; [36] have shown that increasing incident wind angle decreases the induced air flow rate in windcatchers. When a windcatcher is omnidirectional, it provides an inlet at low incident angle to incident wind at every direction.

Studies conducted by Dehghan et al [162] have also shown that curved inlet roof like that featured in the system proposed by the author is superior in inducing air flow better than sloped or square roofs.

The work of Sadeghi et al [163] in quantifying the pressure coefficient on different aspect ratios of spherical domes revealed that pressure difference between windward and leeward ends of domes increases as the aspect ratio (height/diameter) increases. Flow separation also becomes more prominent with a corresponding increase in the amount of suction pressure under the dome. Uematsu et al [164] studied the effect of this aspect ratio in comparison with the aspect ratio of a cylindrical geometry at the base and concluded that pressure coefficients are mainly affected by that of the dome. They also observed that high aspect ratio domes effect suction pressure at the leeward zones due to flow separation. Cheng et al [165] investigated the effects of Reynolds number on the aerodynamic characteristics of hemispherical dome and provided information on the flow separation for smooth and turbulent flow regimes to predict separation points and pressure properties. Sun et al [166] were able to develop a model for generating local pressure fluctuations on spherical domes which can be applied in design.

The proposed system combines properties that have not been found in a single unit across all system mentioned in extensive searches of published scientific literature by the author. These are as follows.

- It utilizes disused chimneys in heritage dwellings.
- Its installation requires no significant modification to building fabric.
- It is fixed with no moving or rotating part.
- It is omnidirectional; able to harvest incident wind from all directions.
- It is a supply and extract system; able to drive extract flow without indoor air buoyancy.
- It has a fixed supply and extract channel i.e. they do not alternate between extract and supply modes.
- It mimics the fundamental geometry of traditional chimney cowls making it suitable for heritage dwellings application.

- It incorporates a low Reynolds number plate heat exchanger combined into the unitary system.

The combination of these properties removes many of the limitations of available systems in making them fit for use in heritage dwellings. The proposed system will be investigated using an iterative procedure to develop the system components. Information on air flow and corresponding thermally will be presented and refinements will be introduced to address deficiencies and realize the desired function. This will provide new knowledge on the properties and generation of counter-current natural ventilation air flow in passive omnidirectional flue-like objects integrated with a plate heat exchanger.

3 AIMS AND OBJECTIVES

This research aims to develop and model in CFD, a prototype of the proposed natural ventilation heat recovery system for heritage dwellings (Figure 1-1) to provide new knowledge on functional design of geometry, operational characteristics and feasibility in terms of ventilation and heat recovery performance.

The objectives include:

- The development from first principles of a passive supply and extract windcatcher. Since the proposed system is aimed at existing heritage dwellings, this will take into consideration the aesthetics, ease of installation, and utilization of the system.
- CFD (Computational Fluid Dynamics) model development of the windcatcher in 3D to identify performance characteristics of geometry in terms of air flow. This will be an iterative process to identify deficiencies in performance and introduce refinements to realize the desired function. The performance of these subsequent refinements will be re-modelled in CFD to verify performance and provide knowledge on the properties and generation of counter-current natural ventilation air flow in passive omnidirectional flue-like objects.
- The development from first principles of a low Reynold's number heat exchanger suitable for naturally driven counter-current flows. This will also be an iterative process to identify an optimal combination of variables to realize the desired function in terms of pressure drop and heat recovery.
- Computational Fluid Dynamics (CFD) analysis of the heat exchanger in 3D to predict performance characteristics of its geometry in terms of air flow pressure drop and thermal effectiveness.

The author has surmised the qualitative performance of the proposed system based on scientific data available in literature. Its actual performance or that it functions in the desired manner cannot be guaranteed. It is intended that issues

in this respect will be highlighted in this research work and associated information made available.

The main risk identified with the windcatcher development concerns the air flow directions in the coaxial supply and extract channels under incident wind conditions without indoor air buoyancy. Unlike conventional windcatchers with extract channels directed away from the incident air direction, the extract channel proposed in this system is open to the incident wind and proposes to generate suction from it using the venturi effect. This is prone to incident wind entry and may not function as an extract channel.

Another risk associated with windcatcher development is the supply of adequate ventilation rate to the attached space at low wind speed. Other issues include flow short-circuit and suitability of overall geometry for heritage dwellings. These issues are mitigated by conducting a review of available scientific literature that address these different aspects of windcatcher design. Available information will enable the author to innovate to realize the desired function of the proposed system.

The task of developing heat exchangers generally involves the balancing of thermal performance with the pressure drop needed to general it. The coaxial flow geometry proposed in this research presents a peculiar problem of how to distribute flow into the alternate channels of the plate heat exchanger. This will be mitigated by studying available information on heat exchanger design and innovating to address this issue. Other issues of inadequate thermal or pressure drop performance will tackled by varying geometry and subsequent modelling in CFD.

The risks posed by the CFD development methodology is mainly the time needed to model the complex geometry of the proposed system. This will be addressed by simplification techniques like optimum meshing, geometry decomposition and use of symmetry planes commonly applied in CFD simulations.

4 METHODOLOGY

Under this heading, the scientific methods used in the development and investigation of the proposed ventilation system are discussed. These are mainly 3D modelling and Computational Fluid Dynamics (CFD) simulations. All CFD simulations were carried out with the wind incident on the windcatcher at 90° on the vertical plane and aligned with the symmetry of the windcatcher.

4.1 3D CAD

All parts were modelled in Autodesk Inventor 2013. Autodesk Inventor is computer aided design software capable of creating 3D digital models that can be used in the design and simulation of products. It uses a parametric based approach to create parts and assemblies [167]. Design intent is usually started with 2D drawings which are then defined by adding dimensions. Different constraints exist to define the relationships between geometric entities in the 2D drawings such as concentricity, tangent, etc. To create 3D models, different operations such as extrusion, sweep etc. is applied to the 2D drawing(s). Assemblies are created from different parts by adding constraints that define how those parts are related. The modelling approach uses an operation tree that details each operation carried out during the modelling process. This enables quick design optimization.

4.2 Computational Fluid Dynamics - CFD

In CFD, numerical method and computers are used to execute the calculations necessary to simulate and optimise the interaction between the different parts of a prototype and the surrounding fluid. CFD has been extensively used in the design and study of ventilation products and has been proven to be reliable when accurate models are utilized. The main disadvantage being the time consumed for computation. Y. Su et al [168] and L. Li et al [108] amongst others [85]; [169]; [170] used CFD in predicting the flow rates in windcatchers and recorded agreements with experimental values. W. Yaici et al [171] used CFD to investigate the performance of a ventilation heat recovery system and confirmed it as an effective means for carrying out detailed development of heat recovery

ventilators. As an alternative, O. Asfour et al [172] in their analysis of wind driven ventilation compared mathematically network models with CFD and confirmed CFD as a robust method of predicting air flow in ventilation systems.

Two commercially available Computational Fluid Dynamics (CFD) programs were used in this research, namely Autodesk CFD 2013 and Ansys FLUENT v14. The choice of using two CFD programs lends credibility to the results obtained and also facilitated a comparison of both software packages for natural ventilation research of the kind conducted in this thesis. Autodesk CFD is a relatively simpler and more user friendly software, and this facilitated rapid development from first principles.

Most of the initial simulations performed to investigate and fine-tune the windcatcher design were done with Autodesk CFD. Autodesk CFD has found numerous applications in scientific research and literature [173]; [174]; [175]; [176]. Burlacu et al. [177] used it to prove the feasibility of a heat recovery system for waste hot water from buildings. Burlacu et al. [178] used it to prove the feasibility of a heat exchanger for waste heat recovery from exhaust flue gases. Nalamwar et al. [179] used it to study ventilation flow pattern in buildings. Abdelhafez et al. [180] used it to optimize building energy consumption in Aswan city located in a hot desert climate. Elrady et al. [181] used it to study heritage dwellings to understand their climate-tempering characteristics and proffer applications to modern dwellings. Eldabosy et al. [182] used it to study thermal comfort in passive design of buildings and observed potential negative effect on indoor environment. Sowgath et al [183] used it to analyse the flow behaviour of gas and heat transfer in a biomass cooking stove. Simulation results matched experimental results with accuracies between 95%-97%. Xie et al. [184] also compared Autodesk CFD results with experimental measurements and recorded accuracies around 95% when they studied the thermal performance of smartphone chip and device skin under different component loading conditions. Albatayneh et al. [185] highlighted issues with it when used for long term simulation of internal building air temperature and proposed the addition of two types of external boundary conditions to mitigate. Gaurav et al. [186] also used it

in the modelling of thermal and fluid flow interactions with an electronic enclosure and recorded good agreement with empirical values.

Ansys FLUENT is a popular CFD program for academic research and in most hi-tech industries. Its robustness and accuracy in accurately predicting fluid flow parameters has been validated by numerous scientific research work [187]; [188]; [189]; [190]; [191]; [192]; [193]; [194]. Thus, the utilization of this code lends credibility to the work done in this research.

4.2.1 Assumptions

In using both CFD software programs, a general assumption of steady incompressible, turbulent fluid flow was made. The compressibility or incompressibility of a fluid depends on the relationship between its density and pressure. If density doesn't change with pressure, the flow is incompressible. Generally free flows moving at speeds less than Mach 0.3 such as those typical of ventilation systems, can be accurately assumed to be incompressible in CFD calculations [195]. Above Mach 0.3, compressibility becomes more prominent and should be taken into consideration to get accurate solutions in CFD calculations. Furthermore, fluctuating or agitated flows, like that experienced by the flow field as it makes contact with the system parts, are generally turbulent and is treated as such.

4.2.2 CFD Theory

The partial differential equations governing fluid flow and heat transfer include the continuity equation, the Navier-Stokes equations and the energy equation. The computational resource needed to simulate the turbulent scales in a fluid flow represented by these equations is prohibitive [116]; [196]. Hence, In CFD, an averaging procedure is applied to smooth the turbulent spectrum. The technique used in both Autodesk CFD 2013 and Ansys FLUENT v14, is Reynold's-averaging to give the Reynold's Averaged Navier-Stokes Equations (RANS) below [197].

$$\frac{\partial \rho}{\partial t} + \frac{\partial(\rho \bar{u})}{\partial x} + \frac{\partial(\rho \bar{v})}{\partial y} = 0 \quad (1)$$

$$\begin{aligned} & \frac{\partial(\rho\bar{u})}{\partial t} + \frac{\partial(\rho\bar{u}\bar{u})}{\partial x} + \frac{\partial(\rho\bar{v}\bar{u})}{\partial y} \quad (2) \\ = & -\frac{\partial\bar{p}}{\partial x} + \frac{\partial}{\partial x}\left(\mu\frac{\partial\bar{u}}{\partial x}\right) + \frac{\partial}{\partial y}\left(\mu\frac{\partial\bar{u}}{\partial y}\right) + \frac{\partial}{\partial x}\left[\mu\frac{\partial\bar{u}}{\partial x}\right] + \frac{\partial}{\partial y}\left[\mu\frac{\partial\bar{v}}{\partial x}\right] \\ & - \left[\frac{\partial(\rho\bar{u}\bar{u}')}{\partial x} + \frac{\partial(\rho\bar{v}\bar{u}')}{\partial y} \right] \end{aligned}$$

(3)

$$\begin{aligned} & \frac{\partial(\rho\bar{v})}{\partial t} + \frac{\partial(\rho\bar{u}\bar{v})}{\partial x} + \frac{\partial(\rho\bar{v}\bar{v})}{\partial y} \\ = & -\frac{\partial\bar{p}}{\partial y} + \frac{\partial}{\partial x}\left(\mu\frac{\partial\bar{v}}{\partial x}\right) + \frac{\partial}{\partial y}\left(\mu\frac{\partial\bar{v}}{\partial y}\right) + \frac{\partial}{\partial x}\left[\mu\frac{\partial\bar{u}}{\partial y}\right] + \frac{\partial}{\partial y}\left[\mu\frac{\partial\bar{v}}{\partial y}\right] \\ & - \left[\frac{\partial(\rho\bar{u}\bar{v}')}{\partial x} + \frac{\partial(\rho\bar{v}\bar{v}')}{\partial y} \right] \end{aligned}$$

$$\begin{aligned} & \frac{\partial(\rho\bar{T})}{\partial t} + \frac{\partial(\rho\bar{u}\bar{T})}{\partial x} + \frac{\partial(\rho\bar{v}\bar{T})}{\partial y} \quad (4) \\ = & \frac{\partial}{\partial x}\left(\frac{K}{C_p}\frac{\partial\bar{T}}{\partial x}\right) + \frac{\partial}{\partial y}\left(\frac{K}{C_p}\frac{\partial\bar{T}}{\partial y}\right) - \left[\frac{\partial(\rho\bar{u}\bar{T}')}{\partial x} + \frac{\partial(\rho\bar{v}\bar{T}')}{\partial y} \right] \end{aligned}$$

Where $\bar{u}, \bar{v}, \bar{p}$, and \bar{T} are mean values and $\bar{u}', \bar{v}', \bar{p}'$, and \bar{T}' are turbulent fluctuations. In three dimensions, these produce nine unknowns known as the Reynold's stress terms in the time-averaged momentum equations. For incompressible, two-dimensional equations of continuity and the non-conservative forms of momentum and energy, the time-averaged governing equations can be expressed as below [197].

$$\frac{\partial\bar{u}}{\partial x} + \frac{\partial\bar{v}}{\partial y} = 0 \quad (5)$$

$$\frac{\partial\bar{u}}{\partial t} + \frac{\partial(\bar{u}\bar{u})}{\partial x} + \frac{\partial(\bar{v}\bar{u})}{\partial y} \quad (6)$$

$$\begin{aligned}
&= -\frac{1}{\rho} \frac{\partial \bar{p}}{\partial x} + \frac{\partial}{\partial x} \left(v \frac{\partial \bar{u}}{\partial x} \right) + \frac{\partial}{\partial y} \left(v \frac{\partial \bar{u}}{\partial y} \right) + \frac{\partial}{\partial x} \left[v \frac{\partial \bar{u}}{\partial x} \right] + \frac{\partial}{\partial y} \left[v \frac{\partial \bar{v}}{\partial x} \right] \\
&\quad - \left[\frac{\partial(\overline{u'u'})}{\partial x} + \frac{\partial(\overline{u'v'})}{\partial y} \right] \\
&\quad \frac{\partial v}{\partial t} + \frac{\partial(\overline{uv})}{\partial x} + \frac{\partial(\overline{v\bar{v}})}{\partial y}
\end{aligned} \tag{7}$$

$$\begin{aligned}
&= -\frac{1}{\rho} \frac{\partial \bar{p}}{\partial y} + \frac{\partial}{\partial x} \left(v \frac{\partial \bar{v}}{\partial x} \right) + \frac{\partial}{\partial y} \left(v \frac{\partial \bar{v}}{\partial y} \right) + \frac{\partial}{\partial x} \left[v \frac{\partial \bar{u}}{\partial y} \right] + \frac{\partial}{\partial y} \left[v \frac{\partial \bar{v}}{\partial y} \right] \\
&\quad - \left[\frac{\partial(\overline{u'v'})}{\partial x} + \frac{\partial(\overline{v'v'})}{\partial y} \right] \\
&\quad \frac{\partial \bar{T}}{\partial t} + \frac{\partial(\overline{u\bar{T}})}{\partial x} + \frac{\partial(\overline{v\bar{T}})}{\partial y}
\end{aligned} \tag{8}$$

$$= \frac{\partial}{\partial x} \left(\frac{K}{\rho C_p} \frac{\partial \bar{T}}{\partial x} \right) + \frac{\partial}{\partial y} \left(\frac{K}{\rho C_p} \frac{\partial \bar{T}}{\partial y} \right) - \left[\frac{\partial(\overline{u'T'})}{\partial x} + \frac{\partial(\overline{v'T'})}{\partial y} \right]$$

Where $\left(\frac{K}{\rho C_p} \right)$ is the thermal diffusivity α of the fluid.

The Reynold's stress terms need to be modelled to close the RANS equations. Several models are available and are generally referred to as Turbulence RANS models [198]. The following sections describe the methods used in the two CFD programs used in this research, to determine approximate solutions to the fluid flow and heat transfer equations.

4.2.3 Turbulence Modelling

Turbulent flows are unsteady, irregular stochastic fluid motion in which transported quantities fluctuate in time and space. Enhanced mixing of these quantities results from the fluctuations and are unpredictable in detail. The small eddies in turbulent flows are more universal in structure while the large eddies are not. In turbulent flows, the large-scale eddies receive their energy from the mean flow. As the flow develops and the eddies stretch and interact, the energy is transferred to smaller eddies and eventually gets converted into internal energy

in the fluid due to viscous dissipation [199]. Modelling this individual fluid motion is prohibitive [196], so Reynold's averaging is employed and the resulting equation closed with a turbulence model. The resultant of this is that the turbulent flow contains only values of the mean flow variables. This is the widely-accepted method in academic research because it provides a good balance between accuracy and the computational resources required [116]; [196]; [200].

To close the RANS equation, the Boussinesq approximation method which defines an eddy viscosity and conductivity is used. This implies that the effect of turbulence is isotropic [201].

$$\begin{aligned} -\rho\overline{u'u'} &= 2\mu_t \frac{\partial \bar{u}}{\partial x} - \frac{2}{3}\rho k; & -\rho\overline{v'v'} &= 2\mu_t \frac{\partial \bar{v}}{\partial y} - \frac{2}{3}\rho k; & -\rho\overline{u'v'} \\ &= \mu_t \frac{\partial \bar{u}}{\partial x} - \left(\frac{\partial \bar{v}}{\partial x} + \frac{\partial \bar{u}}{\partial y} \right) \end{aligned} \quad (9)$$

where μ_t = turbulent eddy viscosity and k = turbulent kinetic energy

The turbulent momentum transport is assumed to be proportional to the mean gradients of velocity. Similarly, the turbulent transport of temperature is taken to be proportional to the gradient of the mean value of the transported quantity.

$$-\rho\overline{u'T'} = \Gamma_t \frac{\partial \bar{T}}{\partial x}; \quad -\rho\overline{v'T'} = \Gamma_t \frac{\partial \bar{T}}{\partial y} \quad (10)$$

Where Γ_t is the turbulent diffusivity.

Since the turbulent transport of momentum and heat is due to the same mechanisms of eddy mixing, the value of the turbulent viscosity can be taken to be close to that of turbulent viscosity μ_t . Based on the definition of the turbulent Prandtl number Pr_T , we obtain

$$Pr_T = \frac{\mu_t}{\Gamma_t} \quad (11)$$

Most CFD procedures assume that this ratio is constant and use values of Pr_T around unity [197].

By substituting the Reynolds stress expressions in equations (2), (3), (6), and (7) and the extra temperature transport terms in equations (4) and (8), removing the overbar that is by default indicating the average quantities, we obtain the incompressible form of the governing equations as below [197].

$$\frac{\partial u}{\partial x} + \frac{\partial v}{\partial y} = 0 \quad (12)$$

$$\frac{\partial u}{\partial t} + \frac{\partial(uu)}{\partial x} + \frac{\partial(vu)}{\partial y} \quad (13)$$

$$= -\frac{1\partial\bar{p}}{\rho\partial x} + \frac{\partial}{\partial x} \left[(v + v_T) \frac{\partial u}{\partial x} \right] + \frac{\partial}{\partial y} \left[(v + v_T) \frac{\partial u}{\partial y} \right] + \frac{\partial}{\partial x} \left[(v + v_T) \frac{\partial u}{\partial x} \right] \\ + \frac{\partial}{\partial y} \left[(v + v_T) \frac{\partial v}{\partial x} \right]$$

$$\frac{\partial v}{\partial t} + \frac{\partial(uv)}{\partial x} + \frac{\partial(vv)}{\partial y} \quad (14)$$

$$= -\frac{1\partial\bar{p}}{\rho\partial y} + \frac{\partial}{\partial x} \left[(v + v_T) \frac{\partial v}{\partial x} \right] + \frac{\partial}{\partial y} \left[(v + v_T) \frac{\partial v}{\partial y} \right] + \frac{\partial}{\partial x} \left[(v + v_T) \frac{\partial u}{\partial y} \right] \\ + \frac{\partial}{\partial y} \left[(v + v_T) \frac{\partial v}{\partial y} \right]$$

$$\frac{\partial T}{\partial t} + \frac{\partial(uT)}{\partial x} + \frac{\partial(vT)}{\partial y} \quad (15)$$

$$= \frac{\partial}{\partial x} \left[\left(\frac{v}{Pr} + \frac{v}{Pr_T} \right) \frac{\partial T}{\partial x} \right] + \frac{\partial}{\partial y} \left[\left(\frac{v}{Pr} + \frac{v}{Pr_T} \right) \frac{\partial T}{\partial y} \right]$$

A two-equation turbulence model is used to resolve the eddy viscosity and conductivity. Ansys Fluent v14 and Autodesk CFD 2013 provide different options to model turbulence. The models available include standard k- ϵ , SST k- ω , SST k- ω SAS, SST k- ω DES, etc. Of relevance to this research, are standard k- ϵ and Shear Stress Transport (SST) k- ω models.

The standard k- ϵ model has been used extensively to study the performance of windcatchers with good agreement with experimental flow values [36]; [168]; [202]; [203]; [204]; [205]; [206]; [207]; [208]; [209]; [210]. A sensitivity analysis of

turbulence models carried out by Nejat et al [203] when they evaluated a new design of windcatcher concluded that the $k-\epsilon$ model provided the best agreement with experimental data of flow values in the windcatcher channels. In their study, it showed a variance of +/-11% when compared to the $k-\epsilon$ RNG and $k-\epsilon$ realizable models.

While this model proves adequate for bulk values of flow quantities in windcatcher design, when windcatchers are integrated with heat exchangers, the accuracy of the flow field near the heat exchanger wall is particularly important for wall-to-fluid heat transfer calculations. The standard $k-\epsilon$ model is not always able to correctly simulate the fluid flow in the viscous sublayer of the boundary layer, except the turbulent sublayer where the velocity profiles shape is of a logarithmic type [211]; [212]; [213]; [214]. The SST $k-\omega$ allows for a better near wall treatment by combining the original Wilcox $k-\omega$ model for use near walls and the standard $k-\epsilon$ model away from walls using a blending function [215]. This combination presents a significant advantage over the $k-\epsilon$ model in predicting flow and heat transfer. However, the computational time needed for the SST $k-\omega$ model is higher due to the higher number of meshes needed to resolve the boundary layer. The SST $k-\omega$ model has been used extensively to study flow and heat transfer in heat exchangers with good agreement between experimental and numerical flow and heat transfer values [216]; [212]; [213]; [214]; [217]; [218]; [219]; [220]; [221]; [222].

4.2.3.1 Standard $k-\epsilon$ Turbulence Model

The default turbulence model in Autodesk CFD 2013 is the high Reynold's number $k-\epsilon$ model. This was used for quick development from initial concept in windcatcher simulations. It is the CFD industry work horse and is adequate for many simulations [223]; [224]; [225]; [226]. The $k-\epsilon$ model equations define the transport of the turbulent kinetic energy, k and the turbulent energy dissipation ϵ .

Values for k and ϵ must be specified at the domain inlets during simulation set up. At the inlet to the simulation domain, Autodesk CFD 2013 automatically computes the turbulence kinetic energy "k" based on the velocity distribution using the equation below[201].

Inlet Turbulence Kinetic Energy based on velocity distribution:

$$k = \frac{1}{2} [(IU)^2 + (IV)^2 + (IW)^2] \quad (16)$$

Where I

= Turbulence Intensity and U, V and W are fluctuating components of velocity

The default value of turbulence intensity is 5% at domain inlets.

The value for the turbulent energy dissipation at domain inlets is calculated automatically using the equation below. In the equation, the length scale is automatically computed by the software based on the size of the model.

$$\varepsilon = C_{\mu} \frac{k^{1.5}}{\delta_s} \quad (17)$$

Where δ_s = Length Scale and C_{μ} = Empirical Constant

4.2.3.2 SST $k - \omega$ Model

The Shear Stress Transport (SST) $k - \omega$ turbulence model was used in Ansys Fluent v14 and Autodesk CFD for simulations of final prototypes of the heat exchanger and windcatcher. Its model equations define the transport of the turbulent kinetic energy k and the specific dissipation rate ω . ω is effectively the ratio of k to ε . The SST $k - \omega$ combines the good performance of the $k - \varepsilon$ model in the free-stream region of fluid flow with that of a modified Low Reynold's number $k - \omega$ model. A blending function is used which activates each turbulence model in the respective regions. Hence, the SST $k - \omega$ is accurate in more simulation scenarios and presents a significant advantage over the $k - \varepsilon$ model in predicting flow separation and heat transfer [211]. The prototype windcatcher is cylindrical and presents an obstructive element to the normal wind flow, Therefore, flow separation is expected in the flow fields within it, and is expected to impact on its ventilation performance. The transport equations for K and ω are given below [211].

$$\frac{\partial}{\partial t}(\rho k) + \frac{\partial}{\partial x_i}(\rho k u_i) = \frac{\partial}{\partial x_j} \left(\Gamma_k \frac{\partial k}{\partial x_j} \right) + G_k - Y_k + S_k \quad (18)$$

$$\frac{\partial}{\partial t}(\rho \omega) + \frac{\partial}{\partial x_j}(\rho k \omega) = \frac{\partial}{\partial x_j} \left(\Gamma_\omega \frac{\partial \omega}{\partial x_j} \right) + G_\omega - Y_\omega + D_\omega + S_\omega \quad (19)$$

Where G_k = the production of turbulent kinetic energy and

G_ω = generation of ω

Γ_k and Γ_ω are the diffusivity of k and ω respectively and Y_k

and Y_ω are the turbulent dissipation of k and ω

D_ω is the cross diffusion term and S_k and S_ω are user defined source terms

4.2.4 Near Wall Treatment

Near wall flow profile are often predictable [227]. Hence, functions can be used to represent the velocity profile in these areas instead of resolving them with fine meshes. This approach reduces the computational resources needed. Wall functions have limitations. In cases where there is flow separation, the wall functions cannot accurately predict the boundary layer profile because the universal near-wall flow profile is not valid when there's a separated flow. Hence, the flow must be resolved with boundary layer meshes (prism elements) [227]; [228].

4.2.4.1 Autodesk CFD

Autodesk CFD 2013 provides a mesh enhancement function to define boundary layer elements in terms of total height, number of elements and gradation. Wall functions are used with high Reynolds number turbulence models like the $k - \varepsilon$ model to treat the near wall regions. At the walls, the fluid flow is modelled by enforcing the law of the wall.

The law of the wall can be written as [201]:

$$U^+ = \frac{1}{k} \log y^+ + B \quad (20)$$

Where B and K are dimensionless constants.

U^+ and y^+ are defined as:

$$U^+ = \frac{U_t}{\sqrt{\frac{\tau_w}{\rho}}} \quad (21)$$

$$y^+ = \frac{\delta \sqrt{\frac{\tau_w}{\rho}}}{\nu} \quad (22)$$

Where U^+ = Velocity Tangent to the wall,
 τ_w = Wall shear stress, ρ = Density, δ = Distance from Wall

and ν = Kinematic viscosity

Autodesk CFD 2013 uses an intelligent scalable wall formulation which adjusts the wall effective viscosity based on the velocity and fluid properties next to the wall to enforce the Law of the Wall. This performs better for the range of y^+ values encountered in near wall flow simulations [229].

When using the SST $k - \omega$ model, especially in flows where separation is expected, it is recommended to resolve the boundary flow with at least 10 prism element layers. This model does not utilise the wall function in Autodesk CFD 2013.

4.2.4.2 Ansys Fluent

Ansys Fluent v14 offers y^+ -independent enhanced formulation for treating the near wall region in wall-bounded turbulent flows. Despite this, good resolution of the boundary layer with prism mesh layers is essential for getting highly accurate solutions for the near wall region [228]; especially in heat transfer simulations. Ansys recommends between 10-20 layers with 15 or more nodes covering the boundary flow, to accurately resolve a boundary flow. The software automatically employs the two-layer model from earlier versions of the software, the law of the wall, or a blending function of the two. This approach is more forgiving in terms of y^+ , but a y^+ value less or equal to 1 is still needed if the laminar sub-layer needs to be captured. Values of y^+ need to be checked after the simulation to be within these values.

The inner region of the boundary layer is known as the law of the wall zone. This zone is divided into a viscous lower layer and, a turbulent upper layer where the

non-dimensional velocity U^+ varies in a log-linear manner. y^+ is the normal distance from the solid boundary to the first grid point and is assumed that $y^+ \equiv U^+$. Generally, within the boundary layer, CFD codes start to apply the log-linear variation to U^+ at the value of y^+ specified. Hence, a very fine boundary mesh where the first grid point is deep within the *real* viscous layer will force the code to apply the log-linear variation too close to the wall and result in an over-prediction of the near wall velocity. On the other hand, a high y^+ value will place the first grid point well near the centre of the flow and result in an under-prediction. In order to estimate the normal distance to the first grid point for a y^+ value, the Schlichting skin-friction correlation was used as shown below.

$$\begin{aligned} & \text{Turbulent Boundary Layer Skin friction } C_f \\ & = [2\log_{10}(Re_x) - 0.65]^{-2.3} \text{ (For values of } Re_x < 10^9) \end{aligned}$$

$$\text{Wall Shear Stress } \tau_\omega = C_f \frac{1}{2} \rho U^2$$

$$\text{Friction Velocity } U_* = \sqrt{\frac{\tau_\omega}{\rho}}$$

$$\text{Distance to first grid point in meters} = \frac{\mu y^+}{\rho U_*}$$

$$\text{Where } \mu = \text{Dynamic viscosity in } \frac{kg}{ms},$$

$$\rho = \text{Density in } \frac{kg}{m^3} \text{ and } U = \text{velocity in } m/s$$

It is recommended to check maximum turbulent viscosity at the walls after initial solutions are obtained in simulations. This gives an indication of the boundary layer as its thickness is twice the thickness of the maximum turbulent viscosity. It is important not to confine boundary layer growth. Hence, the Author made sure the prism layers extended beyond the boundary layer in all simulation cases.

The first cell height was estimated to achieve the desired y^+ value from calculations of the Reynold's number, wall shear stress and friction velocity skin friction using the Schlichting skin-friction correlation. Online calculators utilizing

this technique are common and available here: [230]. This was used in specifying the first cell height for the creation of inflation layers in the Ansys software. The maximum, minimum and face average of y^+ values were checked after solution convergence to verify they are approximately 1. This is achieved by generating reports of surface integrals for the windcatcher and heat exchanger.

4.2.5 Meshing

Meshing is required to discretize the flow region into small domains within which the flow governing equations can be applied and approximated over the larger flow domain. Meshes can be classified into structured mesh, unstructured mesh or a hybrid of both. Structured meshes have regular connectivity and are composed of 3D hexahedral elements in 3D simulations. The structure of these grid makes it easy to calculate the neighbouring cell indices without needing to store them. Unstructured mesh use tetrahedral elements to discretize the solution domain. They are characterized by irregular connectivity and relationship indices with neighbouring cells have to be stored. This requires a larger amount of computational memory compared to structured meshes. Hybrid meshing seek to efficiently combine structured and unstructured meshes, whereby complex geometries within a solution domain are meshed with unstructured grids and simpler ones with structured grids.

The choice between structured and unstructured grids is a balance between setup time, computational expense and accuracy. The alignment of structured meshes along flow direction aids convergence and they are easier to implement on simple geometries. On complex geometries within a larger simple domain such as in this research work, large differences are required between mesh scales in the larger wind domain and the smaller wind catcher geometry. Unstructured meshes allows resolution refinement over the complex geometry without significantly increasing the cell count. Structured meshes tend to result in significantly high cell count when used in the same scenario. When meshes are well refined, the solution error and numerical diffusion are minimized. Solutions are also more accurate when meshes are aligned with flow. In simple flows, such as in pipes, this is more readily achieved with structured meshes. However, in

complex flow scenarios, flow with mesh alignment might not occur and resolution of the geometry becomes more important thereby necessitating an unstructured mesh.

The mesh must be fine enough to capture the variations in fluid behaviour and satisfy CFD numerical requirements [231]. A combination of techniques and settings to avoid numerical diffusion from large cell size gradients were implemented at the geometry construction stage to assist meshing.

In many simulation scenarios, the CAD model was divided up. As an example, for the wind tunnel simulation of the windcatcher, the geometry was divided into 3 sections. The first area (Area 1) which represents the bulk of the model covers areas within the wind tunnel where the presence of the model is not expected to generate relatively high gradients in the fluid flow properties. This area was meshed with the biggest size of elements. Area 2 surrounds the windcatcher and chimney to cover the impact region before the windcatcher and the wake region behind the windcatcher. A finer element size was used for this region to ease the accurate resolution of flow properties variation in these areas. Area 3 represents the fluid region within the windcatcher. High level of turbulence and flow separation coupled with high gradients in the flow properties of pressure and velocity is expected within the windcatcher. Hence, this area was meshed with the finest element size.

It is essential to capture the boundary flow accurately with the mesh. To this end, Inflation prism layers were used to provide a good resolution of boundary layer flow within the flow field [228]. They were generated at all solid boundaries of the model and chimney, including the tunnel floor.

When the quantities of interest in a CFD simulation has converged and reached a steady solution, to be accurate, they need not to vary with mesh resolution [232]. To check this phenomenon, a mesh independency study was conducted for each simulation. The meshes were repeatedly refined after each converged solution until the changes in solutions between subsequent runs are negligible.

4.2.5.1 Autodesk CFD Meshing

For simulations performed on Autodesk CFD 2013, the automatic mesh sizing function was used to define an optimum tetrahedral mesh-size with 10 wall layers based on the curvature of the model geometry.

There are numerous other options to refine and optimise the mesh by reducing resolution and distribution in areas where flow variables are expected to exhibit high gradients. Good representation of the geometry is necessary to obtain high fidelity solutions and accurately represent areas where high gradients are present. High quality, high density meshes generally contribute significantly to accuracy of solutions. The initial run on the default coarse mesh is not highly accurate but it reveals areas where higher mesh density is required. Accuracy is sufficient when further mesh refinements doesn't result in significantly different values for a critical results like flow velocity and pressure. Autodesk CFD 2013 incorporates an adaptive meshing feature which helps to fine tune the mesh after successive runs. The mesh is refined based on gradients of flow parameters like pressure and velocity (and temperature in heat transfer simulation) after each successive complete run. This results in an efficient mesh, finer in areas with high gradients and coarser in other places. At the end of each run, the software reports the mesh independence status. On the average, each final mesh in this study attained a 95% mesh independency on pressure and velocity results.

4.2.5.2 Ansys Meshing

Ansys Fluent v14 meshing provides more options for meshing models. Simulations performed in this study utilised tetrahedral meshes. These were generated with a high level of smoothing using the meshing software's inbuilt size function to resolve curved geometry and areas within close proximity. The number of cells across gaps was chosen to be 5 and transition between mesh sizes were kept slow with a growth rate of 1.2.

Surface inflation prism layers were generated based on the first cell aspect ratio. This option was chosen to generate 10 layers with cell aspect ratio of 5 and growth rate of 1.2 to avoid a large volumetric gradient at the interface between the prismatic inflation layers and main mesh elements. By using enhanced wall

treatment option in Ansys Fluent v14, the simulation solution becomes insensitive to the value of y^+ and places more emphasis on accurately resolving the boundary layers with at least 10 layers and maintaining $y^+ \sim 1$ for heat transfer calculations. y^+ is the normal distance from the solid boundary to the first grid point.

The equations of flow being solved assume the cells in the mesh are relatively ideal in terms of angles and form. Therefore, the quality of the mesh must be examined to enable the computation to converge successfully. Two measures of mesh element quality available in Ansys Fluent v14 meshing were considered in this study i.e. skewness and orthogonal quality.

Skewness reveals how close to ideal a cell in the mesh is. Hence a perfect cell has a skewness of 0 and a degenerate one has a skewness value of 1. For all meshes, an average skewness of 0.1 was maintained.

Orthogonal quality is a measure of the deviation between the direct connection of the neighbouring element centre to the median line of that side face. A value of 1 denotes a perfect orthogonal quality which is reached when equal sided tetrahedrons with uniform sizes are present. All meshes were generated with an average orthogonal quality of 0.97

In contrast to Autodesk CFD 2013, when performing mesh independence studies, mesh adaptation is not only automatic and can be performed manually by marking cells for refinement. The mesh was adapted based on scaled gradients of velocity in the entire domain after each successive run. All regions with gradients higher than 10% of the maximum were marked and adapted until the simulation solution became mesh independent.

4.2.6 Discretization

In CFD, the partial differential equations governing fluid flow and heat transfer must be discretized or converted into a set of non-continuous equations suitable for solving on a computer.

Discretization methods refer to the methods used in interpolating the flow variables from the cell centroid where they are calculated, to the cell faces where values are needed to compute fluxes and gradients. This is generally achieved using an upwind scheme where the face values of variables are gotten from magnitudes in the cell upstream in the normal flow direction.

4.2.6.1 Autodesk CFD

In Autodesk Simulation CFD 2013, the finite element method is used to reduce the governing partial differential equations (pdes) to a set of algebraic equations. In this method, the dependent variables are represented by polynomial shape functions over a small area or volume (element). These representations are substituted into the governing pdes and then the weighted integral of these equations over the element is taken where the weight function is chosen to be the same as the shape function. The result is a set of algebraic equations for the dependent variable at the nodes on every element.

The described formulation is used on the diffusion and source terms in the governing equations. However, for numerical stability, the advection terms are treated with upwind methods along with the weighted integral method. Five upwind methods of varying orders are available in Autodesk CFD 2013. The “ADV 1: Monotone streamline upwind (1<order<2)” method was selected for its numerical stability [201]. Numerical stability refers to how a malformed input affects the execution of an algorithm. In a numerically stable algorithm, errors in the input lessen in significance as the algorithm executes, having little effect on the final output. On the other hand, in a numerically unstable algorithm, errors in the input cause a considerably larger error in the final output. The selected method is also recommended by Autodesk for geometries with many internal flow obstructions such as that present in the windcatcher model [201].

4.2.6.2 Ansys Fluent

Ansys Fluent v14 also allows different upwind schemes to interpolate advection terms in the flow equations being solved. In the simulations carried out here, second order discretization scheme was used. This is essential when using tetrahedral meshes or when flow is not aligned with grid. Generally, higher order

discretization schemes ensure the solution is less diffusive. When the flow is aligned with the grid as can be found in a laminar flow simulation meshed with structured hexahedral elements, first-order upwind discretization may be acceptable. When the flow is not aligned with the grid (i.e., when it crosses the grid lines obliquely), first-order convective discretization increases the numerical discretization error (numerical diffusion) [233]. For triangular and tetrahedral grids, since the flow is never aligned with the grid, accurate results are generally obtained by using the second-order discretization. For structured grids, better results are also obtainable by using the second-order discretization, especially for complex flows [234].

Gradients of solutions variables are required to evaluate diffusive fluxes, velocity derivatives and for higher order discretization schemes; to obtain values of a scalar at cell faces. The Green Gauss node-based method was generally selected for Ansys Fluent v14 simulations. Here the value at each node of a cell are taken from a weighted average of the surrounding cell and the node values are averaged to obtain the face values before the Green Gauss theorem is applied. This scheme reconstructs exact values of a linear function at a node from surrounding cell-centred values on unstructured meshes by solving a constrained minimization problem, preserving a second-order spatial accuracy [235]. This is more accurate and recommended by Ansys for unstructured meshes [233]. In fluent it is good practice to start out a simulation with a rough solution to provide some initialisation of the numerical solution before proceeding on to higher order more accurate discretization solutions to prevent convergence stalling. Hence 150 iterations were done in all cases with first order schemes before switching to second order.

4.2.7 Solver Settings

Discretization produces matrix-form algebraic equations at the nodes. These must be solved in an iterative manner using a matrix solver. Algorithms are used in implementing this solver and solving the matrix. In using an algorithm, the missing pressure equation in the discretized equations must be determined.

Autodesk CFD 2013 implements an iterative matrix solver i.e. the iterative conjugate gradient solver using a segregated velocity-pressure algorithm where the variables are calculated separately in a sequence. A variant of the SIMPLE-R pressure-velocity coupling algorithm [201] is used to determine the pressure equation in the discretized equations. The iterative solving procedure produces residual norms which should get smaller as the solution converges.

Ansys Fluent v14 presents two solvers options i.e. the density based solver and Pressure Based Solver (PBS). The PBS was chosen for all simulations. The PBS takes its name from the way mass continuity is achieved in the numerical solution. The numerical algorithms couple pressure and velocity and express the continuity equation in terms of a pressure correction. The pressure correction equation is then solved and used to correct the velocity field obtained by the solutions to the momentum equations to ensure continuity is satisfied. There are two versions i.e. the segregated and the coupled versions. In the segregated solver, the momentum equations are solved in turn and then the continuity pressure equation. In the coupled version, all the equations are solved simultaneously. For both, every other present equation of energy or turbulence is solved in a sequential manner afterwards. The PBS coupled solver yields superior performance in low-speed incompressible flow calculation especially in cases where there's a strong coupling between pressure and velocity [236]. It also generally converges with less iteration [236]. Hence, it was used in all Ansys Fluent v14 Simulations.

CFD requires all variables be given an initial value before iteration can begin. A realistic initial guess improves solution stability and accelerates convergence. Autodesk CFD 2013 offers an Auto-Start-up function that provides initial guesses for the simulation by running 10 iterations using a constant eddy viscosity model, before the selected turbulence model is started. This function is 'on' by default. In Ansys Fluent v14 Hybrid initialization was utilized. It solves Laplace's equation to approximate the velocity and flow fields. All other variables are patched based on domain averaged values.

4.2.8 Convergence

In use, any CFD solver must perform enough iterations to achieve a converged solution. At convergence,

- a. All discrete conservation equations (momentum, energy etc.) are obeyed in all cells to a specified tolerance in the decrease of residuals, or the solution stops changing.
- b. overall mass, momentum energy and scalar balances are achieved
- c. target quantities reach constant values

Autodesk CFD 2013 uses an Intelligent Solution Control for convergence control. This was enabled and set at the default level. Intelligent Solution Control function uses control theory to examine the trends of each degree of freedom and automatically adjusts the convergence controls and time step size to attain a solution without any manual intervention. Automatic Convergence Assessment works out when the solution stops changing and stops the calculation. This considers the value of 4 different parameters. Instantaneous Convergence Slope evaluates the slopes of the convergence quantities from one iteration to the next. Time Averaged Convergence Slope does the same over several iterations using the mean values to satisfy a value of a set tolerance. The third criterion, Time Averaged Convergence Concavity, takes the derivative of the maximum time averaged convergence slope to measure the concavity of solution variables; when the concavity falls below the set value, this criterion is satisfied. Lastly, Field Variable Fluctuations measures the standard deviation of variables about a mean value to determine convergence. In the wind catcher simulations carried out in this research with Autodesk CFD, solution variables were deemed to be converged when fluctuations are generally below $1e-05$ [237].

In Ansys v14 CFD, solution monitors were set to monitor the integrated quantities of heat transfer coefficient and flow velocity at the heat exchanger surface and flow inlets and outlets. The values recorded at these points were used to judge the convergence state of the solution in addition to absolute values of scaled residuals of the velocity vectors, continuity, energy and turbulence parameters

i.e. the solution was thought to have converged when the solution remained unchanged, the solution residuals were below a 10^{-3} tolerance, and for energy, below 10^{-6} . Mass balance between inflow and outflow was specified to a tolerance of $10e-4$.

4.2.9 Post Processing

Post processing of simulation results from Autodesk CFD is carried out from the “Result” tab on the software. Summary planes were created at surfaces of interest from which mass-weighted average values of pressure, temperature and velocity were calculated using the “Bulk calculator” function. Velocity vectors can also be displayed and contoured with other variables on surfaces and planes. The software has a plot function that allows simulation variables to be plotted along planes and surfaces by manually selecting points on the model. Particle traces are conceptually similar to an injected dye stream in the flow domain. They are used to visualize flow movement and Autodesk CFD allows for different types of traces to reflect different flow variables in its contouring along the flow path. Traces can be seeded from existing surfaces or planes created in the model. Individual traces can be created by selecting points on the model, or patterns created by using the pattern function. It also has functions to display iso-surfaces which can be contoured with other variables and vectors. An iso surface is a surface of constant value. The iso-surface shape indicates everywhere in the model that has the same specified value of a variable. The iso-volume improves on this by showing the volume of a model that falls within a specified range of a result quantity value. These functions were used on each model to create the corresponding features on planes and surfaces of interest. Then the summaries are used in the “Decision Centre” to visually compare results from multiple scenarios for the same feature.

The Autodesk CFD Decision Centre tab is the environment for comparing design alternatives. Dynamic images were also created from this tab which can be viewed and manipulated using Autodesk CFD viewer software for creating visualizations. The Autodesk CFD Viewer reads Dynamic Images which contain the model geometry, results, display attributes, and animation settings. They are

fully navigable unlike static images, and allow direct interaction for a deeper understanding of the results.

Ansys Fluent also offers all the post processing feature described for Autodesk CFD. A similar process was followed to visualize simulation results. Contours and vectors were created on planes and surfaces of interest and features like vector, contours and pathlines were added to visualize flow and thermal properties in the simulation domain. Results of variables from surface and planes were taken as mass-weighted averages of the variables. Post processing was completed in Ansys CFD-Post. CFD-Post enables easy visualization and quantitative analysis of CFD simulation results from Ansys Fluent.

4.2.10 Validation

Windcatchers in literature are intended as energy efficient ventilation units for new buildings, or purpose built structures for summer cooling of vernacular buildings in arid regions [35]. It follows from these purposes that the main aim in windcatcher development has largely been in optimizing the induced air flow into these units. Numerical and experimental works in scientific literature has shown that while cylindrical windcatchers perform adequately, square sided windcatchers generally induce more incident air flow compared to other geometries [36]; [35]; [238]. This is due to the sharp edges of the square geometry which causes a big region of flow separation when wind is incident on it. This results in a large pressure difference across the unit that drives air flow. Thus, it is no surprise that most available works in literature are on developing square-sided windcatchers [35]. The unique requirements of the proposed system in this research to be omnidirectional and suitable for integration into disused chimneys of heritage dwellings has informed the trade-off between these requirements and the enhanced flow performance of square sided windcatchers. There is a dearth of research around cylindrical windcatchers.

In validating the windcatcher CFD results in this study, reference is made to qualitative results from the experimental work conducted by Montazeri [36] when he investigated the flow performance of 5 cylindrical windcatchers with different numbers of openings to quantify the amount of supply air flow induced and

determine the effect of incident wind angles on the induced air flow. In his experiment, scaled versions of the windcatchers were studied in a uniform flow wind tunnel at a wind speed of 19m/s to replicate full scale Reynold's number. Induced air flow through the windcatcher channels were measured with multiple small pitot and static tubes installed at the top and bottom of the channels to measure inflow and outflow. The air flow decreased as the number of channels increased, and outflow was observed from leeward end windcatcher channels. His work made no observation of the flow path of this outflow to reveal whether it is short-circuited flow which recirculates directly into the extract channels at the base of windcatcher when the attached room is air-tight. However, he identified the windcatcher channels in supply and extract modes for each channel number configuration. He also presented data on the sensitivity of the number of windcatcher channels to incident wind angle and concluded that the sensitivity decreases as the number of channels increases, with the 12 channels windcatcher displaying a variance of approximately 5%.

Qualitative results from heat exchanger results are compared with experimental work carried out by Simonetti et al [86] on a 1m long low Reynold's flow multi-channel plate heat exchanger intended for natural ventilation applications in buildings. Thermal and pressure drop performance was investigated for a 5⁰C outdoor temperature and 20⁰C indoor temperature entering on either side of the heat exchanger in a counter flow configuration at a volume flow rate of 300m³/hr. They also investigated the effect of different turbulators to determine an optimal geometry to enhance heat transfer in the device without causing excessive pressure drop. In their numerical simulations the hot air stream reduced to an average of 14⁰C while the cold air stream gained an average of 5⁰C with average pressure drop of 5.5 Pa. Heat exchanger effectiveness was an average of 38%.

They followed with an experimental setup to investigate the system performance. The heat exchanger was coupled to two air handling units equipped with heating elements on either side and tested at volume flow rates between 100m³/hr and 500m³/hr. Pressure drop increased from approximately 1Pa to 19 Pa as flow rate increased. Heat exchanger efficiency calculated at 200m³/hr, 300m³/hr,

$400\text{m}^3/\text{hr}$ and $470\text{m}^3/\text{hr}$ decreased from 45% to 42% with a $\pm 5\%$ error band which gives good agreement with their CFD results at $300\text{m}^3/\text{hr}$. They concluded that the low velocity in these type of heat exchangers achieves higher outflow temperature differences for the fluid streams, but lower amounts of energy is exchanged. The size of the fluid passage cross-sections also affects the thermal performance. As the cross-section size increases, the thermal performance reduces due to the fluid flow at the core being shielded from the effect of the thermal boundary layer at the walls.

5 WINDCATCHER DEVELOPMENT

The proposed windcatcher was developed by an iterative process whereby its characteristic constraints are firstly defined both in performance and geometry, then innovative initial concepts are developed from first principles within these constraints. The initial concepts are put through a series of iterative prototyping and rapid analysis with Autodesk CFD 2013 to arrive at a Base Model that largely satisfies defined basic requirements. This Base Model is then further analysed using Ansys Fluent v14 to understand and present information on fluid flow interactions in the system. Afterwards, refinements are carried out to overcome identified deficiencies in performance before a final prototype is presented and simulated in Ansys Fluent. The following headings present this development process for the windcatcher.

5.1 Theory and Concept

While design inspirations can be taken from the pros and cons of existing types of windcatchers, to effectively cater to the retrofit needs common to heritage dwellings, the characteristics of the windcatcher component of the heat recovery system proposed in this research need to satisfy the following functional requirements.

- a. It must be a supply and extract unit i.e. the supply of ventilation air to the connected living space and its extract from same, must be accomplished within the physical dimensions of the single windcatcher.
- b. The windcatcher must be able to do its air supply and extract function in varying wind speed conditions and constantly changing wind directions. This necessitates an omnidirectional windcatcher that also has a fixed air supply and extract flow path i.e. there must be dedicated supply and extract flow channels without the possibility of them alternating between supply and extract modes. This is to enable the addition of a heat exchanger with distinct hot and cold fluid paths.
- c. It must respect the aesthetic and historic value of heritage dwelling in user expectations and space requirement. This is to preserve the character of

- the building and facilitate easy installation that does not require extensive building fabric modifications. It is also crucial to commercial success; gaining housing authority approval and easy uptake of the system. Thus, it needs to closely mimic the appearance of chimney pots in appearance, fundamental form and size; since this is the feature it is meant to replace.
- d. Though chimney tops are not easily accessible locations, regular maintenance of any component fitted atop a chimney will require working at height. Working at height is major cause of fatalities and injuries. The work at height regulations 2005 [239] discourages it and places an onus on designers to avoid it where reasonably practicable. Hence a need has been established to have, as close as possible, a zero-maintenance windcatcher to reduce maintenance to the barest minimum, eliminate mechanical breakdown and consequently reduce noise. To this end, it has been concluded that the windcatcher should contain minimal moving parts.
 - e. Also, the windcatcher needs to supply air to, and extract air from, the connected living space at an acceptable flow rate for ventilation.

In a room containing temperature stratified air, air movement out of an opening located at high level is largely influenced by the force of buoyancy generated above the neutral level in the room. The neutral level is the level at which the pressure inside the room and that of the ambient are equal. Generally, air will naturally flow out of the room through openings above the neutral level and into the room via openings below the neutral level. When the room air is not stratified, the neutral level is erased and buoyancy force is largely diminished in its ability to drive air movement. The room air is said to be well mixed in this scenario [240]. Within the living space it is desirable to keep the temperature relatively constant by providing a well-mixed room air condition or ensuring the living space remains below the neutral layer. The latter being largely applicable to spaces with high ceilings [240].

Supplying warm air at high level in a room does little to upset natural temperature stratification. However, warm ventilation air supply at low level mixes up the denser low level cold air and brings it close to the

temperature of higher air layers. Consequently, the available buoyancy force to drive natural extract through an opening at height is reduced [240]. This is the case with the proposed system because warm air will be supplied at room level through a disused chimney opening. Therefore, the flow needs to be largely driven by other natural means. Apart from the heat in the room air, only the external wind brings energy into the system interactions. Hence, the windcatcher must be able to harness incident wind energy to drive both the supply and extract flows.

The cooling down of the extract air through the heat exchanger and consequent loss of buoyancy also necessitates air extraction to be aided by the windcatcher.

To arrive at a Base Model for the windcatcher, the requirements stated under points a, b, c and d above were prioritised. The main challenge was achieving a fixed channel supply and extract flow independent of incident wind direction within a passive cowl-like geometry.

17 initial concepts for the windcatcher were modelled in 3D CAD and simulated in Autodesk CFD 2013 by the Author at 3.5m/s wind speed (see Appendix A). Successive geometries were remodelled with features aimed at achieving the correct flow directions in the supply and extract channels. The ensuing base geometry is shown below in Figure 5-2. It consists of two coaxial cylinders and a dome cap. The supply channel is annular surrounding a central channel which acts as the extract channel. The annular section is divided into 8 equal channels by plate sections which extend upwards into the dome cap further dividing the area under it into 8 sections with a slight extension into the central extract channel.

The total supply channels area is 0.023m^2 which is approximately twice that of the extract channel at 0.011m^2 . This ratio was chosen to take into consideration that in operation, approximately half of the supply channels will be facing the prevailing wind direction. Effectively this makes the extract and supply channel equal. This is important to minimize the pressurization of the connected living space to reduce infiltration. When positive or negative pressure is created in the

dwelling, some volume of air enters passes through leaks in the dwelling rather than via the ventilation system. A ventilation system with heat recovery should always operate in balanced way that do not pressurize the dwelling.

The channel areas correspond to an outer body diameter of 220mm when the material thickness is 5mm. This is limited by the size of existing flues and aesthetics since the proposed system is supposed to mimic the appearance of traditional chimney cowls. It is expected that most flues will be compatible with this dimension as the minimum flue diameter specified for open fireplaces is 200mm according to Approved Document J of the UK building regulations [241].

The windcatcher has an overall height of 600mm, and dome cap diameter of 345mm. These are in line with the average dimensions of chimney pots currently available on the market [242] and were chosen for aesthetic reasons. Although, outside the scope of this research work, it is envisaged that the dome cap overhang can be exploited to provide passive protection against driving rain for the wind catcher by determining applicable rain fall trajectories and implementing design and performance refinements. Driving rain is defined as the quantity of rain that passes through a vertical plane in the atmosphere. It occurs because raindrops which are falling to the ground at their terminal velocity are blown sideways by the speed of the wind at any given height above grade. The work done by Straube [243] is useful in this respect.

Incident air on the windcatcher from any direction flows down into the facing annular channel to supply the living space. Part of this incident flow also flows through the constriction under the dome created by the dividing plates. This creates a venturi effect that drives air extraction through the central channel. In operation, this will be boosted by additional buoyancy force within the ventilated space.

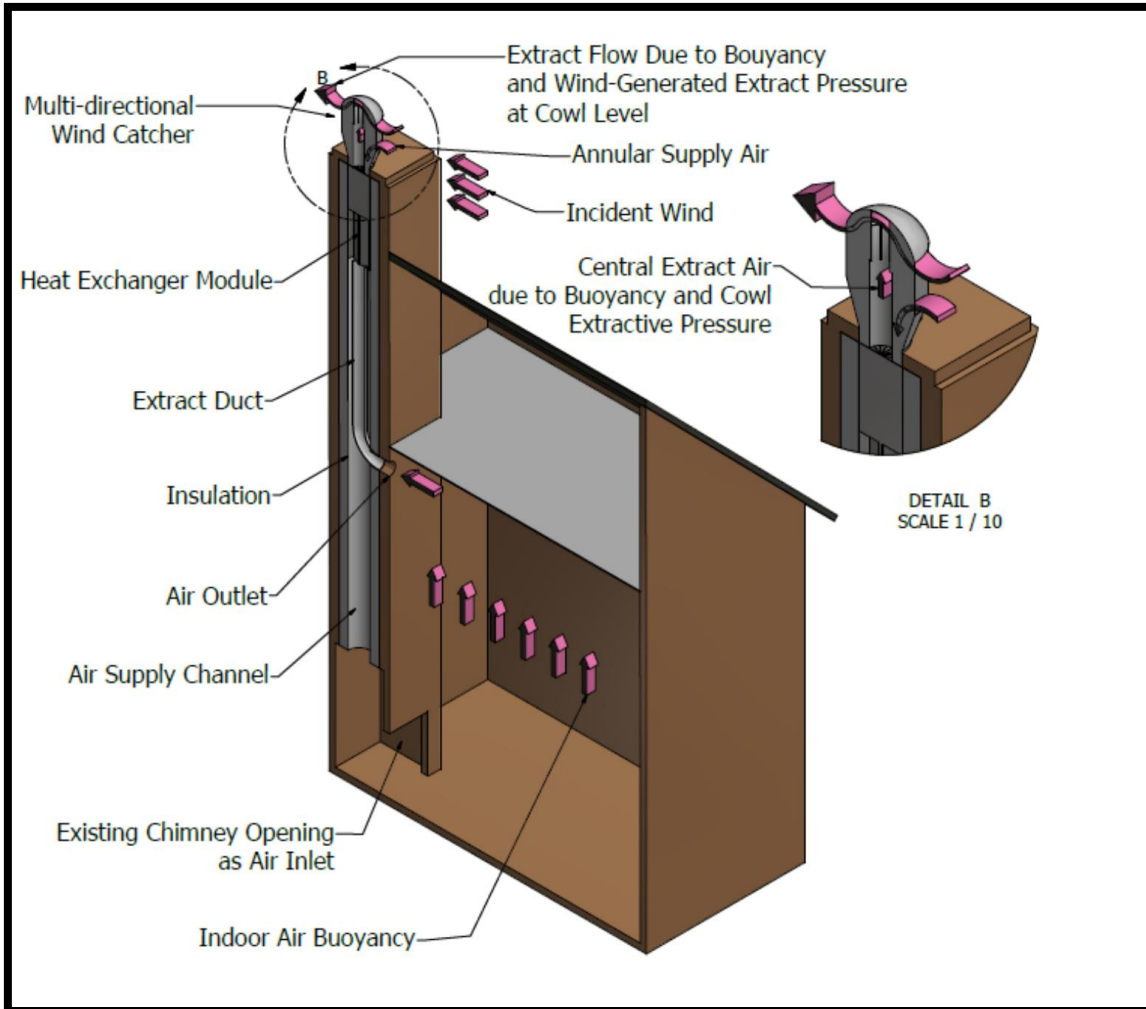


Figure 5-1 System Flow Structure

The task of optimising the flow rates through the windcatcher to meet required ventilation flow rates at foreseeable operating conditions was undertaken and is reported under subsequent sub-headings. Analysis of the windcatcher extract mechanism and investigation into the problem of flow short-circuiting at the base of the windcatcher are also presented.

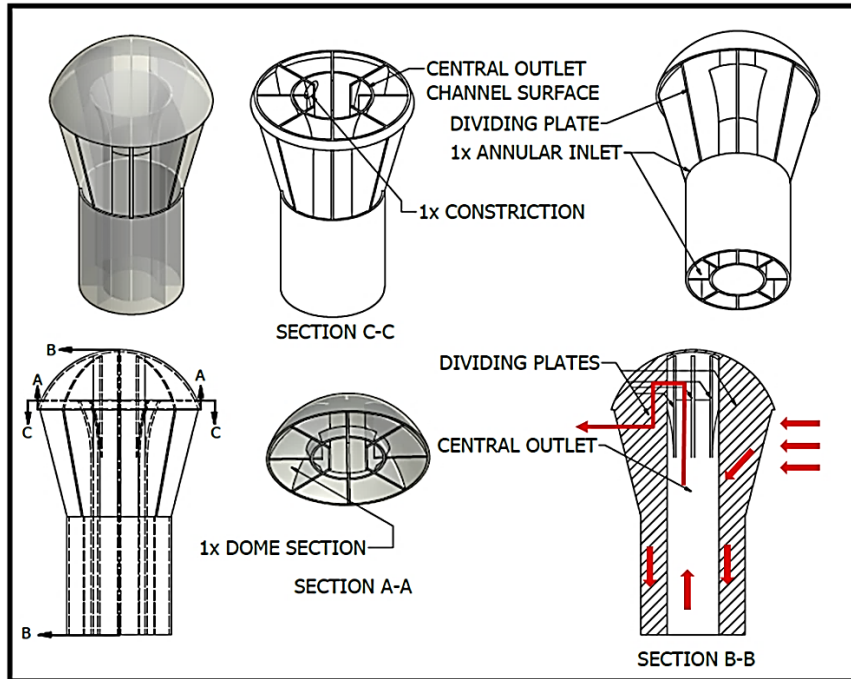


Figure 5-2: Windcatcher Base Model

5.2 Analysis and Results

5.2.1 Air Flow Rate Analysis

As stated under point “e” of heading 5.1, the ability of the windcatcher to supply ventilation air to the connected living space and extract it from same at an acceptable flow rate, is a functional requirement. Table 3.1 of CIBSE guide B2 [23] recommend an air exchange rate of 0.5ach–1ach for domestic dwellings in England. In the light of the above, a need was established for the windcatcher to provide at a minimum of 0.7ach for a room of 2.75m x 4.18m x 2.33m (W x D x H). This is according to the UK Technical housing standard for a double room [244]. The floor dimensions also correspond to the minimum standards for living rooms in a single bed house in 10 London boroughs [245]. The air flow into the room to satisfy the condition is calculated as follows:

$$\text{Room Volume} \approx 27\text{m}^3$$

$$\begin{aligned} \text{Ventilation rate} &= 0.7 \text{ ach} = 0.7 * 27 = 18.9 \text{ m}^3/\text{hr} \\ &= 0.00525 \text{ m}^3/\text{s} \end{aligned} \quad (1)$$

The total cross sectional area of the wind – catcher inlet annulus = 0.023m²

Required average air velocity through wind – catcher inlet

$$= \frac{0.00525 \text{ m}^3/\text{s}}{0.023 \text{ m}^2} = 0.2 \text{ m/s} \quad (2)$$

Five refinements were carried out on the windcatcher Base Model to arrive at a final prototype that satisfies this ventilation air flow rate requirement as a minimum. For larger rooms the adequacy of the system can be assessed by calculating the required ventilation rate for the room and extrapolating the air flow performance figures for the windcatcher at the prevailing wind speed where the room is located.

5.2.1.1 Simulation Models

All models of the windcatcher and physical test scenario were modelled and assembled in 3D using Autodesk Inventor 2013. As shown in Figure 5-3, the wind catcher is fixed atop a 1m tall chimney at the centre of a 14m x 8m x 52m (Width x Height x Depth) wind tunnel. The domain size and location of model were based on the best practice guideline by Franke et al. [246] for environmental wind flow studies. This suggests a maximum blockage of 3%, where the blockage is defined as the ratio of the projected area of the object of interest in flow direction to the free cross section of the computational domain. They also recommend a minimum of 8H for the distance between the inflow boundary and the object of interest, where H is the height of the structure on which the object is positioned. Recommendation for the wake region is an extension of at least 15H to allow for flow redevelopment as fully developed flow is normally used as a boundary condition in steady RANS calculation. Domain vertical expansion should be at least 5H.

The solid windcatcher and chimney parts were removed to derive a 3D section representing just the air flow fluid part. To reduce the computational effort

required for the simulations, the model was divided at the vertical midsection. The surface created by dividing the whole model is that of symmetry and flow properties on either side mirrors the other. The outlet and inlet air sections of the windcatcher channels were extended downwards (Inlet/supply channel =8m, Outlet/extract channel =5m) to model air flow lengths in a single storey building installation with the air extract terminal at high level on the ground floor room above a chimney opening which serves as the air supply vent. Calculated blockage for the chosen domain size is approximately 2%.

Simulations were carried out using Autodesk CFD 2013 at steady state wind speeds of 0.5m/s, 1.5m/s, 2.5m/s, 3.5m/s and 4.5m/s incident on the windcatcher at 90 degrees. The wind speeds are a conservative take on the average wind speeds 10m above ground level in the UK. This is to understand and design for optimal performance at low wind speeds especially in cases where the urban terrain largely inhibits air flow. Wind speeds vary rapidly over very short periods of time. This transient behaviour cannot be easily replicated in validation exercises. Experimental investigations into air flow in windcatchers have also not revealed significant transient behaviour. Variation between small intervals of incident wind speeds produce linear relationships between air flow supply and the incident wind speed [168]. Steady state wind speeds are widely used in the investigation of windcatcher ventilation systems [35]; [149]; [168]; [203]; [247]; [248].

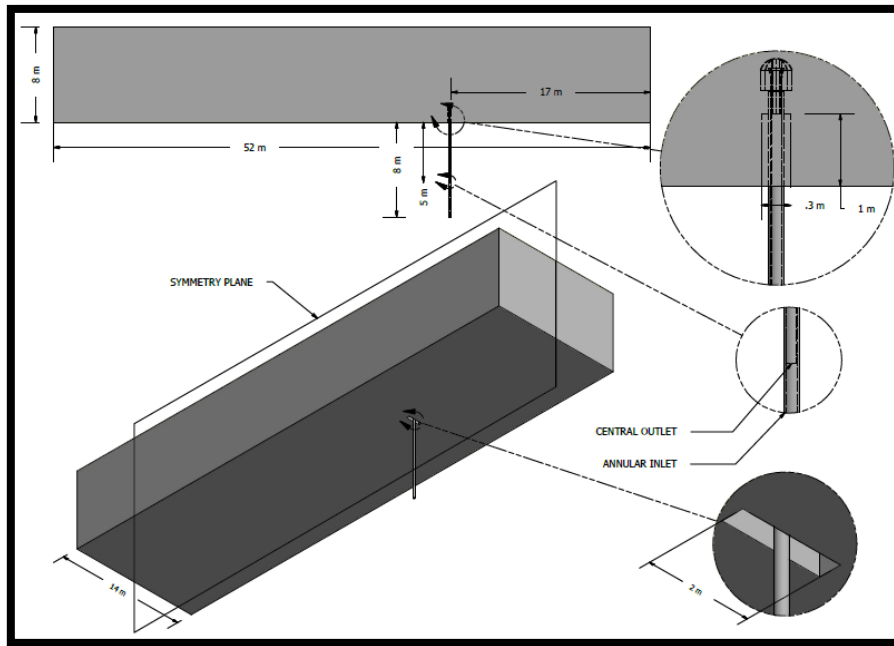
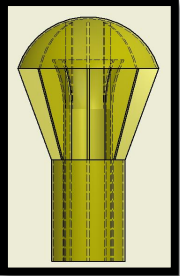


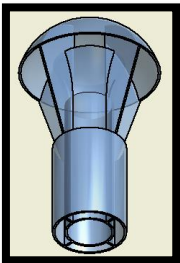
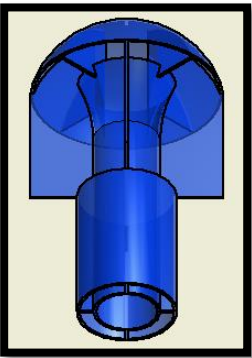
Figure 5-3: Simulation Model Domain

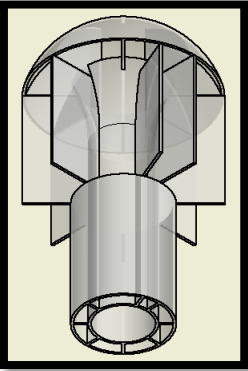
A summary of the windcatcher geometries simulated is shown on Table 5-1 below. The columns summarize the subsequent geometric refinement made to each model based on the analysis of CFD results from preceding designs.

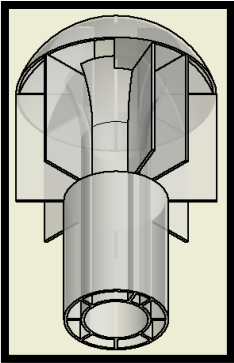
Table 5-1: Simulated Models for Windcatcher Supply and Extract Flow Rate Optimization

Model Geometry	Equal Annular Inlet Channels	Equal Sections Under Dome	Geometry of Dividing Plates	Rationale
 <p data-bbox="203 919 322 951">Model 1</p>	8	8	<ul style="list-style-type: none"> • 8 in total. • Slanted from dome edge to the inlet annulus. • Rigidly jointed to dome and annulus divisions. 	<ul style="list-style-type: none"> • Base Model <p>This model geometry fulfils the requirements for the windcatcher as listed under heading 2.2.2. It is completely passive with no moving parts. The annular channel is omnidirectional and open to incident wind from all directions. The central outlet is also fixed and supported within the annulus by dividing plates which narrow the facing air flow towards the centre of the unit. The narrowing terminates on the outside of the central channel for its straight length. However, at its funnel section the dividing plates extend into the extract channel to narrow the incident air flow part towards the centre of the funnel. This area is covered</p>

Model Geometry	Equal Annular Inlet Channels	Equal Sections Under Dome	Geometry of Dividing Plates	Rationale
				<p>by the dome which provide a low-pressure region to drive extraction when wind is incident on the windcatcher. The narrowing flow paths created under the dome by the dividing plate provides a venturi-like flow path for air flow under the dome to also aid extraction. The combined effects of these extractive pressures is intended to drive air extraction without requiring buoyancy. The dome cap has been extended downwards over the funnel to provide covering and maintain a low-pressure area over the extract channel surface to prevent air inflow into the channel. The entire unit maintains the external appearance of traditional chimney pots.</p>

Model Geometry	Equal Annular Inlet Channels	Equal Sections Under Dome	Geometry of Dividing Plates	Rationale
 <p data-bbox="203 810 327 842">Model 2</p>	4	4	<ul data-bbox="824 499 1330 754" style="list-style-type: none"> • 4 in total. • Slanted from dome edge to the inlet annulus. • Rigidly jointed to dome and annulus divisions. 	<ul data-bbox="1402 483 2116 683" style="list-style-type: none"> • Each annular inlet channel size is increased to increase the amount of incident air captured and boost inlet flow rates. This model is similar in geometry to the Ventive system [24].
 <p data-bbox="203 1294 327 1326">Model 3</p>	4	8	<ul data-bbox="824 887 1308 1310" style="list-style-type: none"> • 4 in total. • Extended outwards squarely and cut flush with the inlet annulus. • Rigidly jointed to annulus divisions. • Rigidly jointed to every second division under the dome. 	<ul data-bbox="1402 871 2116 1182" style="list-style-type: none"> • Each annular inlet channel size is increased to boost inlet flow rates. • Fully extended dividing plates to induce more air flow into the inlet channels by capturing air that would otherwise flow past the sides of the windcatcher.

Model Geometry	Equal Annular Inlet Channels	Equal Sections Under Dome	Geometry of Dividing Plates	Rationale
				<ul style="list-style-type: none"> • 8 dome sections to assist air extract flow through the central outlet. Extract flow mechanism is discussed under heading 5.2.2
 <p data-bbox="203 1090 327 1118">Model 4</p>	<p data-bbox="495 675 510 703">8</p>	<p data-bbox="669 675 685 703">8</p>	<ul style="list-style-type: none"> • 8 in total. • Rigidly jointed to annulus divisions • Not jointed to any division under the dome. • The rigidly jointed dividing plates and annulus divisions are free to rotate in the annulus around the central extract channel. • On impact, incident wind will rotate the relevant plate(s) to a 	<ul style="list-style-type: none"> • The number of inlet channels is increased back to 8 to reduce supply flow rate sensitivity to incident wind direction [95]. • Actively increased inlet channel size at every prevailing wind direction. • 8 dome sections to assist air extract flow through the central outlet.

Model Geometry	Equal Annular Inlet Channels	Equal Sections Under Dome	Geometry of Dividing Plates	Rationale
			<p>maximum extent thereby enlarging the corresponding inlet channel through the annulus. Simulations are carried out for a fully extended plate.</p>	
 <p>Model 5</p>	<p>8</p>	<p>8</p>	<ul style="list-style-type: none"> • 8 in total. • Rigidly jointed to annulus divisions • Jointed to division under the dome with a retractable blind. • Rigidly jointed dividing plates and annulus divisions are free to rotate around the central extract channel. 	<ul style="list-style-type: none"> • 8 dome sections with blinds to restrict air flow into dome to only windward sections in line with the impacted dividing plates before impact. This is to aid extract flow through the central outlet. • Actively increased inlet channel size at every incident wind direction.

Model Geometry	Equal Annular Inlet Channels	Equal Sections Under Dome	Geometry of Dividing Plates	Rationale
			<ul style="list-style-type: none"> • On impact, incident wind will rotate the relevant plate(s) to a maximum extent thereby enlarging the corresponding inlet channel through the annulus. • Retractable blind fans out to cover adjacent dome section as any windward plate rotates under the impact of incident wind. 	

5.2.1.2 Simulation Set-up

The following sub-sections discuss the Autodesk CFD settings applied in carrying out the windcatcher performance simulations.

5.2.1.2.1 Material

The material was set as air with fixed properties at 101325Pa and 19.85°C. As the windcatcher investigation does not involve temperature or density changes, material properties will not vary significantly. This is a safe assumption in incompressible flow simulations where air velocities are well below Mach 0.3.

5.2.1.2.2 Boundary Conditions

Boundary conditions are needed to bound the simulation domain and define its interaction with the environment beyond it. The following boundary conditions were generally applied for all simulations.

By default, all boundaries between solid and fluid were treated as smooth walls where a no-slip condition is enforced and the viscous fluid has zero velocity relative to the wall. No values were entered for shear stress and surface roughness because flow losses in the simulated models are largely produced by form drag due to prototype geometry as opposed to shear losses along the walls.

Symmetry boundary condition is applied at the vertical symmetry surfaces, top and opposite sides of the simulation domain. This defines a slip wall with zero shear and zero normal velocity and gradients. Flux across the symmetry plane is zero and the halves of the model are a mirror of each other.

As the windcatcher is supposed to drive both extract and supply air flows itself, the surfaces of the supply and extract channels at the base of the windcatcher, were set at a static gauge pressure of 0Pa i.e. pressure outlet, to allow inflow or outflow. To aid numerical convergence, the back-flow direction was correspondingly specified for the extract channel. The CFD code calculates the flow direction in the adjacent cell layer to the boundary to determine flow direction. The outlet from the simulation domain was also set as a pressure outlet. Turbulent viscosity and turbulent intensity at this point were set at 10 and 10%

respectively, to account for flow disturbance experienced through the simulation domain.

Only the normal component of velocity was used to compute the mass flow rate and fluxes into the domain in all simulated scenarios. The quantity specified at the velocity inlet is applied uniformly across the boundary surface. Therefore, the elongated upstream air section allowed the flow to develop properly before impacting the windcatcher. The inlet to the simulation domain was set at the different simulated incident wind speeds in directions normal to its surface.

Earlier experimental and simulations carried out by Montazeri [36] on the performance of cylindrical multi-opening windcatchers has already revealed that the sensitivity of these windcatchers against incident wind angle decreases as the number of openings increases. In his experiment the flow rate per channel of 4-opening windcatcher only varied by a maximum of ~10% as the incident wind angle was varied between 0° and 180° . This variation decreased to ~5% for a 12-section model. The proposed windcatcher in this study is an 8-sided windcatcher with a similar geometry to that investigated by Montazeri. As such, the variation of flow performance with incident wind angle is expected to be minimal and within the range observed in his experiment.

Turbulent intensity and viscosity ratios at all incident wind speeds were set to 5% and 10 respectively. These are typical prescribed values for external flows [130]; [249]; [250]; [251].

5.2.1.2.3 Meshing

Autodesk CFD's automatic sizing and adjustment function concentrate smaller elements in areas of strong curvature, gradient and close proximity to neighbouring geometry. This function was used to define an optimum tetrahedral mesh which was adjusted using the size slider to give a finer element factor of 0.73. The mesh enhancement function was used in defining uniform inflation layers on wall boundaries. The height of these layers is uniform across a surface and based on the smallest length scale on that surface. This in turn transitions smoothly across the model surfaces. 10 inflation layers were specified and the

enhancement blending option was chosen to cause a gradual transition between the inflation layers and adjacent tetrahedral elements. The layer factor controls the total height of inflation layers on each surface depending on local isotropic length scale while the layer gradation function controls the rate of growth of inflation layers. A layer factor of 0.2 and gradation of 1.3 was specified. Mesh refinement regions were created to cover the windcatcher and wake region behind it. This provides a better resolution of flow properties variations in this region. Meshing resolution, volume growth rate, limiting aspect ratio and other advanced meshing controls were left at their default values.

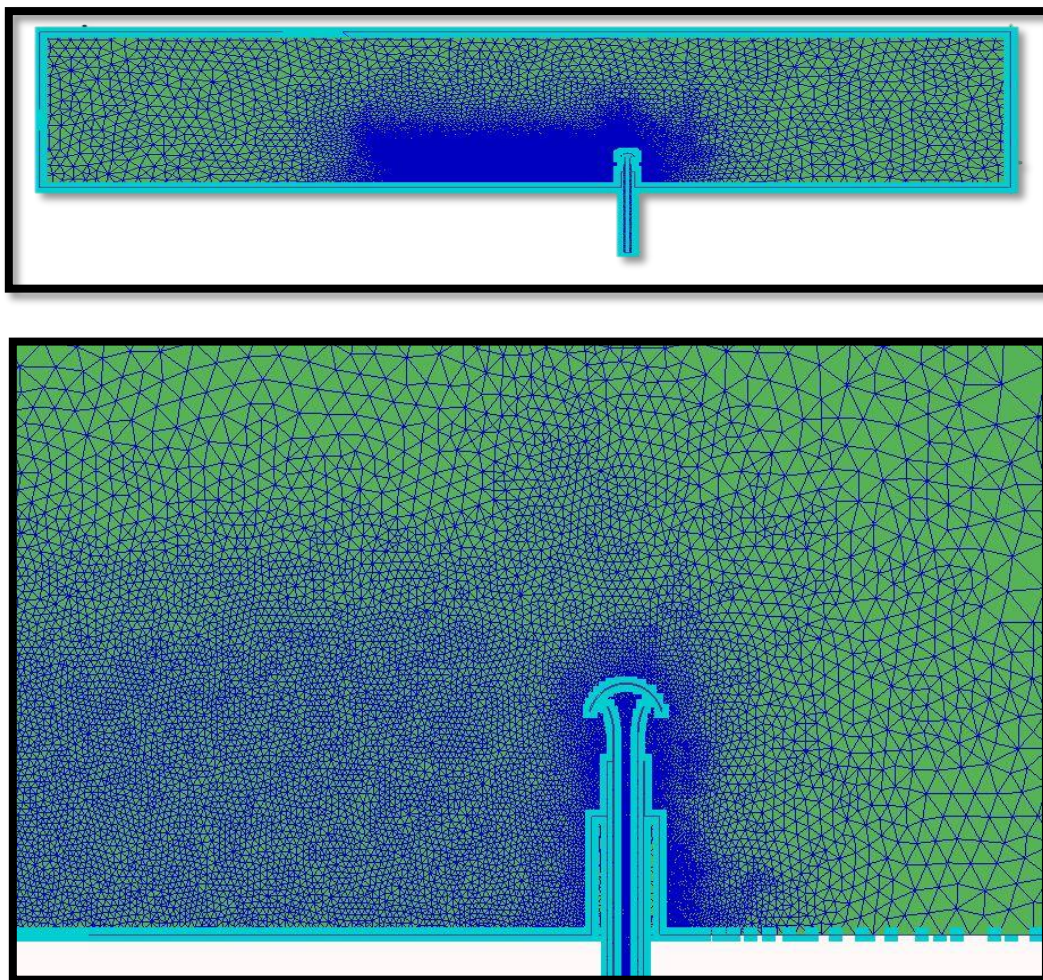


Figure 5-4: Autodesk CFD Mesh (Wake region to the left)

Three mesh adaptation cycles which allowed mesh coarsening were specified for each simulation. Ordinarily the mesh is refined based on gradients of pressure and velocity (and temperature in heat transfer simulation). However, additional adaptation criteria of flow-angularity, free-shear layer and external flow were specified for the simulations. The Flow Angularity option enables refinement in regions that contain large amounts of flow separation. 'Free Shear Layers' adaptation enables adaptation in free shear layers occurring between the free stream velocity and much slower flows, as found in wake or separation regions. And, the 'External Flow' option factors in large domains of unbounded flow during free shear layer adaptation. The final element count was between 18million and 20million for all simulated scenarios.

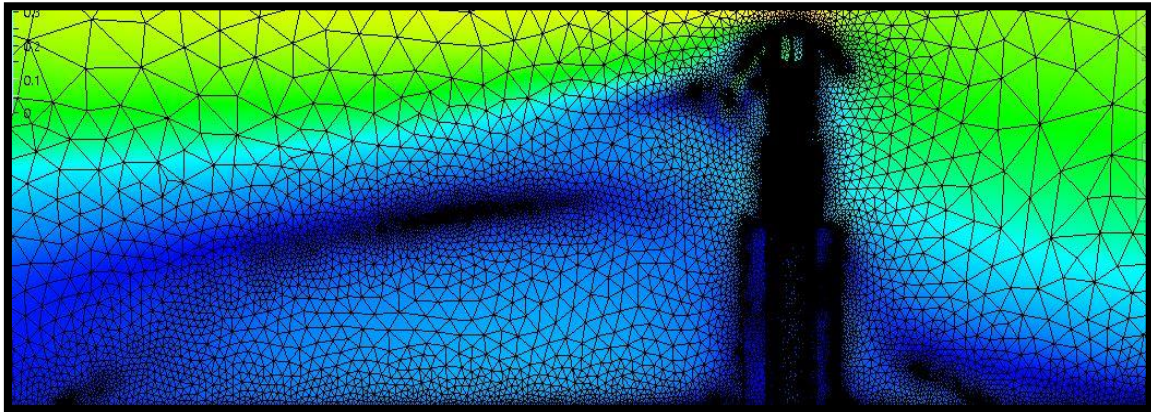


Figure 5-5: Autodesk CFD Adapted Mesh

5.2.1.2.4 Solving

1000 iterations were specified in all cases using the k-epsilon turbulence model. For convergence control, Intelligent Solution Control was enabled and Automatic Convergence Assessment was set to 'tight' using the slider bar. The 'tight' setting is satisfied when the maximum instantaneous slope in all iterations is below 0.0001, 'Time Averaged Convergence Slope' is below 0.01, the 'Concavity' of solutions falls below 0.01, and 'Field Variable Fluctuations' are below 1e-05. All other settings for body force, advection scheme (ADV 1: Monotone streamline up) etc. were left at their default values.

5.2.1.3 CFD Simulation Results

Below, Individual model results are compared with the desired flow rate calculated as $0.00525 \text{ m}^3/\text{s}$ for a single room size, and flow directions in both inlet and outlet channels are analysed. The analysis of each preceding model results is used as basis for the adjusted features of the subsequent model.

5.2.1.3.1 Model 1

Model 1 is the Base Model as shown on Table 5-1. It has 8 annular air supply channels. The dividing plates are fixed in place and slant from the dome to the inlet annulus. These plates also extend into the dome to divide the area underneath it into 8 sections.

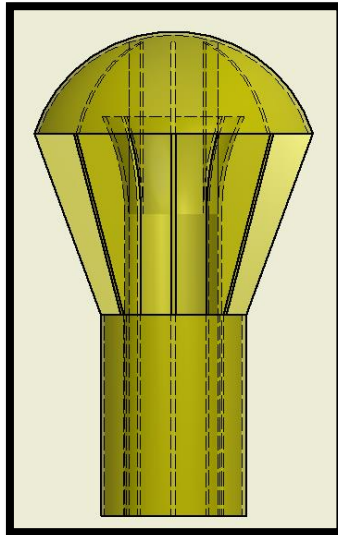


Figure 5-6: Model 1 (Base Model)

A. Supply Air Flow

Velocity vectors on the symmetry plane have been plotted in Figure 5-7 for the different incident wind speeds simulated. At all wind speeds, it is observed that the air stream entering the windcatcher separates into two flow paths. A proportion goes down into the front (windward) annular inlet channels and the other flows upwards into the dome.

The central outlet channel exhibits the desired flow direction i.e. it shows an upwards extract flow facilitated by low pressure generated by the incident wind

accelerating over its upper surface through the constricted sections under the dome. However, a vortex is developed around the outlet of the extract channel at all wind speeds. The vortex takes up a considerable area at the mouth of the outlet. This has the undesirable effect of reducing the extract air flow rate and consequently the windcatcher performance.

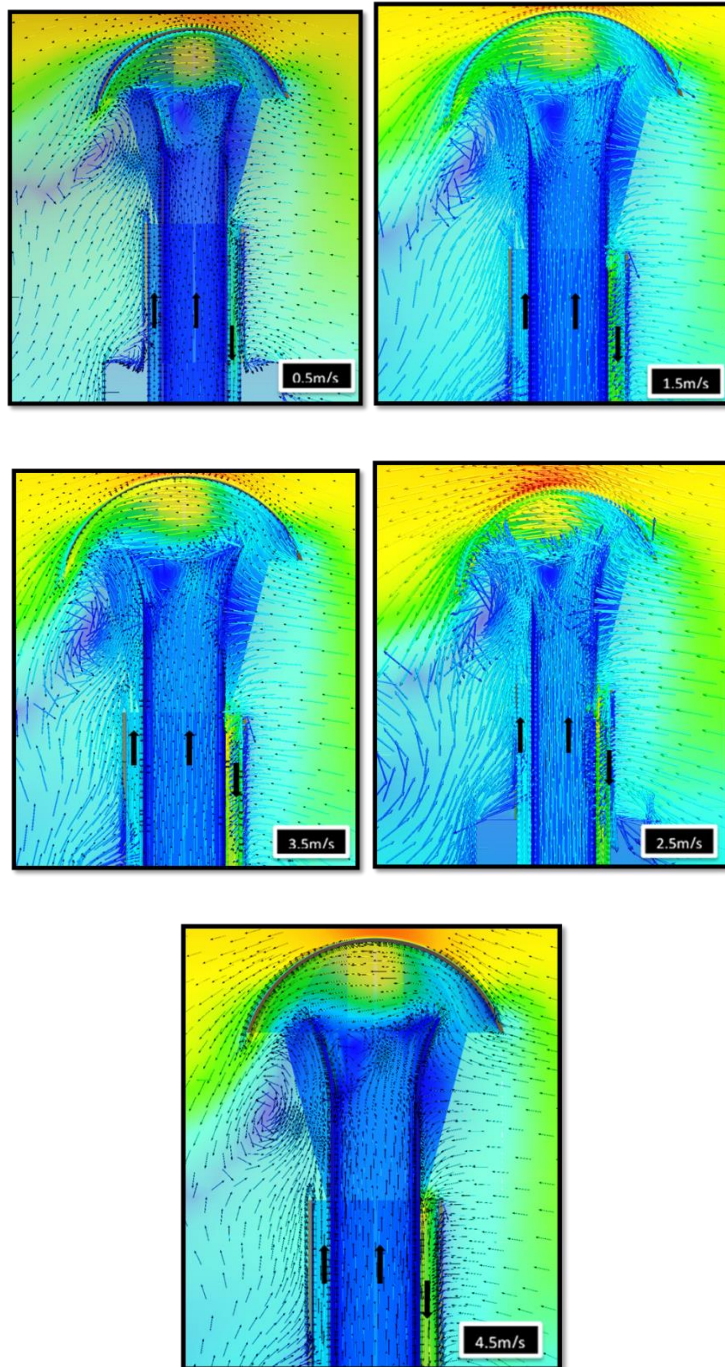


Figure 5-7: Model 1 Velocity Vector Plots

A vortex is also developed at the leeward end of the windcatcher model. It can be observed that the combined effect of the leeward end vortex and low pressure in this wake region induces suction in the leeward end annular supply channel. Hence the upward flow direction in this channel. The resultant of this phenomenon is a short circuit, i.e. the flow recirculates at the base of the windcatcher directly into the leeward end inlet channel as shown Figure 5-8. A short circuit has the effect of significantly reducing the ventilation effectiveness of the supply air at removing the stale room air and contaminants.

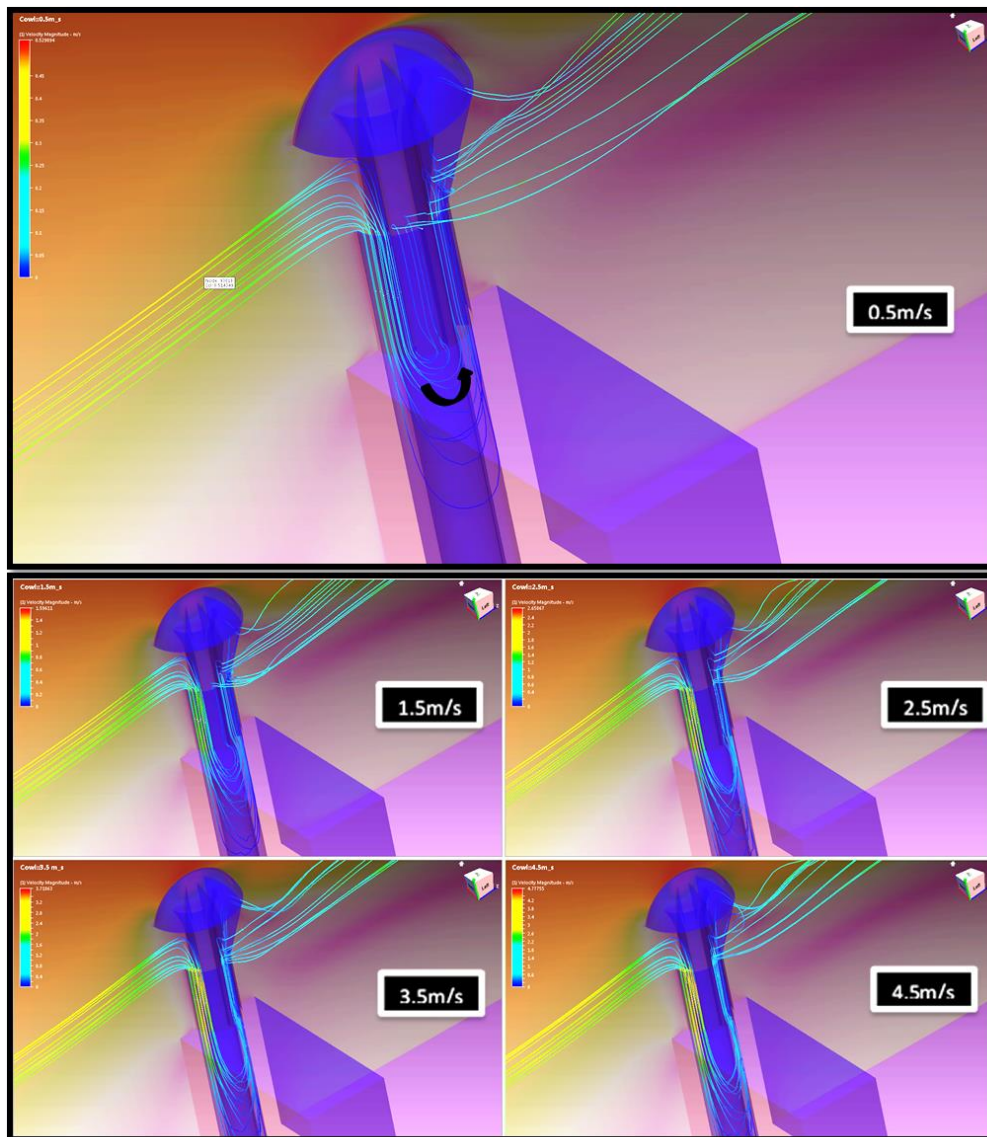


Figure 5-8: Model 1 Flow Short-Circuiting at 1.5m/s to 4.5m/s

Short-circuit flow was observed at all simulated incident wind speeds. However, it was more prominent at low wind speeds. At 0.5m/s incident wind speed, the captured air readily flows in a short circuit into leeward end channels. Thus, no air flow was delivered at the room level. Instead, a minimal extraction of air was observed.

As the incident wind speed increases, the point of recirculation beneath the windcatcher is pushed further downwards and some air flow goes down the channel (into the room). Hence, the proportion of air short-circuited decreases as incident wind speed increases. This can be observed on Figure 5-9; the incident wind approaches from the right side of the model. This should theoretically flow down the annular supply channel and exit at the room level. Thus, a trace of the flow stream taken on the surface of the supply air inlet at room level should show fluid paths originating from the right side of the model which is where the wind is coming from. However, at 0.5m/s wind speed, the trace is observed to be towards the left side of the model. This is because the entire flow captured in the windward inlet channels is short-circuited and extracted at the leeward channels. At the same time, the general flow direction in the annulus is completely reversed and the channel is effectively in extraction mode. For this reason, the flow path lines shown for the 0.5m/s wind speed scenario actually represent flow in the upwards direction as opposed to downwards for the other scenarios. The flow direction is magnified in Figure 5-10

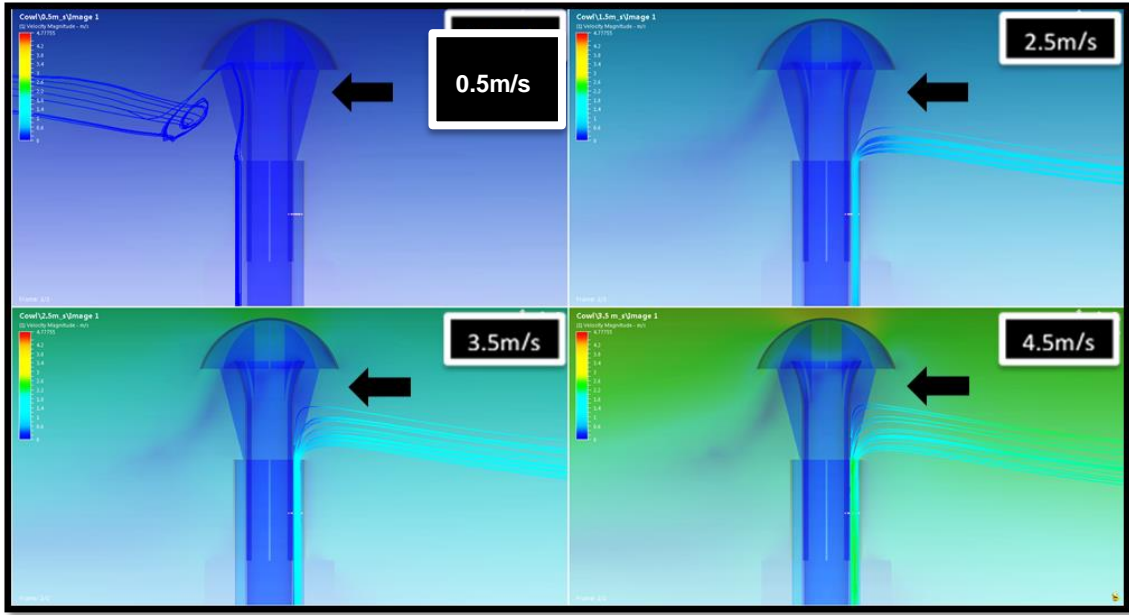


Figure 5-9: Model 1 Annular Inlet Channel Flow Path

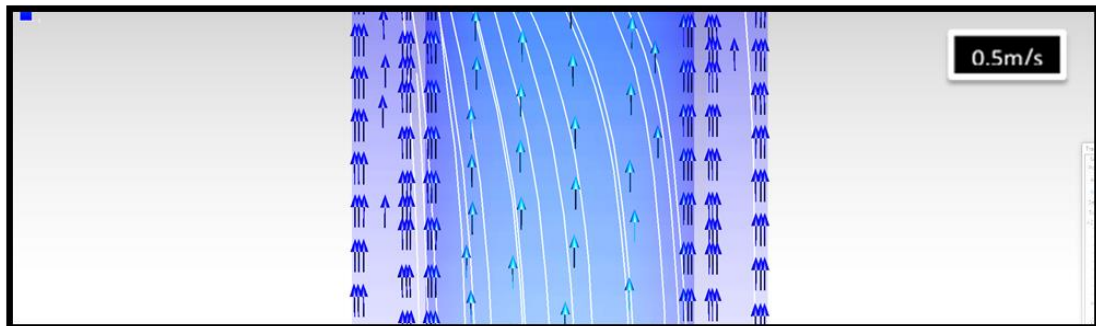


Figure 5-10: Model 1 Annular Inlet Flow Path at 0.5m/s Wind Speed (Zoomed)

Figure 5-11 gives a plot of the volume flow rates through the annular supply channel at room level. It can be observed that at low wind speed i.e. 0.5m/s the volume flow rate is very minimal and in the opposite direction. This validates the earlier observation of a reversed direction flow in the supply channel. Overall, the induced flow rate into the room increases linearly as the incident wind speed increases and peaks at 0.72m³/hr for an incident wind speed of 4.5m/s. This is very small compared with the limiting flow rate of 18.9m³/hr (Equation 1). Thus, the current design doesn't perform well in air supply.

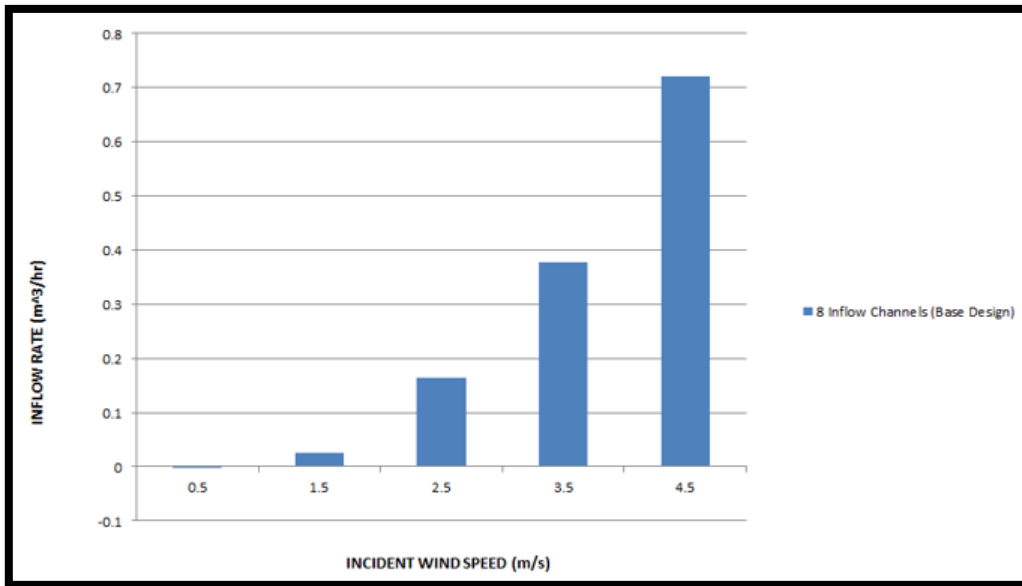


Figure 5-11: Model 1 (Base Model) Supply Air Volume Flow Rate

In Figure 5-12 below, a plot of incident wind flow path reveals an appreciable portion of air flow by-passing the windcatcher. Air capture into the annular supply channel occurs only at the channel directly facing the incident wind direction. The separated air flow at the windward dividing plate does not encounter appreciable redirection by the side dividing plates into the side annular channels. This suggests that the area of the dividing plate available to capture and induce air into the supply channel is limited.

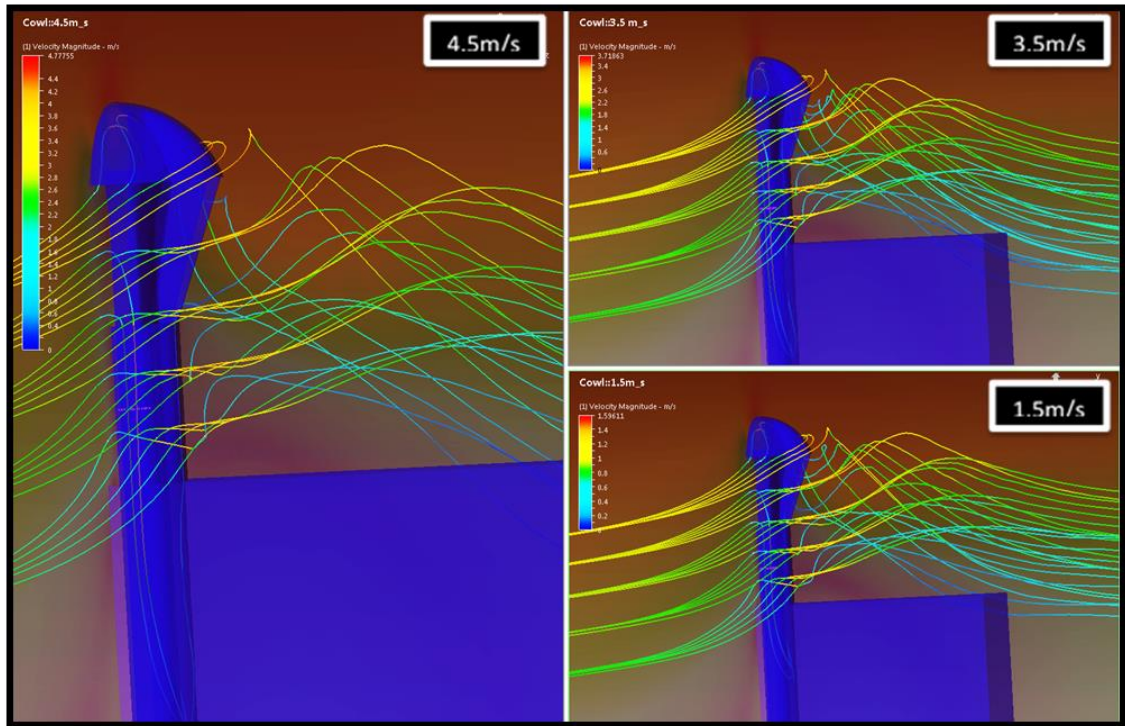


Figure 5-12: Incident Wind By-Passing Windcatcher

B. Extract Air Flow

The extract flow through the central channel of the windcatcher performed significantly better than the supply (Figure 5-13). The flow rate increased linearly as the wind speed increased reaching a maximum value of 18m³/hr at 4.5m/s wind speed. In an ideal airtight room, this high flow rate will serve to induce more flow down the supply channel into the room. Hence, the inadequate volume inlet flow rate observed earlier will be marginally enhanced. However, it is noted that as the extract opening will be located above the disused chimney supply point in the room, a significantly stronger extract will tend to enhance short-circuiting of air flow at the room level and inhibit adequate air distribution within the occupied zone. Furthermore, as buildings themselves are not absolutely air tight, the low pressure created because of the extract flow rate may also induce external air into the room through cracks and openings thereby reducing the efficiency of the entire system in operation. The air supply flow rate induced by the windcatcher into the room should closely match that of the extract without any significant

requirement for pressure interactions at room level to aid it. This will limit air room infiltration rates and ventilation air short circuiting within the room.

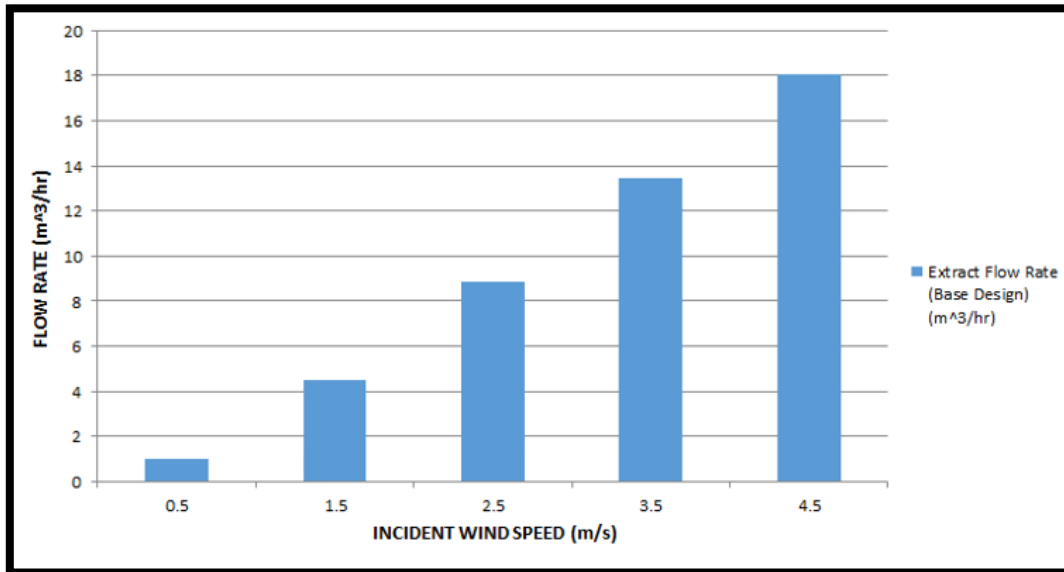


Figure 5-13: Model 1 Central Outlet Flow Rate

5.2.1.3.2 Model 2

H. Montazeri [36] in his experimental study of the performance of a cylindrical wind catcher with different numbers of flow channels concluded that the induced air flow rate decreases by increasing the number of channels. Therefore, the first approach employed in this CFD study was to reduce the number of channels to increase the air flow rate delivered at room level. In Model 2, the number of windcatcher supply channels has been decreased to 4 while keeping all other dimensions constant. Consequently, the size of each supply channel has been increased. The dividing plates slant from the dome to the inlet annulus. These plates also extend into the dome to divide the area underneath it into 4 sections. The outlet channel has remained unchanged from Model 1.

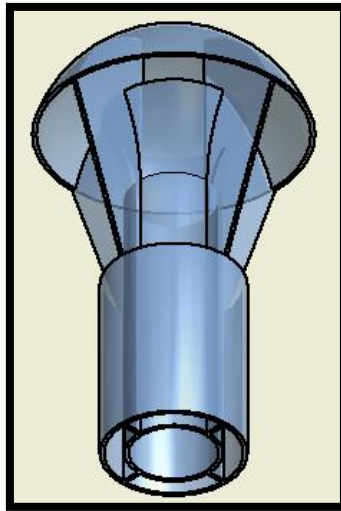


Figure 5-14: Model 2

A. Supply Air Flow

Supply flow rates are taken at the supply/inlet surface at room level. A significant increase in the supply flow rate was observed as shown on Figure 5-15. The flow rate increased linearly and peaked at $3.6\text{m}^3/\text{hr}$ compared to $0.72\text{m}^3/\text{hr}$ for the 8 channel Model 1. It performed significantly better at all incident wind speed scenarios. This follows from earlier observations made in experiments with similar cross-section windcatchers [36]. However, the supply flow rate values are still significantly lower than the limiting value of $18.9\text{m}^3/\text{hr}$ required for adequate ventilation. Hence, further geometrical alterations are required to enhance the flow rate.

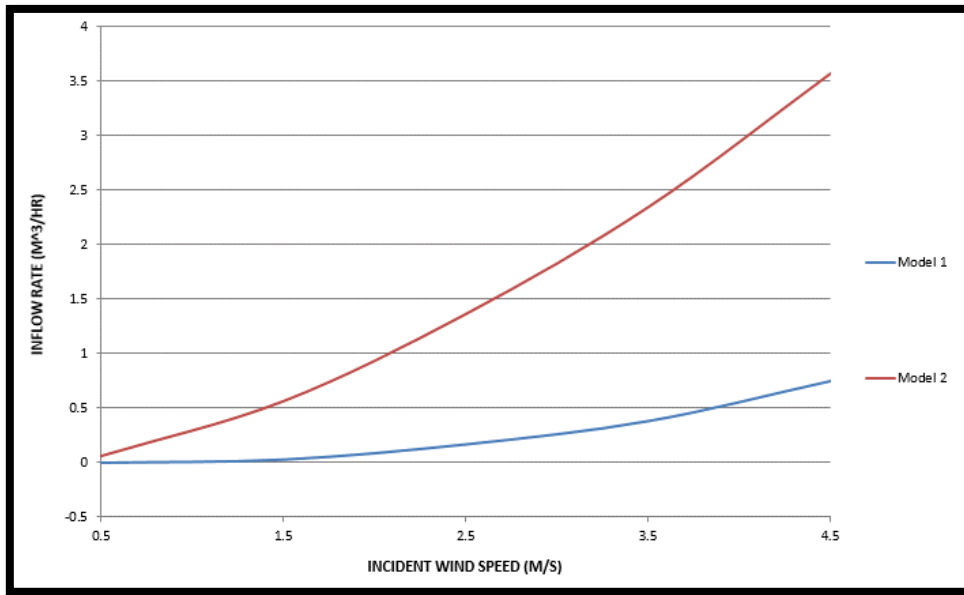


Figure 5-15: Supply Air Flow Rates for Models 1 and 2

A significant level of flow short-circuiting still occurs due to the low pressure on the leeward side (Figure 5-16). Compared to Model 1, the point along the supply channel where the flow recirculates to the leeward end does not change with wind speed. This is chiefly due to the larger inlet channels which does not constrict the flow path as in Model 1. Consequently, the flow down the supply channel is not as accelerated. As such, it quickly flows into the low pressure leeward side at the base of the windcatcher.

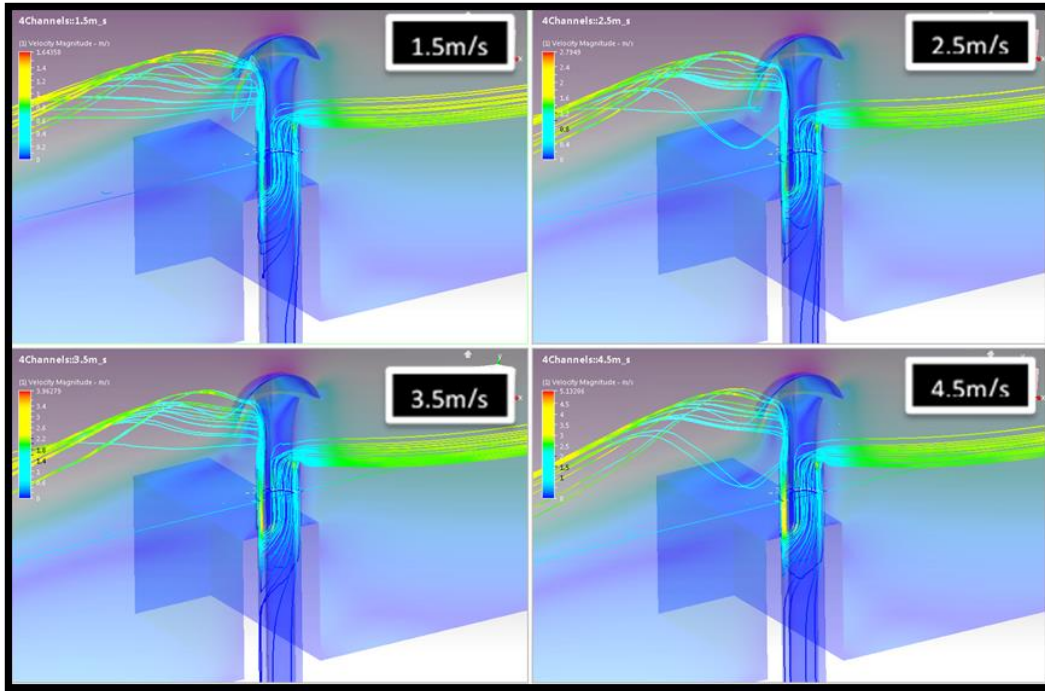


Figure 5-16: Model 2 Supply Air Short- Circuit Flow Path

B. Extract Air Flow

Vector plots indicating flow direction reveals an abnormality for this model. At all incident wind speeds, the flow in the central extract channel is in the reverse direction as shown on Figure 5-17.

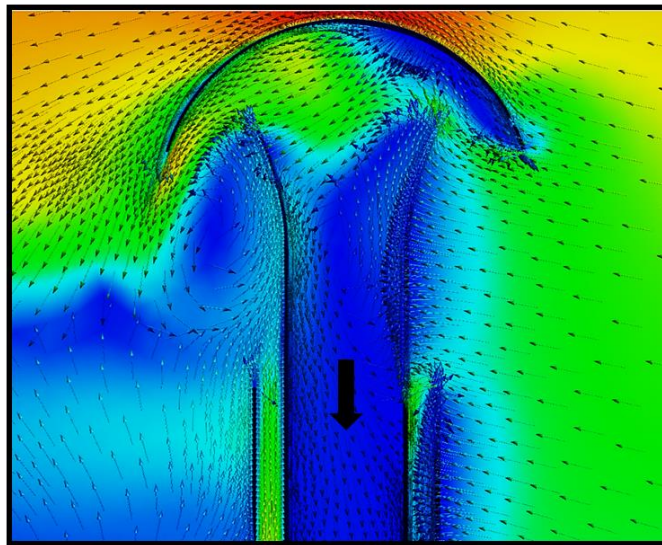


Figure 5-17: Model 2 Extract Air Flow Vector Plot

This is due to the reduced number of sections under the dome cap. For Model 1 with 8 sections under the dome, the incident wind is accelerated through the smaller divisions and over the central extract channel, consequently inducing negative suction pressure at its surface under the dome cap. Figure 5-18 is a plot of the pressure variation over the surface of the extract channel along its diameter in the incident flow direction as indicated with the red line.

For Model 2, the low-pressure suction effect is significantly reduced. Over a greater part of the surface, the pressure is high (and positive), causing flow down into the extract channel. This is contrast to the plot for Model 1 which shows negative suction pressure at most points along the surface diameter. Thus, the presence of eight sections under the dome enabled the extract channel to function in extract mode

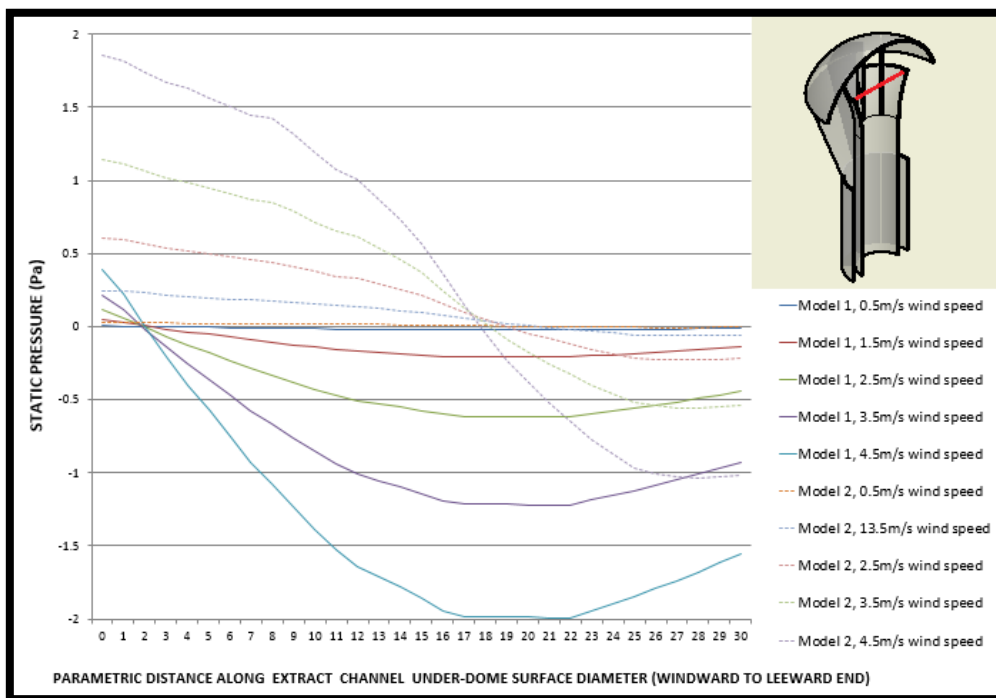


Figure 5-18: Pressure Variation over Extract Channel Surface

5.2.1.3.3 Model 3

In Model 3, four annular supply channels are combined with eight dome sections to achieve a functional extract channel as observed in Model 1 and the increased supply flow rate observed in Model 2. The dome geometry remained same with eight sections under it. Only every second dividing plate is extended downwards beyond the underside edge of the dome into the supply channel. Thus, the windcatcher maintained 8 sections under the dome and 4 supply channels at the annulus. Furthermore, to curtail the phenomenon of air bypassing the windcatcher as observed in Model 1 (Figure 5-12), the dividing plates are larger in this model. They are not slanted towards the annulus; they are extended downwards squarely and cut flush with the inlet annulus. This is to induce more air flow into the annular supply channels by capturing air that would otherwise flow past the sides of the windcatcher. The central extract channel has remained unchanged.

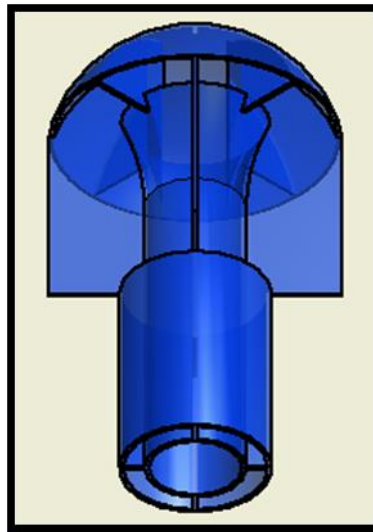


Figure 5-19: Model 3

A. Supply Air Flow

Model 3 showed a significant improvement in the supply flow rate which peaked at $8.3\text{m}^3/\text{hr}$ for an incident wind speed of 4.5 m/s (Figure 5-20). Nonetheless, this value is still significantly lower than that required to adequately ventilate the subject room. The supply flow rate is twice as much, even though this model has

the same size of supply channels as Model 2. This is due to the increased area of dividing plates which captured more air and induced it into the annular channels.

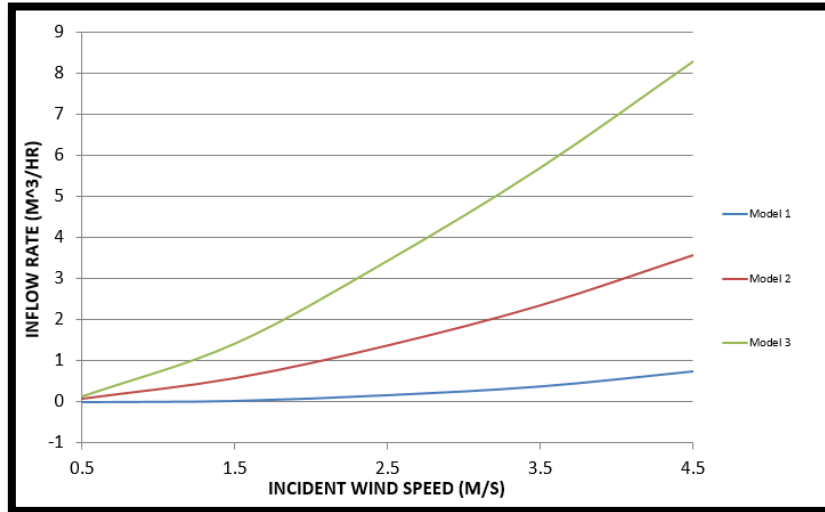


Figure 5-20: Inlet Air Flow Rates for Models 1, 2 and 3

B. Extract Air Flow

At all incident wind speeds, the flow in the windcatcher central extract was reversed i.e. air flowed down the channel instead of flowing out (Figure 5-21).

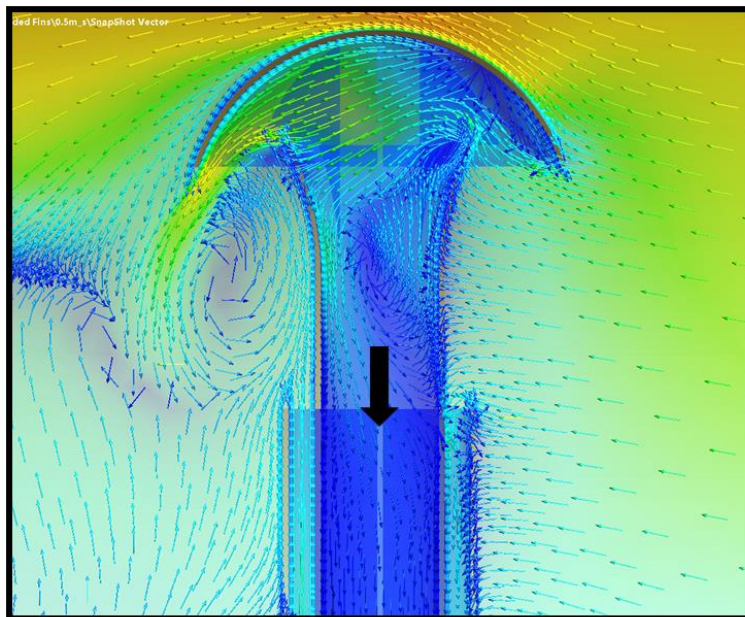


Figure 5-21: Model 3 Extract Air Flow Vector Plot

This model has the same number of dome sections as Model 1. However, in contrast to Model 1, this has not aided extraction through the central extract channel. This can be explained by observing how the incident air flow is divided between the windward dome sections (in one half of a symmetric model as simulated). Figure 5-22 shows the flows ratios through the two windward dome sections for Model 1 and Model 3 at 4.5m/s incident wind speed. This is measured on plane c-c as shown in Figure 5-2 as the mass-weighted average of volume flow rate through the area of the opening. For Model 1, 70% of the flow accelerates through the constriction at section 1 to induce a low suction pressure over the extract channel. Because this flow is significantly stronger, the disruption in flow path caused by the other flow from section 2 is not consequential. In comparison, for Model 3, the incident air flow is split almost evenly between the two dome sections. The velocities are almost the same for the two flows and are directed towards the centre of the extract channel. Consequently, both flows collide over the central extract channel causing turbulence and disrupting the setup of any pressure system that will aid extractive flow out of the central channel. Thus, the flow diverts into the outlet channel.

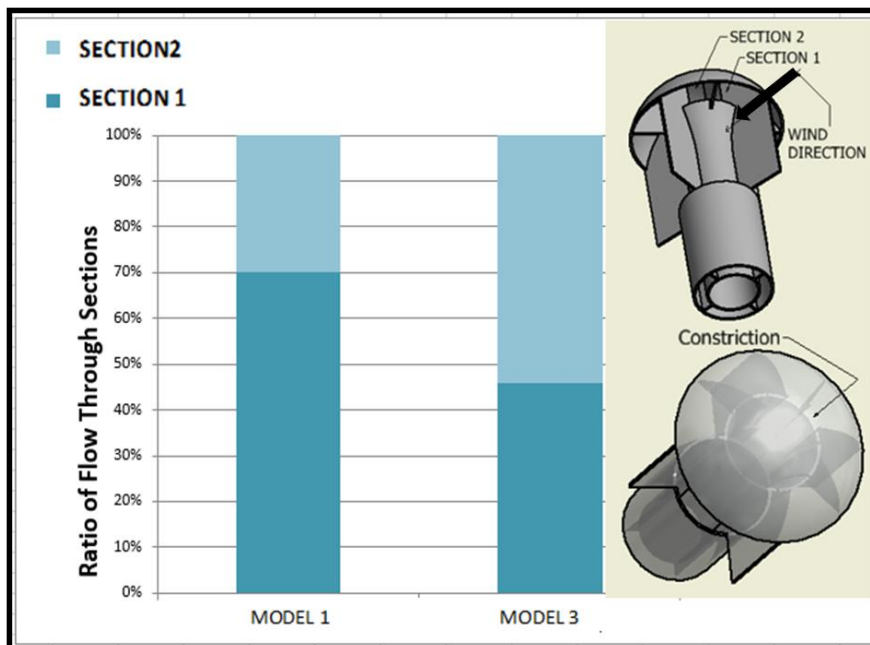


Figure 5-22: Model 3 Flow Ratios through Windward Dome Sections

A plot of the pressure variation over the outlet channel surface revealed a variation similar to that of Model 2 with 4 sections under the dome (Figure 5-23). The pressure remained positive over a large portion of the extract channel surface with a small section of negative suction pressure at the leeward end. This confirmed that a sweeping negative suction pressure over the central outlet as exhibited by Model 1 is necessary for extraction flow and reinforces the option of 8 sections under the dome as a prerequisite for the outlet channel to function in extract mode.

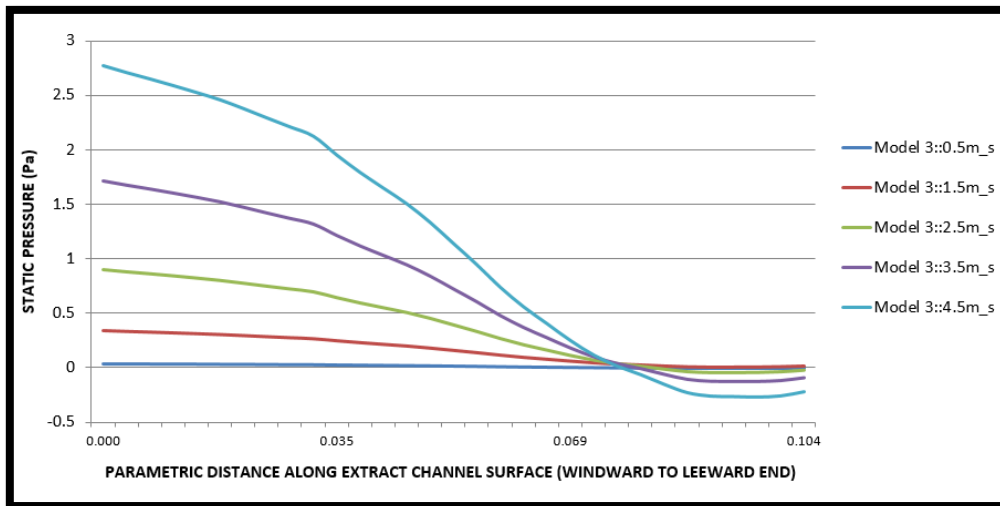


Figure 5-23: Model 3 Pressure Variation Over Outlet Channel Surface

5.2.1.3.4 Model 4

It has been established in previous models, that a dome divided into 8 sections is necessary to generate the low pressure required to extract air through the central outlet. In the last section, an analysis of the flow ratios through the windward dome sections also revealed that air flow must be concentrated in one section, to effect this extraction. Hence, Model 4, like Model 1 has the annular inlet channel and dome sections divided into 8, except with non-slanting dividing plates. The plates are extended downwards squarely and cut flush with the inlet annulus to induce more air flow into the inlet channels. In this Model, however,

each plate is cut into two, level with the lower edge of the dome. This separates each dividing plate into a rigid upper part, under the dome, and a loosely movable lower part. The rigid upper part keeps the original 8 dome sections intact, while the lower part is loosely movable and rotates in the annulus around the y-axis of the windcatcher. On impact, the incident wind rotates the relevant plate to its maximum extent thereby enlarging the corresponding inlet channel through the annulus. At its maximum extent, each dividing plate is set to expose its corresponding dome sections in a 70%-30% ratio with the directly windward facing section equating to 70% of the total opening.

This geometry introduces two things;

- The flexibility of having larger inlets through the annulus depending on the force of incident wind; larger inlets have been established as a necessity for increased air flow through the annulus.
- The incident air flowing into the dome section travels primarily through the windward dome section. This follows from the dome section flow ratio analysis done under Model 3, where it was observed that air flow into the dome must be primarily through one dome section to effect extraction through the windcatcher's central outlet.

The central outlet channel has remained unchanged from the Model 1.

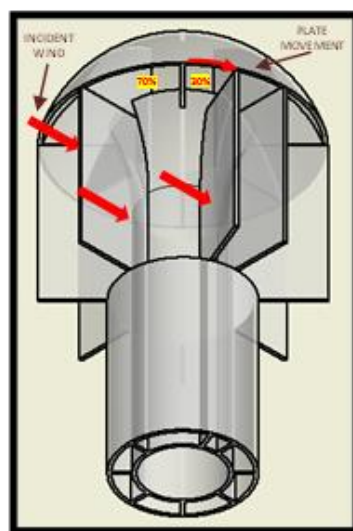


Figure 5-24: Model

A. Supply Air Flow

As with previous Models, the amount of induced inlet air flow increased linearly with increasing wind speeds; peaking at around $6m^3/hr$. Air flow rates through the annular inlet have been plotted on Figure 5-25. It shows how the annular inlet flow rates for Model 4 compares with that of all previous Models. An earlier investigation made by Montazeri et al [36] into the aerodynamics of a cylindrical windcatchers concluded that an increase in the number of inlet channels reduces the volume of air induced into a windcatcher at a given incident wind speed. A similar observation can be made here when Model 4 is compared with Model 2. An increase in the number of inlet channels from 4 to 8 has resulted into lower inlet flow rates at all simulated wind speeds.

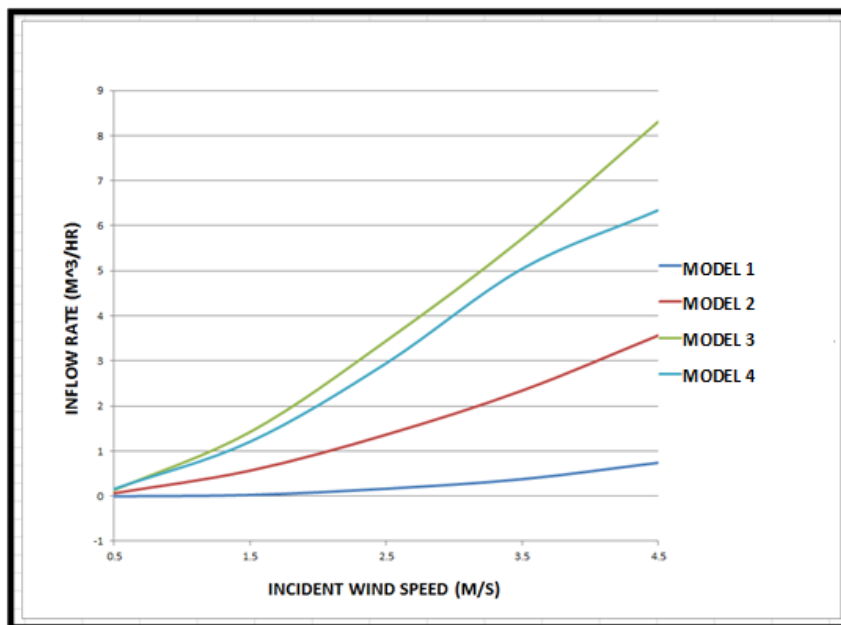


Figure 5-25: Supply Air Flow Rates for Models 1, 2, 3 and 4

B. Extract Flow

The extract flow through the central outlet was reversed at all incident wind speeds up to $3.5 m/s$. However, at $4.5m/s$, the outlet flow direction normalized and flowed upwards out of the outlet. An observation of the pressure distribution over the surface of the central outlet under the dome revealed that it was largely

positive at all wind speeds up to 3.5 m/s . At 4.5 m/s , a slight negative pressure was seen and this produced a weak extract flow out of the central outlet.

This observation can be explained by recognising a critical air velocity, above which air flow over the central outlet (under the dome) will gain enough momentum through the dome section constriction and generate low pressure to produce an extract flow through the central outlet [38]. In Model 4, incident air flow is divided between the windward dome sections. Consequently, the flow rate and velocity through the larger section (70% opening) is reduced. This slow-moving air does not produce the negative pressure above the extract channel required to drive extraction at all incident wind speeds up to 3.5 m/s . However, at an incident air velocity of 4.5 m/s , the increased incident air velocity also increases the air flow over the central channel. Hence, the extract flow observed.

5.2.1.3.5 Model 5

Model 5 retained the geometry of Model 4 with a slight addition. A geometry has been imagined which incorporates a spring-loaded blind connecting the top and lower divisions of the dividing plate at the plane flush with dome edge. At rest the blind is wound up in its spring mechanism and the top and bottom plates are aligned. However, in operation the blind fan out to cover the adjacent dome section as the plates open under the pressure of the incident wind. This limits the incident air flow to one dome section when the dividing plates open. The velocity magnitude of this air flow through the relevant constriction is expected to be, at a minimum, equal to that present when the dividing plate has not moved from its rest position. Hence, at wind speeds high enough to move the relevant dividing plate, extract performance through the central outlet should be higher, while at the same time, presenting proportionally larger inlet opening at the annulus.

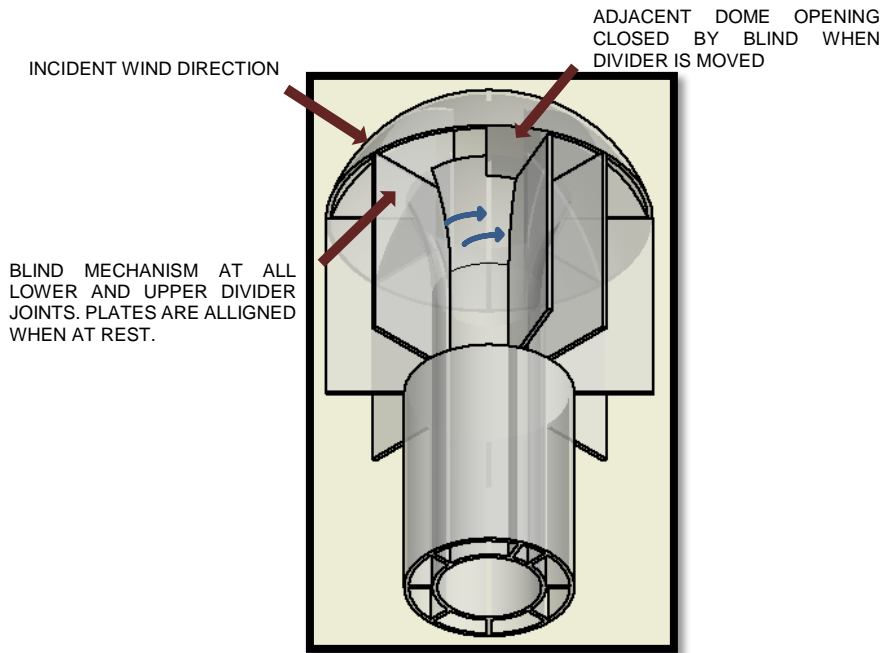


Figure 5-26: Model 5

A. Supply Air Flow

The inflow rate at room level through the annular inlet peaked at 5.4m³/hr for 4.5m/s incident wind speed and compares with all other simulated geometries as shown on Figure 5-27.

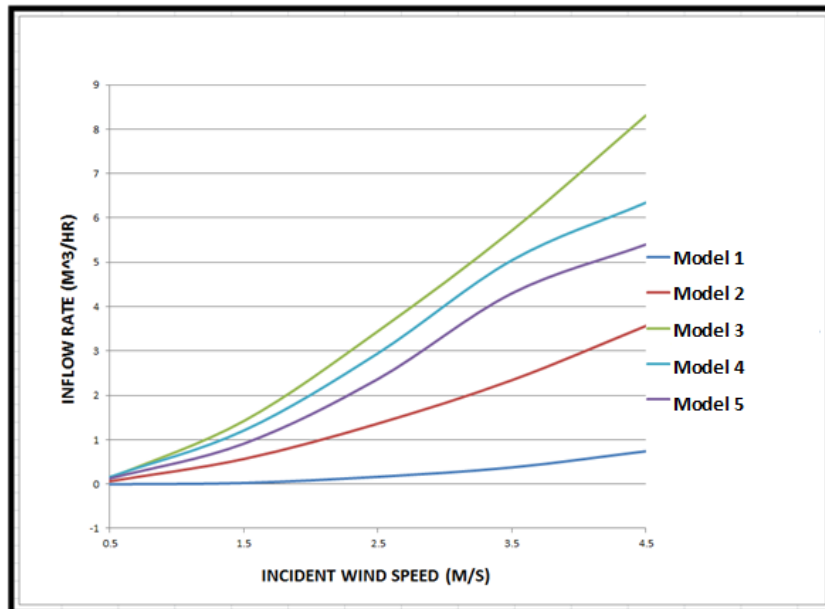


Figure 5-27: Supply Air Flow Rates for Models 1, 2, 3, 4 and 5

Even though the area of annular opening on this model and Model 4 are the same, the supply/inlet air flow at room level is less. This can be explained by observing the short circuit flow. As seen on Figure 5-8, some of the air flow induced in the windward annular inlet recirculates into the leeward end inlets. This short-circuit flow reduces the volume of air available at room level. Thus, a model with high short-circuit flow will provide less air flow at room level when compared with a similar model with the same inlet opening but lesser short-circuit flow.

For Model 5, the negative suction pressure induced at the leeward end annular channels of the windcatcher was much more than that for Model 4 which had no blinding under the adjacent dome section. Hence the percentage of the supply flow that went into short-circuit flow was larger as shown on Figure 5-28.

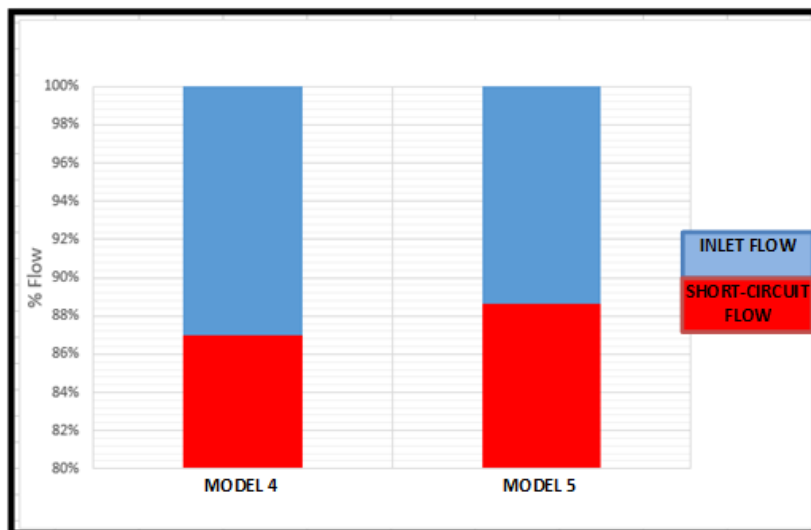


Figure 5-28: Ratio of Supply and Short-Circuit Flows for Model 4 and 5

B. Extract Flow

The required flow performance was realised through the central outlet. The blind restricted air flow to only the dome section directly facing the prevailing wind making the flow concentrated and accelerated through it. Negative suction pressure regions were created at the other sections under the dome and over the extract channel surface. This assisted the extract flow rate considerably with

values reaching 30m³/hr at 4.5m/s incident wind speed. Previously, Model 1 (Base Model) showed the highest extract flow rate, Figure 5-29 shows how it compares to that of Model 5.

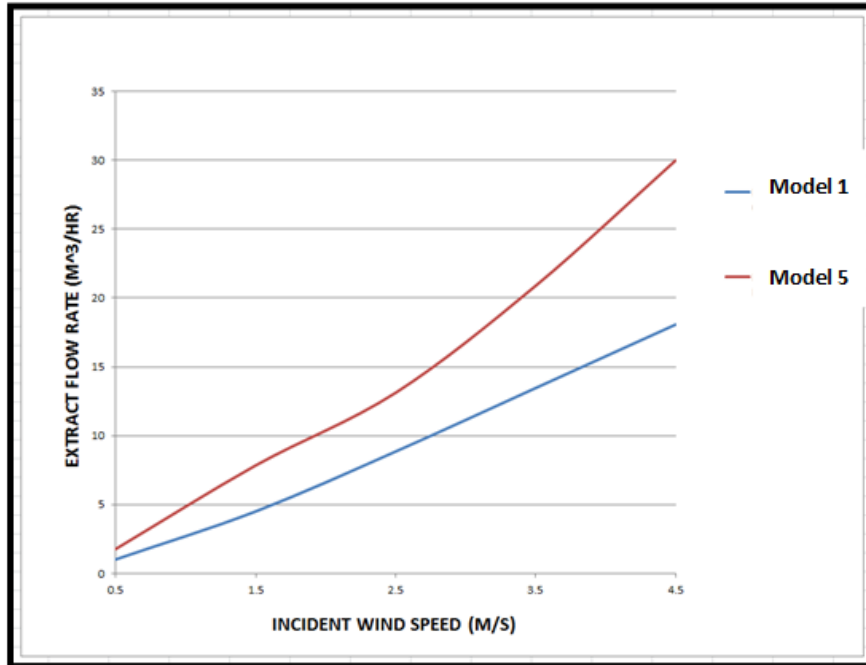


Figure 5-29: Extract Flow Rates for Models 1 and 5

5.2.2 Extract Flow Analysis

Model 1 is used here to understand the central outlet extract flow pattern and reveal the air flow characteristics under the dome. This is the same for the final prototype as the only significant difference in geometry is that of the bigger dividing plates which only serves to induce supply air into the annular inlets. With reference to Figure 5-30 below, when incident air flows under the windcatcher dome, negative pressure is generated at the side dome sections due to flow separation. This negative pressure induces suction over the central outlet. In comparison, the venturi effect created by the accelerated air flow over the extract channel has a smaller effect in trailing the extract air flow to the leeward exit region outside the dome. Consequently, the primary exit path(s) for the extract air flow is through the dome section(s) at the sides.

Depending on the flow velocity, incident air flow into the windward dome sections tends to flow directly over the central outlet into the leeward end dome section. Unavoidably, some goes into the central outlet and gets readily extracted through the side dome sections.

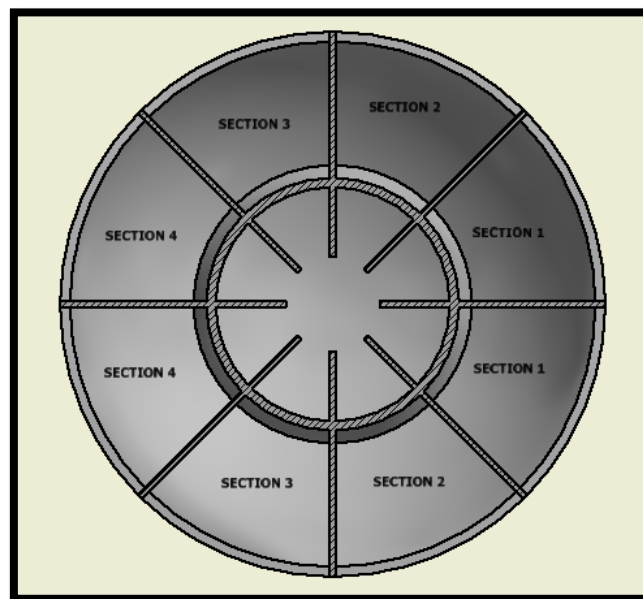
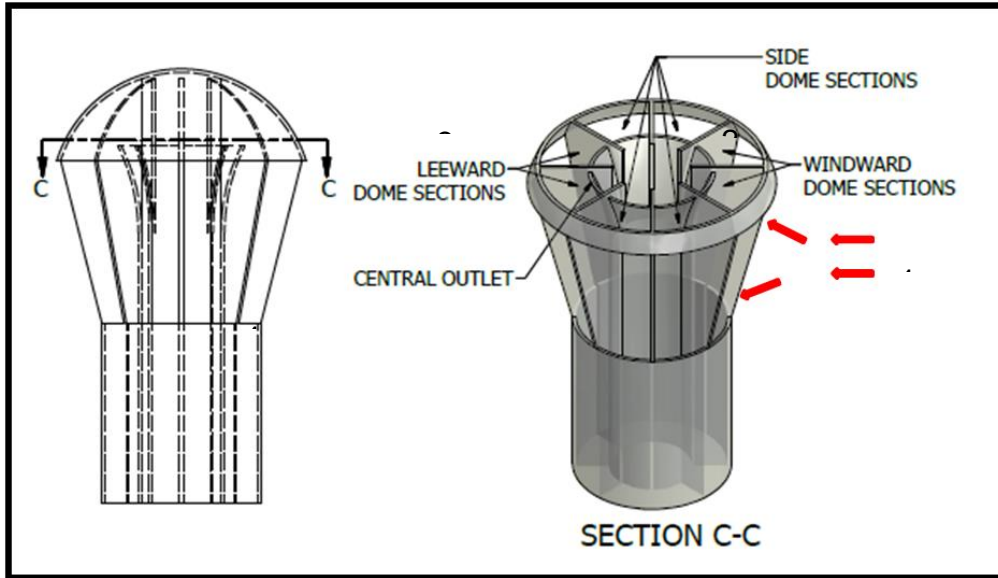


Figure 5-30: Extraction Sections

Figure 5-31 compares, the inflows and outflows at a converged time instant for all sections under the dome at the indicated cut plane c-c for one half of the symmetrical Model 1. The total volume inflow at both windward sections (1&2) is 31.4m³/hr with 28.8m³/hr of it coming in through Section 1. This stream exits at Section 4 and an outflow value of 27.1m³/hr can be read at the region. The difference of 4.3m³/hr is the part of the stream flowing downwards into the extract channel as shown on Figure 5-32. The 13.37m³/hr flow recorded exiting at Section 3 comprises of the 4.3 m³/hr difference in the windward flow stream, and an additional 9.07m³/hr extracted from the extract channel. For a full model, this 9.07m³/hr doubles up into 18.14m³/hr, which was the recorded extract rate for this Model 1 (see Figure 5-11).

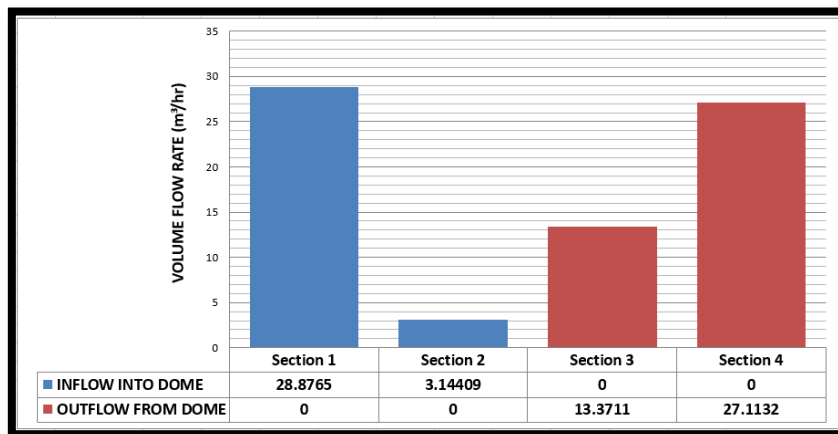


Figure 5-31: Model 1 Dome Sections Flow Rates

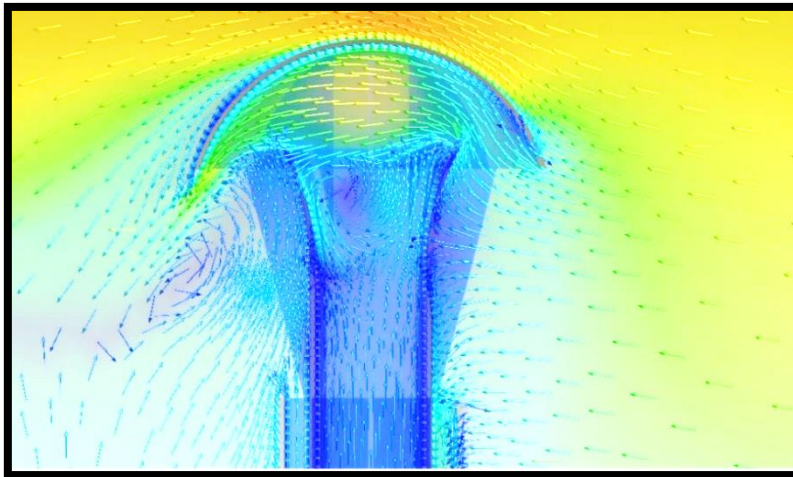


Figure 5-32: Model 1 Extract Channel Velocity Vector Plot

5.2.3 Short Circuit Flow Analysis

Short-circuiting of ventilation air flow in windcatchers have been shown to inhibit proper ventilation of an attached space [169]; [252]. An analysis of the short circuit flow phenomenon by observing the flow rates and pressures is presented below.

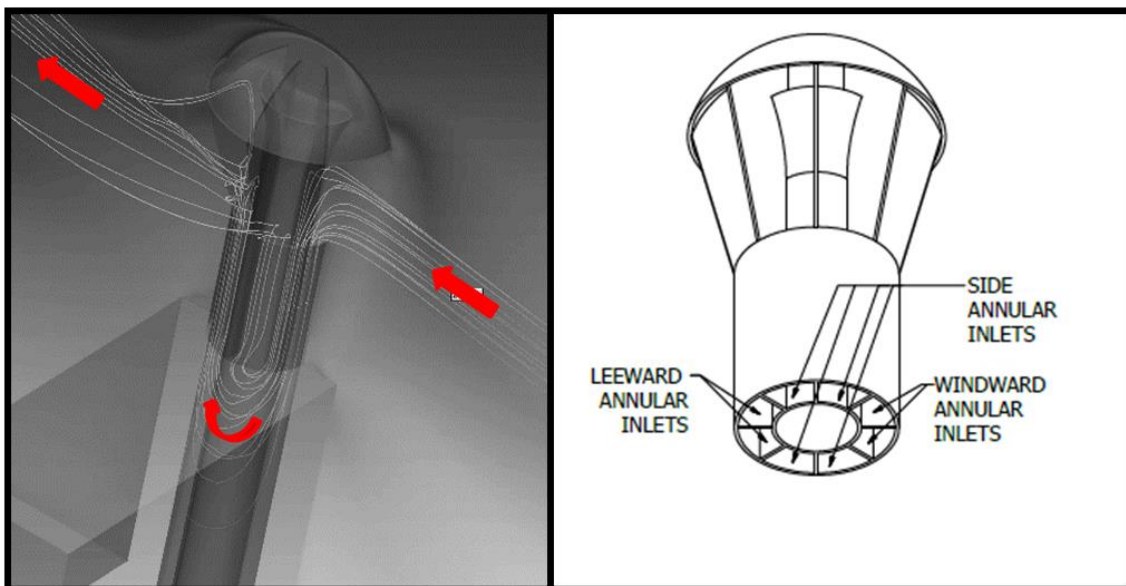


Figure 5-33: Short Circuit Flow

5.2.3.1 Flow Rates

A substantial percentage of the captured flows in all models escape via the leeward annular inlets of the windcatcher. The captured air stream goes down the windward inlets and short-circuits at the base of the windcatcher as shown on Figure 5-33, with only a proportion going down into the annular air supply channel. Figure 5-34 and Figure 5-35 shows the ratio of short-circuit air flow to that supplied at room level, for all the windcatcher models at 4.5m/s and 0.5m/s incident wind speed.

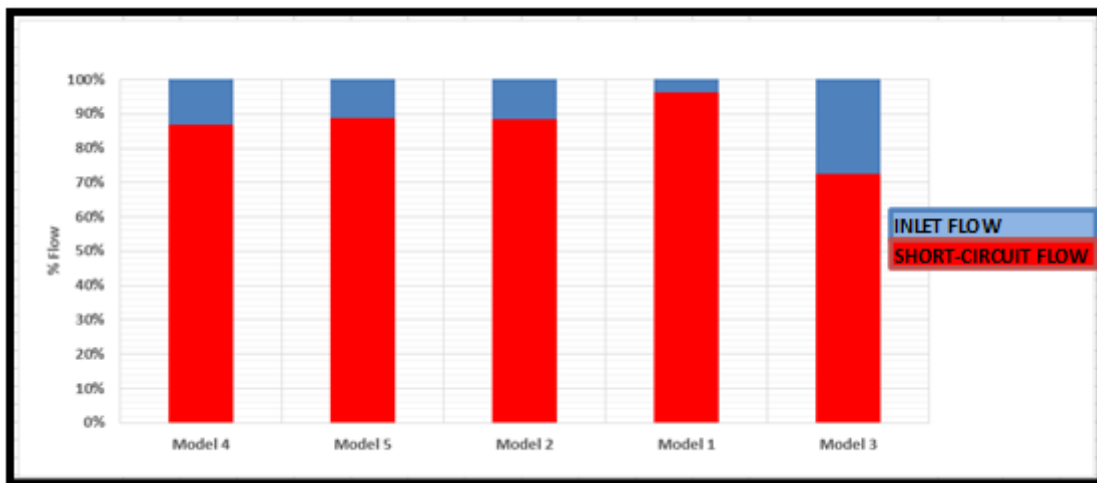


Figure 5-34: Percentage Short Circuit Flow at 4.5m/s Incident Wind Speed

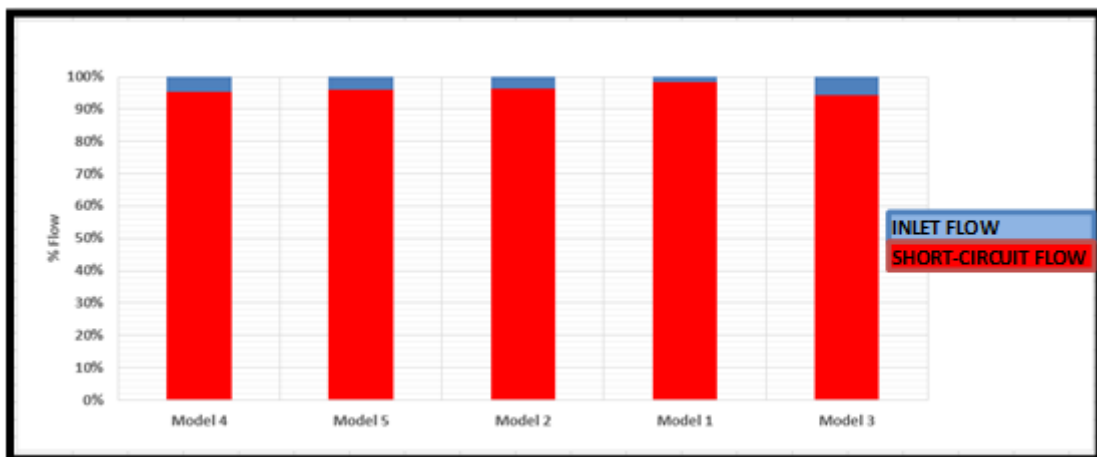


Figure 5-35: Percentage Short Circuit Flow at 0.5m/s Incident Wind Speed

Figure 5-36 and Figure 5-37 shows the actual short circuit and air supply flow rates for all simulated windcatcher models at 0.5m/s and 4.5 m/s incident wind speed.

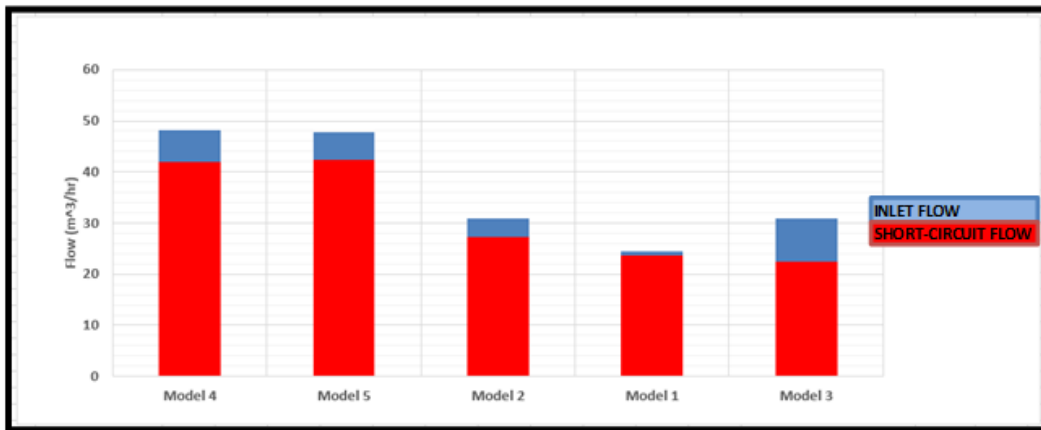


Figure 5-36: Actual Short Circuit flow at 4.5m/s Incident Wind Speed

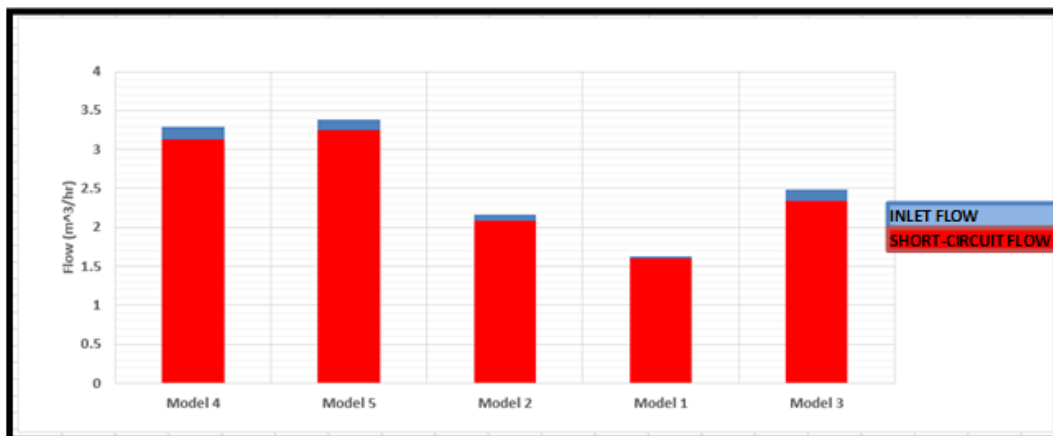


Figure 5-37: Actual Short Circuit flow at 0.5m/s Incident Wind Speed

Even though the 4 inlets geometry of Model 2 presented a larger surface area per annular inlet, Models 4 and 5 induced more flow than all other models. The acute angle presented by the moved plate in Models 4 and 5 plates, channelled most of the flow incident on it into the inflow channel. Same cannot be said of the

plate for Model 2 with 4 channels as some of the air stream incident on it flows sideways away from the supply channel. This phenomenon is illustrated in Figure 5-38.

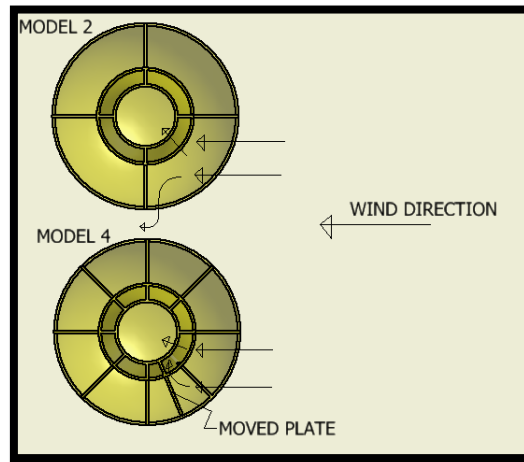


Figure 5-38: Incident Wind Direction

Models 2 and 3 both have their annular inlets divided into 4. However, the dividing plates on Model 2 are slanted while those on Model 3 are full and extruded to the extents of the dome. A look at the total volume flow rate induced into the supply channel for both, shows that the bigger dividing plates facilitated a higher flow rate at low incident wind speed (Figure 5-37) but this becomes less at the higher wind speed. As shown on Figure 5-36, at 4.5m/s wind speed, the total induced volume flow rates for both models are almost equal. The extended plates did not produce a significant increase in inflow; most flow streams incident on extra extruded section of plate escaped and flowed sideways along the side of the windcatcher as the stagnation pressure of the early fluid stream hitting the plates builds up and pushes the later streams further sideways. Since the extruded fins induced more flow at a low incident wind speed they can be thought of as a self-regulating feature of this windcatcher model which induces more air flow at low wind speeds and becomes less effective as wind speed increases. This serves to provide relatively constant air flow irrespective of the prevailing wind speed.

Model 1 captured the least total inlet volume flow rate. This is mainly due to the surface area presented by the dividing plates and smaller area per annular inlet compared to those on all other windcatcher models.

Generally, a closer look at the total values of the induced flow rates into the supply channels shows them to be adequate for all geometries if the short-circuit flow can be eliminated.

5.2.3.2 Pressure

Short-circuit flow is largely due to flow separation which causes negative suction pressure to be generated at the leeward end annular inlets. Figure 5-39 shows the pressures at each annular inlet for Model 1. The values are taken just below the annular inlet surface for one half of the model. As discussed under heading 5.2.1.1, all the models are symmetrical about the vertical plane and only one half was used in CFD simulations.

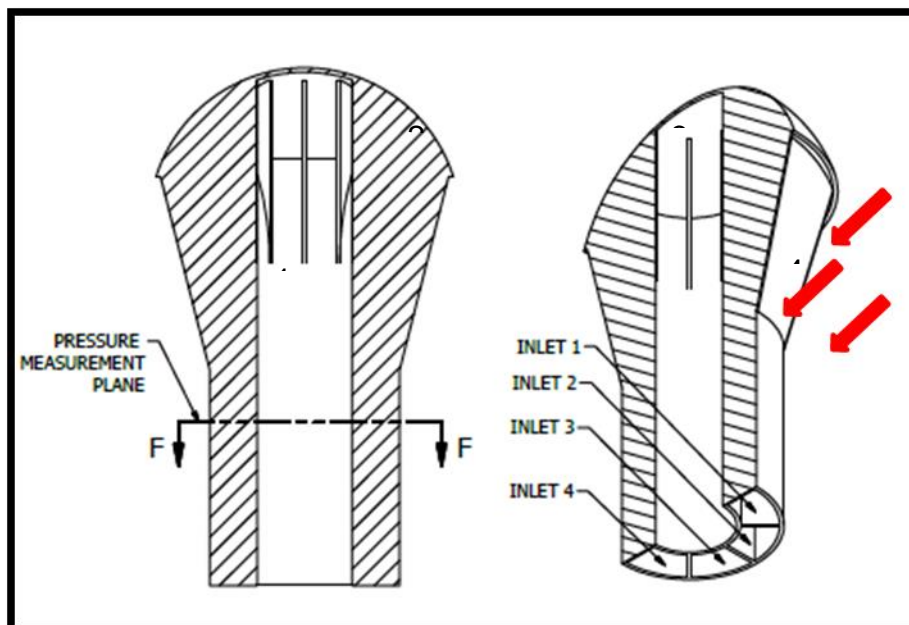


Figure 5-39: Model 1 Reference

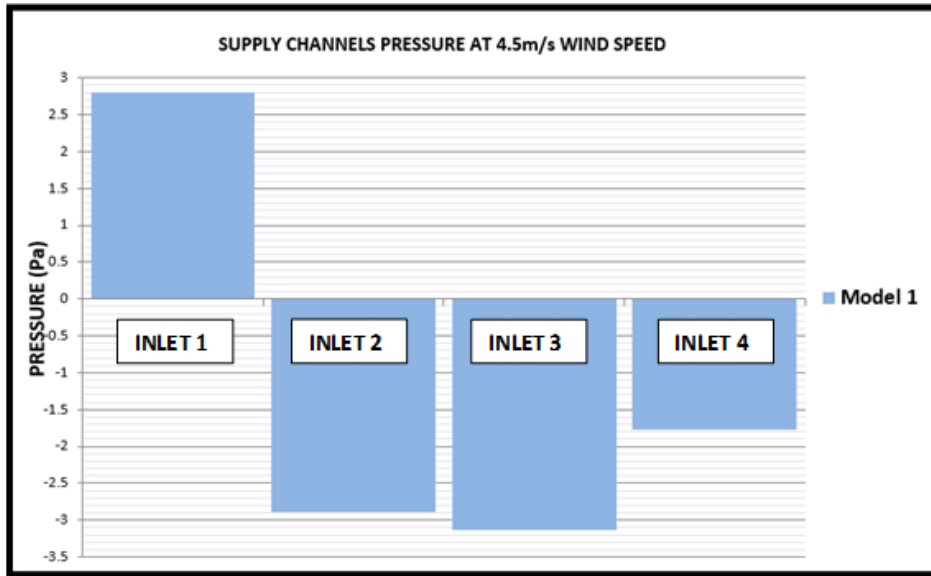


Figure 5-40: Model 1 Supply Channels Pressures At 4.5m/s Incident Wind Speed

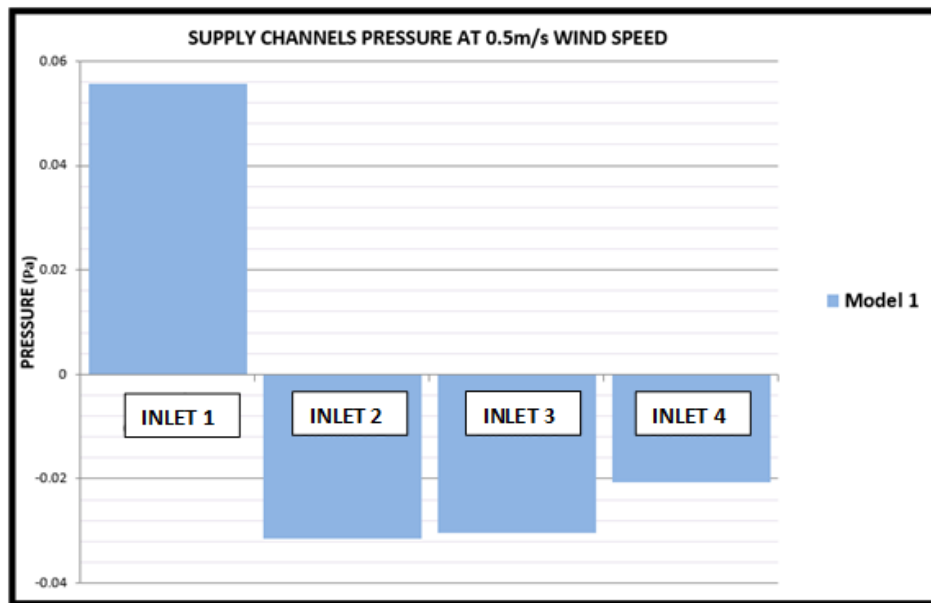


Figure 5-41: Model 1 Supply Channels Pressures At 0.5m/s Incident Wind Speed

The negative pressures indicate that the relevant annular inlet is in suction while positive pressures indicate an inflow down into the inlet. In Model 1, the smallest suction pressure occurs at inlet 4 which is the leeward end inlet channel. (Figure

5-40 and Figure 5-41). Inlets 2 and 3 have the highest suction pressures with that in inlet 2 as the lesser. This is caused by the little incident wind which gets into inlet 2 compared to inlet 3 which is totally shielded from the incident flow. This also follows earlier observation under heading 5.2.2, where it was observed that extract flow from the central outlet is mainly through the side dome sections because of the high negative suction pressure there.

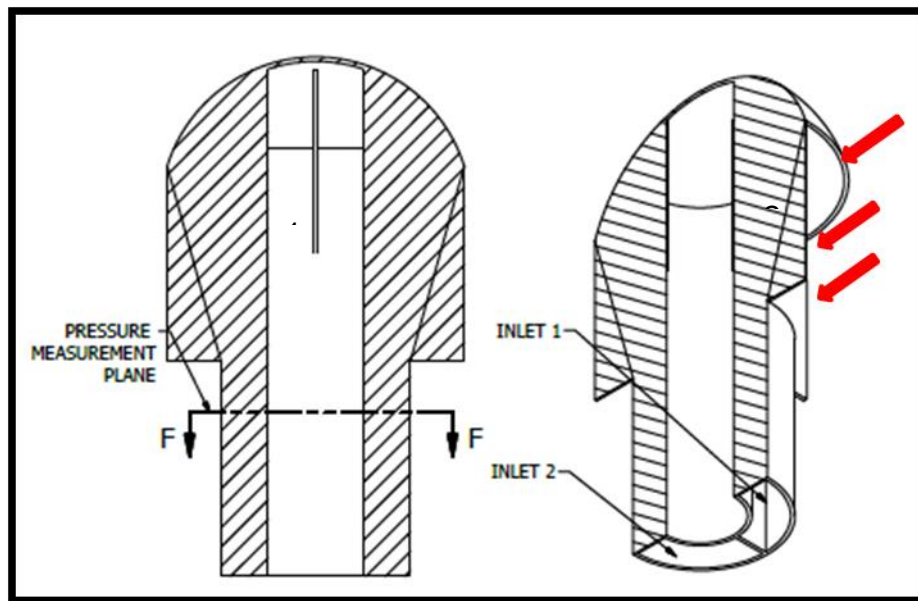


Figure 5-42: Model 2 & 3 Reference

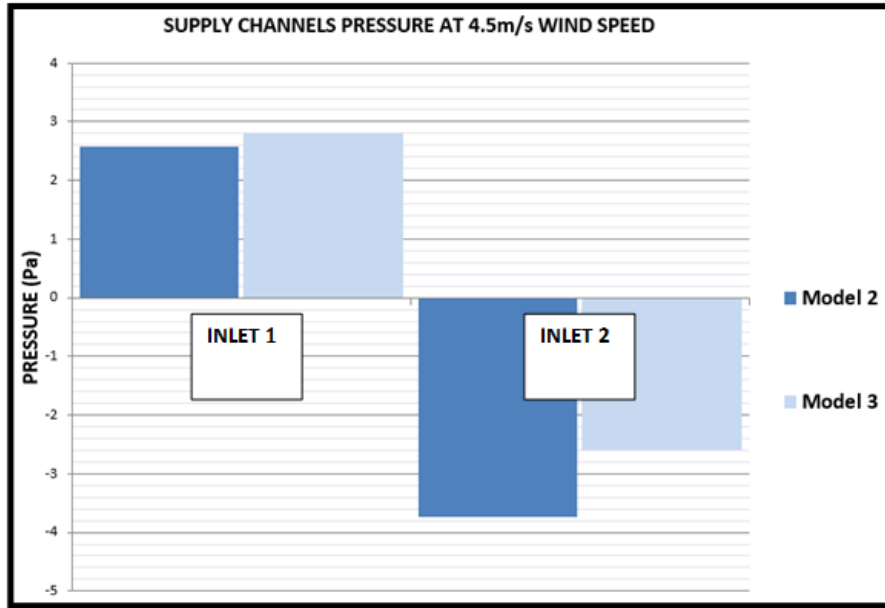


Figure 5-43: Models 2&3 Supply Channels Pressures at 4.5m/s Incident Wind Speed

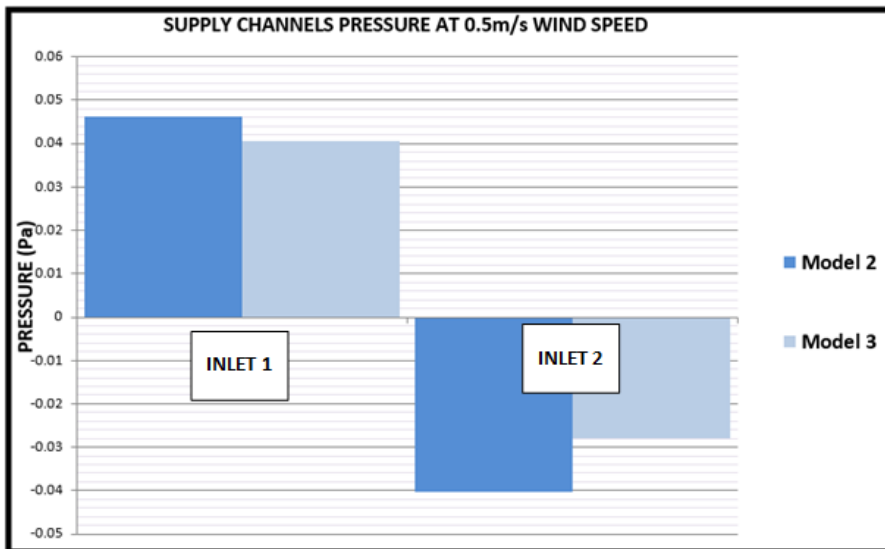


Figure 5-44: Models 2&3 Supply Channels Pressures at 0.5m/s Incident Wind Speed

Model 2 and 3 have the same number of annular inlets with the only difference being in the size of dividing plates and the number of sections under the dome.

As explained under heading 5.2.2, the dividing plates play a role in providing higher supply volume flow rates for Model 3 up to 4.5m/s incident wind speed, at which the total induced supply flow rate become almost equal with that of Model 2. However, Figure 5-20 shows an annular inlet flow rate at room level for Model 3 which is around twice as much as that for Model 2 at 4.5m/s wind speed. This is caused by a difference in the leeward end negative suction pressure for both models. The flow exiting the dome section at the leeward end also contributes to the negative pressure effect there. For Model 2, because a significant proportion of the incident flow stream under the dome is directly obstructed by the dividing plates at right angles to the flow path and it flows down into the central outlet, a higher negative pressure is induced at the leeward end. In contrast, the incident air flow in the windward dome section in Model 3 tapers the flow stream through the constriction and a larger proportion exits at the leeward end. The induced negative suction pressure at the leeward end is greater for Model 2 compared to Model 3. This has the effect of increasing the ratio of the captured incident flow that goes into short-circuit for Model 2 giving Model 3 a higher inlet flow rate at room level (Figure 5-36 and Figure 5-37).

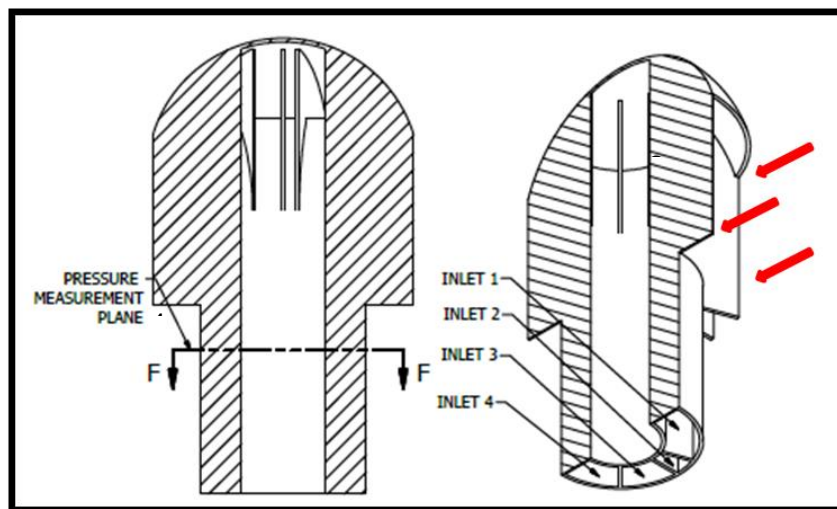


Figure 5-45: Models 4&5 Reference

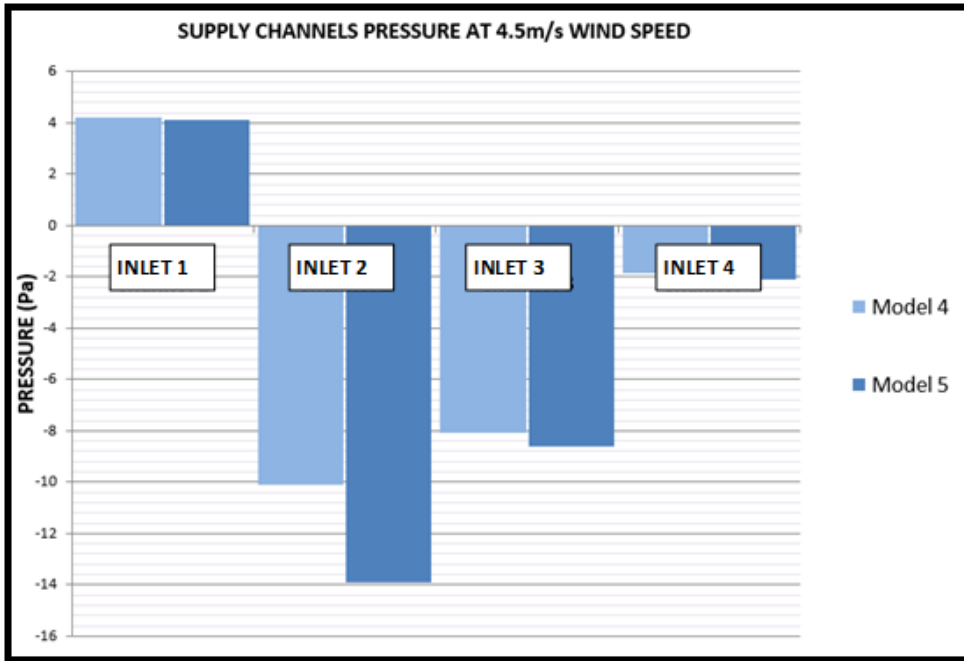


Figure 5-46: Models 4&5 Supply Channels Pressures at 4.5m/s Incident Wind Speed

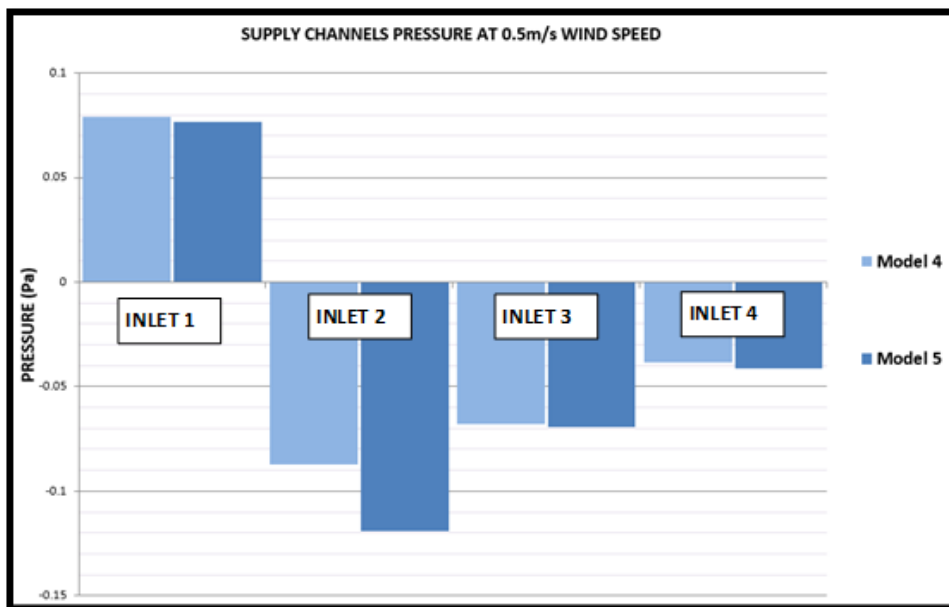


Figure 5-47: Models 4&5 Supply Channels Pressures at 0.5m/s Incident Wind Speed

A comparison of Models 4 & 5 (Figure 5-46 and Figure 5-47) show similar trend to that of Model 1 with the greatest suction occurring at the side inlets. However, in this case, the greatest suction occurs in inlet 2 because most of the incident wind is captured through inlet 1 and the smaller inlet 2 sees relatively lesser incident wind compared to that in Model 1. Thus, it experiences a greater negative pressure.

The negative pressure induced in inlet 2 is marginally greater at all wind speeds for the Model 5, hence more of the inflow is lost for that geometry compared to Model 4.

5.2.4 Final Prototype

It is proposed that the inclusion of a lightweight non return valve mechanism in the annular inlets could help reduce or eliminate the short-circuit flow. The non-return valve would take the form shown below, which consists of a simple lightweight rigid material hinged on the outer wall of the central outlet at one end and rested on a tiny wedge on the same outer wall at its other end. The rest position of this valve is in the fully open position. In operation, the valve arrangement will permit unrestricted flow downwards into the air supply inlets but any outflow pressure will swing it from its rest position to block the channel, thereby preventing further outflow. It is expected that, with the mechanism described above, only the minimal outflow required to raise the valve plate to shut the relevant inlet will be lost in operation and the bulk of the flow values shown in Figure 5-36 and Figure 5-37 will be available at room level. A 2D representation of the gate valve is shown below.

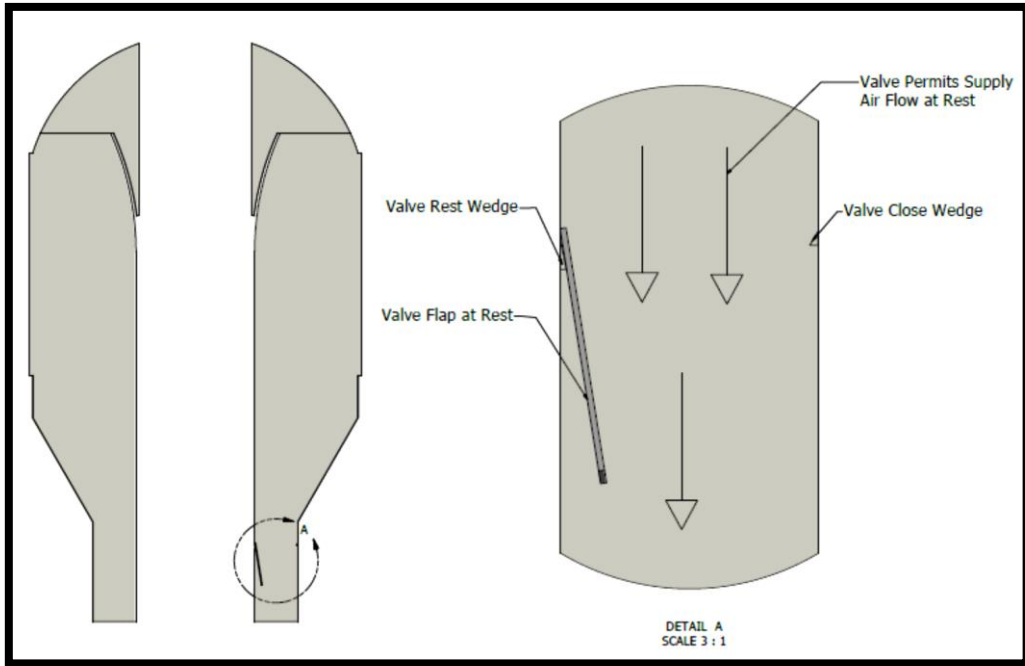


Figure 5-48 Valve at Rest Position

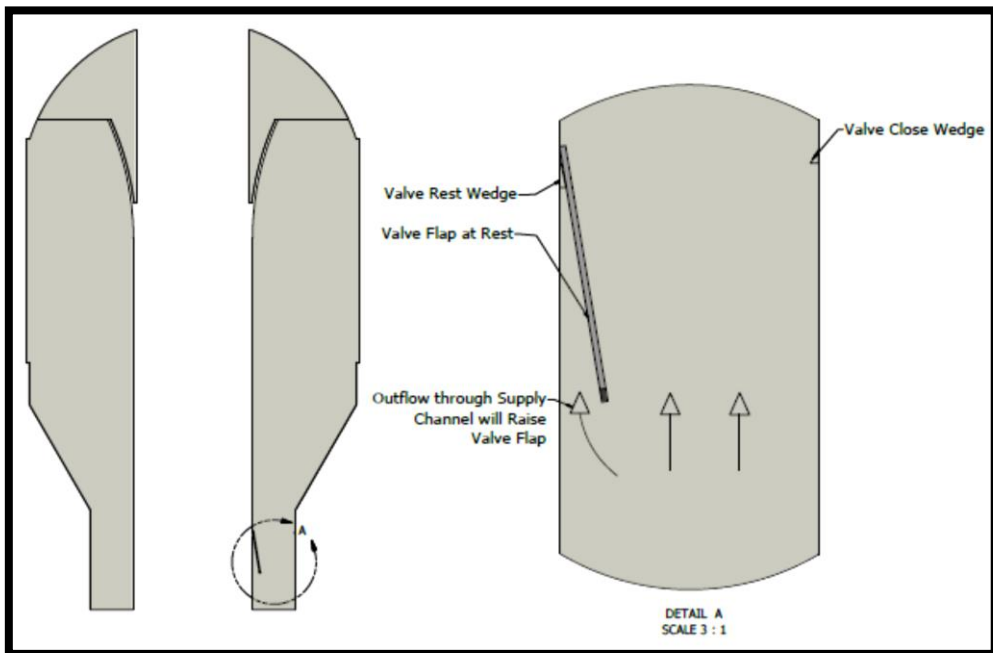


Figure 5-49 Valve Action against Outflow

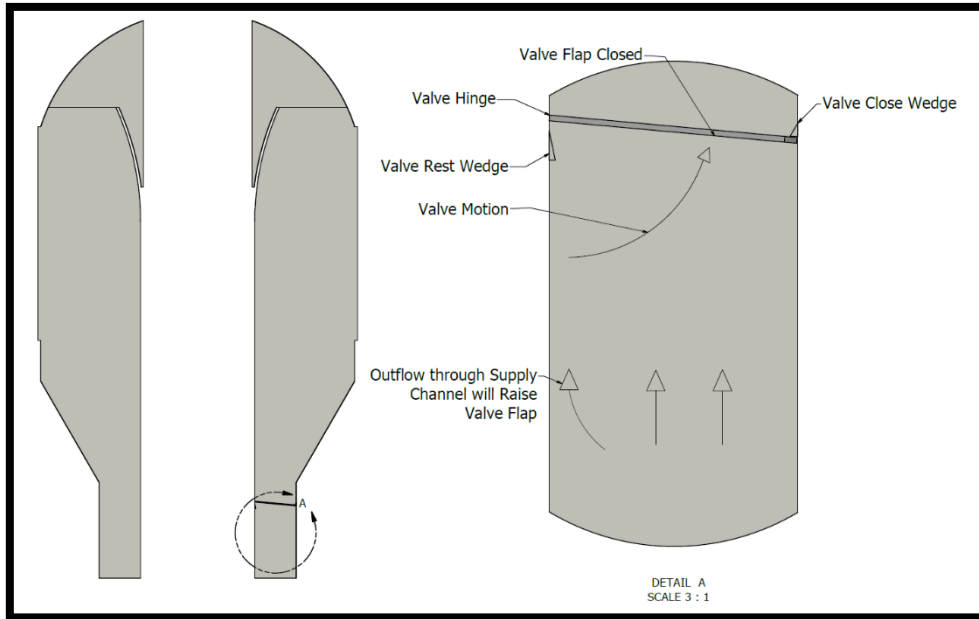


Figure 5-50 Valve in Closed Position Preventing Further Outflow

To make the above the valve mechanism resilient to flow variations, a three-gate interacting arrangement can be used which locates one gate on the side walls and back wall of each channel. This arrangement will be able to utilise channel flow of varying intensity where the portion of the fluid flow containing the most energy is not close to the back wall (hinge location). While this introduces more moving parts into the windcatcher, it offers a better coverage of the annular channel for short-circuit flow regulation. A representation of the three-gate mechanism is shown below for one annular channel.

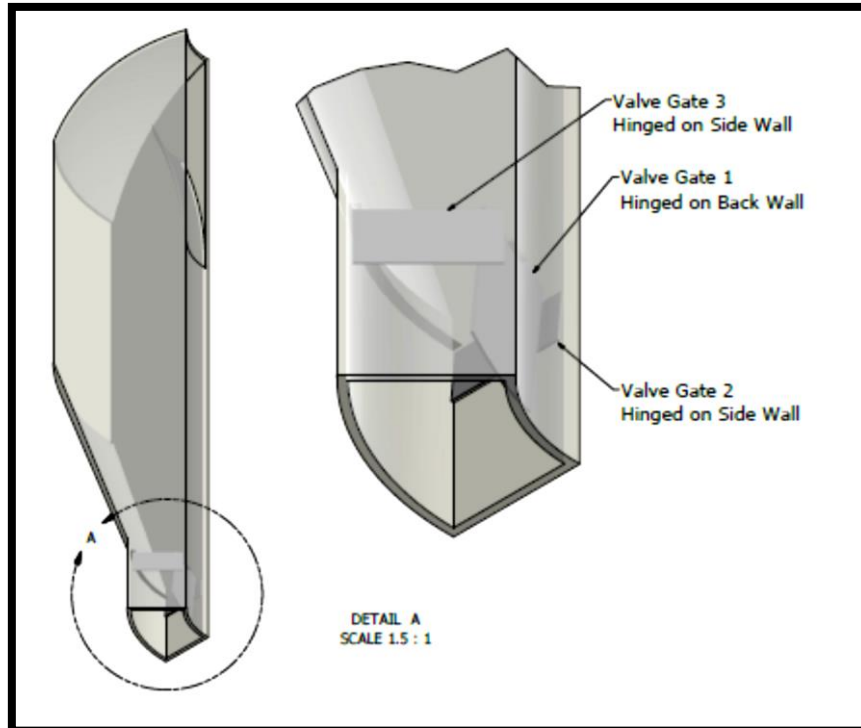


Figure 5-51 Three-Gate Valve Arrangement

Though Model 5 presented the best air flow characteristics, the proposed mechanism of non-return valve is not suited to that geometry because of the moving plates. Hence, a variation of Model 1 has been resolved to be the most suitable. An extruded plate has been added to it to enhance the flow rates at low wind speeds. The annulus has also been enlarged and a funnel section added to it. The windcatcher has a height of 600m, body diameter of 213mm and dome cap diameter of 336mm. The centre extract channel has a surface area of $0.011m^2$ and the annular supply channels have a total surface area of $0.023m^2$. The final prototype windcatcher is shown below in Figure 5-52.

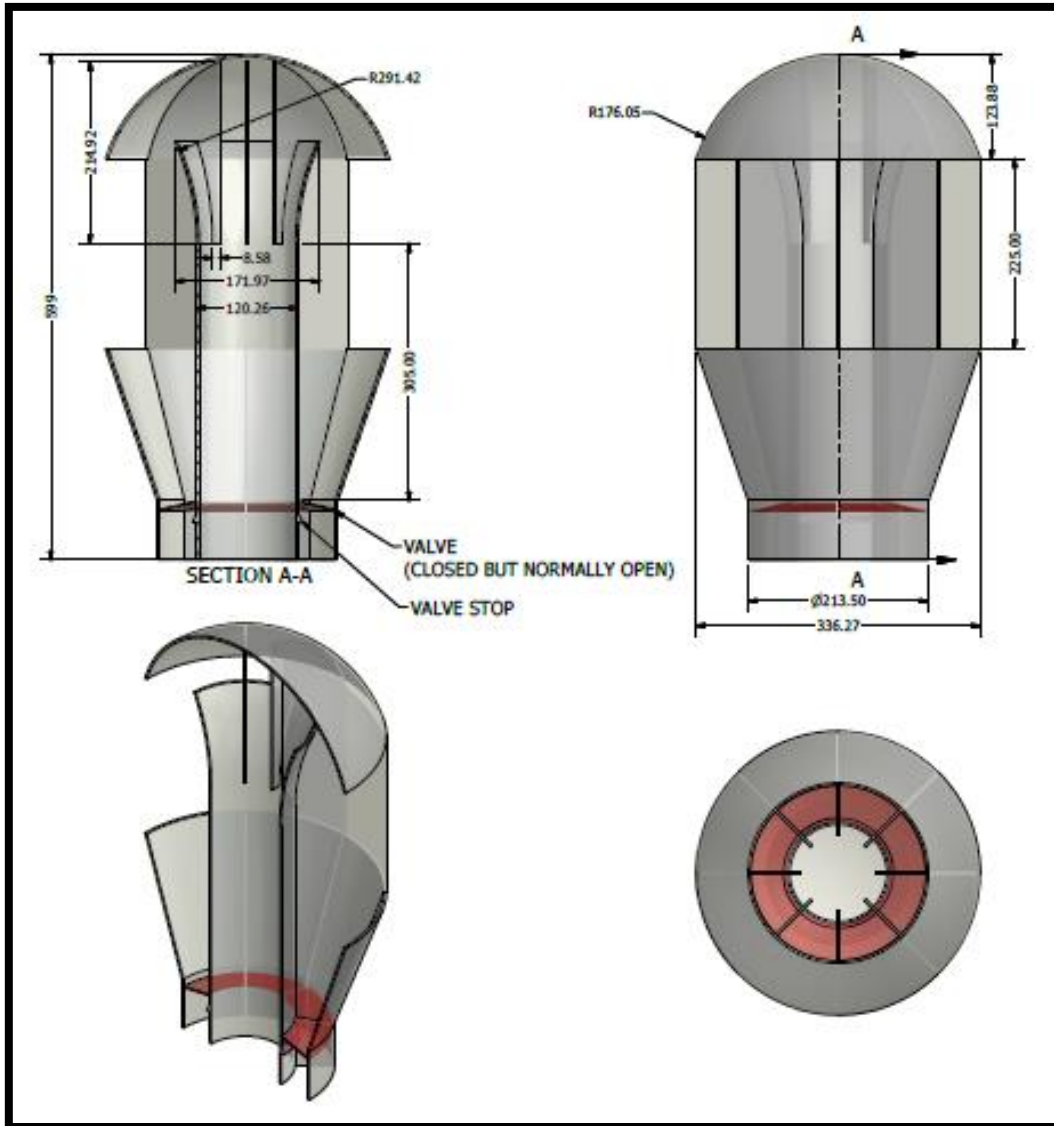


Figure 5-52: Final Prototype with Non-Return Valve (units in mm)

This final model was simulated in Ansys Fluent v14 to investigate its flow performance.

5.2.4.1 Simulation Set-up

The following sub-sections discuss the Ansys Fluent v14 software settings and specifications applied in carrying out the final windcatcher performance simulations.

5.2.4.1.1 Simulation Model

The simulation model is of the same general dimensions as used in previous Autodesk CFD 2013 simulations (shown in Figure 5-3). Albeit, with this final windcatcher inserted. To mimic a closed valve situation in all annular inlets normally in extraction without the valve arrangement, those inlets were blocked. These were mainly the leeward end ones. As before only the air part was used in simulation. All solid parts were disabled.

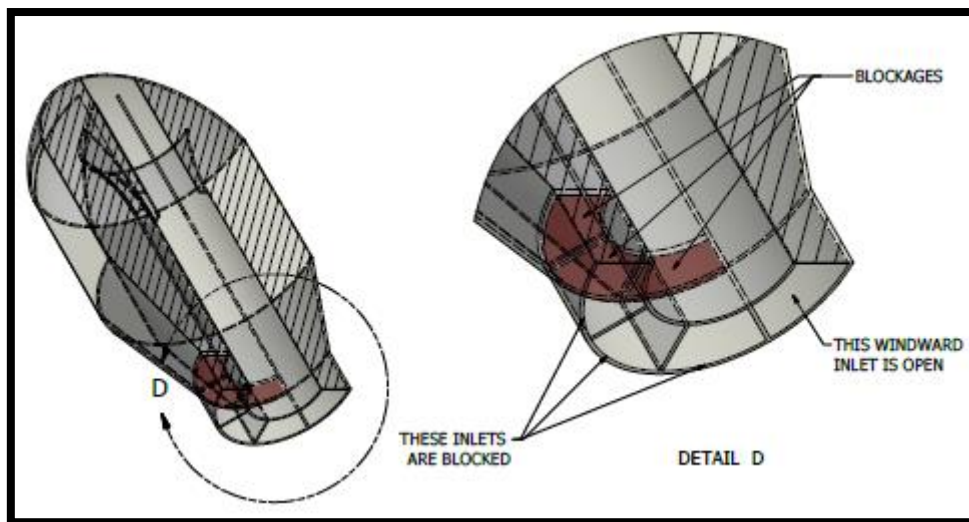


Figure 5-53: Simulation Model

5.2.4.1.2 Material

The material was set as air with fixed properties at 101325Pa and 19.85°C. This is a safe assumption in incompressible forced flow simulations where air velocities are well below Mach 0.3 as the little variations in material properties will not significantly affect the flow results

5.2.4.1.3 Boundary Conditions

Boundary conditions were the same as discussed under heading 5.2.1.2.2. Flow outlets were all set to zero-gauge pressure to simulate an inflow/outflow surface and velocity values were applied at the domain inlet. Symmetry boundary condition was applied at the mid-section plane, top and opposite side of the simulation domain. All other surfaces were treated as walls by default.

5.2.4.1.4 Meshing

Ansys v14 Meshing Advanced Sizing Function defines optimum element sizes to capture areas of strong curvature, and close proximity to neighbouring geometry in the model. This function was used to define a patch conforming tetrahedral mesh for the assembly. This was adjusted using the high smoothing and a “fine” setting for Relevance Centre. 10 inflation layers were specified on the wall boundaries to adequately resolve gradients at the walls. This provides a better representation of flow in this region and increases accuracy of the simulation results. Other meshing controls were left at their default values. The resultant mesh had ~19.3 million cells.

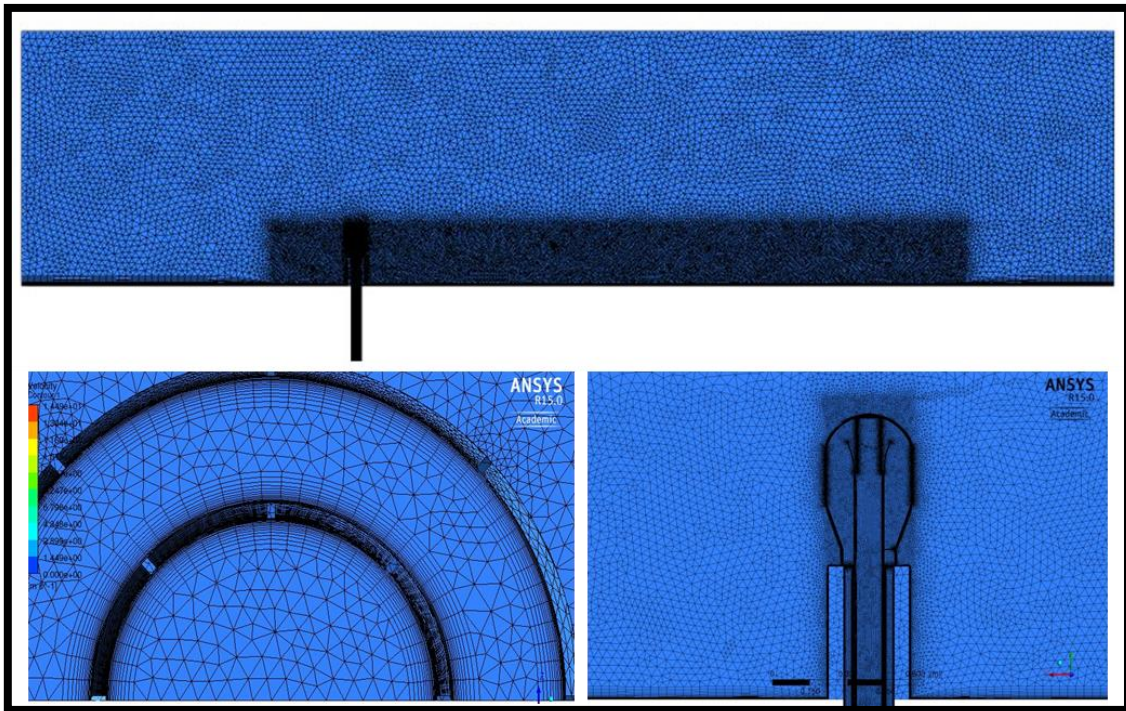


Figure 5-54: Ansys Windcatcher Mesh

5.2.4.1.5 Solving

As this model will be used in combination with the heat exchanger, steady state simulation was done using the SST $k - \omega$ turbulence model and the coupled Pressure-Based Solver (PBS) to carry out 1000 steps of calculation. The PBS

coupled solver yields superior performance and generally converges with less iteration. Hybrid initialization was utilized to give an initial value before iteration can begin. A realistic initial guess improves solution stability and accelerates convergence. Solution monitors were set to monitor air flow rate at the bottom surfaces of the central and annular channels. The values recorded at these points were used to determine the convergence state of the solution i.e. the solution was thought to have converged when the solution remained unchanged, the solution residuals are below a 10^{-3} tolerance and mass balance between inflows and outflows was below a tolerance of $10e-4$.

A mesh independence study was conducted at 0.5m/s domain inlet velocity to determine the optimum mesh for the simulation. At converged solutions, 4 subsequent mesh refinements were performed based on scaled gradients of velocity in the entire domain. All regions with gradients higher than 10% of the maximum were marked and adapted. As shown on Table 5-2, solutions of flow mass-weighted average velocities taken at the channel surfaces were broadly similar for all meshes. Nevertheless, Mesh 3 was chosen as it is close to the number of cells used in previous Autodesk CFD simulations, and it gives a good balance between computational effort and mesh refinement in areas of high gradient.

		Mesh 1	Mesh 2	Mesh 3	Mesh 4
	Cell Count (Millions)	9.5	16.8	19.3	21.0
Annular Channel	Air velocity (m/s)	-0.084	-0.083	-0.083	-0.083
Central Channel	Air velocity (m/s)	0.125	0.099	0.124	0.124

Table 5-2: Mesh Independence Test results

5.2.4.2 CFD Simulation Results and Discussion

The windcatcher model was simulated at incident wind-speeds of 0.5m/s , 1.5m/s , 2.5m/s , 3.5m/s and 4.5m/s . Converged values of air flow rate through the annular and central channels were recorded at each wind speed. The measurement was taken at the respective surfaces of each channel at room level.

Velocity values are mass-weighted average values over the measurement surface.

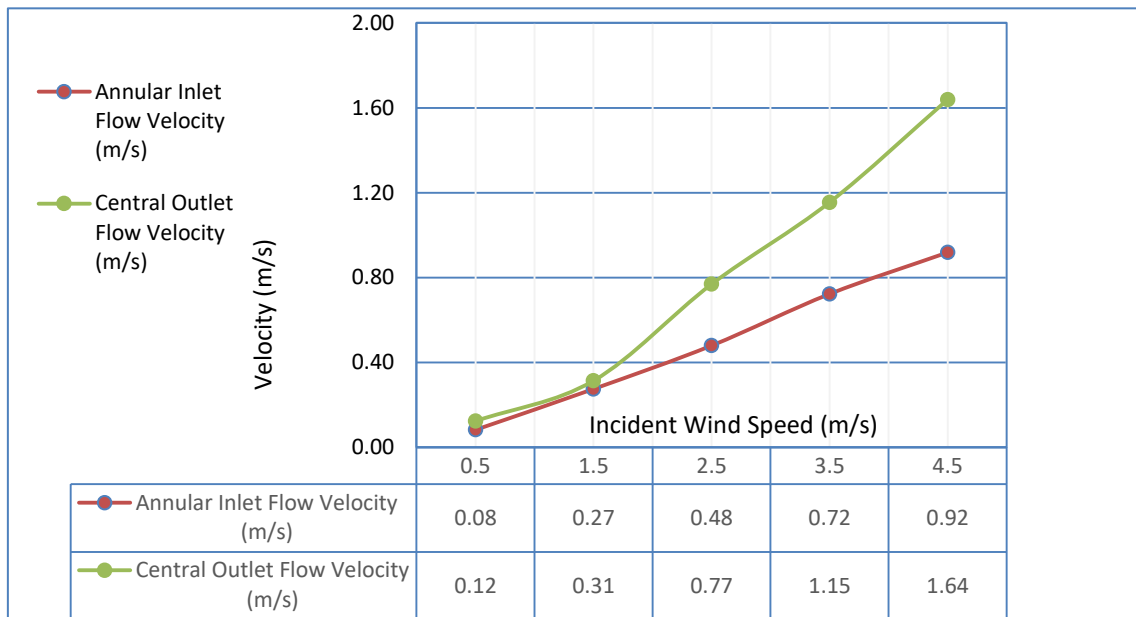


Figure 5-55: Windcatcher Channel Velocities

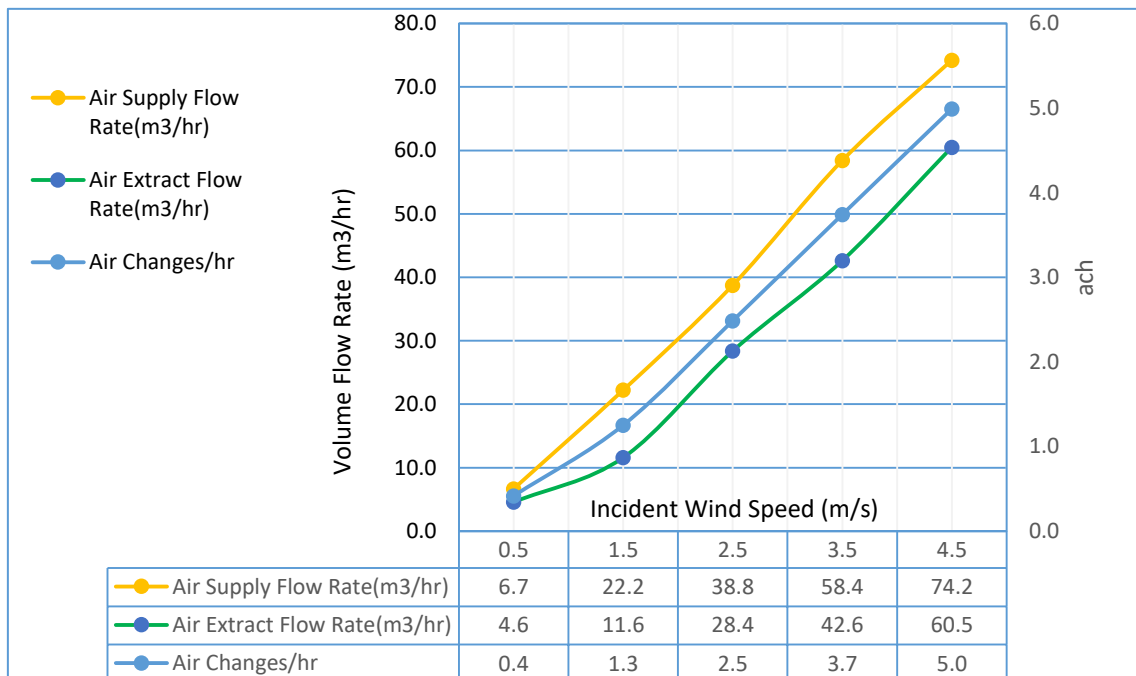


Figure 5-56: Windcatcher Flow Performance

At all wind speeds, the windcatcher exhibited the desired flow pattern with no short-circuit. Incident air flow captured in the annular inlet flowed downwards and extract flow through the central outlet flowed upwards. Values of flow rates through both channels increased steadily as the incident wind speed increased. The ventilation performance was compared in Figure 5-56 with the limit of 0.7ach set under section 5.2.1. The air changes per hour values are also plotted for the design room. At all simulated incident wind speeds above $\sim 1\text{ m/s}$, the windcatcher provided adequate levels of ventilation (limit is 0.7ach). This increased almost linearly to 5 ach at an incident wind speed of 4.5 m/s . Given that the typical low wind speed in UK urban areas is around 3 m/s [253] corresponding to 3 ach for the test room, this result indicated that the windcatcher is capable of providing the required ventilation flow rate.

Figure 5-56 also shows the air supply and extract flow rates at the simulated wind speeds. Across all scenarios, the central outlet extract flow rate was on the average 30% less than that of the inlet supply flow (Figure 5-56). This is desirable as buoyancy will add to the extract flow rate bringing it closer to the supply flow rate. A significantly stronger extract flow through the central channel can induce severe short-circuiting at room level.

5.2.5 Autodesk CFD Results Comparison

The final windcatcher prototype was simulated in Autodesk CFD to compare results from both CFD packages. The same 3D domain was utilized as in Ansys Fluent with the same boundary conditions and material specification. The intelligent adaptation in Autodesk CFD works by running a specified number of times to convergence, then using the gradient of velocity, pressure and temperature to refine the mesh in the simulation domain at the end of each run. The mesh independence values are reported in the output bar for pressure, velocity and temperature. Three adaptation cycles were specified for the simulations and carried out to achieve a mesh independence value of 95% for pressure, 98% for velocity and 97% for temperature. The final mesh had 18million cells. The simulations were carried out as an incompressible flow using the SST $k - \omega$ turbulence model at 0.5 m/s , 1.5 m/s , 2.5 m/s , 3.5 m/s and 4.5 m/s wind

velocity at the domain inlet. All windcatcher channel flow measurements were taken at the surface of the annular and centre channels as mass-weighted average values. Vector plots of the flow direction at the lowest and highest wind speed simulated are shown below.

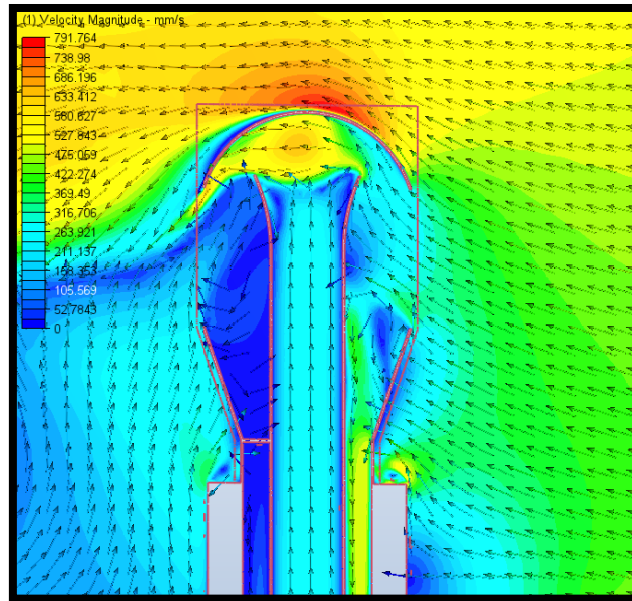


Figure 5-57 Autodesk CFD Windcatcher Velocity Vectors at 0.5m/s Wind

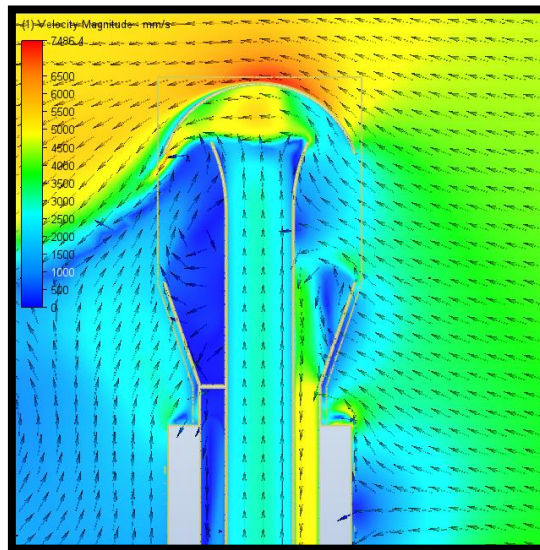


Figure 5-58 Autodesk CFD Windcatcher Velocity Vectors at 4.5m/s Wind

The channel flow directions performed as desired in a same fashion as the Ansys simulation. Flow directions in the annular channels was downwards at all wind speeds simulated and that in the central channel was extractive and upwards. A comparison of the flow velocities for both software packages is presented in Figure 5-59.

The predicted annular and central channel velocities in Autodesk CFD were more than those predicted by Ansys Fluent at all wind speeds. The mass-weighted average velocities in the annular supply channel were on the average 5% less in Ansys Fluent, and those in the central extract channel were 10% less. Within the range of quantities, these are minor differences. Especially as the compared values are surface averages. Differences can be due to many factors within the simulation setup, mesh count and software algorithm.

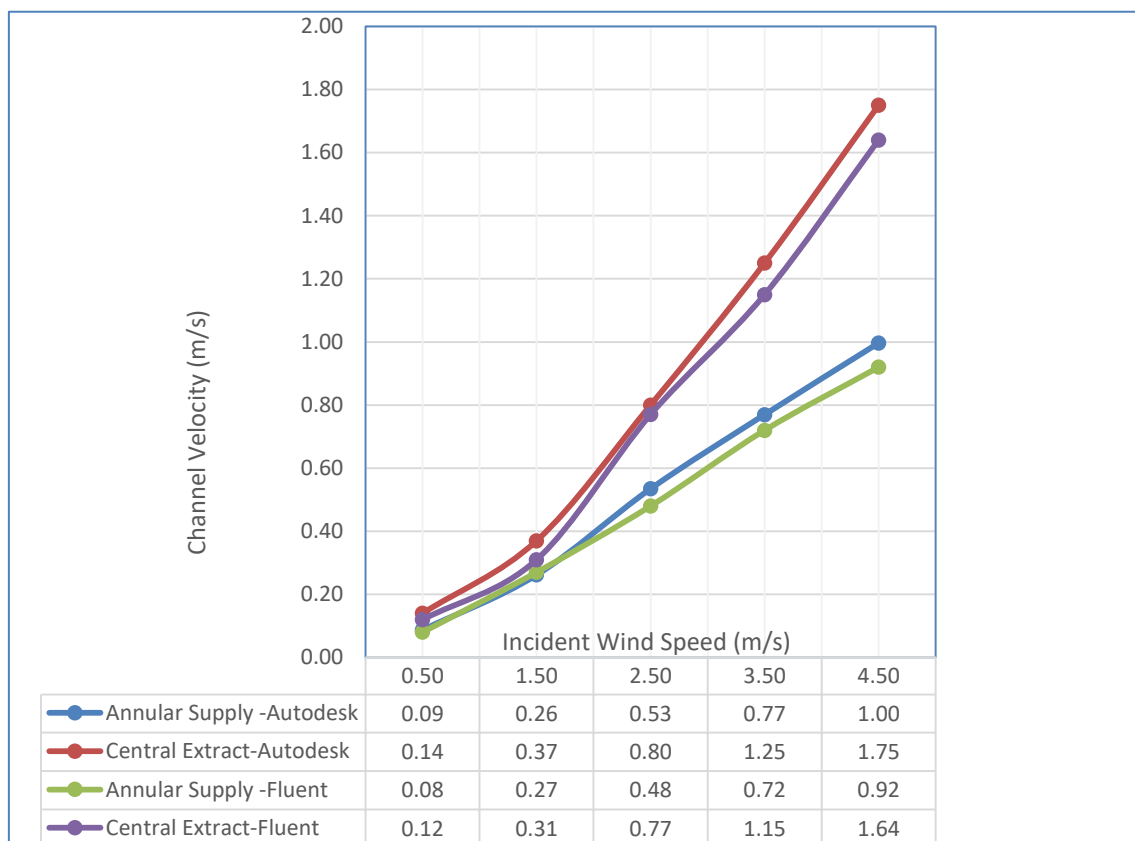


Figure 5-59 Comparison of Predicted Channel Velocities

6 HEAT EXCHANGER DEVELOPMENT

A heat exchanger is any device between two or more materials at different temperatures for the purpose of transferring heat energy between the materials. In most heat exchangers, the materials are never in direct contact. They are separated by a wall which acts as the heat transfer surface. When the heat exchange happens in transient manner, the heat exchanger is broadly known as a recuperator. In contrast, devices which transfer heat at intervals between materials are known as regenerators [40]; [254]. In most recuperators, the heat is simply conducted through the separating wall. In others like heat pipe heat exchangers, a combination of working fluid conduction and convection is involved [255]; [256]. Further classifications of heat exchangers are made based on different characteristics of the device, fluid and heat exchange mechanism. While it is possible to have moving parts such as fans, agitators and stirrers within heat exchangers. Most heat exchangers are passive devices, mainly consisting of the heat transfer element and the fluid distribution element [257].

Existing heat exchanger technologies are discussed under following sections to highlight their pros and cons and examine their suitability for the heat recovery ventilation system proposed in this research.

6.1 Design Considerations

Heat exchangers are very common and different configurations already exist with different modes of operation. Under this heading, existing heat exchanger technologies are reviewed to determine their suitability for the proposed natural ventilation system. While pressure drop and thermal properties are of paramount importance in quantifying the unit performance of heat exchangers, the proposed system presents geometrical and application restrictions which must be satisfied to establish suitability.

6.1.1 Heat Transfer Process in Heat Exchangers

Depending on whether fluid streams come into direct contact or not during heat exchange, heat exchangers can be divided into indirect-contact and direct-contact types [122].

6.1.1.1 Indirect Contact Heat Exchangers

In indirect-contact heat exchangers, fluid streams are kept separate from each other, only exchanging heat through impervious conductive surfaces. These type of heat exchangers can further be divided into direct-transfer and storage types [40].

Direct-transfer indirect-contact heat exchangers are basically recuperators. Transient heat transfer is achieved by the continuous flow of fluids in channels on opposite surfaces of the impervious primary heat transfer surface. They have no moving parts and can come with fins to provide extended heat exchange surfaces. Common examples are the plate heat exchangers, tubular heat exchangers etc. [41]. Plate heat exchangers have seen many uses in ventilation systems. Many commercially available mechanical heat recovery systems contain plate heat exchangers at their core.

In storage-type indirect-contact heat exchangers, the thermally interacting fluids are intermittently passed through a heat storage medium. During the hot blow phase, when hot fluid is passed through the heat exchanger, heat energy is extracted and stored. The cold blow phase introduces the cold fluid which extracts the stored heat. In most cases, parts of the fluids are inevitably retained in the storage medium and a small degree of mixing is present [64]. Hence, this technique is only applicable to processes in which minimal levels of mixing is tolerable. Such applications can be found in processes exchanging heat between similar gases at different temperatures. The heat storage medium usually consists of a matrix of tiny cells of conductive material. However, phase change materials can be used in low-quality heat applications with extended hot/cold blow periods [42]; [258]. This technique is employed in rotary heat exchangers such as can be found in many commercial air handling units for ventilation applications. The heat exchange matrix is rotated by a small variable speed electric motor for

performance control. In natural ventilation systems requiring no electrical power input, the electrical power requirement of this technique makes it unsuitable unless natural means are employed in driving the thermal wheel. In cases where the storage medium is stationary, an intermittent control of the cold and hot air streams is also needed to effect the heat transfer. All these inevitably complicate the system. In a system such as that proposed in this study, the heritage application and physical dimensions of the system makes this onerous to achieve.

6.1.1.2 Direct Contact Heat Exchangers

As the name implies, these types of heat exchangers bring the fluids in contact. This technique is commonly employed when the fluids are chemically compatible and immiscible. Therefore, this technique does not lend itself to use in air to air heat exchangers such as that required for the proposed system. Condensation of oil vapour with water is a common example using immiscible fluids. In addition to heat transfer, mass transfer also occurs as part of the heat transfer process. An example of this can be found in cooling towers of large HVAC systems where water is used to directly cool air with associated evaporation of the water. The absence of a heat transfer surface nullifies the problem of fouling. With the mass transfer inherent in direct contact heat exchangers, very high heat transfer rates are possible [40].

6.1.2 Heat Exchanger Construction

Based on the physical construction, heat exchangers can be broadly classified into tubular, plate, extended surface and regenerative heat exchangers [40].

6.1.2.1 Tubular Heat Exchangers

Tubular heat exchangers generally consist of one or more tubes. They are primary surface heat exchangers and are mostly used in liquid-liquid/gas applications to take advantage of high specific heat capacities of one or both of the heat transfer fluids. They can be found in process industries, where they are used extensively as condensers, boilers, steam generators, evaporators etc.

Common examples of tubular heat exchangers are spiral tube, shell and tube, and double pipe heat exchangers.

Spiral tube heat exchangers are shell and tube in their basic form. However, the tubes are wound in a spiral form to accommodate more heat transfer surface area. They suffer from cleaning problems and are mostly applied in processes where fouling is very little [42].

Shell and tube heat exchangers are particularly very common; they generally consist of a tank or shell containing one process fluid surrounding a bank of tubes carrying the other. Depending on their design, fluids can be made to go through the channels in single or multiple passes to enhance performance. This is easily achieved by bending or coiling the tubes in the tube channel or introducing baffles in the in the shell. High pressure drops are inherent in this technique and it does not lend itself to naturally driven air flows.

Double pipe heat exchangers are relatively better in terms of pressure drop for a heat exchange performance. They are simply concentric tubes with the fluids flowing separately in the central and annular channels, and are usually designed for counter flow applications. However, longer channels are usually required for similar heat exchange performance, and they quickly become relatively expensive per unit heat transfer [42]. The chimney cavity and flow configuration of the proposed system lends itself to the utilization of this heat exchanger construction. However, this must be balanced with allowable pressure drop in the heat exchanger module. The available chimney cavity length available is not limitless. A good design should be compact to facilitate ease of installation and also be efficient in recovering heat per unit length of heat exchanger material or chimney cavity length employed.

6.1.2.2 Plate Heat Exchangers

Plate heat exchangers consist of plate banks with the process fluids flowing on alternate sides of the plates. In common applications, the plates are tightly packed with small channels created between them by patterns of grooves on the plates. High heat transfer rates are achievable as the fluid flow through the

onerous channels and experience high pressure drop [41]. There are several patterns available based on the heat transfer rate and pressure drop desired.

Owing to their construction, plate heat exchangers generally, cannot accommodate high pressures or temperatures and are seldom used in such applications [41]; [257]. The low pressures and temperatures of ventilation air flow makes plate heat exchangers especially suitable. In turbulent flows, the turbulent moving fluids readily attach and detach from the heat exchange surfaces and fouling is seldom a problem [40]; [41]. Plate heat exchangers are also relatively flexible. Common types can be easily taken apart and expanded with more plates to adjust their performance. Also, due to their high heat transfer rates, tubular heat exchangers with comparable performance are usually 6 times larger in size [42].

If the properties and relative simplicity of plate heat exchangers can be combined with the concentric flow path configuration offered by tubular exchangers, an optimal geometry which offers the advantages of both constructions can be found for the ventilation system proposed in this research. Common materials for the plates include stainless steel and copper. In ventilation applications, polymer-based materials have received a lot of attention because of their resistance to fouling and corrosion and potential use for humidity control. [74]; [259]; [260]; [261]. They have been concluded to hold significant promise in ventilation heat recovery applications [67]. However, their relatively low thermal conductivity compared to traditional metallic materials makes their application unfavourable in natural ventilation situations requiring high heat transfer with low pressure drop within a compact geometry [262].

6.1.2.3 Extended Surface Heat Exchangers

The previous heat exchangers discussed under this section are all primary surface heat exchangers. When higher performance is required, especially in a limited space, the primary heat transfer surfaces can be increased by the addition of extended surfaces i.e. fins. Fins can increase performance by up to four times and are particularly useful when one or both of the process fluids is a gas [42]; [263]. Primarily because gases have smaller heat transfer coefficients compared

to liquids. These types of heat exchangers are referred to as extended surface heat exchangers. Careful design is necessary to develop extended surfaces. The additional pressure drop that will be experienced by the fluid must be taken into consideration. Also, depending on where the fins are located, they can either enhance or hinder general heat exchanger performance. In a tubular heat exchanger, fins located inside the tube, can reduce the heat transfer coefficient if not spaced properly. On the other hand, fins on the tube will, in all cases improve the heat transfer coefficient [42]. The fins can be plain, patterned or corrugated to induce turbulence and increase heat transfer.

6.1.2.4 Regenerative Heat Exchangers: Heat Pipe

Heat pipes heat exchangers are vacuum sealed tubular sections partially filled with a working fluid in liquid form. When one end of the section is exposed to hot fluid and the other to colder fluid, the working fluid goes through cycles of condensation and evaporation to do the heat transfer. The fluid at the hot end, absorbs heat from the hot fluid, vaporises and travels through the centre of the tube to the cold end where it releases the heat to the cold fluid and condenses back into liquid. This liquid adheres to the walls of the tube and travels back to the evaporator section. The liquid phase travel can either be driven by gravity, capillary action or a combination of both. Saturated Wick structures incorporated into the inner wall of the tube encourages adhesion and experiences capillary pressure as the liquid is vaporised at the evaporator end. This capillary pressure effectively pumps the liquid phase into the evaporator end. When capillary action is combined with gravity, the orientation of the heat pipe can speed up the capillary pumping or retard it. Hence, tube orientation can be used to regulate heat transfer rate in a heat pipe heat exchanger. In gas to gas applications, fins are usually added to external wall of the pipe to increase the heat transfer surface area and improve performance[255].

Working fluids in heat pipes are chosen based on the temperature of the application and compatibility with the tube material. Popular working fluids include water, ammonia and refrigerants [255]. Heat pipes have found numerous applications in natural ventilation heat recovery due to their high unit thermal

conductance [52]; [139]; [145]; [150]. When employed in natural ventilation systems, an extended heat transfer surface is usually required to effect reasonable heat transfer. Consequently, a balance must be established between pressure drop and thermal performance. The integration of heat pipes into windcatchers also presents its own geometrical problems. On the scale of the system proposed in this research, the integration must be carefully designed to avoid excessive flow obstruction. Overall, a heat pipe design of comparable thermal performance would present a lesser heat transfer surface for air flow. When fouling is considered, small surfaces can be quickly rendered ineffective compared to larger ones, thereby negatively affecting the long-term performance and maintenance requirement in a natural ventilation application. The cost of manufacture of heat pipes is also relatively higher when compared to plate heat exchangers.

6.1.3 Heat Exchanger Compactness

Space restriction in many process applications demands for progressively smaller heat exchangers. Light weight heat exchangers with performance values comparable to larger sized ones are not only attractive but tend to be more structurally robust [42]. A parameter which can be used as a basis for comparing heat exchangers based on their physical sizes is “compactness” [40]; [42].

$$UA = U\beta V = Q / \Delta T_m \quad \text{where } \beta = A/V \quad (3)$$

Where T_m = true mean temperature difference,

A = Heat exchanger surface area(hot/cold),

V = heat exchanger volume(hot/cold) and

β = compactness/heat transfer surface area density.

Actual classification across the different types of heat exchanger configurations is based the value of compactness " β " present in the equation above. It follows from this definition that; a compact heat exchanger will not necessarily be small in size. However, it will have to be bigger to give the same performance in a

specific application [42]; [264]. This classification is applied differently for gas-fluid and liquid-liquid/multiphase heat exchangers.

Gas-fluid heat exchangers with compactness greater than $700m^2/m^3$ are classified as compact if the other fluid is a gas. For heat exchange with a liquid or multiphase fluid, compactness implies a density of $400m^2/m^3$ or more. However, $400m^2/m^3$ in a liquid-liquid/multiphase heat exchanger, on any side of the heat transfer surface, classifies it as a compact heat exchanger [42].

Since gases are generally less dense with smaller heat capacities than liquids. To achieve a good level of heat exchange, gas-gas heat exchangers generally fall in the compact category. They are characterised by multiple flow passages making pressure drop an important factor in their design. To obtain uniform flow along the numerous passages, the design of the fluid distribution element (commonly the header or cap) is also very important.[40]; [42]; [264].

6.1.4 Heat Exchanger Flow Patterns

Depending on the flow direction of the hot and cold stream in heat exchangers, they can be classified into parallel-flow, counter-flow and cross-flow types. An important aspect of the performance of heat exchangers in the different categories is the temperature variation along the heat exchange surfaces. This provides an important tool for establishing the thermal performance of heat exchangers.

6.1.4.1 Parallel-Flow Heat Exchangers

In a parallel-flow heat exchanger, the fluid streams travel in the same direction along the heat exchange surfaces. At the entrance to the heat exchanger, it brings the hottest state of the hot stream, together with the coldest state of the cold stream causing a high temperature differential and heat transfer. This temperature differential gradually reduces asymptotically and approaches the same value along the flow direction. Consequently, only a limited thermal efficiency can be achieved by using a parallel-flow configuration in heat exchangers.

6.1.4.2 Counter-Flow Heat Exchangers

In counter-flow heat exchangers, the hottest state of the hot fluid is brought in contact with the hottest state of the cold fluid. Conversely the both streams are in contact at their coldest states at the other end of the heat exchanger. The thermal efficiency of this flow configuration is relatively high because it provides a nearly constant temperature differential along the heat exchange surface. However, they may require bigger sizes because of the small temperature difference between the fluid streams [43]; [44]; [45]. The counter-current flow configuration of the supply and extract air in the proposed natural ventilation system lends itself to a heat exchanger of this flow type. Therefore, only this flow configuration is considered for the system.

6.1.4.3 Cross-Flow Heat Exchangers

In a cross-flow heat exchanger, one fluid streams flow across the other. The temperature variation pattern in them is more is far more difficult to analyse beyond the scope of this work. They are commonly used as evaporative and condensation heat exchangers, and many different configurations are possible [265].

6.2 Modelling Heat Exchanger Performance

The performance of a heat exchanger can be quantified with some well-established parameters; these are discussed in the following sub-sections. This is an essential part of the design process. It enables design development from first principles and can often provide a good starting point for any heat exchanger design process. The discussion in this section will be in most parts, restricted to the heat exchanger type of interest i.e. counter-flow heat exchangers. The following assumptions are made.

- The mass flow rate of each air stream is constant throughout the process
- The energy-absorbing capacity of each air stream can be represented by a constant value of specific heat capacity over the range of operating temperatures.

- The air at each section across a flow passage is well mixed, so that a single temperature can be found to relate to its energy content.

These restrictions are not of great significance when the temperature ranges are modest, the heat exchange surface is impervious, and the flow channels are generally tube-like cavities along which temperature changes slowly. The parameters useful in modelling and design are discussed below.

6.2.1 Capacity Ratio

The product of the mass flow rate " \dot{m} " and specific heat capacity " c " at a constant pressure is known as the thermal capacity rate for a given fluid.

$$\text{For a hot fluid stream, Thermal capacity rate} = \dot{m}_h c_h \quad (4)$$

$$\text{For a cold fluid stream, Thermal capacity rate} = \dot{m}_c c_c \quad (5)$$

The thermal capacity rate for the hot and cold air determines the maximum amount of heat that may be transferred by a heat exchanger. The ratio of the thermal capacity rate for the hot and cold fluid is defined as the Capacity ratio. Capacity ratio is more important where the heat exchanger fluids are different. Hence, if hot fluid with a larger heat capacity rate is used to heat a cold fluid in a heat exchanger, the hot fluid temperature change will be much lesser than that of the cold fluid [266].

$$\text{Capacity ratio } C = \frac{\dot{m}_c c_c}{\dot{m}_h c_h} \text{ if } \dot{m}_c c_c < \dot{m}_h c_h \quad (6)$$

$$\text{or } \frac{\dot{m}_h c_h}{\dot{m}_c c_c} \text{ if } \dot{m}_h c_h < \dot{m}_c c_c$$

6.2.2 Heat Exchanger Effectiveness

This is defined as the ratio of actual heat transfer to the maximum possible heat transfer for a given configuration [267]; [266] i.e. the heat transfer which would result if the fluid with the smallest thermal capacity undergoes a temperature change equal to the maximum temperature difference available ($t_h - t_c$).

$$\text{Hence, Maximum heat transfer } \dot{Q}_{max} = \dot{m}_c c_c (t_{hi} - t_{ci}) \quad (7)$$

$$\text{if } \dot{m}_c c_c < \dot{m}_h c_h$$

$$\text{OR } \dot{m}_h c_h (t_{hi} - t_{ci}) \text{ if } \dot{m}_h c_h < \dot{m}_c c_c$$

$$\text{Actual Heat Transfer } \dot{Q}_{actual} = \dot{m}_h c_h (t_{hi} - t_{ho}) \text{ or } \dot{m}_c c_c (t_{co} - t_{ci}) \quad (8)$$

$$\text{Hence Effectiveness } E = \frac{(t_{co} - t_{ci})}{(t_{hi} - t_{ci})} \text{ if } \dot{m}_c c_c < \dot{m}_h c_h \quad (9)$$

$$\text{OR } \frac{(t_{hi} - t_{ho})}{(t_{hi} - t_{ci})} \text{ if } \dot{m}_h c_h < \dot{m}_c c_c$$

Where the i and o subscripts denote inlet and outlet respectively

6.2.3 Logarithmic Mean Temperature Differential

In general, the temperature differential that drives heat transfer from the hot fluid to the cooler fluid will vary along the flow passage. The single temperature difference that is representative of the entire process is the logarithmic mean temperature difference (LMTD).

If $\theta_1 =$ temperature difference between the fluid streams

at one end of the heat exchanger

and $\theta_2 =$ temperature difference at the other

$$LMTD = \theta_m = \frac{\theta_1 - \theta_2}{\ln(\theta_1/\theta_2)} \quad (10)$$

In Parallel Flow Heat Exchangers: $\theta_1 = (t_{hi} - t_{ci})$ and $\theta_2 = (t_{ho} - t_{co})$

In Counter Flow Heat Exchangers: $\theta_1 = (t_{hi} - t_{co})$ and $\theta_2 = (t_{ho} - t_{ci})$

In terms of overall heat transfer coefficient for a heat exchanger,

$$\theta_m = \frac{Q}{U_t A} \quad (11)$$

The derivation of the last equation is based on a pure parallel or counter flow of the fluid streams. To allow the equation to be evaluated for a wider range of heat exchangers, it can be generalised as [263]:

$$Q = F U_t A \theta_m \quad (12)$$

Where F = Empirical correction factor

The correction factor compensates for departures from the simple model in geometry, internal temperature variations and configuration.

6.2.4 Heat Transfer Units

The response of the heat exchanger to flow rates and temperatures needs to be quantified. The dimensionless parameter which helps in this regard is the *number of heat transfer units* (NTU). NTU is the ratio of heat transfer capacity of the surface to the smaller of the thermal capacities of the two streams [266].

$$\text{Hence } NTU = \frac{U_t A}{\dot{m}_c c_c} \quad \text{if } \dot{m}_c c_c < \dot{m}_h c_h \quad (13)$$

$$\text{OR } NTU = \frac{U_t A}{\dot{m}_h c_h} \quad \text{if } \dot{m}_h c_h < \dot{m}_c c_c$$

We may relate NTU to heat exchanger effectiveness E

and Capacity ratio C as below

$$\text{Parallel Flow } E = \frac{1 - e^{-NTU(1+C)}}{1 + C} \quad (14)$$

$$\text{Counter Flow } E = \frac{1 - e^{-NTU(1-C)}}{1 - C e^{-NTU(1-C)}} \quad (15)$$

6.3 Theory

6.3.1 Heat Transfer over Flat Plates

Heat can be transmitted in three ways i.e. via conduction, convection and radiation. In many practical problems, these 3 mechanisms combine in different degrees to generate the total energy flow.

One dimensional heat flux via conduction can be written as [263]:

$$q = \frac{Q}{A} = k \frac{\Delta T}{L} \quad (16)$$

Where q = heat flux (heat transfer per unit area),

Q = heat transfer rate in Watts (W),

A = area in m^2 ,

ΔT = Temperature difference in Kelvins,

L = thickness of solid medium in metres

and k = thermal conductivity in $W/m.k$

$$\text{In 3 dimensions, it can be shown that } \nabla^2 T + \frac{\dot{q}}{k} = \frac{\partial T}{\alpha \partial t} \quad (17)$$

$$\text{Where } \nabla^2 T = \frac{\partial^2 T}{\partial x^2} + \frac{\partial^2 T}{\partial y^2} + \frac{\partial^2 T}{\partial z^2} \quad (18)$$

The thermal diffusivity α symbol in the equation above is a measure of how fast a medium can transmit heat and it depends on the conductivity of the medium as well as the volumetric heat capacity c_v of the particles.

$$\alpha \equiv \frac{k}{\rho c_v} \quad (19)$$

Convection is heat energy travel in moving currents through fluids; molecules move away from the heat source carrying heat energy with them. In convection,

the fluid particles in contact with a hot medium move more quickly, become less tightly packed together and spread out, rising through the denser particles and making the cooler particles sink towards the hot surface. Those in turn get heated up and move up again. This sets up a convective current.

In convective heat transfer, the heat transfer rate Q is proportional to the difference between the temperature of a body T_{body} and that of the surrounding fluid T_{∞} . This constant of proportionality is usually derived from experiments and is called the heat transfer coefficient/film coefficient for the body.

$$q = \bar{h}(T_{body} - T_{\infty}) \quad (20)$$

Where

\bar{h} = Average heat transfer coefficient over the body surface in W/m^2K

In this equation, h is over-simplified as it is not always independent of $(T_{body} - T_{\infty})$. However, in cases where the pressure gradient is small and the fluid is experiencing a forced flow, it can be safely considered as independent [263]. This also applies to k in conduction. Within the temperature range of interest, k or h must be assessed to be relatively constant for steady state heat transfer equations to hold.

In dealing with the transient convective cooling of a body in fluid, the following equation can be derived using the first law of thermodynamics.

$$\frac{T - T_{\infty}}{T_i - T_{\infty}} = e^{-t/T} \quad (21)$$

$$\text{Where } T \text{ is the time constant} = \frac{\rho c V}{\bar{h} A} \quad (22)$$

T_{∞} = Fluid Temperature, T_i = Initial Body Temperature, t = time in seconds,

V = Body Volume and A = Body Surface Area

This equation assumes that that body has a uniform temperature and the measure of this state is call the Biot Number. Uniformity can be assumed in situations where the Biot number is less than 1 [263].

$$Biot\ Number = \frac{\bar{h}L}{k} \quad (23)$$

The special case of fluid flow over a flat plate is very relevant to this research work. When fluid particles make contact with a plate surface, a boundary layer develops. The boundary layer profile varies with vertical distance from the wall. In convective heat transfer problems, it is necessary to determine whether the boundary layer is laminar or turbulent. The convective heat transfer coefficient strongly depends on which of these conditions exists. The irregular fluid motion in turbulent boundary layers results in mixing of the flow and enhances \bar{h} significantly [268]; [269]. In contrast, in laminar boundary layers, the fluid motion is highly ordered. For a flat plate experiencing forced fluid flow over its surface, the boundary layer is initially laminar. At some distance from the leading-edge fluid fluctuations begin to develop. This is the transition region. Eventually with increasing distance from the leading edge, transition to turbulence occurs. This is followed by a significant increase in the boundary layer thickness and the convective heat transfer coefficient. Also, at this stage, three different zones can be observed in the turbulent boundary layer; the laminar sub layer, the buffer layer and the turbulent zone where mixing dominates. The location where transition to turbulence exists is determined by the Reynold's number of the boundary flow using the distance from the leading edge as the characteristic length. For Reynolds number less than 5×10^5 flow is generally laminar. Above this value, it becomes turbulent [263].

A thermal boundary layer must develop similar to the velocity boundary layer if the fluid free stream temperature and that of the flat plate are different. The fluid particles that come in contact with the warmer plate achieve thermal equilibrium with the plate's temperature and exchange energy with particles above them. A temperature gradient is therefore established. This temperature gradient

decreases with distance from the leading edge. Hence, \bar{h} decreases with distance.

6.3.2 Heat Transfer Coefficient in Heat Exchangers

The analogy between conductive heat transfer and Ohm's law in electricity helps in analysis of resistance to thermal energy transfer as shown below [263].

$$i.e \ Q = \frac{\Delta T}{L/kA} \approx Q = \frac{\Delta T}{1/A\bar{h}} \approx Q = \frac{\Delta T}{\sum R} \approx I = \frac{E}{R} \quad (24)$$

In the design of heat exchangers, it is often desirable to quantify the total heat transfer resistance of the system. Thus, an overall resistance is defined in terms of the overall heat transfer coefficient " U_t " of a unit. The heat transfer coefficient is independent of the system variables and is defined as shown below.

$$U_t = A \frac{1}{\sum R} \ (W/m^2) \quad Hence, Q = U_t A \Delta T \quad (25)$$

U_t relates to the total heat flow resistance in the system which comprises of conductive, radiative and convective elements depending on the system under consideration. Following from this, it can be deduced that heat exchanger fluids with low heat conductivity will generally reduce U_t and vice versa. During design, we seek to maximise U_t by minimising resistance.

The long-term performance of the unit at duty conditions must be accounted for in designing heat exchangers. While most of the material characteristics might not change depending on the type of heat exchanger, fouling of the heat exchange surfaces of the unit usually occurs in the long term. An empirical value called the *fouling resistance* is thus added to the overall unit resistance when computing the heat transfer coefficient for a unit. Tables of typical fouling resistance values are available in text for different combinations of fluids, operating temperatures, fluid velocities, heat exchanger surfaces and maintenance regimes. Fouling resistances varies widely with operating conditions. Generally, it would increase with age and decrease with increasing fluid velocities [41]. Highly accurate values for fouling resistance can only be

gotten from exact replicas of a heat exchanger system in operation and care must be taken to account for fouling resistances on all surfaces prone to fouling. In gas to gas heat exchangers, it can be observed that fouling does not significantly reduce heat transfer coefficient because of the already relatively low values compared to cases like liquid-liquid heat transfer with high values of U_t . As shown below, in conditions where $U_t < 100 \text{ W/m}^2\text{K}$, it can be safely ignored [42]; [263].

$$\text{if } U_t = 100 \text{ W/m}^2\text{K}$$

$$\begin{aligned} \text{Fouling resistance for most stable gases in shell and tube heat exchanger} \\ = 0.0005 \text{ m}^2\text{K/W} \end{aligned}$$

Accounting for fouling in this condition gives a corrected U_t – value

$$= \frac{1}{\frac{1}{100} + 0.0005} = 95.23 \text{ W/m}^2\text{K} \quad (26)$$

Typical fouling resistance values are given on Figure below

<i>Fluid and Situation</i>	<i>Fouling Resistance R_f (m²K/W)</i>
Distilled water	0.0001
Seawater	0.0001 – 0.0004
Treated boiler feedwater	0.0001 – 0.0002
Clean river or lake water	0.0002 – 0.0006
About the worst waters used in heat exchangers	< 0.0020
No. 6 fuel oil	0.0001
Transformer or lubricating oil	0.0002
Most industrial liquids	0.0002
Most refinery liquids	0.0002 – 0.0009
Steam, non-oil-bearing	0.0001
Steam, oil-bearing (e.g., turbine exhaust)	0.0003
Most stable gases	0.0002 – 0.0004
Flue gases	0.0010 – 0.0020
Refrigerant vapors (oil-bearing)	0.0040

Figure 6-1: Typical Fouling Resistances [263]

6.3.3 Heat Transfer Surfaces

In heat exchangers, the heat transfer elements are the primary surfaces in direct contact with the hot and cold fluids and are responsible for the heat transfer. Since heat transfer is directly proportional to the area available for the process, the heat transfer elements can also include features, such as fins, used to increase the available area for heat transfer. Fins can also be added for structural strength, to direct fluid flow or promote mixing of the material to enhance heat transfer [270]. Factors that influence surface thermal resistance include:

- The thermal conductivity, specific heat and fluid viscosity
- The nature of the fluid flow (laminar/turbulent)
- Surface roughness of the heat exchange surface [42]

The nature of a chosen fluid can't be reasonably changed. Hence, only the last two factors provide an opportunity to augment heat transfer in a heat exchanger. Fins can be introduced to induce turbulence in the flow field and increase surface roughness thereby reducing resistance to the flow of heat [270]. There are reasons for considering very carefully the practicality of using fins in the design of heat exchangers. The introduction of fins obviously leads to an increase in fluid friction [257]; [270]; [271]. With the lack of external pumping power in natural ventilation applications, the avenue for this is very limited. Rather the emphasis should be on improving or increasing the surface available for heat transfer.

The equation below defines the temperature along a thin straight fin of uniform thickness in the flow direction in a heat exchanger and can be used to evaluate the effectiveness of a fin. It is based on the following assumptions [42].

- The convective coefficient is uniform over the fin surface.
- The flow of heat is one dimensional.
- Heat transfer from the outer thickness of the fin is negligible.

$$\frac{T(x) - T_{\infty}}{T_o - T_{\infty}} = \left[\frac{\cosh[m(L - x)]}{\cosh(mL)} \right] \quad (27)$$

$$\text{And } m = \sqrt{\frac{Ph_c}{kA}} \quad (28)$$

Where k = Thermal Conductivity, h_c = Convective heat transfer coefficient,

P = Fin perimeter, A = Area, L = Fin length into the flow,

T_∞ = Fluid temperature,

T_o = Temperature at the root of the fin and

T_x = Temperature at a position x along the fin

The fin efficiency relates the performance of a fin to an ideal fin for which the temperature is uniform over the entire length and is defined below [42].

$$\text{Fin efficiency} = \eta_{fin} = \frac{\tanh(mL)}{mL} \quad (29)$$

6.4 Heat Exchanger Concept

Design was defined by Shah et al [257] as an activity aimed at providing complete unambiguous description of an engineering system, part of a system or component. This description must include a clear specification of the system size, component, performance, function and other characteristics important for subsequent manufacture and utilisation. Depending on the design project, a number of variables are present e.g. cost, size, pressure drop, heat duty, flow configuration, number of passes, shape etc. The design process is an iterative one to get an optimised solution. This process is often carried out in industry using different optimisation techniques. Different combinations of genetic algorithms [119]; [272], constructal theory [267]; [273], particle swarm optimization [274], biogeography-based optimization [275], have all seen uses in heat exchanger design.

The sheer number of variables to be considered in designing conventional heat exchangers (e.g. shell and tube heat exchangers) necessitates the utilisation of these mathematical techniques. In simpler applications, where a small number of

variables can be prioritised, simpler techniques can be employed. Parametric techniques have been used in the development of heat exchangers with good correlation with experimental results [276]; [62]; [277]; [278]; [279]; [280]; [281]. The method presented in this study uses parametric plots as graphical means of quick optimisation. It is based on earlier work done by T.K Poddar et al [282] for the optimisation of a shell and tube heat exchanger. The graphs show the relationship between the geometry and values of pressure drop and heat duty to provide headway in the design process.

For the ventilation system proposed in this research, spatial restriction is prominent since the heat exchanger has to fit within the chimney space below the windcatcher. Hence, the development process starts with a preliminary geometrical design. Following this, a thermal and pressure preliminary sizing of the heat exchanger will be carried out. Lastly, CFD will be used to investigate and enhance the preliminary design. These activities are discussed below.

6.4.1 Problem Specification

The problem specification provides the basis on which the heat exchanger will be designed. The properties that need to be defined at this point are discussed below.

6.4.1.1 Geometry

The concentric air supply and extract channels of the chimney windcatcher places a restriction on applicable heat exchanger geometry. The Base Model design produced by the Author for the heat exchanger is shown below. It is cylindrical with radial plates around a perforated central tubular core. The design features an innovative fluid distribution element. These are end caps on both ends which splits the flow through the heat exchanger making it a counter flow configuration (Figure 6-2).

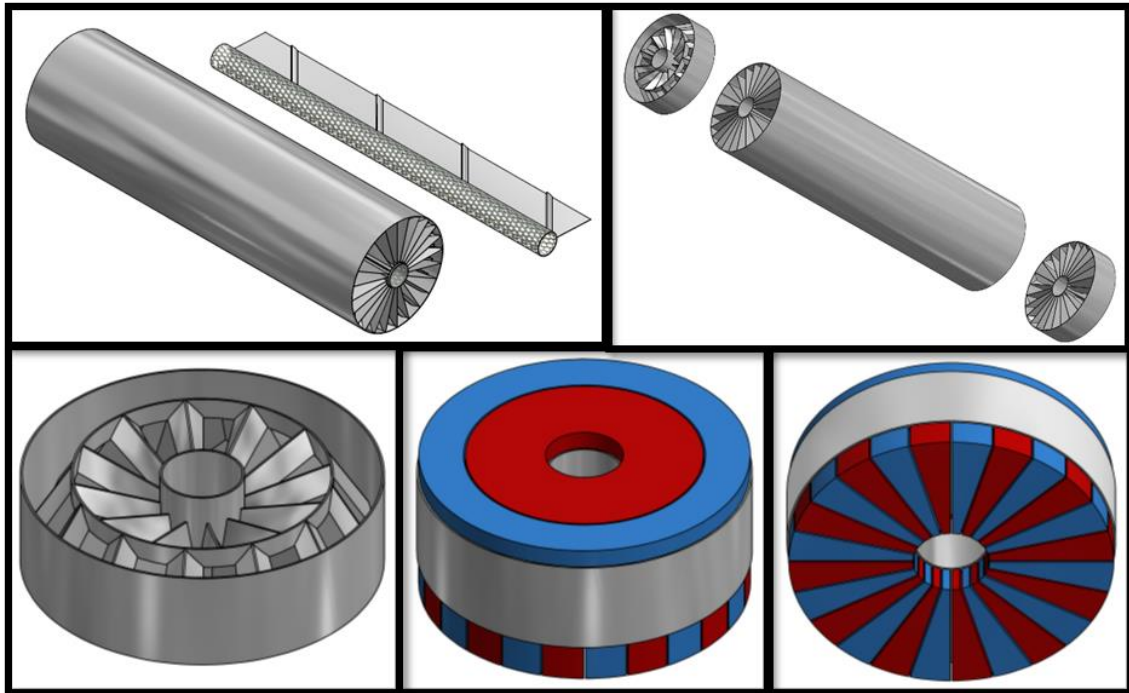


Figure 6-2: Heat Exchanger and End Caps

Inlet air flow from the windcatcher annular section is split into alternate sections of the heat exchanger passages while flow out of the central outlet is through passages in the heat exchanger adjacent to those of the inlet. This is illustrated in Figure 6-3 below; the blue and red sections represent opposite air streams through the end cap. The end caps have been designed by the author to have streamlined surfaces to minimize flow resistance. It is also proposed as a future design addition that grooves as shown can be added on the heat exchanger plate on the side exposed to the outgoing extract air to slant towards the central tubular core. This can act to channel condensate in the heat exchanger towards the perforated tubular core which can hold an inert chemical desiccant to absorb any condensate in the system. The heat exchanger considered in this research is without grooves and condensation is not modelled.

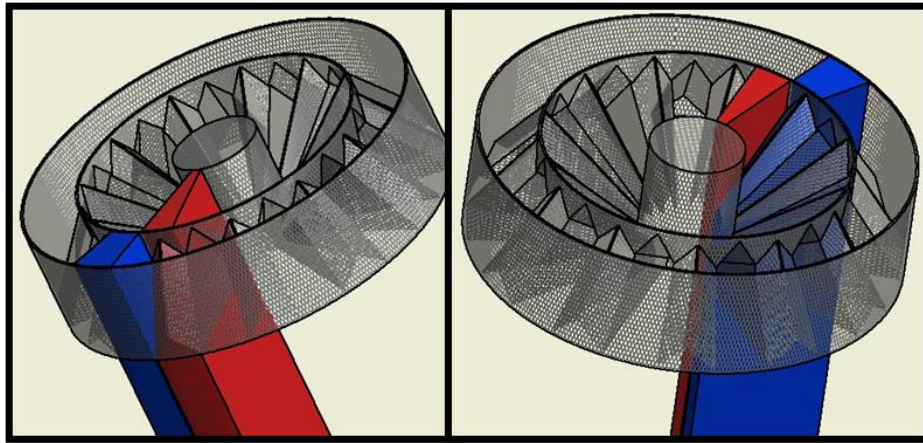


Figure 6-3: Supply and Extract Flow Paths Through End Caps

6.4.1.2 Operating Conditions

Since the primary purpose of the system is to recover otherwise lost ventilation heat, the environmental design point has been chosen to be a winter case with an outdoor temperature of 2°C . The response of the heat exchanger to other flow rates and temperatures can be quantified by dimensionless parameter of heat transfer units discussed under heading 6.2.4. CIBSE recommended indoor design conditions for winter in the UK are at an average temperature of 22°C and 50% relative humidity [23].

As the temperature of air is reduced at this pressure, its capacity to hold water in vapour state reduces and relative humidity (RH) goes up. At 100% RH, the air reaches its dew point. Continual heat recovery from the outgoing indoor air at this point causes its water vapour content to condense in the heat exchanger. Condensation is an efficient heat recovery process. However, it is undesirable in this system. In a heat exchanger mounted outdoors and exposed to cold weather, condensate freezing can occur. Frost formation over the heat exchanger surfaces reduces efficiency and increases pressure drop through the system [45]; [283]; [284]. To this end, the heat exchanger is required not to cool the outgoing indoor air below dew point, which is 11°C at the indoor conditions. Hence 14°C has been chosen by the author as the desired hot stream outlet temperature. The design conditions for the air streams through the heat exchanger is summarised

below. The hot stream flows from the room through the heat exchanger and exits the system through the windcatcher central outlet. While the cold stream is incident air captured through the windcatcher annular inlet and channelled through the heat exchanger into the room. As expected, the cold stream rises in temperature through the heat exchanger. The thermal energy for this rise is derived from the hot stream. Hence, the hot stream reduces in temperature through the heat exchanger.

Hot stream Inlet temperature $T_{hi} = 22^{\circ}C/295.15K$

Hot stream outlet temperature $T_{ho} = 14^{\circ}C/287.15K$

Cold stream Inlet temperature $T_{ci} = 2^{\circ}C/275.15K$

The Author chose $T_{co} = 20^{\circ}C/293.15K$ as the desired temperature to raise the cold stream to. This closely matches the existing indoor comfort temperature and in operation will minimize the experience of cold draughts within the living space. An initial design with the 16 heat exchanger channels has been arbitrarily chosen.

$$\text{Surface area of heat exchanger end} = 0.032m^2.$$

Hence, taking a single channel;

$$\text{Surface Area } A = \frac{0.032}{16} = 0.002m^2 \quad (30)$$

$$\text{Amount of heat to be rejected } Q = \dot{m}c_p(T_{hi} - T_{ho}) \quad (31)$$

Assuming a value of 1m/s as the average velocity "V" of extract air (i. e. Hot Stream)

through the cowl central channel,

$$\text{Mass flow Rate } \dot{m} = VA\rho \quad (32)$$

$$\dot{m} = 1 * 0.002 * 1.2305 = 0.0025kg/m^3$$

$$\text{Required Heat Duty } Q = 0.0025 * 1.00435 * 8 = 20W \quad (33)$$

Where ρ = Air density at the average temperature,

c_p = Air specific heat capacity at constant pressure

6.4.2 Pressure Drop

The heat exchange rate in a heat exchanger is highly dependent on the air velocity over the heat exchange surfaces. The velocity also relates to the pressure drop through the heat exchanger [263]. Hence, successful design of a heat exchanger relies on being able to optimise the pressure drop and the heat transfer for a given operating condition. Pressure drop in the heat exchanger is contributed by fluid friction through the heat exchanger core. However, due to the low velocities of induced air flow through the ventilation system, the pressure drop is expected to be low. This is beneficial because there is no pumping power available to drive air flow through the heat exchanger. It is essential the pressure drop is kept to bare minimum to avoid a stall in the air flow through the system.

One channel of the heat exchanger has been approximated to a rectangular tube section with the longer side of the cross-section fixed at the radius length of the cylinder.

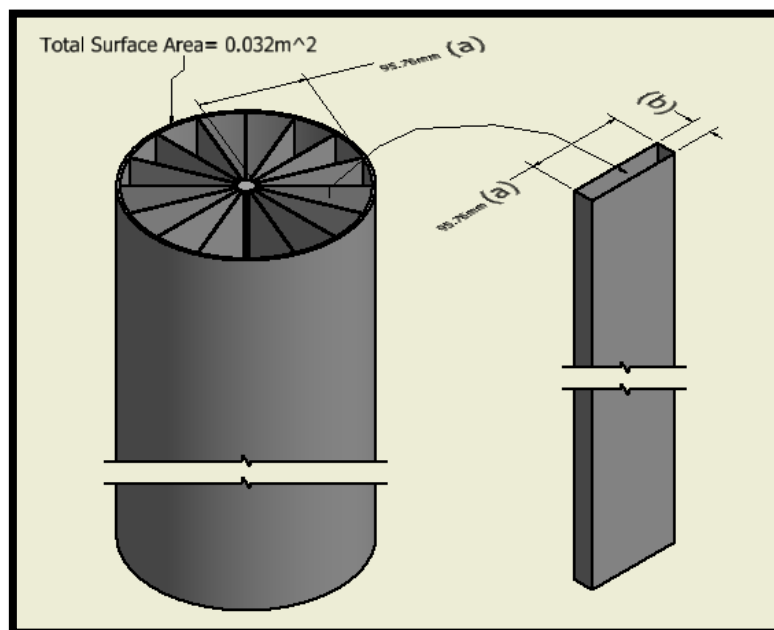


Figure 6-4: Heat Exchanger Channel

A value of 1 Pa has been chosen as the maximum allowable pressure drop per channel of the heat exchanger. Assuming a developed flow, pressure drop is calculated using the Darcy-Weisbach equation.

$$\Delta P = \frac{fl\rho V^2}{2D_h} \quad (34)$$

Where l = channel height, D_h = Hydraulic Diameter of channel,

f = friction factor and V = velocity

$$\text{For a rectangular section with side lengths } a \text{ and } b, D_h = \frac{2ab}{a+b} \quad (35)$$

$$\text{and } f = 70/Re \quad (36)$$

$$V = \frac{\dot{m}}{\rho A} = \frac{\dot{m}}{\rho(ab)} \quad (37)$$

$$Re = \rho V D_h / \mu = \frac{\rho * \left(\frac{\dot{m}}{\rho(ab)}\right) * \left(\frac{2ab}{a+b}\right)}{1.8e^{-5}} \quad (38)$$

$$f = \frac{70}{Re} = \frac{70}{\left(\frac{\rho * \left(\frac{\dot{m}}{\rho(ab)}\right) * \left(\frac{2ab}{a+b}\right)}{1.8e^{-5}}\right)} \quad (39)$$

Hence writing the Darcy – Weisbach equation in terms of a and b gives:

$$\Delta P = \left[\frac{\frac{70}{\left(\frac{\rho * \left(\frac{\dot{m}}{\rho(ab)}\right) * \left(\frac{2ab}{a+b}\right)}{1.8e^{-5}}\right)} * l * \rho * \left(\frac{\dot{m}}{\rho(ab)}\right)^2}{2 * \left(\frac{2ab}{a+b}\right)} \right] \quad (40)$$

We know as stated above, $\Delta P = 1Pa$, $a = 0.096m$ (i.e cylinder radius),

from equation 32, $\dot{m} = 0.0025kg/s$

and $\rho = 1.2305kg/m^3$

This leaves only l (= Height of rectangular heat exchanger channel) and b (= breadth of heat exchanger channel crosssection) as the only unknowns

6.4.3 Heat Duty

The thermal design is based on Newton's law of cooling equations which relates the heat transfer rate with the heat transfer coefficient in an isobaric open non-adiabatic system [257]. Assuming a thermally developed flow;

$$Q = hA(T_s - T_\infty) \quad (41)$$

Where A = Heat transfer surface area, h = Heat transfer Coefficient

T_∞ = Fluid bulk temperature and T_s = Surface Temperature

Using this equation, designing a heat exchanger can be a case of finding the right heat exchanger surface area to satisfy a required value of h and ΔT .

When analysing the heat transfer from a surface exposed to a fluid, the Nusselt number Nu quantifies the ratio of conductive thermal resistance l/K to the convective thermal resistance $1/h$ [285]. This can be used to calculate the value for h as shown below.

$$i. e. Nu = \frac{hD_h}{k}, \text{ Hence, } h = \frac{Nuk}{D_h} \quad (42)$$

Where k = Thermal conductivity of the fluid estimated at film temperature i. e. $(T_s + T_\infty)/2$

Still considering the hot stream as we did in equation 31, we assume that the plate remains at the average temperature of the cold stream

$$i. e. T_s = \frac{T_{co} + T_{ci}}{2} = \frac{293.15 + 275.15}{2} = 284.15K \quad (43)$$

and the fluid bulk temperature is the average of the hot stream temperature

$$i. e. T_\infty = \frac{T_{ho} + T_{hi}}{2} = \frac{295.15 + 287.15}{2} = 291.15K \quad (44)$$

$$\frac{(T_s + T_\infty)}{2} = \frac{284.15 + 291.15}{2} = 287.65K \quad (45)$$

Interpolating for k at 287.65 gives; $k = 0.02526 \text{ W/mK}$ [23]

From the above definition of the Nusselt number, it can be deduced that, when the convective thermal resistance is high, the Nusselt number tends to unity and conduction dominates the heat transfer process. This is typical of laminar flows. On the other hand, in turbulent flows, the convective thermal resistance is low and convective heat transfer dominates the process [268]; [285].

Many empirical correlations are available for quantifying the Nusselt number for different cross-sections. For laminar forced flow heat transfer in vertical rectangular tubes, the Nusselt correlation is given below [286].

$$Nu = 1.94 + 0.659r - 0.02496r^2 = 1.94 + 0.659\frac{a}{b} - 0.0249\left(\frac{a}{b}\right)^2 \quad (46)$$

Where $r = a/b$

$$\text{Thus } h = \frac{\left(1.94 + 0.659\frac{a}{b} - 0.0249\left(\frac{a}{b}\right)^2\right) * k}{\frac{2ab}{a+b}} \quad (47)$$

Writing the Newton's Law of Cooling in terms of a and b gives:

$$Q = \left(\frac{\left(1.94 + 0.659\frac{a}{b} - 0.0249\left(\frac{a}{b}\right)^2\right) * k}{\frac{2ab}{a+b}}\right) * (2(a+b) * l) * (T_s - T_\infty) \quad (48)$$

6.4.4 Sizing

It has been possible to express the thermal and pressure duty of the heat exchanger by taking a single channel and approximating it to a rectangular channel with the breadth fixed at the radius of the cylindrical geometry. The two resultant equations are given below:

$$\Delta P = \left[\frac{\left[\frac{70}{\left(\frac{\rho * \left(\frac{\dot{m}}{\rho(ab)} \right) * \left(\frac{2ab}{a+b} \right)}{1.8e^{-5}} \right) * l * \rho * \left(\frac{\dot{m}}{\rho(ab)} \right)^2} \right]}{2 * \left(\frac{2ab}{a+b} \right)} \right] \quad \text{Equation 40}$$

$$Q = \left(\frac{\left(1.94 + 0.659\frac{a}{b} - 0.0249\left(\frac{a}{b}\right)^2\right) * k}{\frac{2ab}{a+b}} \right) * (2(a+b) * l) * (T_s - T_\infty) \quad \text{Equation 48}$$

Where $\Delta P = 1Pa$, $a = 0.096m$, $\dot{m} = 0.0025 \text{ kg/s}$, $k = 0.02526 \text{ W/mK}$, $\rho = 1.231 \text{ kg/m}^3$, $Q = 20W$

In these equations, the two geometrical parameters l and b are unknowns. These equations can be solved simultaneously and the relationships between the different variables can be explored. In reality, the relationship between these variables is far more complex and the rigorous equation development is beyond the scope of this work as this process is only intended to provide a start point for the heat exchanger development. The pressure drop performance will be prioritised over that of heat exchange.

The graph in Figure 6-5 is a plot of the solution of equations 40 and 48 showing the relationship between pressure drop and heat transfer rate for $l = 0.8m$ at $b = 0.02m$. It can be observed that the heat transfer rate approaches a limiting value.

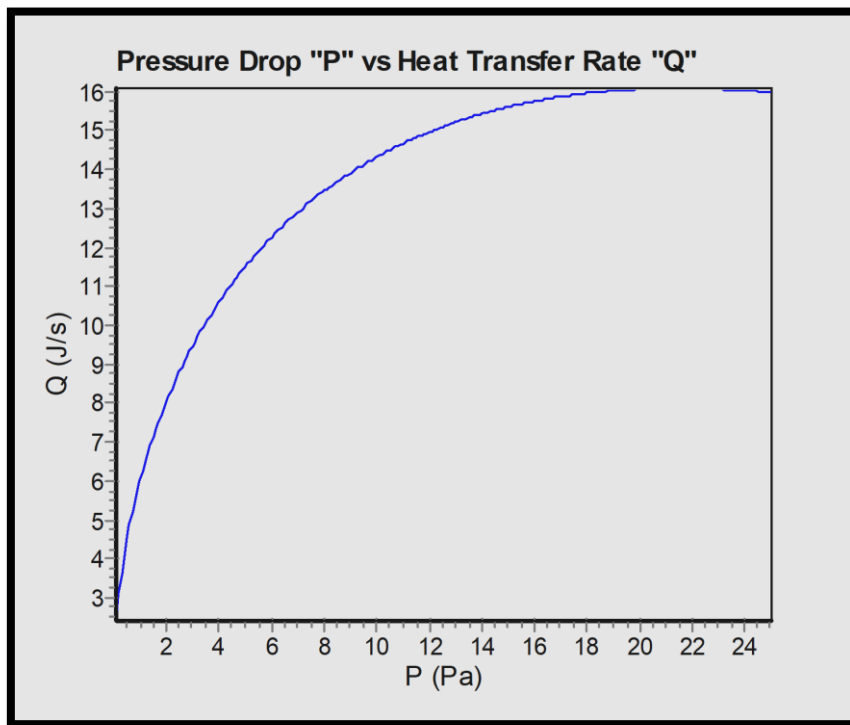


Figure 6-5: Heat Exchanger Pressure vs Heat Transfer Rate Graph

At the same length, the relationship between the channel breadth b and pressure drop is shown in Figure 6-6. As expected, decreasing the value of b progressively

narrows the channel cross-section and increases pressure drop through the channel.

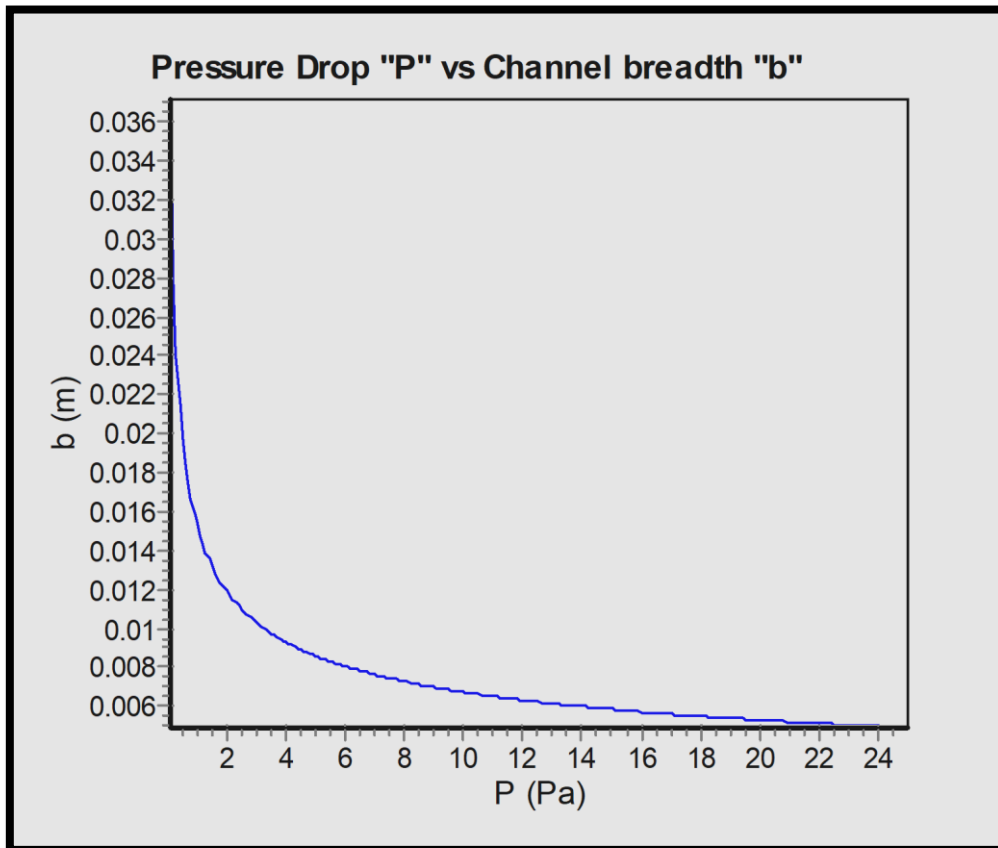


Figure 6-6: Heat Exchanger Pressure Drop vs Channel Breadth Graph

Figure 6-7 shows the relationship between heat transfer rate and channel length l at fixed channel cross-sectional breadth $b = 0.02m$. Increasing channel lengths presents larger heat transfer areas which consequently increases the heat transfer.

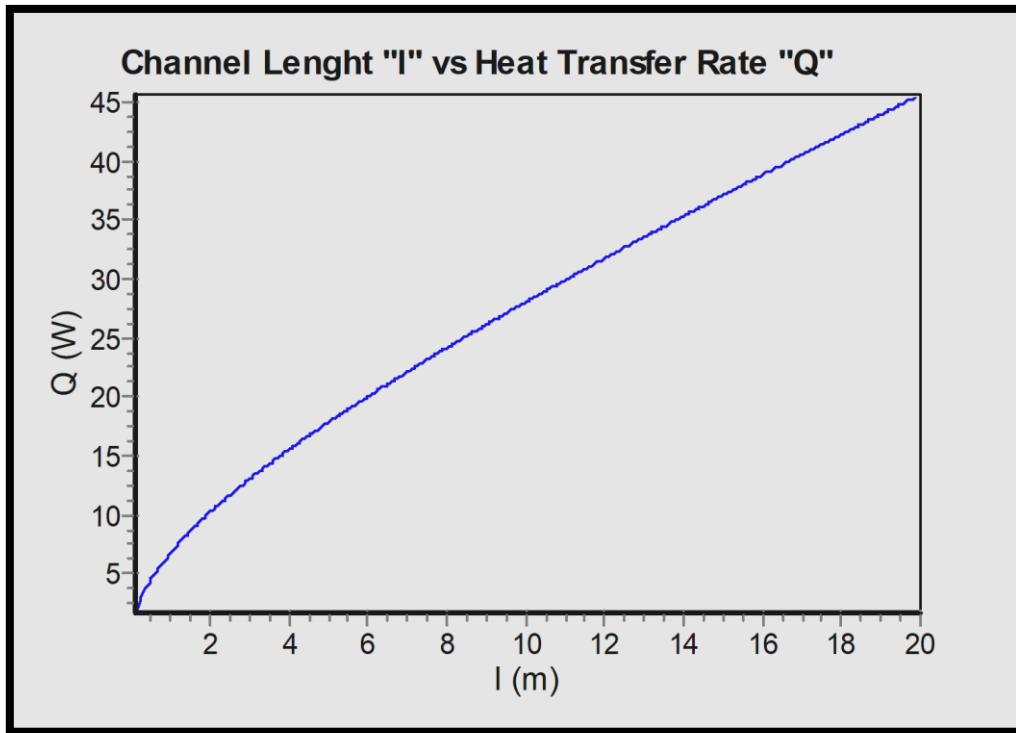


Figure 6-7: Heat Exchanger Channel Length vs Heat Transfer Rate Graph

In Figure 6-8, the pressure drop ΔP is $1Pa$. The relationship between channel length l and breadth b is shown. When the channel length l increases, to maintain the same pressure drop, channel breadth b must also increase accordingly.

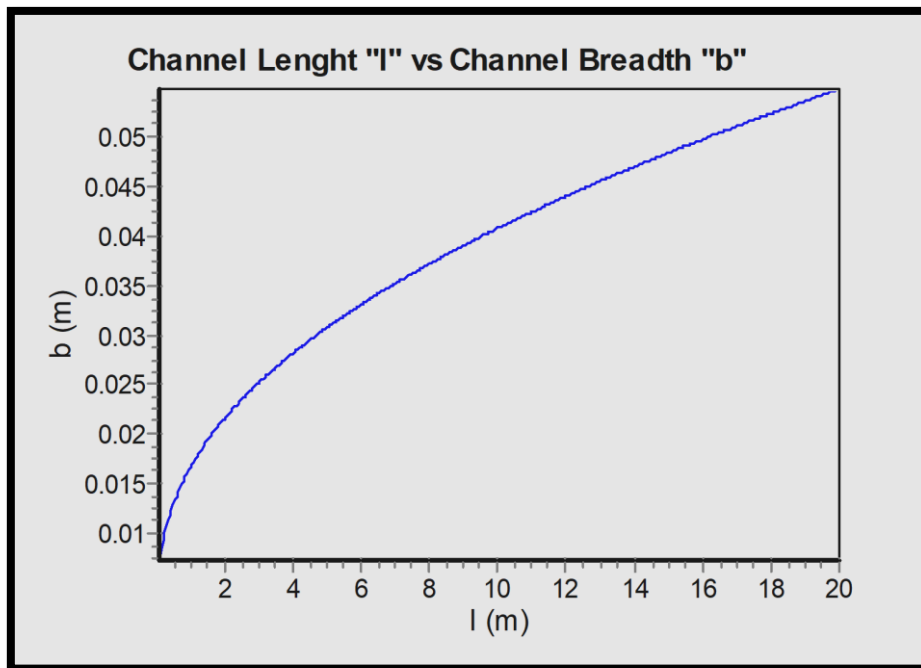


Figure 6-8: Heat Exchanger Channel Length vs Channel Breadth Graph

This method provides a graphical means of optimising the heat exchanger geometry for rapid preliminary design when important design parameters are known. In Figure 6-9, the relationship between channel breadth b , heat transfer rate Q and Pressure drop ΔP at fixed length $l = 0.8m$ is shown.

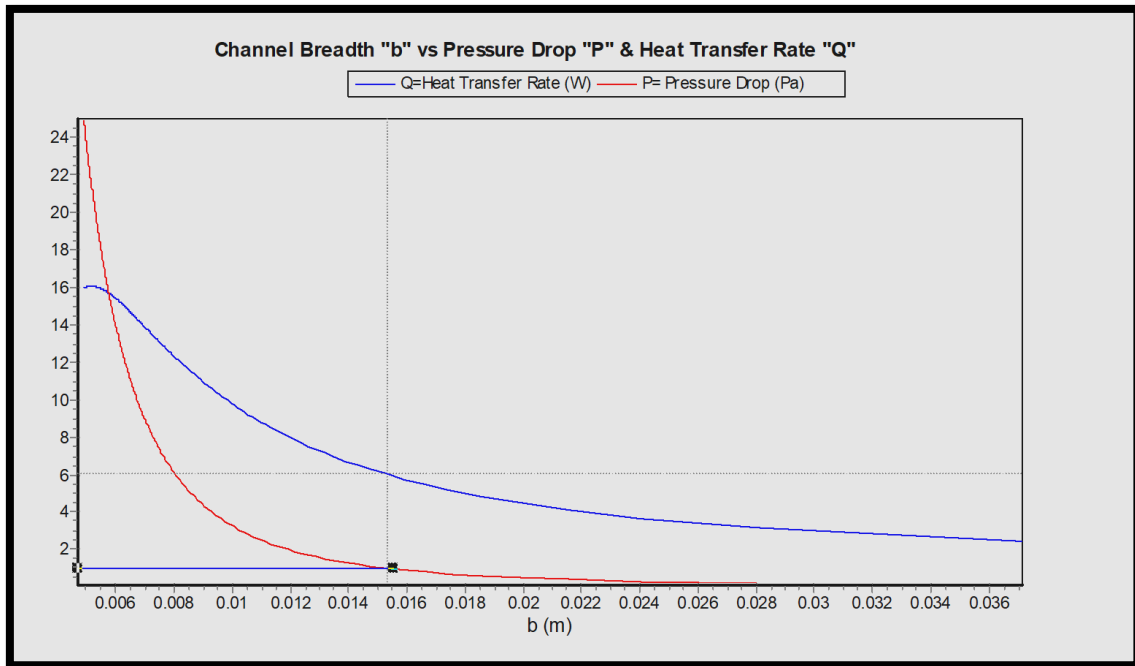


Figure 6-9: Heat Exchanger Design Point Graph

The optimal channel breadth b can be deduced when the pressure drop $P = 1Pa$.
The corresponding heat transfer rate Q can also be read off the graph.

Thus when $P = 1Pa$, $\dot{m} = 0.0025 \text{ kg/s}$, $l = 0.8m$, $a = 0.096m$,

$$b = 0.015m, \text{ and } D_h = 0.026m,$$

$$Q = 6.012W \text{ for a single channel} \quad (49)$$

The sectional dimension of the cylindrical heat exchanger is fixed by that of the windcatcher and equal to the area of its base.

Thus,

$$\text{Cross – sectional area per rectangular channel} = 0.015 * 0.096 \quad (50)$$

$$= 0.00144m^2$$

$$\text{Cross – sectional area of cylindrical heat exchnager} \quad (51)$$

$$= 0.032m^2$$

From the cross – sectional area of the cylinder, we can get

$$\frac{0.032m^2}{0.00144m^2} = 22 \text{ sections of } 0.00144m^2 \text{ each} \quad (52)$$

Only half of these channels will carry the hot stream of air.

Allowing a margin of 30% to account for errors due to differences in channel geometry; the Author has chosen to have 8 channels for each flow stream. This approximation has prioritised the pressure drop performance to provide a start point for the heat exchanger design which is subsequently investigated with CFD. The heat transfer equation (48) is less accurate for the geometric approximation and its more accurate prediction is deferred to CFD analysis.

6.5 Analysis and Results

6.5.1 Heat Transfer Optimization

The heat exchanger is required to temper cold air captured by the wind catcher and supply it to the living space at an acceptable rate. It can do this by satisfying the required heat duty within a band of expected air temperatures without stalling air flow through the central and annular flow channels. A minimum air flow rate of $0.00525 \text{ m}^3/s$ is required for adequate ventilation as established in equation 1. Hence, pressure drop through the heat exchanger should guarantee this flow rate at most external wind conditions as a minimum.

CFD is an established method in the development of heat exchangers [216]. The thermal and flow performance of the heat exchanger was investigated in Ansys Fluent v14. The simulation was carried out as a turbulent incompressible flow at steady state wind speeds.

6.5.2 Final Prototype

The heat exchanger prototype is shown on Figure 6-10. It has 0.8 meters in length with 16 channels; 8 in each flow direction. Staggered columns of 3mm concentric copper rings have been added as shown to induce turbulence in the fluid flow and break up the formation of boundary layers. Passive methods of heat transfer augmentation like this improve heat transfer performance of heat exchangers [270].

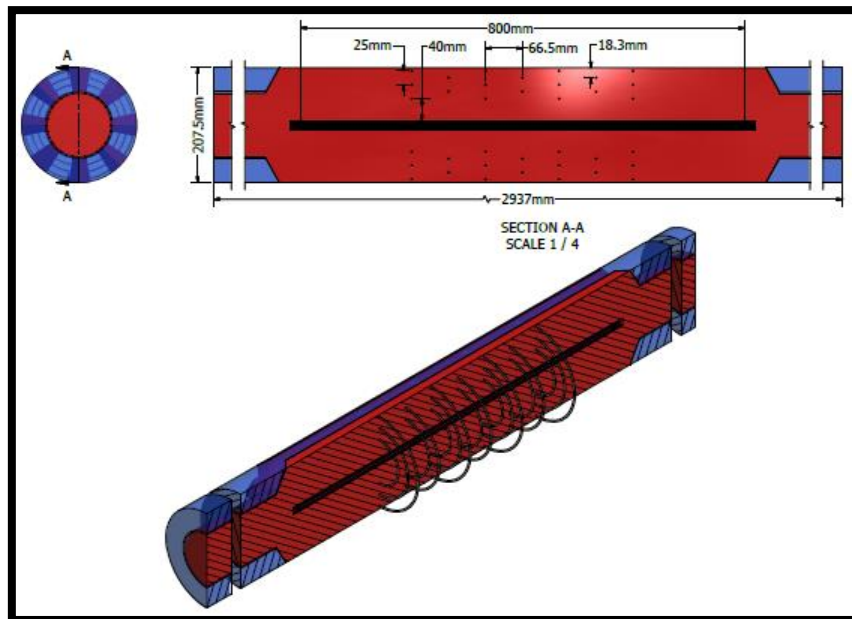


Figure 6-10: Final Prototype

In laminar fluid flow, heat transfer is largely limited to molecular conduction through the layers of fluid [42]. However, in turbulent flows, heat transfer is greatly enhanced by mixing which causes the bulk transport of heat and momentum by turbulent eddies in the fluid [263]. In fluid flow through a fixed length of channel, the onset of turbulent flow is governed by the Reynolds number; consequently, the velocity. Turbulent flows are readily achieved at high velocities. However, the velocity at which turbulence is achieved can be reduced by different means. One way is by introducing geometric features that constantly bursts the build-up of the boundary layer and causes significant mixing of the fluid [287]; [288]; [289]. This has the disadvantage of introducing flow obstructions, consequently increasing pressure drop. The right balance of tolerable pressure drop and heat transfer enhancement must be found. Generally, features like this should be introduced at points where boundary layer thickness build-up starts becoming excessive (e.g. at points well into the channel because boundary layer thickness at entrances are thin) and then at subsequent intervals to prevent downstream re-attachment and build-up.

6.5.2.1 Simulation Set-Up

The following sub-sections discuss the Ansys Fluent v14 software settings and specifications applied in carrying out the heat exchanger simulations.

6.5.2.1.1 Simulation Model

A 3D model of the heat exchanger was modelled and assembled in Autodesk Inventor 2013. The solid heat exchanger and end-cap parts have been removed to derive 3D sections representing just the air fluid parts. As the walls are relatively thin here, they were modelled as 0.3mm thick shells to reduce computational effort. With this option, one layer of virtual cells is created to compute conduction not only in the direction normal to the wall, but also in the plane of the wall.

As shown in Figure 6-11, the resultant simulation model consists of two air sections. The annular air supply section receives inlet air flow from the windcatcher through the heat exchanger end caps. This flows through the heat exchanger interleaved with the central extract flow from the windcatcher central outlet.

The air section in the extract and supply channels were extended by approximately 1m on both sides of the end-caps to allow for flow development before entering the heat exchanger.

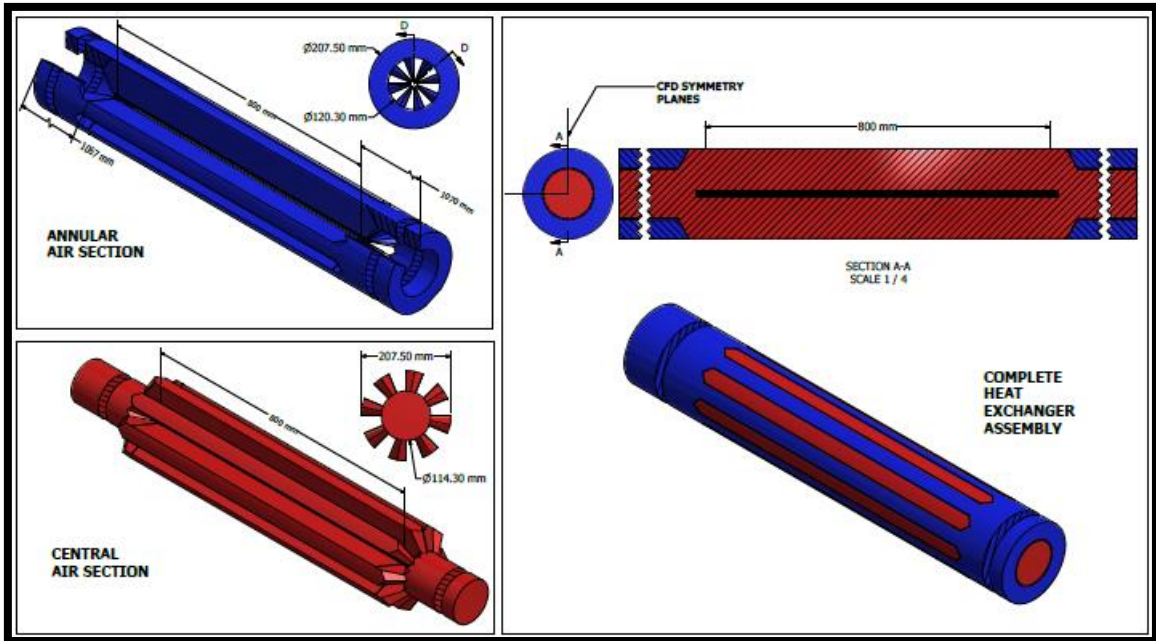


Figure 6-11: Simulation Model (Rings not shown)

To further reduce computational effort, only a quarter of the model was used. The model was divided at the vertical and horizontal planes shown. The surfaces created by dividing the model is that of symmetry where flow properties on either side mirrors the other.

6.5.2.1.2 Material

The material was set as air with the default properties of density, specific heat, thermal conductivity and viscosity. This is a safe assumption in incompressible forced flow simulations where air velocities are well below Mach 0.3 as the little variations in material properties will not significantly affect the flow and heat exchange results [195]. All heat exchange surfaces were specified as 0.3mm thick copper plates with a constant thermal conductivity equal to 387.6 W/mK .

6.5.2.1.3 Boundary Conditions

Since the heat exchanger is a counter-flow configuration, each end has an inlet and outlet for opposite air streams. Flow outlets were set to zero-gauge pressure to simulate an inflow/outflow surface. This static pressure is held constant over these surfaces to represent that of the environment external to the simulation

domain. The two perpendicular symmetry surfaces were modelled as symmetry boundaries where the normal velocity and gradients of all variables are zero.

At inlets, uniform profile of the simulated velocities was applied normal to the surface of each channel. The velocities were obtained from the results of the final windcatcher simulations as shown on Figure 5-55. They are mass-weighted averages taken at the relevant channel surfaces. “Annular Inlet velocities” were applied at the annular supply channel inlets and “Central outlet velocities” were applied at the central extract channel inlets. This is representative of average flow velocities through the heat exchanger at the corresponding incident air speeds.

Two thermal boundary conditions were applied; the air through the annular channel was set at 2°C at its inlet and that of the central channel was also set at 22°C at its inlet at the opposite end.

All other surfaces were left in their default state. Ansys Fluent v14 automatically model these surfaces as smooth non-slip walls where tangential fluid velocity is equal to that of the wall (equal to zero) and normal velocity component is zero.

6.5.2.1.4 Meshing

Ansys v14 Meshing Advanced Sizing Function defines optimum element sizes to capture areas of strong curvature, and close proximity to neighbouring geometry in the model. This function was used to define a patch conforming tetrahedral mesh for the assembly. This was adjusted using the high smoothing and a “fine” setting for Relevance Centre. 20 inflation layers were specified on the wall boundaries to adequately resolve gradients at the walls using a y^+ value of 1. This provides a better resolution of flow in this region. Other meshing controls were left at their default values as summarised in Figure 6-12. The resultant mesh has 8.7 million cells.

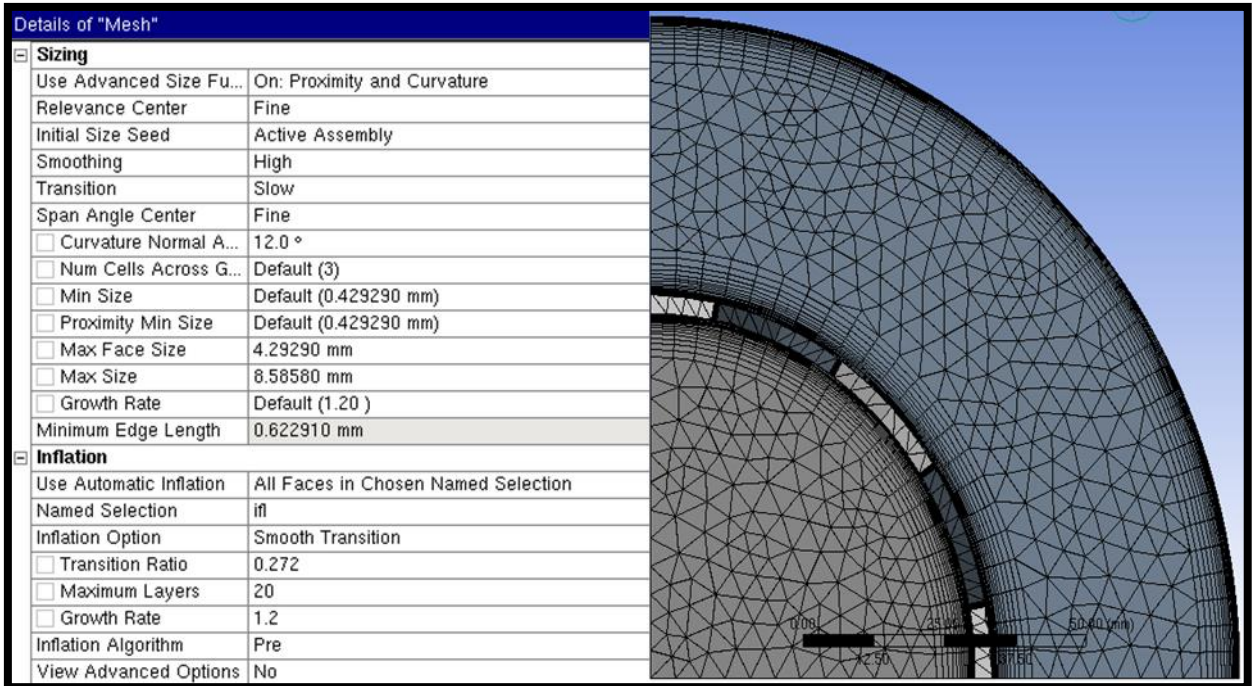


Figure 6-12: Ansys Mesh Settings

6.5.2.1.5 Solving

1000 Steady state simulations were specified using the SST K-Omega turbulence model. The coupled Pressure-Based Solver was chosen for simulations. Hybrid initialization was utilized to give an initial value before iteration can begin. A realistic initial guess improves solution stability and accelerates convergence. Solution monitors were set to monitor air outlet temperatures and pressures. The values recorded at these points were used to determine the convergence state of the solution i.e. the solution was thought to have converged when the solution remained unchanged, the solution residuals are below a 10^{-3} tolerance and for energy, below 10^{-6} . Mass balance between inflow and outflow was specified to a tolerance of $10e-4$.

A mesh independence study was conducted at 2.5 m/s flow velocity and inlet temperatures of 2°C (annular channel) and 22°C (central channel) to determine the optimum mesh for the simulation. At converged solutions, 4 subsequent mesh refinements were performed based on scaled gradients of velocity in the entire domain. All regions with gradients higher than 10% of the maximum were marked and adapted. As shown on Table 6-1 solutions of pressure drop and temperature

change for the flow streams were broadly similar for all meshes in both channels. Nevertheless, Mesh 3 was chosen as it gives a good balance between computational effort and mesh refinement in areas of high gradient.

		Mesh 1	Mesh 2	Mesh 3	Mesh 4
	Cell count (millions)	8.7	10.3	12.9	16.4
Supply Channel	Pressure Drop (Pa)	3.52	3.79	4.10	4.09
	Temperature Change (Kelvins)	2.78	3.33	3.56	3.56
Extract Channel	Pressure Drop (Pa)	1.22	1.54	1.88	1.86
	Temperature Change (Kelvins)	7.87	8.21	8.70	8.69

Table 6-1: Mesh Independence Test results

6.5.2.2 CFD Simulation Results and Discussion

The following sub-sections discuss the thermal and flow results from CFD simulations

6.5.2.2.1 Thermal Performance:

Figure 6-13 below shows the temperature change for each air stream through the heat exchanger. At the lowest wind speed, a significant proportion of heat contained in the extract flow was recovered causing a fluid temperature drop of $14^{\circ}C$. This temperature difference readily decreases as the air flow rate increases. At flow rates generated by a 4.5 m/s wind incident on the windcatcher, the temperature drop reduces to $6.96^{\circ}C$.

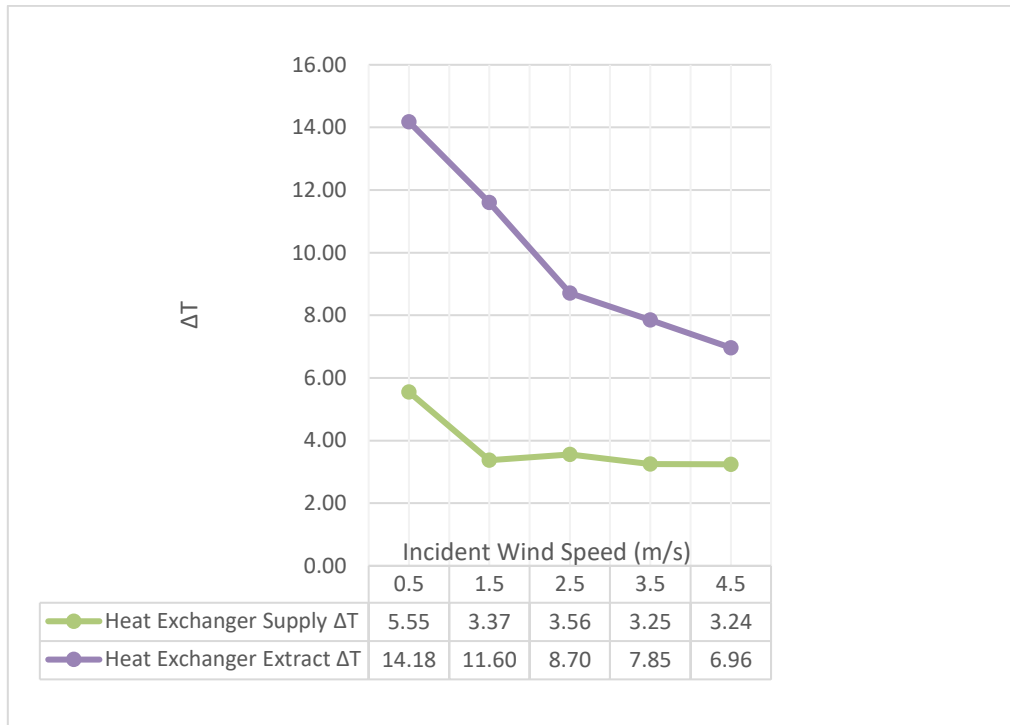


Figure 6-13: Supply and Extract Flow Temperature Change

Incident Wind Speed (m/s)	Annular Inlet Flow Velocity (m/s)	Central Outlet Flow Velocity (m/s)
0.50	0.08	0.12
1.50	0.27	0.31
2.50	0.48	0.77
3.50	0.72	1.15
4.50	0.92	1.64

Table 6-2 Equivalent Channel Velocities at Wind Speeds

The focus here is on the extract flow because it contains the heat energy to be recovered, and the performance of the heat exchanger is based on its ability to do this recovery. The temperature rise of the supply flow is largely dependent on

its flow rate. In the planned operation of this system, the air supply flow rate will be adjustable at room level inlet with a damper. It follows that at high flow rates, the temperature gain of the supply air will be low and at low flow rates, it will be high. This corresponds to results gotten by M. Simonetti et al [86] in their study of a low Reynolds number plate heat exchanger with rectangular channels.

Figure 6-14 shows the heat exchanger effectiveness. At low flow rates equivalent to low incident wind speeds on the windcatcher, it is quite high at 71%. This readily reduces to 35% as the flow rate through the heat exchanger increases.

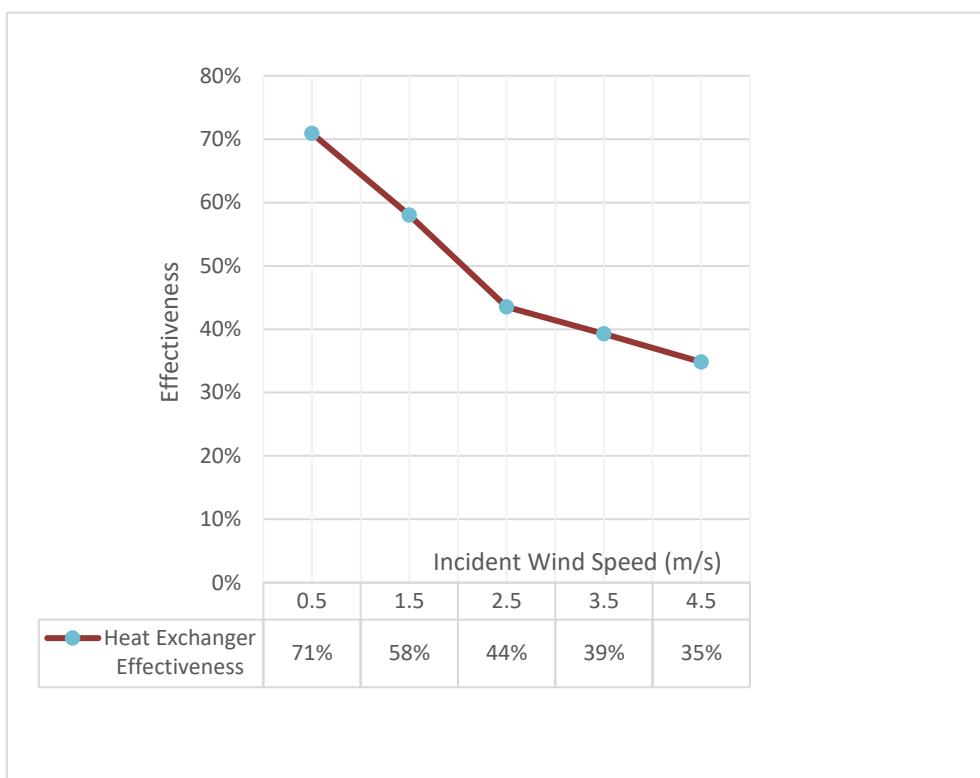


Figure 6-14: Heat Exchanger Effectiveness

Figure 6-15 to Figure 6-17 shows the distribution of temperature and flow through the heat exchanger at flow rates generated by a 2.5m/s incident wind on the windcatcher. Similar patterns were observed for all simulated scenarios. A gradual temperature change in each flow stream can be seen. Velocity distribution shows an area of flow separation towards the heat exchanger axis at the inlets. The heat flux at this location is very low and the heat transfer surface

is not efficiently used, thereby affecting overall performance of the heat exchanger [290]. The evidence of this can be seen on the heat flux contour in Figure 6-18 as the deep blue area.

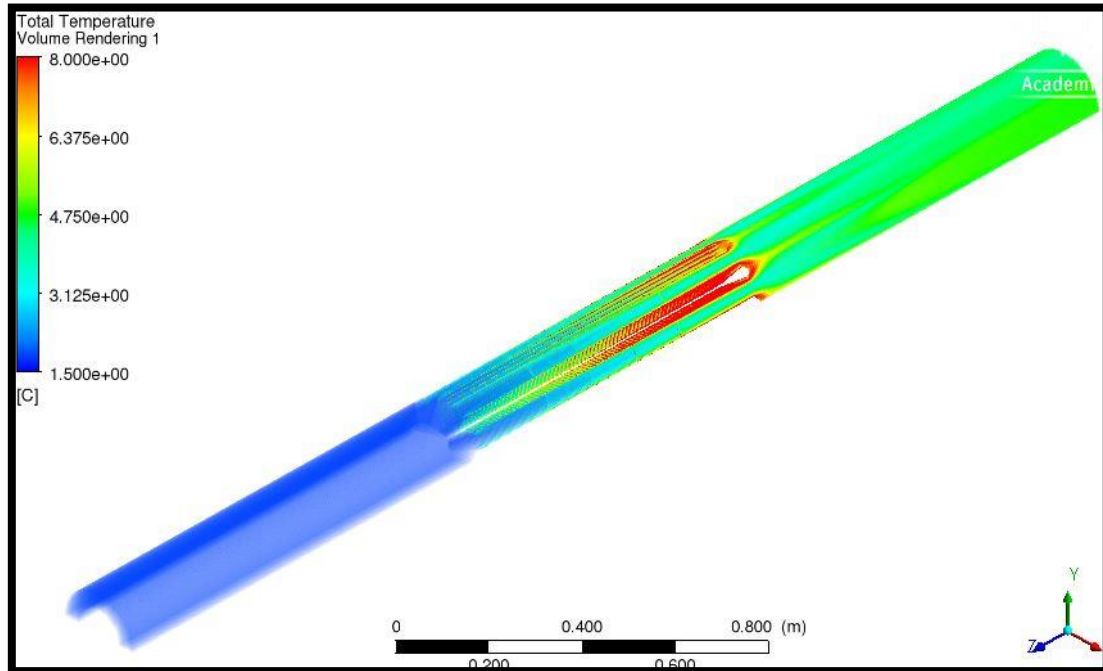


Figure 6-15: Annular Supply Flow Temperature Contour

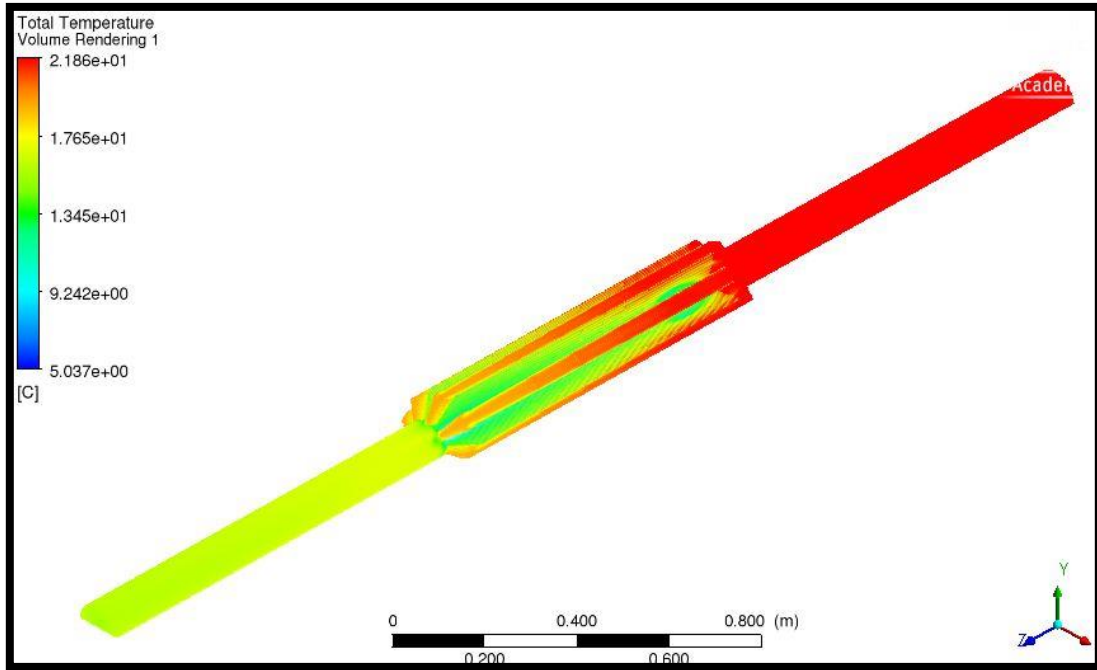


Figure 6-16: Centre Extract Flow Temperature Contour

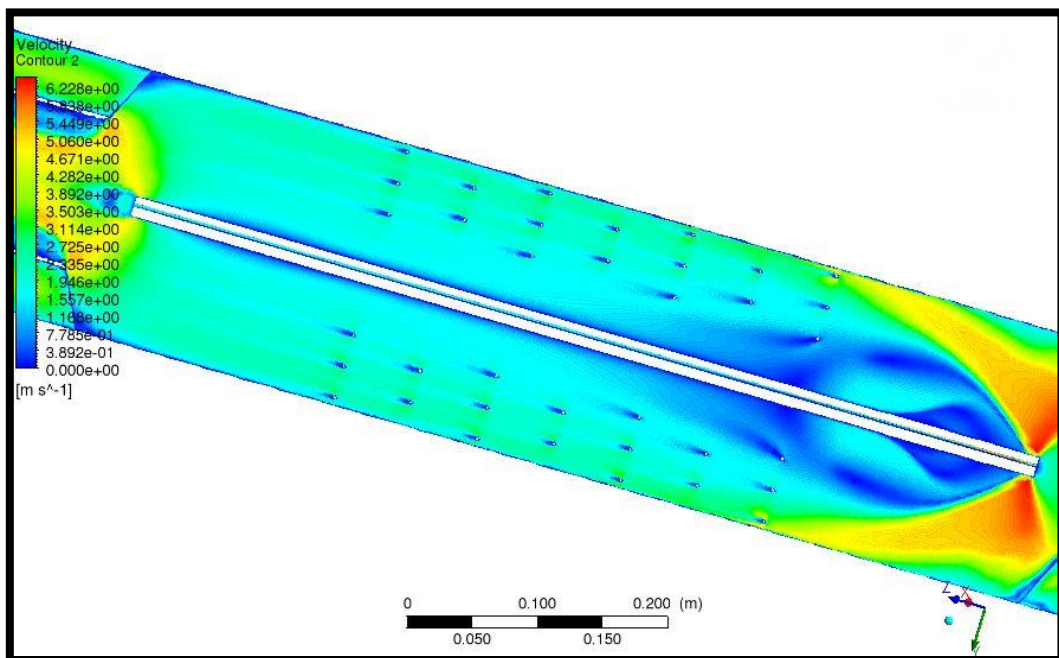


Figure 6-17: Velocity Contour of Centre Channel Flow through Heat Exchanger

An observation of the heat flux distribution over the heat exchange surfaces shows that it is relatively constant along the flow direction. This is characteristic of counter flow heat exchangers. There is an increase at the flow inlet area where the air velocity is higher and, around the rings where turbulence is induced. In areas where the rings are absent, a reduced heat flux is observed. Therefore, the introduction of these features in these areas served to increase the heat flux.

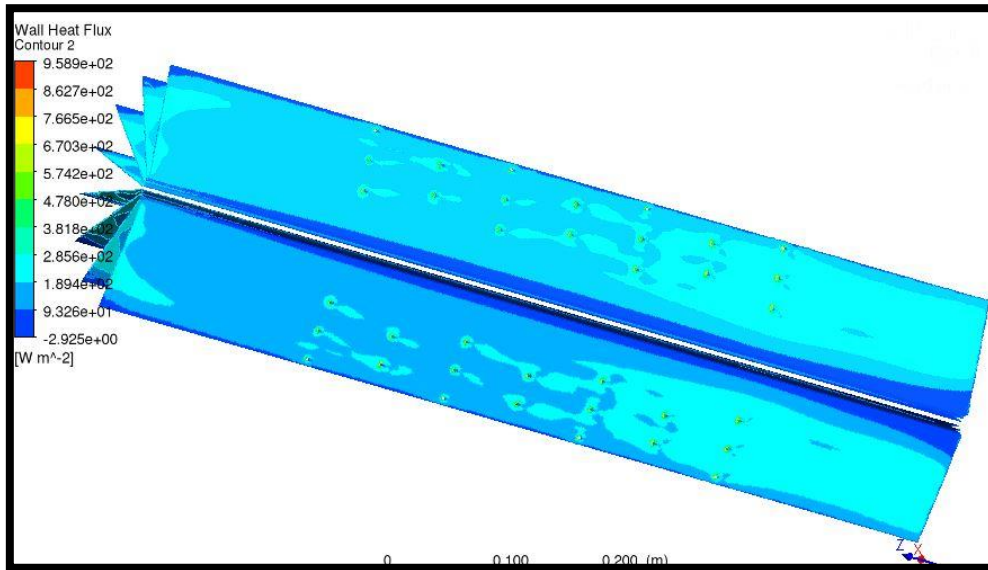


Figure 6-18: Heat Flux on Heat Transfer Surfaces of Heat Exchanger

As expected the staggered arrangement of cylindrical ring turbulators introduce some turbulence into the flow as shown on the plot of turbulence intensity. This increases the average turbulence of the entire flow and consequently the heat transfer. This corresponds to results gotten by T. Tahseen et al [291] when they investigated different arrangement of cylindrical turbulators. This is more evident towards the flow outlets where it can be seen that turbulence is generally decreased except around the pins.

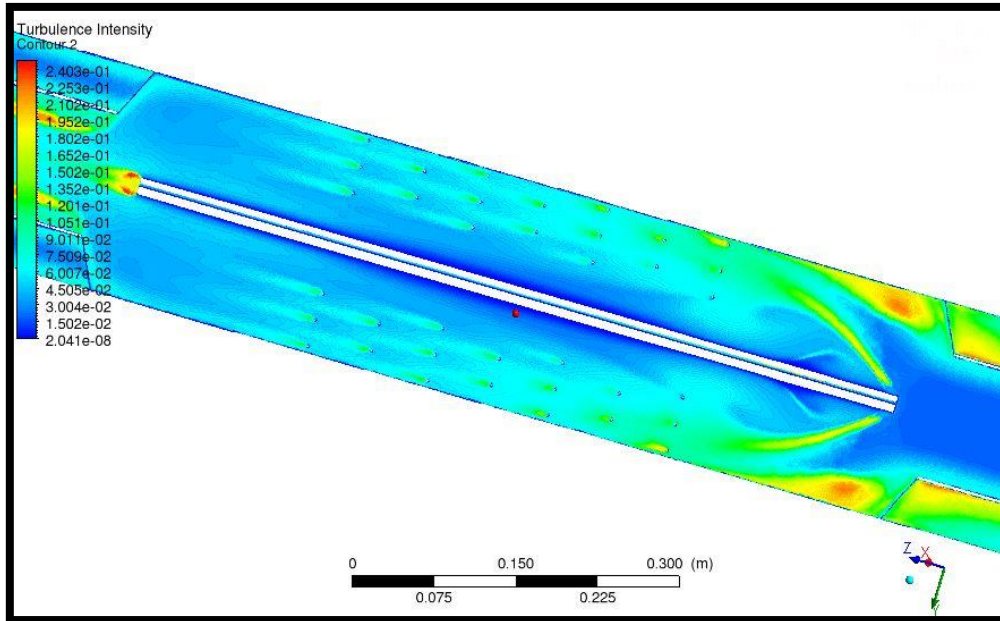


Figure 6-19: Turbulence Intensity Through Heat Exchanger Channel

6.5.2.2.2 Pressure Performance:

The graph in Figure 6-20 shows the pressure drop across the heat exchanger at the incident wind speeds shown. These are mass-weighted values of total pressure taken at planes parallel to the heat exchanger end cap outer end locations. As expected, the pressure drop is quite low at low flow velocities but increases as the incident wind speed increases. The trends for both annular and centre channels of the heat exchanger are also similar with the annular supply section experiencing a bigger pressure drop compared to the centre extract flow. Values for pressure drop are shown below on Figure 6-20. Pressure drop was less than 1Pa at 0.5m/s. This increased to a maximum of 13Pa through the Supply channel at 4.5m/s wind speed.

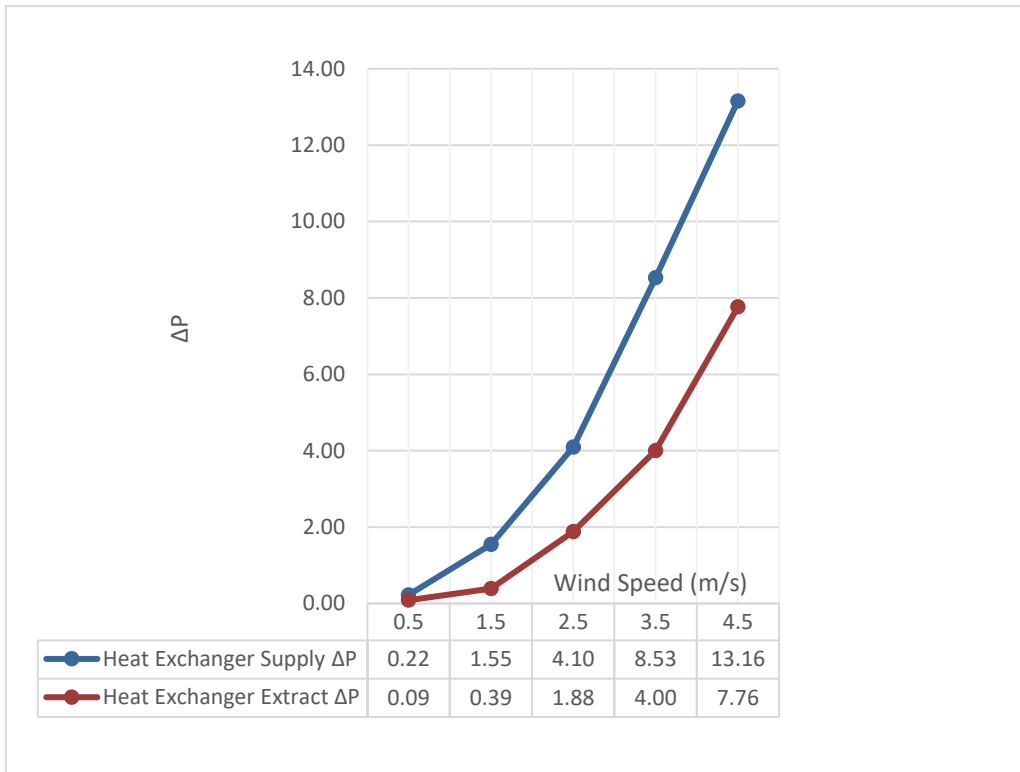


Figure 6-20: Heat Exchanger Pressure Drop

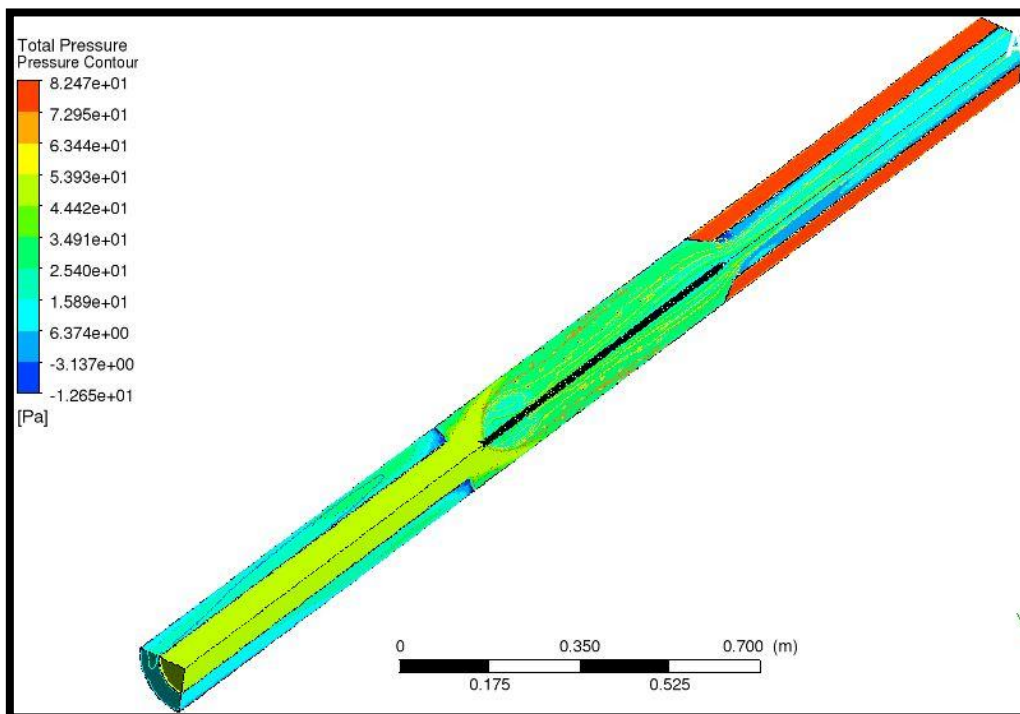


Figure 6-21: Contour of Pressure Distribution at 2.5m/s Incident Wind Speed

6.5.2.3 Whole System Performance

A CFD investigation was carried out on the proposed system as a unit consisting of the windcatcher with heat the exchanger attached to its base. This was simulated in Ansys Fluent in 3D and reported in the following sections.

6.5.2.3.1 Simulation Model

Some simplifications were carried out to reduce computational effort for this larger model. All solid parts have been removed to derive sections only representing the fluid flow. The simulation was also carried out for half of the entire system along its vertical symmetry as done for previous simulations in this study. The heat exchanger walls were modelled as 0.3mm thick copper shells. This allowed the computation of conduction in both the normal and planar direction of the wall. The heat exchanger's cylindrical ring turbulators were also extracted from the model to reduce computational effort. The effect of the turbulators would be to increase thermal performance of the system with minimal pressure drop. This can be thought of as additive performance quantities that can be easily accounted for after a simulation without these features. The simulation domain is also reduced in size. The lower limits of domain size recommendations from Franke et al [246] has been adopted. In previous simulations, the domain size was generous and above these minimums. Following techniques adopted in previous simulations to make meshing easier, the domain has also been divided into 4 parts representing the annular, central, cowl and wind air sections. The interfaces of these parts have shared topology and are modelled as internal surfaces. With this option Fluent treat the interfaces as internal domains of the fluid and they are meshed together. The symmetry through the heat exchanger was cut at a plane through the fluid streams to create four cold stream of annular supply air flow bounded on both sides by three full and two halves of extract flow hot streams. The annular and central sections of air flow were extended by 1.5m below the heat exchanger to allow for flow development. All values for post-processing were taken at the relevant domain planes as mass-weighted average values of the quantity of interest.

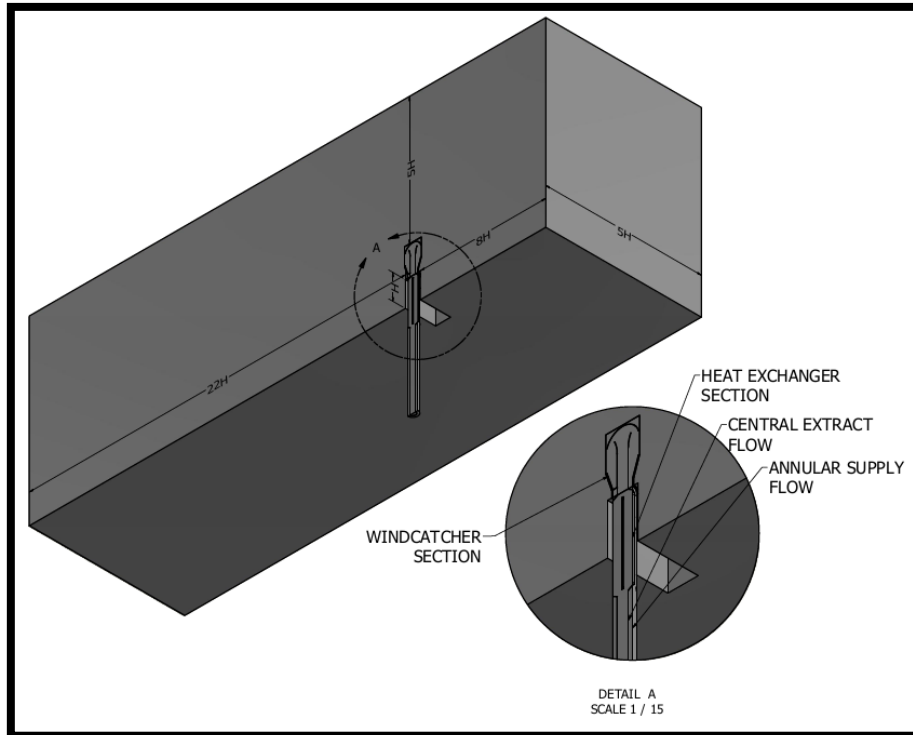


Figure 6-22 Whole System Simulation Domain

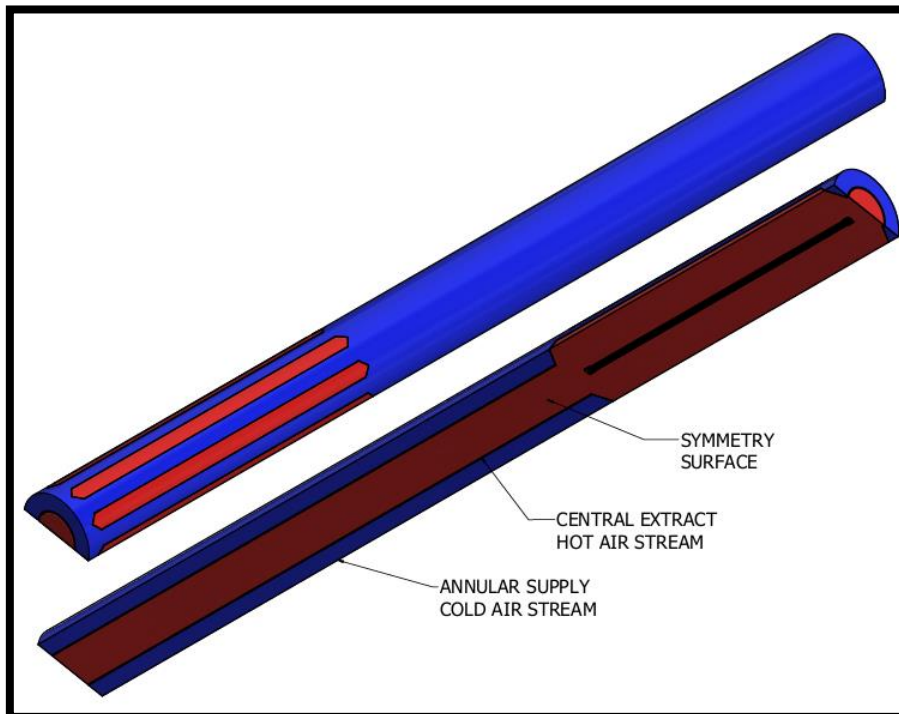


Figure 6-23 Symmetry through Heat Exchanger

6.5.2.3.2 Boundary Conditions

The cell zone conditions were set as air. Uniform velocity boundary conditions of 0.5m/s, 1.5m/s, 2.5m/s, 3.5m/s and 4.5m/s were applied normal to the domain inlet to create 5 simulation scenarios representative of these wind speeds. The opposite domain outlet and terminal surfaces of the annular and central channels were all set as pressure outlets. Symmetry boundary condition was also applied at the model symmetry plane, top and opposite side of the domain. Two thermal boundary conditions were applied. The applied air velocities at the domain inlet were all set at a temperature of 2⁰C. At the lower part of the domain on the surface of the central channel, a temperature of 22⁰C was applied. These are representative of a cold outdoor winter condition and a heated indoor condition as defined in section 6.4.1.2 under operating conditions. All other surfaces were left in their default state. Ansys Fluent automatically model these surfaces as smooth non-slip walls.

6.5.2.3.3 Meshing

Ansys Meshing was used to define optimum tetrahedral element sizes for each part making up the model to capture areas of strong curvature and close proximity especially within the heat exchanger. The model was subsequently meshed sequentially starting with the annular section, the cowl section, the central air section, then the wind section. This allowed for optimum part-based mesh generation. 10 inflation layers were specified on all wall boundaries to adequately resolve gradients at the walls using a y^+ value of 1. This provides a better resolution of flow in this region. The resultant mesh had 12 million cells. A mesh independence study was carried out at 2.5m/s wind speed where subsequent simulation were run to convergence and checked for the value of y^+ within the cowl and heat exchanger flow sections. Mesh refinements were also carried out based on gradient and curvature of velocity within the general flow domain. The average through the channel sections were monitored alongside the air temperature change. Mesh 3 (Table 6-3) provided the best balance between computational resource and accuracy. The final mesh count after 4 refinements was 19.5 million cells.

		Mesh 1	Mesh 2	Mesh 3	Mesh 4
	Cell count (millions)	12	17	19.5	23
Supply Channel	Mass-weighted average velocity(m/s)	0.6	0.45	0.48	0.47
	Temperature Change (Kelvins)	5	5.5	5.67	5.65
Extract Channel	Mass-weighted average velocity(m/s)	0.55	0.58	0.6	0.6
	Temperature Change (Kelvins)	2.02	2.24	2.26	2.25

Table 6-3 Whole System Mesh Independence Study

6.5.2.3.4 Solving

2000 Steady state simulations were specified using the SST K-Omega turbulence model and coupled Pressure-Based Solver. Solution monitors were set to monitor air outlet temperatures and velocities. These were used in conjunction with the solution residuals to judge convergence. The solution was thought to have converged when the solutions remained unchanged, the solution residuals are below a 10^{-3} tolerance and for energy, below 10^{-6} .

6.5.2.3.5 Flow Performance

At all simulated wind speeds the system channels showed the desired flow configuration i.e flow in the annular channels was downwards as supply and that in the central channel was upwards as extract flow.

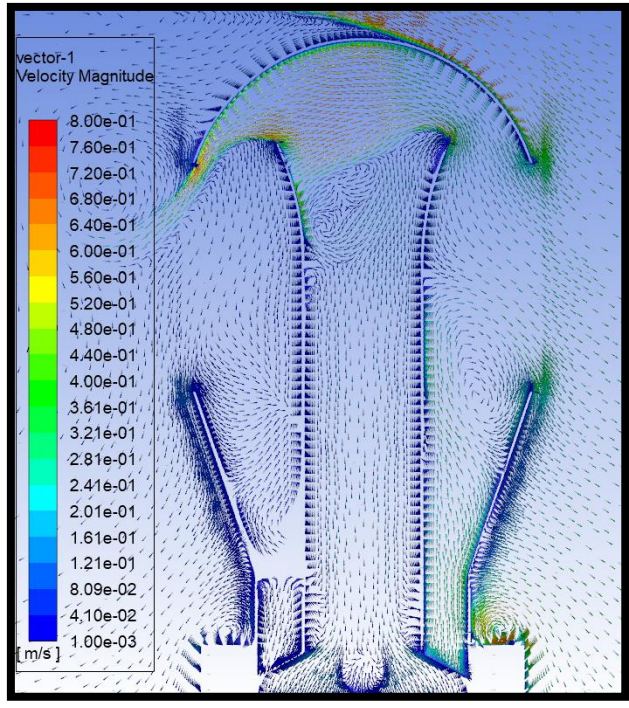


Figure 6-24 System Windcatcher Velocity Vector at 0.5m/s Wind Speed

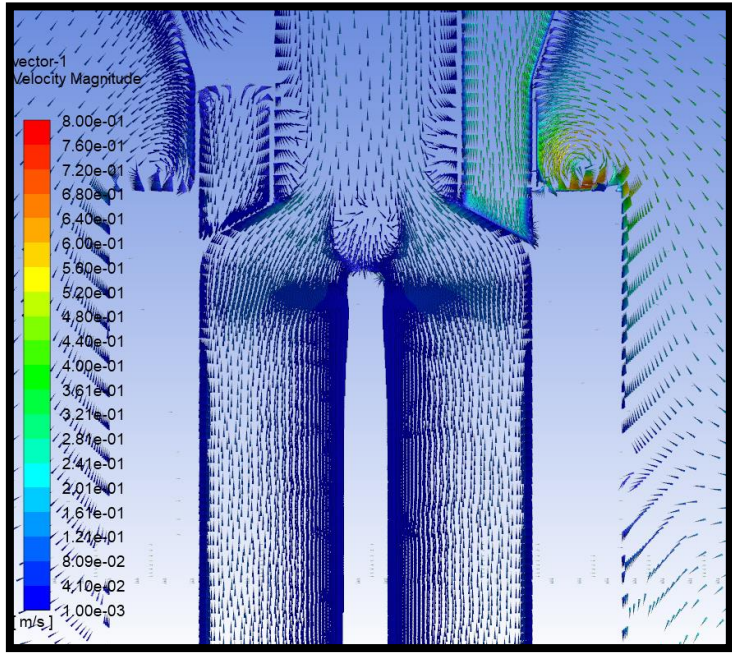


Figure 6-25 System Heat Exchanger Extract Velocity Vector t 0.5 m/s Wind Speed

The flow through the supply channel increased from 0.07m/s at 0.5m/s incident wind speed to 0.94m/s at 4.5m/s incident wind speed (Figure 6-26). The extract flow was faster at all wind speeds. However, due to the difference in channel cross-sectional area (The annular supply channel total cross-sectional area is twice that of the central extract channel), the volume flow rates through both channels differ in value in the reverse order (Figure 6-27). Across all scenarios, the central outlet extract flow rate was on the average 37% less than that of the inlet supply flow. This is desirable as buoyancy will add to the extract flow rate bringing it closer to the supply flow rate. A significantly stronger extract flow through the central channel can induce severe short-circuiting at room level.

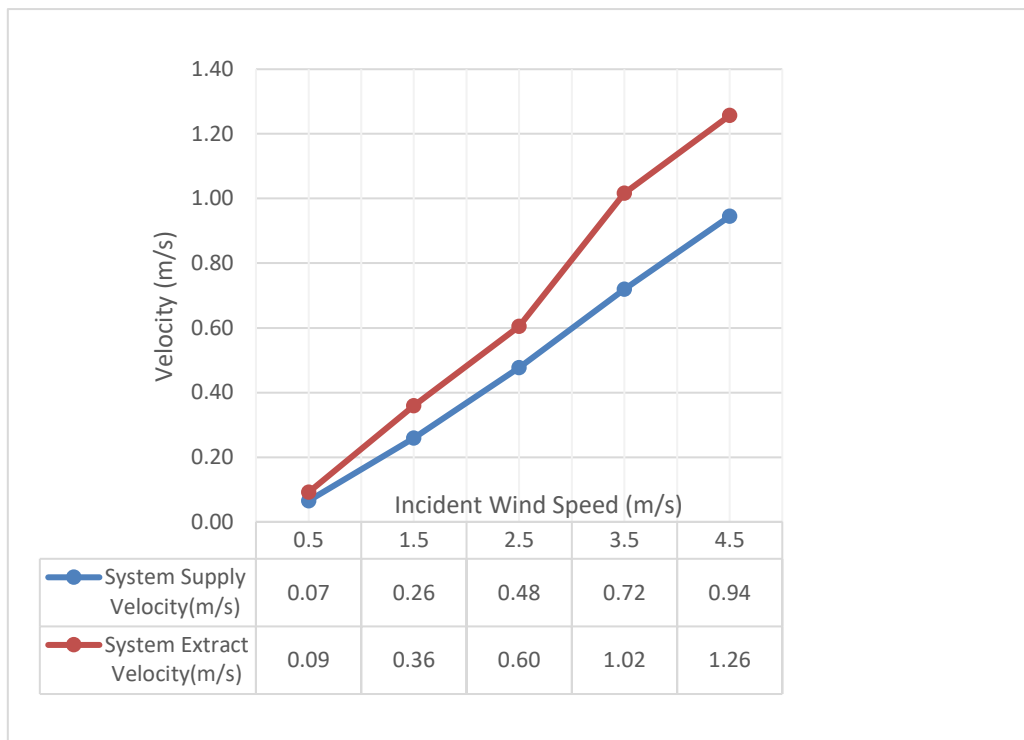


Figure 6-26 System Channel Velocities

Ventilation performance for $27m^3$ test room is plotted on Figure 6-27. At every simulated wind speed above $\sim 1m/s$, the system was able to supply ventilation air flow above the CIBSE recommended minimum of 0.7ach. The ventilation performance was 0.3ach at 0.5m/s incident wind speed. This increased to 4.5ach at 4.5m/s incident wind speed. The ventilation performance of the system as a unit (windcatcher and heat exchanger) is compared on Figure 6-28 with that of

the windcatcher alone from Figure 5-56. The system ventilation performance was 10% lower on the average due to the heat exchanger resistance in the flow path.

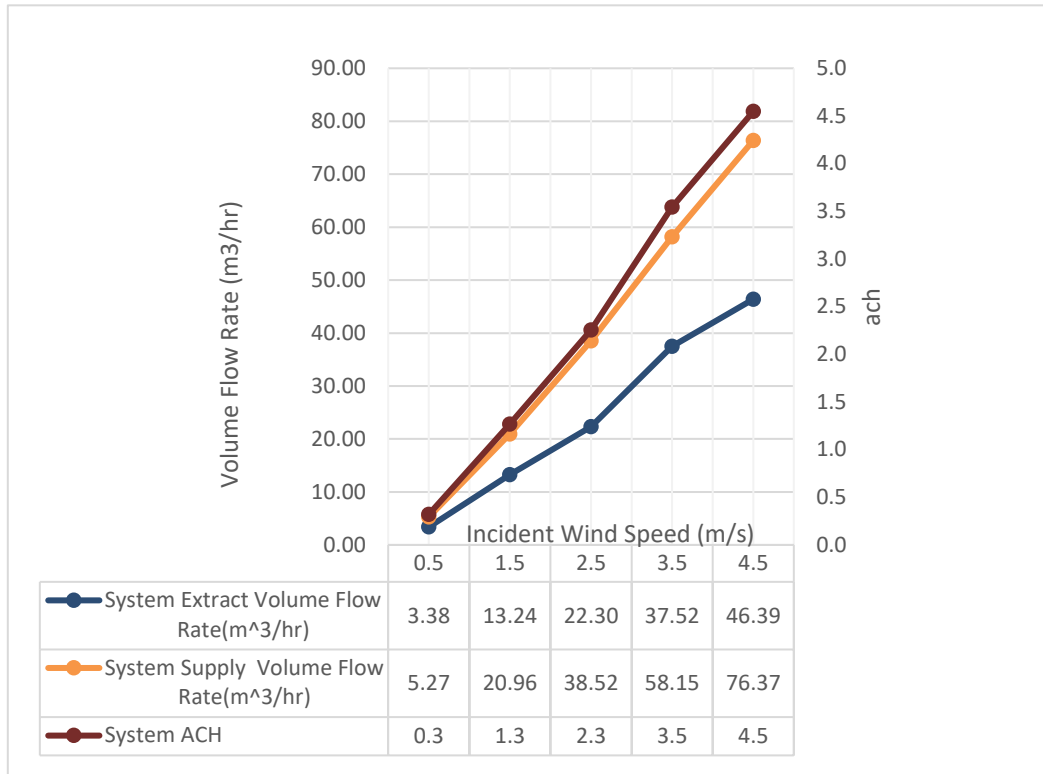


Figure 6-27 System Ventilation Performance

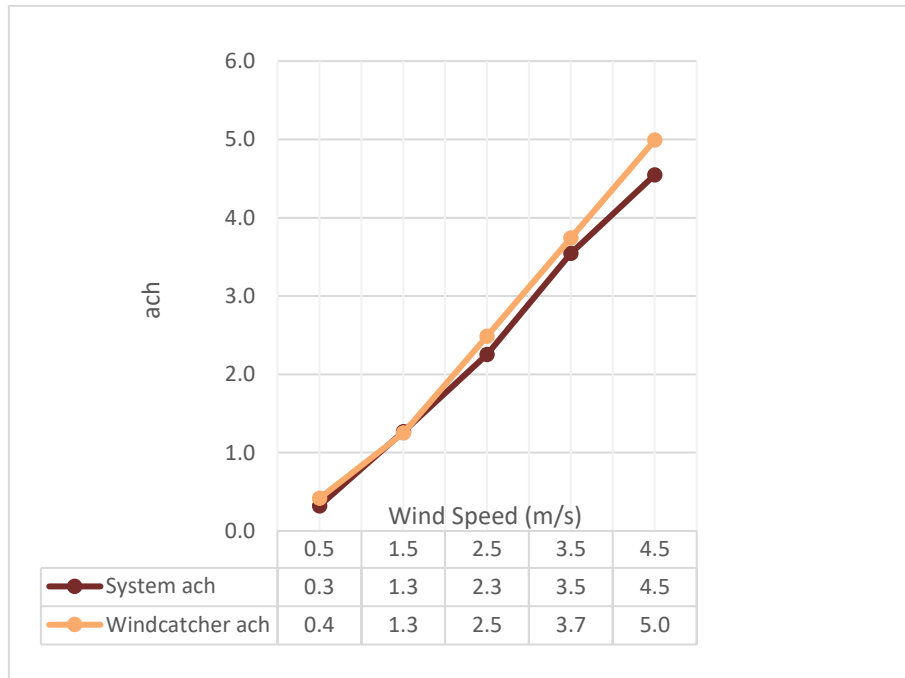


Figure 6-28 System vs Windcatcher Ventilation Performance

The flow through the system was also not uniform. The flow through the heat exchanger-only model was uniform across the cross-section compared to that of the system scenario where flow entry was through frontal annular supply channel with all others closed. The section facing the incident wind direction showed an overall faster air flow through the entire system. The heat exchanger did not temper this flow non-uniformity as high energy flow was still observed on the frontal side of the annular supply channel below the heat exchanger. In contrast, flow through the central extract channel was relatively uniform.

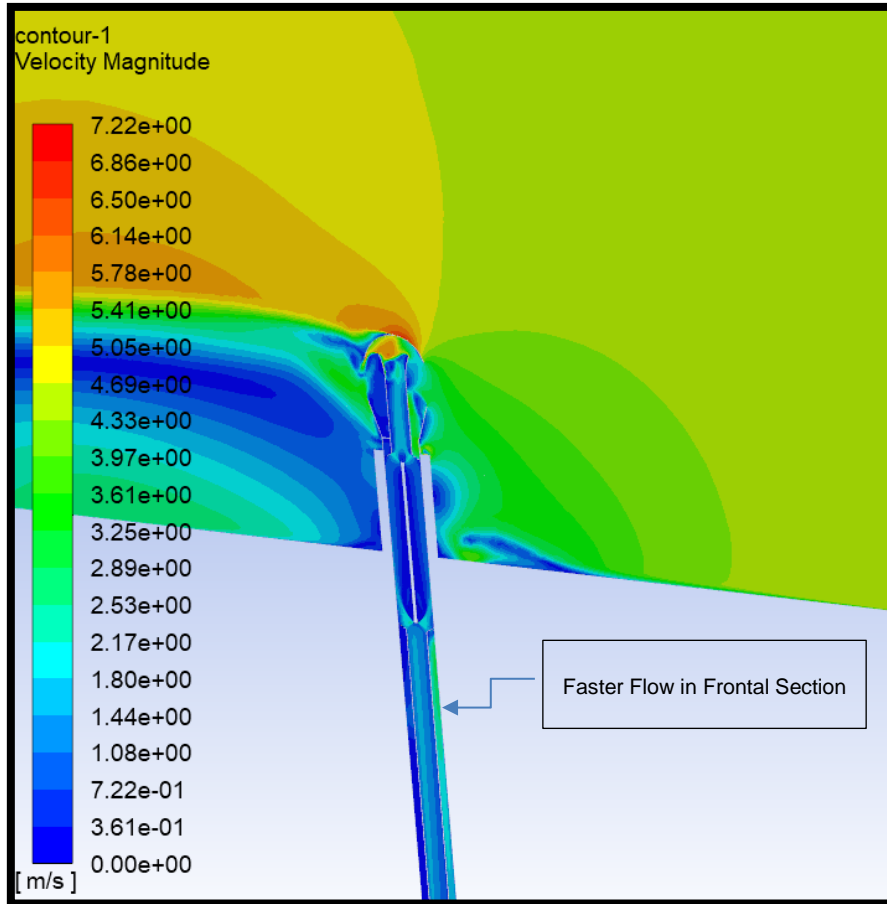


Figure 6-29 Velocity Contour 4.5m/s Wind Speed

6.5.2.3.6 Thermal Performance

Figure 6-30 shows the temperature change of each channel flow through the system. The slower annular supply flow gained 9 degrees as it flowed through the system when the wind was incident at 0.5m/s. This decreased to about 4.5 degrees as the wind speed increased to 4.5m/s. The temperature change in the central extract flow varied in the reverse order by increasing from 1 degree to 2.71 degrees. This is due to the flow rate variation (Figure 6-27). As the wind speed increases, the difference in flow rate through the channels become larger with the supply flow rate peaking significantly above that of the extract flow rate at 4.5m/s wind speed. This has the effect of removing more energy from the extract flow at higher wind speeds while decreasing the bulk temperature gain of the supply flow.

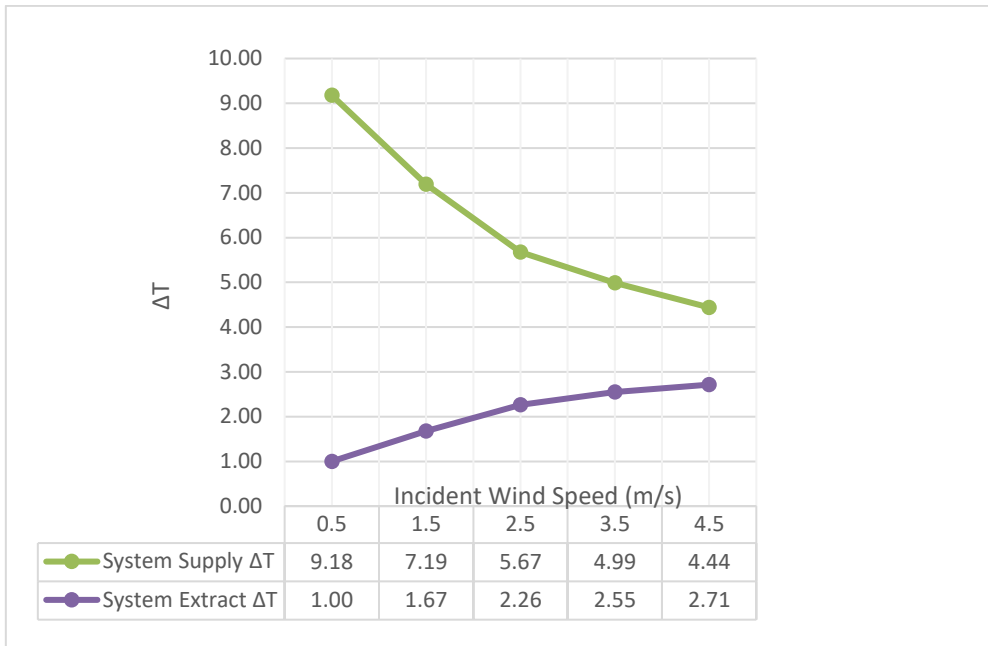


Figure 6-30 System Channel Flow Temperature Change

In Figure 6-31, the heat exchanger effectiveness of the system has been plotted and compared with that of the heat exchanger alone from Figure 6-13. Effectiveness for the system peaked at 46% at 0.5m/s wind speed. This steadily decreased to 22% at 4.5m/s wind speed. In comparison with the heat exchanger unit performance. The thermal performance was reduced by an average of 27% when the system is integrated as a unit.

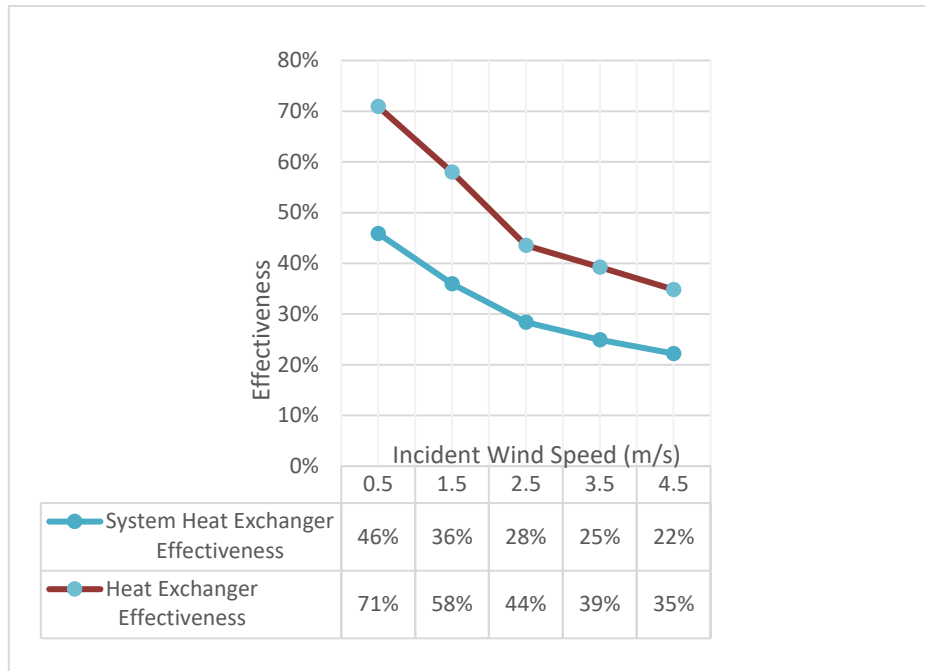


Figure 6-31 System vs Heat Exchanger Effectiveness

This performance reduction can be attributed to the non-uniform pattern of annular supply flow through the system (Figure 6-29). In the heat exchanger-only simulation from Figure 6-13, the flow values were uniformly applied at the channel inlets. In this simulation, flow through the heat exchanger was unevenly distributed at all wind speeds with high energy flow towards the frontal portion of the supply channel. This created colder high heat exchange conditions in this region compared to hotspots at the back section (Figure 6-32, Figure 6-33 and, Figure 6-34).

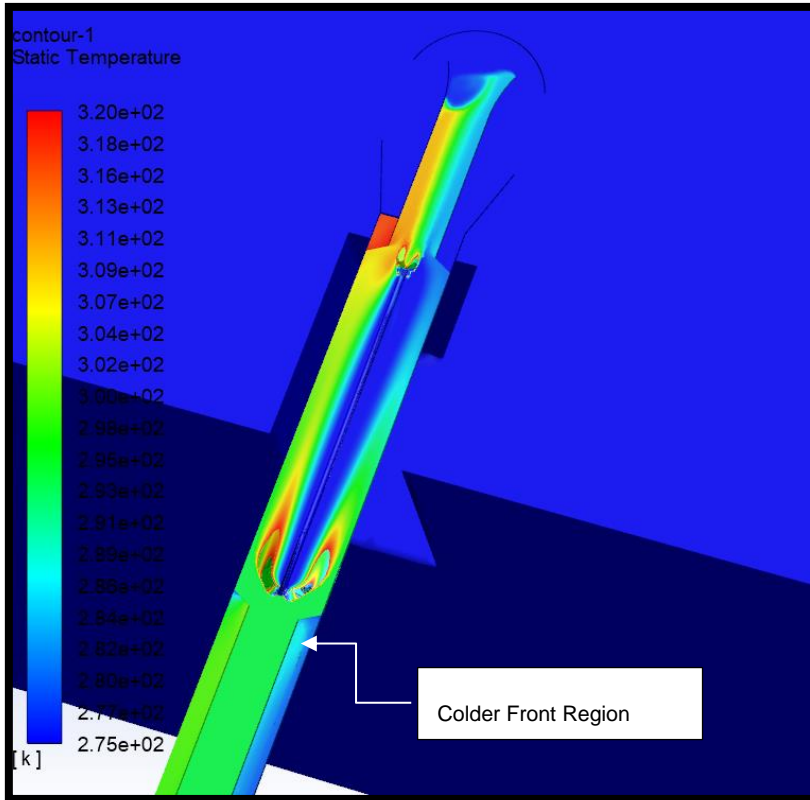


Figure 6-32 Temperature Contour at 0.5m/s Wind Speed

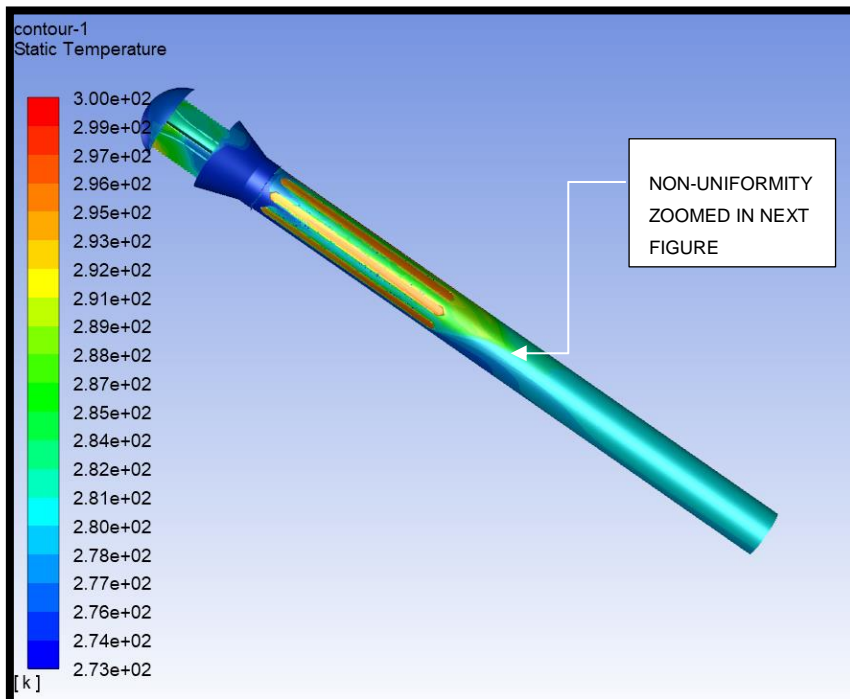


Figure 6-33 System Temperature Contour at 4.5m/s Wind Speed

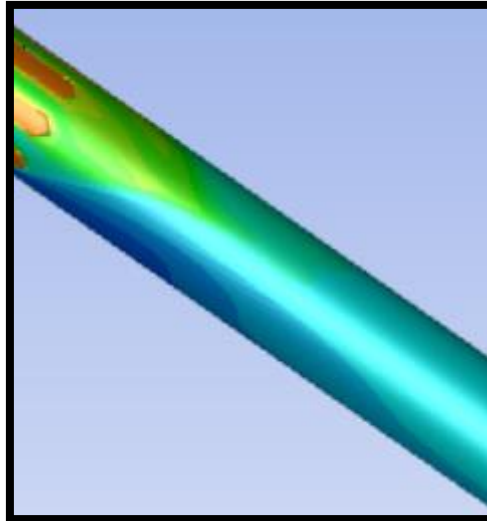


Figure 6-34 Temperature Contour- Zoomed

The temperature contour also confirmed an earlier observation made in section 5.2.2 regarding the extract flow path. It was mentioned that the primary exit path(s) for the extract air flow is through the dome section(s) at the sides. Temperature contours of the windcatcher revealed this at every wind speed as the warm extract air flow warmed up the side dome sections of the windcatcher (Figure 6-35).

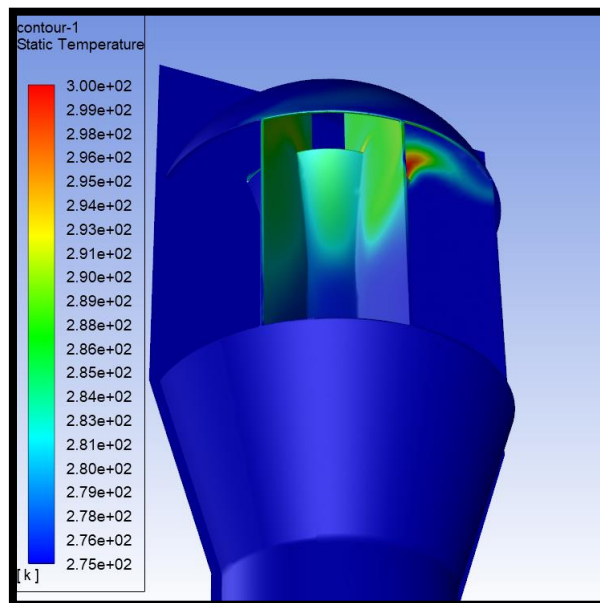


Figure 6-35 Windcatcher Temperature Contour at 0.5m/s Wind Speed

6.5.2.3.7 Pressure Performance

The pressure performance is plotted on Figure 6-36 below and compared with the heat exchanger-only scenario. As shown below, the pressure drop values are quite low at low flow velocities but increases as the incident wind speed increases. The trends for both annular and centre channels of the system are also similar to those of the heat exchanger alone. The pressure drop for the system as a whole was lower at all wind speeds compared to that of the heat-exchanger. This difference can also be attributed to the non-uniformity of flow within the system compared to that of the heat-exchanger alone scenario. Pressure drop through the system was negligible and less than 0.1Pa at 0.5m/s and this increased to a maximum of 7.12 Pa through the Supply channel at 4.5m/s wind speed.

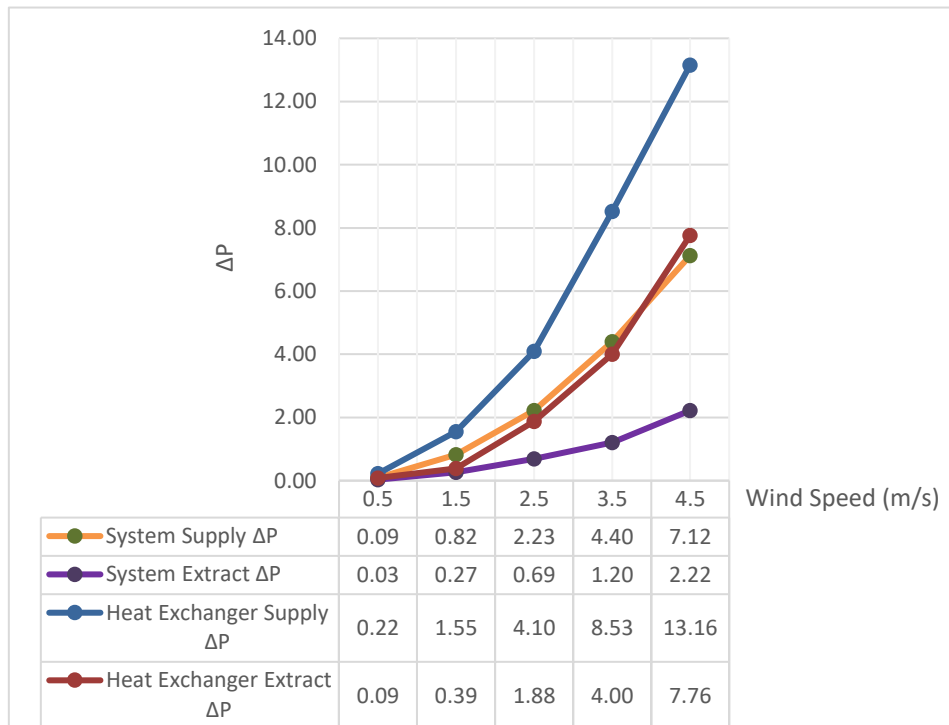


Figure 6-36 System vs Heat Exchanger Pressure Drop

7 DESIGN OF VALIDATION EXPERIMENTS

The need for experimental testing is borne out of the limitations imposed by numerical CFD techniques. These limitations are largely the range of assumptions made in CFD to make computation easier. Although, the theory and numerical approximations of incompressible flows in CFD has been highly developed and resilient, there are many important features of fluid flow and interactions like turbulence and boundary layer interactions that cannot be fully accounted for. While advanced CFD techniques like Large Eddy Simulation (LES) presents a more accurate method in theory to predict fluid behaviour, the computational resources required for it is immense. Investigative work such as carried out in this research will typically require up to 100million elements when meshed and will take up to 16 days to simulate a 30 second event [196]. Hence, experimentation is indispensable because it provides concrete data which can be used to further refine theories and determine the influence of various interactions within a fluid flow field. In general, therefore, numerical studies need to be supplemented by experiments. The following sections detail proposals for thermal comfort study, large-scale test, and wind tunnel testing of the windcatcher.

The thermal comfort study extends the theoretical and numerical studies that can be performed on the proposed system to provide data on indoor conditions achievable with the system. Definitive data on thermal comfort are best achieved during in situ testing over an extended period. This calls for large scale experiments on which information has also been included to provide guidance on carrying out the task. Data from the large-scale test can be used in confirming the numerical thermal comfort model which can be more conveniently extended or modified for system performance prediction in different space and building configurations.

Wind tunnel experiments which often is most convenient to conduct on scaled models, is proposed for the experimental investigation of the proposed windcatcher unit performance. From the perspective of design of fluid flow geometries, wind tunnel experiments have two principal uses. Firstly, they make

it possible to determine the influence of the various features of the design, and of modifications to them, in a manner which is relatively safe, quick, and cheap compared to in-situ tests in real life conditions. Such tests are usually very straight forward and conditions which can only materialize over a long period in situ can be replicated quickly and conveniently. The second use of wind tunnel experiments is for provision of information of a fundamental nature, usually in conjunction with theoretical work like CFD numerical modelling. By experimental means, the theoretical work is confirmed, so laying the foundation for further design improvements or refinement of the system under investigation.

7.1 Thermal Comfort Study

To study the impact of the ventilation system on thermal comfort, TRNSYS 17® can be used. TRNSYS 17® is computer simulation software that can simulate the transient performance of thermal systems in buildings. It works by employing a modular approach whereby the user specifies the components that constitute the system and the way they are connected [292]. The TRNSYS 17® library consists of many components called 'Types' found in thermal energy systems, as well as components to handle the input of different weather data for different locations around the world. Of relevance is the Type 56 Multi- Zone building. This component deals with the thermal balances of a building having up to 25 thermal zones. The building model in Type 56 is designed in such a way that its different physical characteristics and adjacencies of the zones can be specified. The flexibility of TRNSYS 17® allows the modelling of new technologies with Fortran compilers and quick incorporation into its software library [293]. Analytical models of similar technologies to the one in this research are available.

TRNSYS 17® has been employed widely in the simulation of indoor environment when studying HVAC systems. S.Lu et al [294] validated a group of TRNSYS types when they simulated the performance of PCM panels in a room and concluded that both the trend and simulated data agreed with experimental values with 90%-98% accuracy. R. Chargui et al [295] further used TRNSYS in predicting the indoor environment performance of a dual source heat pump in winter and A. Hobbi et al [296] used it to study a solar water heating system for

residential unit in Canada. The versatility of TRNSYS was demonstrated by B.L. Gowreesunker et al [297] when they coupled it with Ansys Fluent CFD software to predict the performance of ventilation system in an airport departure hall. R.Eldeeb et al [298] expanded the use of the software to studying the humidity conditions in a room when heat and moisture transfer panels are employed, and A. Wills et al [299] and M.L. Sweet et al [300] both used TRNSYS to study solar heating in a single house over yearlong seasonal variations. A. Wills et al [299] concluded that TRNSYS 17®'s flexibility and unit modular nature enables scientists to readily analyse new sustainable technologies. Further pointing out that this presents a big improvement over the modelling capabilities of similar software.

7.2 Wind Tunnel Testing of Windcatcher.

Wind tunnel testing has been widely applied in investigating the performance of ventilation systems [115]; [128]; [129]; [130]; [131]; [132]; [133]; [134]; [135]; [136]. Specifically, in the field of natural ventilation, it has been confirmed a robust technique in natural ventilation system development; H. Montazeri et al [95] used wind tunnel testing to study the flow through a wind catcher natural ventilation device, M. Esfeh et al [96] used it to determine the optimal wind catcher roof geometry for a natural ventilation system, Y. Su et al [70] used it in evaluating a commercially available wind catcher system, etc.

The proposed system in this study can be tested in a wind tunnel at different wind speeds to quantify performance and correlate the results with those gotten from CFD simulations.

7.2.1 Test Model

The full-size prototype of the windcatcher measures 600mm in height. Considering the practical constraints in testing a full-size prototype in a wind tunnel, a reduced scale model; half of the full size can be used. The ability of measurements taken from reduced scale models in a wind tunnel to predict flow characteristics in a full-size model is highly dependent on being able to replicate aspects of the real flow in the scaled experiment. Although desirable, not all

aspects can be replicated at the same time. Thus, the properties of interest, if replicated successfully can suffice in wind tunnel experiments.

The first obvious similarity criterion between reduced scale and full-size models is geometric. Scaled models must have geometric dimensions that are a ratio of the full-size dimensions on all dimensions. For the scaled model to properly replicate the fluid flow properties of a full-size model, they also must be kinematically and dynamically similar. Kinematic similarity requires that the velocity at corresponding positions have the same direction and a constant ratio of their magnitudes. Dynamic similarity on the other hand, requires that corresponding forces have the same directions and a constant ratio of their magnitudes. When two flows are similar, results collected from one can be used for prediction in the other after scaling. Scaling is the process of non-dimensionalization of the experimental result quantities to produce quantities that are independent of the unit system [301]. In a system consisting of a model in a fluid flow stream, dynamic similarity between a scaled and full-size system can be established if the relationship between physical properties of both systems is the same.

In steady incompressible subsonic viscous flows, the force experienced by a body in a moving fluid depends mainly on the relative velocity " U ", the size of the body defined by a characteristic length " l " and on the kinematic viscosity " ν " of the fluid. The theory of dynamic similarity shows that if the Reynolds number Ul/ν is the same for two fluid flow systems (i.e. a full and a scaled one), the pressures at the same points on both models is proportional to ρU^2 [302]. Therefore, provided the Reynolds number for both flows is the same, the non-dimensional functions of fluid velocity components like pressure coefficient will be the same for scaled and full model. When other properties of the fluid play an important role in the fluid motion, other non-dimensional parameters must be matched in the scaled model. In flows heavily influenced by the weight of the fluid, it is important to match the Froude number. While those involving heat induced motion must consider the Prandtl and Grashof numbers [302]. These parameters are defined below:

$$Fr = U/gl^{1/2} \quad (53)$$

$$\sigma = \mu C_p/k \quad (54)$$

$$Gr = l^3 g \Delta T / \nu^2 T_0 \quad (55)$$

Where $Fr = Froude Number$, $\sigma = Prandtl Number$, $Gr = Grashof Number$,

$U = velocity$, $g = acceleration due to gravity$, $l = characteristic length$, $\mu = dynamic viscosity$,

$C_p = specific heat$, $k = thermal conductivity$, $\nu = kinematic viscosity$,

$\Delta T = temperature difference$, $T_0 = surface temperature$

In the experimental setup of concern, only the Reynolds number is required to be matched. The test air speeds should be within the operational range of the available wind tunnel and representative of the UK urban average at 10m above ground. An example is calculated as shown below.

*The kinematic viscosity of air at room temperature = $15.11 * 10^{-6} (m^2/s)$*

Full model characteristic length $l = 0.6 m$

UK Average Urban High Wind Speed at 10m height = $7 m/s$

Reynold's number at $7 m/s = 277961$

UK Average Urban Wind Speed at 10m height = $5 m/s$

Reynold's number at $5 m/s = 198544$

UK Average Urban Low Wind Speed at 10m height = $3 m/s$

Reynold's number at $3 m/s = 119126$

Hence, the wind tunnel test velocities are as follows:

Scaled model characteristic length $l = 0.3 m$

At equal Reynold's number, Wind Tunnel Test Velocities
= 14 m/s, 10 m/s, 6 m/s

In an ideal incompressible fluid, the criterion for similarity of the pressures at corresponding points in the flow field is [302]:

$$C_p = 1 - \left(\frac{U_1}{U_0}\right)^2 = 1 - \left(\frac{U_2}{U_0}\right)^2 \quad (56)$$

Where C_p = Pressure Coefficient

U_0 = Free stream velocity,

and the subscripts 1 = full model and 2 = scaled model

The generation of adequately high speeds may not be feasible in some wind tunnels. Reynold's number effects on properly non-dimensionalized forces, pressures, etc., as well as on flow patterns like flow separation are known to be weak for large Reynold's numbers [301]. Thus, it may be acceptable to conduct model tests at lower Reynold's number and extrapolate trends to higher Reynold's numbers.

Another important property to measure and match between CFD simulation and the wind tunnel experiment, is the turbulence intensity. Mean flow velocity in a fluid flow speed is usually made up of little velocity fluctuations within the field. The ratio of the root mean square (*rms*) value of these fluctuations to the mean velocity is called the turbulence intensity (ε) of the undisturbed flow. Flow management devices can be used to generate flows with a desired variation in turbulence structure. The statistically simplest type of turbulence is homogenous and isotropic, namely a flow whose statistical moments and other averaged properties are independent of location and orientation. This is a good environment for studying the effect of turbulence on a variety of models [301]. Turbulence intensity can be measured with a hot wire anemometer.

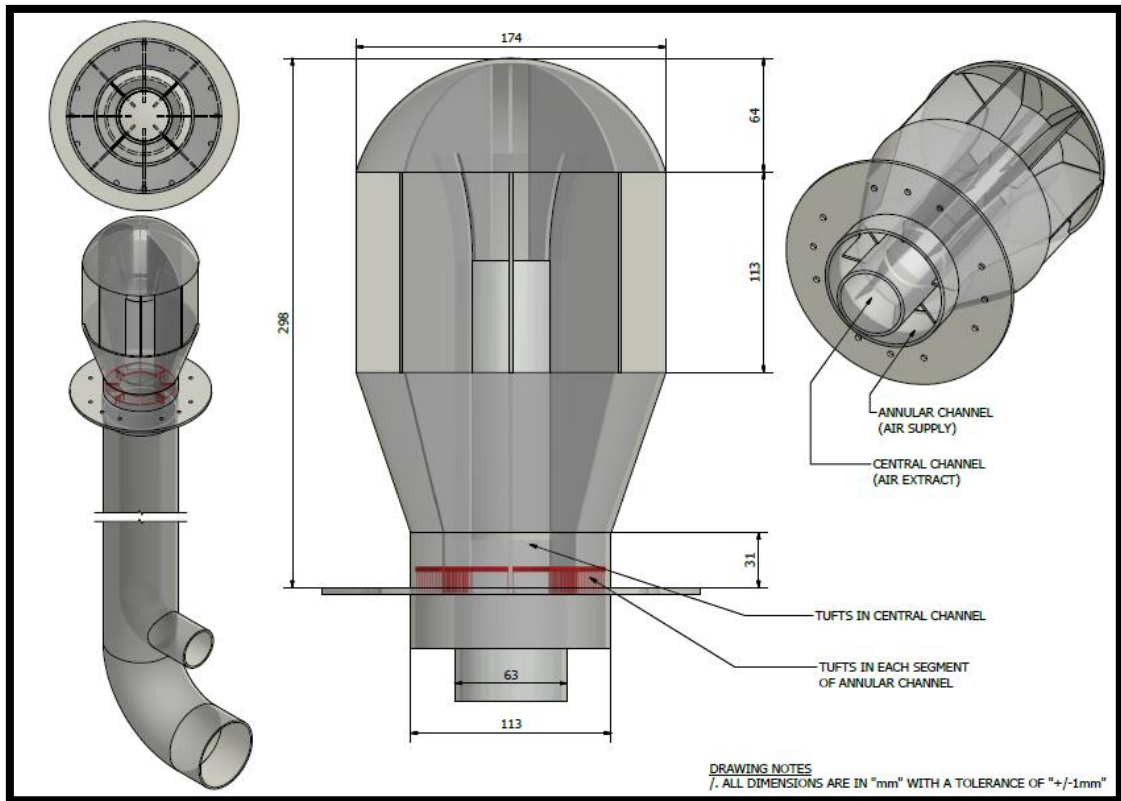


Figure 7-1: Test Model

A reduced scale test model is shown in Figure 7-1. It consists of the windcatcher attached to two concentric plastic pipes at the base. These are separated at a distance below the windcatcher to carry the opposing extract and supply flows in distinct ducts to allow for separate air velocity measurements. The windcatcher itself is made from clear acrylic and has tufts fixed in each annular channel plus the central channel to visualize flow direction during the experiment. Styrofoam cut-outs in the shape of the annular inlets can be used in sealing annular inlets to mimic the closing of sealed non-return valves in the full-scale prototype when in extraction mode. The disc around the base of the windcatcher is required to bolt it down in the wind tunnel during testing.

7.2.2 The Wind Tunnel

Wind tunnels are ducts containing a controlled flow of air used for the study of air flow past models. General purpose wind tunnels are usually of the low speed type with wind speeds considerably lower than 100m/s to reduce compressibility effects. They can be of the suction open-circuit type where air is drawn into the duct by a fan located downstream of the test section. Suction wind tunnels are generally cheaper to build and occupy less physical space. While they are less prone to disturbances caused by an upstream fan, they are vulnerable to external disturbances from the environment.

Another common arrangement for open-circuit wind tunnels is the blow down wind tunnel with the fan mounted upstream of the duct. While this seem to present more flow disturbances than the suction wind tunnel, it does allow for better flow control and utilization of various flow management devices.

Open wind tunnels generally suffer from environmental contamination and are less suitable for studies that require smoke visualization or seeding of particles. Closed circuit wind tunnels feature a recirculating flow path and better flow management with higher power efficiency [301]. They have reduced noise and contamination levels but are prone to self-heating. This must be taken into consideration in experiments where thermal and aerodynamic effects are coupled. Some variants feature cooling units to eliminate this effect. The wind tunnel available at Cranfield university where this research was carried out is an open circuit blow down type. A diagrammatic representation of the wind tunnel is given in Figure 7-2. Flow losses due to skin friction, vorticity and eddying motion etc. occur in wind tunnels. To provide air movement against these losses, the wind tunnel is equipped with a fan which accelerates the air to the required speed for the working section.

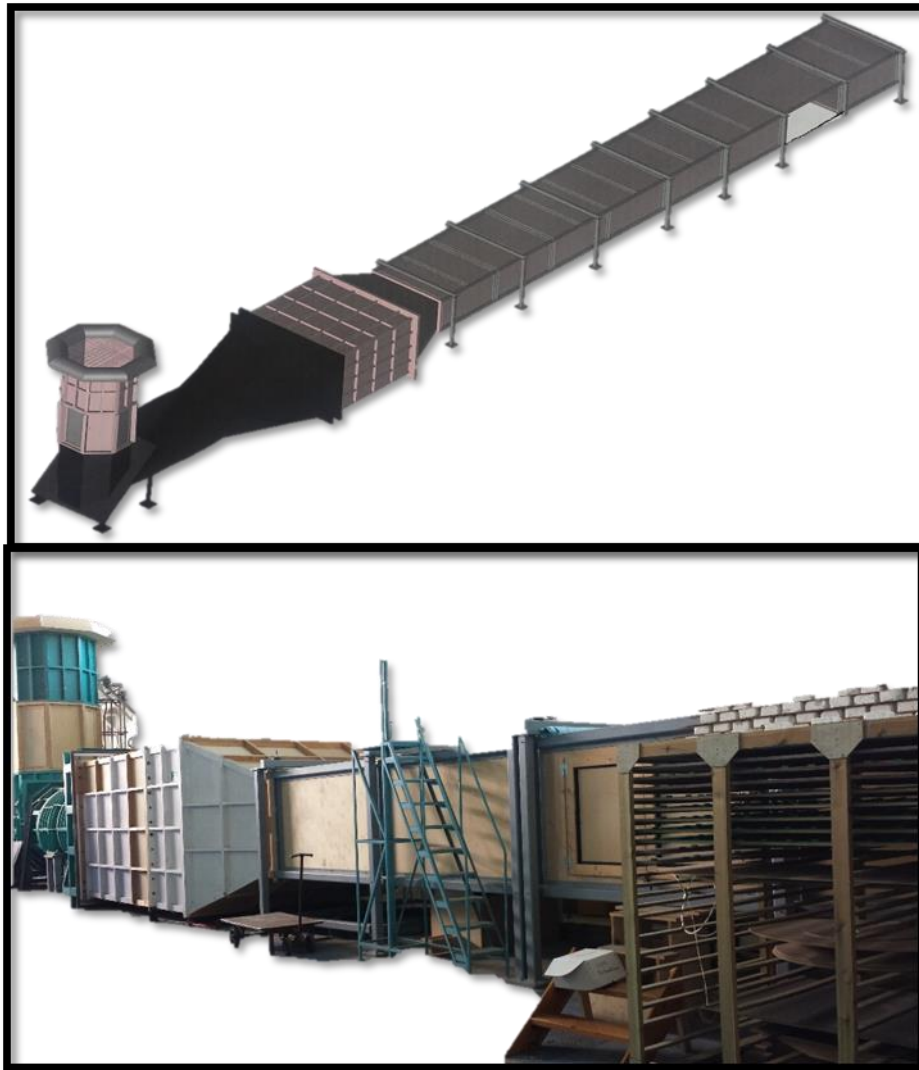


Figure 7-2: Wind Tunnel

The working section of the wind tunnel is of the closed type. It is 2.4m by 1.2m in size with an observation glass on one side. The section upstream contains flow management objects to reduce turbulence and produce uniform airstream at the working section. Flow management objects are of different types to manage different aspects of the air flow before the working section.

Flow straighteners are employed in the tunnel to remove air flow swirl in the tunnel. The most common device for flow straightening in wind tunnels is the honeycomb device which consists of an array of hexagonal cellular channel through which the flow is forced to pass. Common sizes range between 0.5mm

and 20mm in length with solidity between 1% and 5%. An alternative or cheaper arrangement can be made by packing plastic drinking straws. Flow straighteners pose little flow resistance in the wind tunnel, but they serve a useful purpose by obstructing transverse velocity components and swirl by producing flows that is nearly parallel to their walls. This does not remove streamwise velocity non-uniformity in the flow. These properties are tempered by screens.

Screens are used to improve streamwise flow and reduce turbulence. Especially in the vicinity of dominant eddies in the fluid path. They are mostly a fine mesh or grid of material mounted across the flow stream. A flow normal to a screen whose scale of spatially varying velocity is larger than the screen's mesh size will experience a reduction in peaks of velocity and increase in valleys resulting into a more uniform flow by the breakdown of larger eddies into smaller ones. These smaller eddies are more prone to viscous dissipation downstream of the flow. Multiple screens should be utilized for better flow uniformity instead of one equal in pressure-loss to the two. These should be spaced sufficiently to allow the viscous dissipation of smaller eddies from an upstream screen. Downstream of the working section, the diffuser section serves to dissipate the kinetic energy of the fluid leaving the working section as efficiently as possible.

7.2.3 Air Flow Measurement

Velocity measurements will be required at different points in the experimental setup to quantify the tunnel mean speed required for each test scenario and to determine the air flow through the channels of the model. Descriptions of suggested techniques at the different locations are as follows.

7.2.3.1 Tunnel Mean Velocity

The tunnel mean velocity is defined as the mean speed in the working section when it is unoccupied. This measurement can be taken by Pitot - static tube measuring system usually integral to the wind tunnel.

Pitot-static tubes consist of two concentric tubes i.e. the Pitot tube and the Static tube with a manometer attached at the end of their stems to record the pressure. The Pitot tube measures the total pressure while the static tube measures the

static pressure. These values of pressure are used to determine the velocity of air flow in the wind tunnel [303]. The relationship between pressure and velocity in subsonic fluid flow is given by the equation below.

$$P_T - P_S = \rho U^2 / 2 \quad (57)$$

Where P_T = Total Pressure, P_S = Static Pressure, U = Velocity

and ρ = Density

The Pitot-static tube is placed parallel to the axis of the flow direction with one opening facing the incoming flow. The opposite end of the tube is connected to a manometer which measures the pressure difference between the fluid and ambient. In most cases like this where point measurements are taken axially in a channel, mean velocity is determined by preliminary calibration e.g. by pitot transverse method [304]. This relationship should have been determined during wind tunnel commissioning and compensated for in the manometer readings.

The arrangement used in the measurement of total head by pitot tubes rests on the premise that in subsonic fluid flow, the pressure generated at the stagnation point of a bluff body placed in a moving fluid is closely equal to the total head of the fluid flow [304]. While the accuracy of a pitot tube is independent of the head shape or the length of its downstream section, it is largely affected by yaw (inclination of the axis to the stream direction) in its placement. Hence, it is important for the axis to lie along the direction of an undisturbed stream of fluid to record accurate pressures [305]. A visual inspection should be done to verify the integrity of the positioning before experiments are performed.

Generally, error in measurements with a pitot-static tube due to yaw reduces with an increase in the ratio of the tube bore to the external diameter [302]. Other factors that affect the accuracy of pitot readings include fluid viscosity [306] and turbulence [307]. The effect of fluid viscosity at low velocities is negligible if the product of the tube diameter (*in inches*) and air speed (*in ft/s*) exceeds 0.1 [308].

The hole(s) drilled around the surface of the tube on a common radial plane at a distance from a solid nose, constitute the static tube part of the Pitot - static tube. 4 holes are usually sufficient for small diameter tubes to minimize the effects of yaw [302]. Since a boundary layer is also formed over the instrument surface, it is necessary for the pressure in the free stream to be transmitted without change across the boundary layer on the instrument surface. This is easily achieved in subsonic flows [302]. There is evidence that the ratio of the hole depth (thickness of the wall) of the tube to the diameter of the hole i.e. (thickness/diameter) doesn't have an effect on pressure measurements as long as it exceeds a value of 2 [302]. However, the distance of the holes from the nose and stem does. The nose serves to accelerate the flow over the holes thereby reducing the measured pressure relative to that in the free stream. Conversely, the bent stem does the opposite; it tends to slow the fluid flow down thereby increasing the measured pressure. Hence, the plane of the holes, in standard equipment, is chosen in a way to make this opposite effect balance out and improve accuracy. At subsonic flows, this can be achieved by locating the holes at a distance downstream of the nose of about 6 x the external diameter of the tube and the stem being situated 8x diameters farther downstream [302]. The minimum air speed measurable with an accuracy of 1 percent is usually is usually around 5m/s. Static pressure measurements are more sensitive to yaw than pitot measurements. The effect of turbulent flow is also pronounced for static tubes [307].

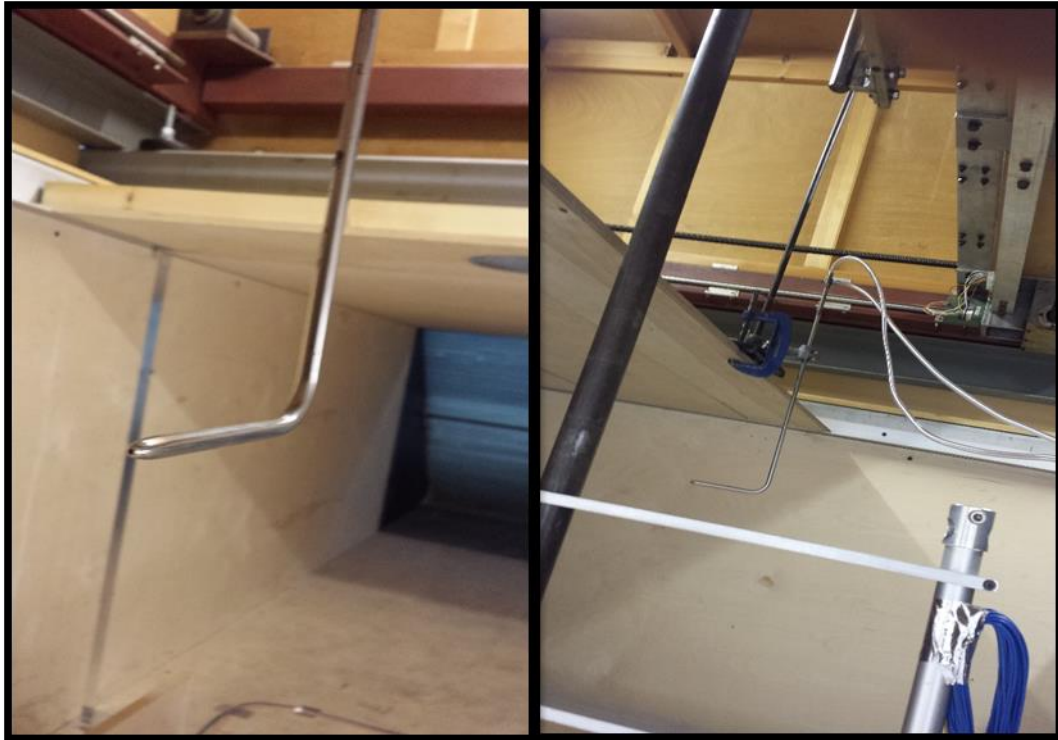


Figure 7-3: Pitot - Static Tube in Wind Tunnel

Manometers are required to measure the pressures sensed by the Pitot - static tube. These pressure values are used to derive flow speeds. Manometers are available for a large range of pressures and one should be chosen within the range of expected pressures to obtain a good level of accuracy. Generally, as the pressure range decreases, the manometer becomes more sensitive and consequently more accurate.

A good manometer is the KIMO® INSTRUMENTS CP302 electronic neutral gas pressure transmitter. It contains an interchangeable piezo-resistive strain gauge (SPI 500) which uses the piezo-resistive effect of bonded or formed strain gauges to detect strain due to applied pressure. This measuring element is very sensitive and responds quickly to pressure changes. In minimally unstable air streams, the fluctuating measurements can be problematic. Thus, it incorporates an integration coefficient (0 to 9) which serves to average out the measurements to present stable values. It is self-calibrating and capable of working with differential probes. Air velocity is calculated using the function below [309].

$$\text{Air Velocity (m/s)} = C_M * C_C * C_T * \sqrt{(\Delta\text{Pressure (pa)})} \quad (58)$$

Where C_M = Coefficient of differential probe

C_C = Coefficient of adaptation

C_T = Coefficient of Temperature Compensation (59)

$$= \sqrt{\frac{574.2 * \text{temp}(\text{°C}) + 156842.77}{101325}}$$

The instrument can be configured to make temperature compensations in real time by the addition of a thermocouple. This generally presents more accurate data for experiments. Since air temperature is not expected to vary significantly during the wind tunnel test, this function is not required. A single constant C_T can be applied at the test ambient temperature.

The properties of the unit are summarised below.

Pressure Measurement Range:	-500/+500 Pa
Air Velocity Measurement Range:	2 to 22m/s
Working Temperature:	0 to +50 °C
Response Time:	0.3 sec.
Accuracy:	±0.5% of reading ±1Pa
Resolution:	1pa

It is important that the flow pattern remains relatively undisturbed with the introduction of any measuring device. Care should be taken in positioning the tubes leading to the manometer to keep them clear of the air path.



Figure 7-4: Kimo cp302 Manometer

7.2.3.2 Ventilation Flow Rate

Because of the low flow velocities expected, it is important that the measuring system be non-intrusive. Also, the expected flows in the two pipes will be in opposite directions to indicate extract and supply ventilation air. Hence, the additional functionality of being able to determine the flow direction is required. Clamp-on Flexim FLUXUS® G601 Ultrasonic Flow Meters can be used at the separate inlet and outlet pipes of the test model to determine the overall ventilation flow rate achievable. The G601 Flowmeter uses the transit-time flow measurement technique. With this technique, a pair of transducer is clamped around each pipe; one at a location upstream and the other downstream of the flow. During measurement, each transducer sends and receives coded ultrasonic signals, which are analysed for transit times. When there is fluid flow in the pipe, the travel times of the signals downstream and upstream will differ depending on the fluid velocity i.e. a signal travelling downstream in the direction of the fluid flow will have a shorter transit time compared with one traveling upstream against the fluid flow. The difference between these transit times is proportional to velocity of air in the pipe. The calculated velocity is adjusted for the kind of pipe material before the flow rate is computed using the cross-sectional area of the pipe.

Depending on the application and pipe size, the transducer mounting can be chosen to improve accuracy in measurement. Generally, the transducers are mounted on the sides of the pipe in a Z, V or W pattern, which denotes the travel path of the measurement sounded waves emitted by the instrument transducers. In both V and W arrangements, the transducers are mounted on the same side of the pipe some distance apart. The spacing for the V arrangement allows the sound signal from one transducer to reflect once at the opposite pipe wall before reaching the other. In the W arrangement, the transducers are further apart and the signal transverses the fluid 4 times. These multiple signal reflections provide better accuracy in measurements [310]. The instrument can be configured to make temperature and pressure compensations in real time by using additional sensors. Since these values are not expected to vary significantly during the wind tunnel test, the operational pressure and temperature of the air can be entered directly as fixed values into the transmitter.

The air flow rate can be deduced from the ultrasonic signal transit times as follows:

$$Q_v = k_{Re} * A * k_a * \Delta t / (2 * t_{fl}) \quad (60)$$

Where: Q_v = Volume Flow Rate

k_{Re} = Fluid mechanics calibration factor, A

= Internal Cross – Sectional Area of the Pipe,

k_a = Acoustical Calibration Factor, Δt = transit time difference

t_{fl} = Transit Time in fluid

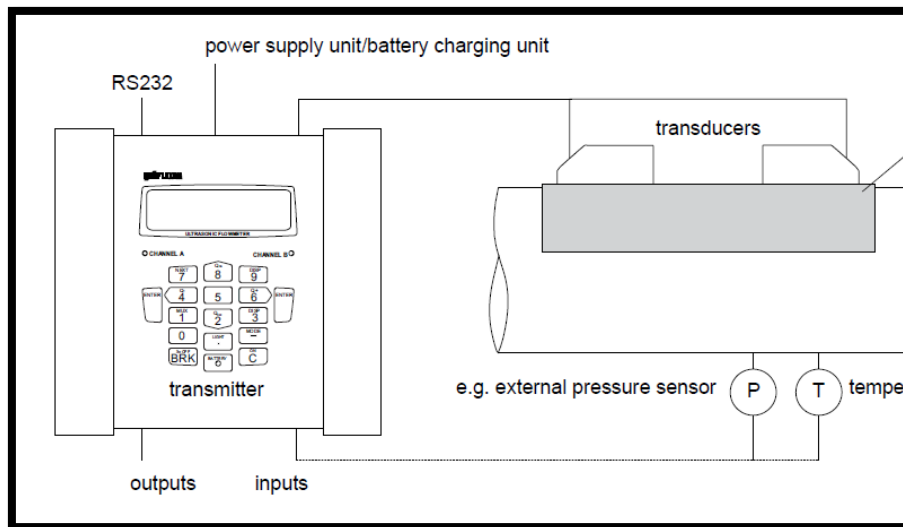


Figure 7-5: Ultrasonic Flow Meter Set-Up [310]

The unit comes with an integral LCD screen to view real time data and trends. 100,000 data points can be logged with an accuracy of $\pm 0.5\%$ of reading ± 0.01 m/s repeatable with 0.15% of reading ± 0.01 m/s.

7.2.4 Fluid Motion Visualization

7.2.4.1 Tuft

The use of fine threads or tufts attached to the walls of the channels provides a general indication of the fluid flow direction close to their points of attachment. Tufts are made of fine fabric, frayed at one end and attached smoothly to the surface of the channels at the other. Tufts can also give a good indication of the boundary layer flow. A steady tuft generally indicates a laminar boundary layer, but they flutter considerably in areas of turbulence. The properties that affect the performance of tufts are their density, stiffness and length. The dynamic responsiveness of tufts increases as the value of these properties diminish [301]. To improve visibility, tufts may be dipped in fluorescent dyes and illuminated with monochromatic light during an experiment. In addition to being attached to surfaces, tufts can be installed mid-stream across the channels by using a tuft

screen which comprises of a thin mesh of wires stretched across a flow channel with tufts attached at the mesh nodes. This may also take the form of a single straight wire stretched across the flow channel. Tufts installed in each segment of the annular channel will help to observe the flow direction. Flow direction in the non-segmented central channel will be indicated by measuring equipment and can also be observed with the tufts installed in it. Generally, care should be taken to make sure the tufts do not introduce undesirable aerodynamic effects into the flow.

7.2.5 Experimental Setup

A sample experimental setup to investigate the windcatcher flow performance is shown in Figure 7-6. It consists of the reduced scale windcatcher fixed atop a wooden box to mimic a chimney. The box has a hole in the middle in line with a similar sized hole cut in a round table forming the base of the wind-tunnel test section. The ducts are bent 90 degrees below the wind tunnel and extended outside to allow clamp-on flow meter attachments.

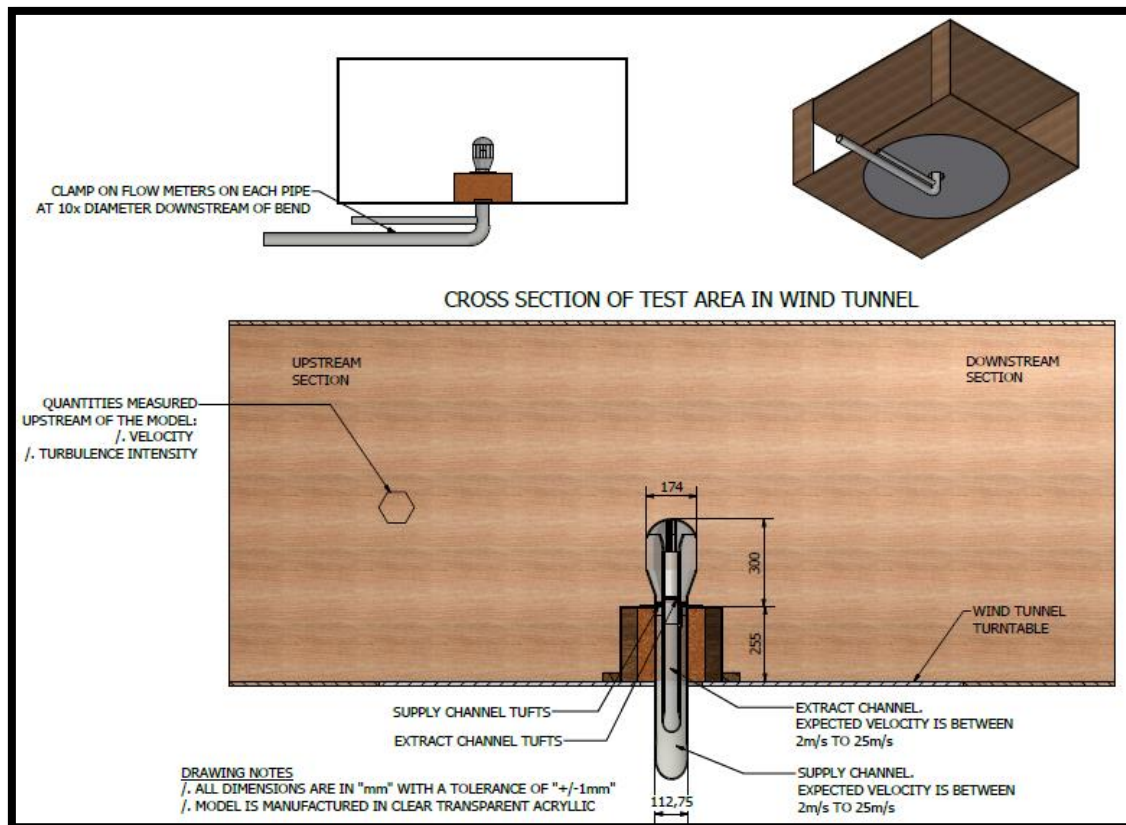


Figure 7-6: Experimental Set-Up

The arrangement above allows for various testing scenarios beyond that of a perpendicular incident wind on the windcatcher. The effect of incident wind angles can be investigated by rotating the turn table. Other objects can also be introduced into the wind tunnel to investigate the effect of structures in air flow path to the windcatcher. Smoke visualization can be particularly useful in visualizing flow patterns external to the windcatcher.

7.2.6 Experimental Error Sources

Although an acceptable level of similitude can be achieved by matching the Reynolds number between the scaled and actual fluid flow system, the boundary imposed by the limited cross-section of the tunnel introduces some errors in the wind tunnel experiment. Sound waves and other transit phenomena also introduces errors in wind tunnel measurements [302].

In closed section wind tunnels, when a solid model is inserted in duct flow, it blocks part of the stream which is diverted around the model. It may also alter the flow in ways that would not occur in unconfined flows. The general effect is an increase in the velocity intersecting the model compared to the reference velocity in the duct. Blockage also causes an increase in static pressure drop across the model in the wake region. In an open working section, the constraint can be thought of as a constraint to the pressure field and it is a complicated phenomenon to explain [302]. Generally, in allowing for tunnel interference effects of walls, it is acceptable to assume that these interactions are independent and additive. Hence they can be catered for simply adding quantities to the measured values [302]. To reduce errors, the various dimensionless parameters should be evaluated taking into consideration this increase. Several types of corrections for blockage effects are available in literature derived from theoretical and experimental studies on confined flows around bluff and streamlined bodies. However, in incompressible single phase flows where the projected frontal area of the test model is less than 1% of the test-section area, it is generally accepted that the effects of blockage may be neglected [301].

The measuring system consist of several interconnected components such as sensors, data acquisition and processing devices and software. All these are subject to undesirable inputs which can interfere with measurements inputs and bring about the modification of inputs. An interfering input is a property to which measurement systems are sensitive and a modifying input modifies the response to a desired input. A good example given by Tavoularis [301] involves the measurement of air velocity of a jet issuing from a nozzle in a room by a hot-wire anemometer. The draft of the air in the room acts as an interfering input because it distorts the jet's velocity field. While a change in the room temperature will cause a modification of the anemometer's heating circuit. Undesirable input cause measurement errors and may even produce outputs in the absence of desired inputs. For accurate measurements, these errors must be identified, and their effects estimated. If found significant, these must be accounted for or mitigated.

A measurable property has a true value that ideally matches the magnitude of the physical property of interest. The determination of this true value is the objective of measurements. The measured value is an estimate of this true value provided by the measuring system within a band of absolute measurement error. This inherent inaccuracy may be caused by errors in calibration, data acquisition or reduction in the measuring system. In calibrating, the values of inputs are measured independently by another instrument whose response is known and that serves as a standard. Therefore, the selection of the calibrating instrument is important as accuracy depends on it. It is good practice to maintain all interfering and modifying inputs at the same levels as those during actual measurement during calibration [301].

To minimize errors, instruments must also be selected with the right properties for the measurement regime. The dynamic range of measurement system is the ratio of the largest to the smallest values of input that the system can measure. This must be selected to suit the input range being measured with the right level of threshold and resolution. Threshold is the smallest input value that will produce a detectable output. Resolution defines the smallest input change that will produce a detectable input change. Scale readability of analogue instruments can also introduce human errors. It defines the minimum change in output that can be recognized by an observer. In this regard instrument with digital outputs are preferable.

A common error in electronic measurement systems is due to signal conditioning which occurs in the translation of analogue measurement signals to discrete digital values. Care must be taken in processing electrical signals at low levels from instruments like transducers and thermocouples. It is advisable to amplify these signals using low noise instrument amplifiers before processing. Filters are also useful in removing undesirable effects like noise in electronic measuring equipment.

The physical presence or operation of measurement instruments also introduce errors to the measurements. Common adverse effects include flow distortion, loading and instrument cross-talk. Instruments inserted in flows cause distortion

of a certain amount to the flow such as blockage, streamline displacement, instability, vortex shedding and turbulence. Loading occurs when the measurement equipment extracts power from the flow and alters the measured quantities. An example is the use of a measurement turbine for flow rates which may introduce resistance in the flow path and reduce flow rates. Proper design of experiments and utilization of non-obstructive measuring techniques can minimize this error. Cross-talk occurs when a measuring equipment is coupled in its operation with another measuring equipment. An example is the thermal cross-talk between two closely positioned heated thermal anemometers in which the wakes from one can affect measurement from the other. Cross-talk in experiments must be identified and eliminated to reduce errors.

7.3 Large Scale Testing

Large scale tests will involve installing the proposed system in a chimney connected to a test room installed in a climate chamber to mimic winter conditions. The room should contain a means of mimicking indoor heat gains like an electric heater. The ventilation effectiveness can be evaluated using CO₂ decay measurements. Temperatures and air velocity measurements should be taken at the room level vents to evaluate thermal and flow performance of the ventilation system. All surface and air (indoor and outdoor) temperatures can be measured using RTD sensors. Mean radiant temperature in the room is an indicator of thermal comfort. This measurement can be taken at a height of 100mm below the ceiling centre by a type K thermocouple at the centre of a 101.6mm diameter black copper sphere as described by EN ISO 7726. The acquisition of real time data from the sensors can be done using Pico TC 08 data loggers or similar. Its real time graphical display will provide an avenue to monitor the experiment and ensure every sensor was in working order.

The tests should be carried out in two sets; the first without the ventilation system to establish a baseline for comparison, and the second after the system is installed. This arrangement can also be utilized for the investigation of condensation and freezing in the proposed system by utilizing a humidifier in the test room.

8 CONCLUSION AND RECOMMENDATIONS

8.1 Conclusion

A review of available literature revealed that the UK housing stock contains a significant proportion of dwellings constructed pre-1945. These dwellings form part of the cultural heritage of the country. They currently make up 36% of the total dwellings for England, 32% for Scotland, 50% for Wales and 18% of those in Northern Ireland. Structural features incorporated at the time of their construction were intentional to create high infiltration rates conducive for the lifestyle of the period and method of indoor heating using fireplaces connected to chimneys.

Modern heating systems have led to the disuse of many fireplaces and these dwellings are mostly fitted with central heating system. With their characteristic high infiltration rates and subpar fabric thermal performance, the issue of high energy consumption in these dwellings have become very important.

Reviewed scientific literature revealed that heat loss through ventilation accounts for up to 30% of energy loss in these dwellings. Recent government incentives have contributed to improving thermal performance of these buildings through fabric insulation and making them airtight. Controlled ventilation is then provided for occupant's thermal comfort and humidity control. Hence heat loss through ventilation has become very prominent.

Systems available for controlled ventilation are mostly mechanical heat recovery systems that require extensive ducting and unwanted modifications. Numerous scientific studies revealed problems with energy and comfort performance claimed by the manufacturers of these systems and its variability with in-situ and human factors. Recent developments in improving their heat exchange performance have investigated the use membranes in the recovery of total energy. Studies in literature show these to be promising in improving the total efficiency, especially in climes with high humidity.

Natural ventilation heat recovery systems are also an option for these dwellings, and literature revealed numerous scientific investigations into their design,

performance and analysis. These mostly consist of two functional parts; the windcatcher element providing ventilation, and the heat exchanger element extracting heat from extract flow and pre-warming supply air with it.

Literature revealed many to be of satisfactory performance both in thermal and pressure terms. Available ones have a combination of functional characteristics but not one has all of those listed below in a unitary system.

- a. Aesthetic suitability for heritage dwellings
- b. Utilizing existing disused part of building fabric thereby not necessitating extensive modification.
- c. Fixed with no moving or rotating part.
- d. Omnidirectional; able to harvest incident wind from all directions.
- e. Supply and extract system; not requiring buoyancy of indoor air to drive extract flow.
- f. Incorporates an effective plate heat exchanger combined into the unitary system.
- g. Fixed supply and extract channel i.e. they do not alternate between extract and supply modes.

The properties listed in a-f above are particularly important for applicability to heritage dwellings. As such, the Author's original proposal is that of a novel system that combines all these properties.

It consists of a windcatcher with a plate heat exchanger unit attached to its base and designed to sit atop a disused chimney with the heat exchanger within the chimney void. A central air path connected to a duct terminating at high level within the attached space, acts as the extract air flow path. While the connected fireplace acts as the supply air terminal supplied from an annular flow path around the central one. The heat exchanger maintains this configuration at its entry and exit terminals, but within, it is a plate heat exchanger with 16 counter-current flow paths. The external windcatcher element is fixed, omnidirectional and mimics the geometry of traditional chimney cowls.

An iterative procedure was carried out to develop the two system components using Autodesk Inventor 2013 3D modelling, parametric plots and CFD simulations. Many scientific works in literature agree that these are robust methods in the design and analysis of natural heat recovery ventilation systems.

Two commercial CFD programs were employed namely Autodesk CFD 2013 and Ansys Fluent v14 to perform RANS simulation of models. The standard $k - \epsilon$ turbulence model was used in Autodesk CFD to investigate initial models of the windcatcher, while SST $k - \omega$ was used in Ansys Fluent and Autodesk CFD to investigate final prototypes of the windcatcher and heat exchanger.

8.1.1 Windcatcher

For the windcatcher development, the Autodesk CFD software was used for analysis of 17 initial concepts to arrive at a Base Model. Five subsequent iterations of the Base Model (Model 1 - 5) were carried out to resolve identified deficiencies in performance and present information on fluid flow interactions in the system. A final prototype is then presented and simulated in Ansys Fluent and Autodesk CFD to present qualitative and quantitative performance data in terms of supply and extract air flow and ventilation rate, and also compare the performance of both software packages for the investigation of the ventilation heat recovery device.

The chosen test room is $27m^3$ in volume with a CIBSE prescribed ventilation flow rate of 0.7ach. This equates to a flow rate of $18.9m^3/hr$.

The simulation model consisted of the relevant windcatcher model fixed atop a 1m tall chimney at the centre of a flow domain. Simulations were carried out at steady state wind speeds of 0.5m/s, 1.5m/s, 2.5m/s, 3.5m/s and 4.5m/s incident on the windcatcher at 90 degrees on the vertical plane of symmetry through the unit.

Model 1 (Base Model) central outlet channel exhibited the desired flow direction i.e. it shows an upwards extract flow facilitated by low pressure generated by accelerated flow its upper surface through the constricted sections under the dome. This was $1m^3/hr$ at 0.5m/s incident wind speed and peaked at $18m^3/hr$ for

4.5m/s incident wind speed. Low pressure in the windcatcher wake region induced suction in the leeward end annular supply channel causing the induced supply air flow to short circuit at the base of the windcatcher. This is consistent with the work of B. Hughes et al [311] when they investigated a square windcatcher. Although not of the same cross-section, the dividing plates in this cylindrical windcatcher also presents a wide stagnation surface for the flow as the square section they investigated. Short-circuit stalled air supply at incident wind speed of 0.5m/s and was observed at all other speeds. Supply air flow rates peaked at 0.72m³/hr well short of the 18.9m³/hr required.

Model 2 sought to induce more flow into the annular inlet at all wind speeds to achieve the required flow rate despite the short-circuit phenomenon. To this end, the size of each annular channel was increased in line with the corresponding dome sections. The resultant windcatcher had 4 larger annular inlets and dome sections. The supply flow rate was increased peaking at 3.6m³/hr (still lower than required). This is in line with earlier observations made by H. Montazeri [36]. With this model, the extract flow was reversed at all wind speeds. Air flow into the dome section was direct onto the perpendicular dome plate divider and did not generate low extractive pressure over the central outlet.

Model 3 combined the 4 larger annular channels of Model 2 with the 8 dome sections required for extract performance as observed for Model 1. It also incorporated a larger dividing plate to induce more air flow into the annular inlets. The dividing plates enabled higher supply air flow rate at increasing incident wind speed. This peaked at 8.3m³/hr for an incident wind speed of 4.5 m/s. Despite the 8 dome sections, incident air flow was evenly divided between the windward dome sections compared to Model 1 where flow was concentrated in one dome section. This caused a failure in air extraction.

Model 4 is a variation of Model 1 with the larger dividing plate observed to increase supply flow rates in Model 3. This design also sought to incorporate the larger supply channels of Model 2 by cutting the dividing plates into two, level with the lower edge of the dome. This separated each dividing plate into a rigid upper part, under the dome, and a loosely movable lower part. The rigid upper

part keeps the original 8 dome sections intact, while the lower part is loosely movable and rotates in the annulus around the y-axis of the windcatcher to enlarge the corresponding annular channel on wind impact. Following from observations in Model 3, extract flow is allowed for by making sure the movable dividing plate only open to a minimal extent beyond its corresponding dome section plate to concentrate incident air flow into the dome section in the windward direction.

Resultant supply air flow was reduced from Model 3 due to the smaller annular inlets. Performance was similar at 0.5 m/s incident wind speed but peaked lower at $6\text{m}^3/\text{hr}$.

This model failed in extract at all incident wind speeds except 4.5m/s when the increased incident air velocity also increases the air flow over the central channel enough to generate the low pressure required for extraction flow.

Model 5 is the same as Model 4, only with a blind covering the adjacent dome section when the windward dividing plate moves to enlarge its corresponding annular inlet on wind impact. Supply flow rate peaked below that of Model 4, even though the annular channels are the same. This results from the blind which induced higher suction pressure in the leeward end annular channel for the same windward opening. Hence, short-circuit flow was stronger and supply flow rates reduced.

As expected the extraction performed well reaching $30\text{m}^3/\text{hr}$ at 4.5m/s incident wind speed. This is well beyond that of Model 1 ($18\text{m}^3/\text{hr}$) which is the only model with a functional extraction up till this point.

An analysis of the extract flow through the central channel using Model 1 showed that negative pressure generated at the side dome sections due to flow separation of incident air flow has a significant effect in driving the extract air flow in addition to the venturi effect of air flow through the dome constrictions. The primary exit paths for the extract air flow was found to be through the side dome sections.

A comparison of short-circuit flow for all simulated models revealed significant proportion of induced air going into short circuit. Models 1 and 5 which both functioned in supply and extraction induced enough supply air flow to satisfy the limiting requirement of 18.9m³/hr, if not for short-circuit. Thus, a variation of the less complex and completely passive Model 1 was modified with bigger dividing plates and funnel shaped annular inlet and presented as the final prototype. This included a lightweight not return valve in the annular inlets to eliminate the short-circuit flow.

Ansys Fluent v14 simulation of this prototype with the valves closed exhibited the desired flow pattern with no short-circuit. At all simulated incident wind speeds above 1 m/s, the windcatcher performance provided sufficient levels of ventilation. Given that the typical low wind speed in UK urban areas is around 3m/s corresponding to 3 ach for the test room, this result indicated that the windcatcher can provide the required ventilation flow rate.

A comparison of flow results from CFD simulation using Autodesk CFD showed maximum difference of 10% in the average air flow values. The values predicted by this software were marginally higher than those from Ansys Fluent. This proved the comparable accuracy of this simpler and user-friendly software when compared with the more established Ansys Fluent.

8.1.2 Heat Exchanger

In investigating possible configurations for the heat exchanger, scientific literature revealed the different heat transfer processes available in heat exchangers. Counter-flow plate heat exchangers were found to be advantageous because high heat transfer rates are achievable, and they are comparatively compact. This makes them particularly suited to gases which generally have low heat capacities. The design of the fluid distribution element (commonly the header or cap) is also very important to achieve good heat exchange and flow performance. Pressure drop through common plate heat exchangers are generally high. Thus, the introduction of extended surfaces like fins that adds to pressure drop is undesirable.

For the heat exchanger development, the problem was specified in terms of geometry and operating conditions. Then parametric simultaneous equations representing the desired pressure and thermal duty were developed. Parametric plots were used for sizing the length and number of flow channels within the cylindrical geometry of the heat exchanger to satisfy the required pressure drop. This provided a Base Model which was further developed by simulation in Ansys Fluent v14 to present performance information in terms of heat exchange and pressure drop.

The cylindrical geometry of the windcatcher placed a restriction on the shape of the applicable heat exchanger that can be attached to it. Hence, a cylindrical heat exchanger was chosen. The proposed heat exchanger Base Model has 16 channels with grooved radial plates around a perforated central tubular core which holds an inert desiccant to remove condensate flow into it from grooves. The grooves are on the side exposed to the outgoing extract air which is likely to have higher humidity content.

The annular and central air flow paths necessitated the design of a novel fluid distribution element that re-directs these flows into alternate channels of the cylindrical plate heat exchanger.

Operating conditions were chosen to be representative typical of indoor and outdoor temperatures in UK winter, taking care not to cool the extract air to its dew point and induce condensation in the system.

Hot stream Inlet temperature $T_{hi} = 22^{\circ}C/295.15K$

Hot stream outlet temperature $T_{ho} = 14^{\circ}C/287.15K$

Cold stream Inlet temperature $T_{ci} = 2^{\circ}C/275.15K$

The Author chose $T_{co} = 20^{\circ}C/293.15K$ as the temperature to raise the cold stream to.

The required heat duty to cool the hot stream in a single channel to its outlet temperature was calculated as 20W for a flow velocity of 1m/s. This equated to a mass flow rate of $0.0025kg/m^3$.

The Author chose 1 Pa as the design pressure drop through a single channel and approximated one channel into a rectangular cylinder with the longer cross-sectional dimension “a” fixed at the heat exchanger’s radius. The pressure drop was expressed in terms of the channel cross-sectional dimensions “a” and “b” in an equation. The heat duty to cool the hot stream to its outlet temperature if the channel remains at the average temperature of the cold stream was also expressed in terms of “a” and “b”. These two simultaneous equations representing the heat exchangers performance and geometric parameters was plotted to reveal the relationships between them.

As plate exchangers suffer more in terms of pressure drop performance, the pressure drop was prioritised in sizing the heat exchanger using these equations. The equation for pressure loss is also more deterministic than that of heat transfer rate for the geometric approximations made. A more accurate prediction of heat transfer performance was deferred to the CFD simulation.

The parametric plots of these equations showed that at fixed dimensions of channel length $l = 0.8m$ and channel cross-sectional breadth $b = 0.02m$, the heat transfer rate increased with pressure drop. At the same fixed channel length, decreasing the value of b progressively narrows the channel cross-section and increases pressure drop. When b is fixed, increasing the channel length presented more heat exchange surface and higher heat transfer rates. An optimal channel breadth $b = 0.015m$ was chosen equivalent to 16 air flow passages through the heat exchanger; 8 for each stream

Ansys Fluent v14 was used to simulate the heat exchanger performance using resultant channel velocities corresponding to the incident wind speeds from the windcatcher prototype simulation.

At low incident wind speeds on the windcatcher, heat exchanger effectiveness was quite high at 71%. This readily reduces to 35% as the flow rate through the heat exchanger increased. This trend match that gotten by M. Simonetti et al [86] when they investigated a rectangular channel low Reynolds flow heat exchanger.

Pressure drop was less than 1Pa at 0.5m/s. This increased to a maximum of 13Pa through the Supply channel at 4.5m/s wind speed.

8.1.3 Whole System

Lastly, a CFD simulation of the whole system was carried out using Ansys Fluent. At every simulated wind speed above 1m/s, the system was able to supply ventilation air flow above the CIBSE recommended minimum of 0.7ach. The ventilation performance was 0.3ach at 0.5m/s incident wind speed. This increased to 4.5ach at 4.5m/s incident wind speed. When compared with that of the windcatcher alone. The system ventilation performance was 10% lower on the average due to the heat exchanger resistance in the flow path.

Heat exchanger effectiveness of the system was compared with that of the heat exchanger alone. Effectiveness for the system peaked at 46% at 0.5m/s wind speed. This steadily decreased to 22% at 4.5m/s wind speed. In comparison with the heat exchanger unit performance. The thermal performance was reduced by an average of 27% when the system is integrated as a unit. This performance reduction can be attributed to the non-uniform pattern of annular supply flow through the system.

In this research process, the characteristics air flow through the proposed windcatcher revealed a novel method of generating counter-current supply and extract flow through an omnidirectional windcatcher suited to heritage dwellings. The heat exchanger development showed a novel fluid distribution element developed by the author for converting counter current annular and tubular flows for use in a plate heat exchanger. The developed cylindrical low Reynolds number plate heat exchanger also proved suitable for the proposed system and contributed to the dearth of information in this area of research.

8.2 Recommendations for Future Work

As the ventilation system studied in the thesis is an original proposal by the author, there is a dearth of research work into it. However, this thesis has made apparent different areas where further study would be immensely useful.

Immediately obvious is a lack of information on the performance of the system as a whole when indoor buoyancy is factored in. Information obtained from CFD simulation of this will present holistic assessment of the system's performance. With the buoyancy of heated indoor air included in the simulation, it will further match real life operational scenarios.

Condensation and freezing are possible conditions in the operation of ventilation heat recovery systems especially in very cold climes where the proposed system might be beneficial. A method of collecting the condensate with an inert descant was proposed under section 6.4.1.1. This can be further modelled in very cold climes to investigate freezing.

The windcatcher models investigated in this research all have 4 or 8 annular inlets with wind incident on them at 90° to them on the vertical plane. It would be beneficial to study the performance of the windcatcher with different numbers of annular inlets in different operational scenarios to obtain an optimal configuration for possible operational conditions of incident wind speed angle, direction and other flow properties.

The investigations carried out in this work were also done for steady state wind speeds. This is not ever the case for atmospheric winds. Varying strength of gusts may lead to unsteady conditions of air flow within the ventilation system and impact its performance and level thermal comfort achievable at room level. Investigation into these aspects of the system's operation would further help to validate performance and feasibility of the system. Gusty flow can also produce noise. Thus, acoustical performance is another area a researcher might be interested in.

As the system has no filter, geometrical modifications or parts are required to prevent fouling and driving rain ingress. Driving rain is defined as the quantity of rain that passes through a vertical plane in the atmosphere. Driving rain occurs because raindrops which are falling to the ground at their terminal velocity are blown sideways at the speed of the wind at any given height above grade. Passive design of the dome overhang can be investigated to provide protection against rain ingress by determining applicable rain fall trajectories and

implementing design and performance refinements. The work done by Straube [243] is useful in this respect. This is an important area of further development that presents an opportunity to make the proposed system highly practical. The effect of fouling on the heat exchanger performance also need to be assessed.

Lastly, proposals for experimental testing of the system have been included in Chapter 7 of this thesis. These can be implemented to provide experimental validation of the system's performance.

REFERENCES

- [1] National Building Specification. (2015) *Conservation of fuel and power in existing dwellings, incorporating 2010, 2011 and 2013 amendments : conservation of fuel and power in existing dwellings, incorporating 2010, 2011 and 2013 amendments*. RIBA. Available at: https://www.planningportal.co.uk/info/200135/approved_documents/74/part_1_-_conservation_of_fuel_and_power/2 (Accessed: 4 January 2018).
- [2] Malpass, P. (2008) 'Housing,'Heritage'and Community', *Housing Studies Association Annual Conference, University of York*, (April). Available at: <https://www.york.ac.uk/chp/hsa/spring08/presentations/malpass.doc> (Accessed: 4 January 2018).
- [3] Department for Communities and Local Government (2012) *English Housing Survey HOMES 2010*. Available at: https://www.gov.uk/government/uploads/system/uploads/attachment_data/file/6748/2173483.pdf (Accessed: 1 October 2016).
- [4] Historic Scotland (2008) *Energy Efficiency and traditional buildings – Historic Scotland 's work*. Available at: <http://www.historic-scotland.gov.uk/energyefficiencyandtraditionalbuildings.pdf> (Accessed: 1 October 2014).
- [5] Architects, P. A. (2010) *Energy Efficiency in Traditional Buildings*.
- [6] Rudge, J. (2012) 'Coal fires, fresh air and the hardy British: A historical view of domestic energy efficiency and thermal comfort in Britain', *Energy Policy*. Elsevier, 49, pp. 6–11. doi: 10.1016/j.enpol.2011.11.064.
- [7] Brown, P. (2002) '50 years after the great smog, a new killer arises', *The Guardian*, 30 November. Available at: http://www.theguardian.com/uk_news/story/0,3604,850909,00.html.
- [8] Government, D. for C. and L. (2015) *English Housing Survey Headline Report 2013-14*. Available at: https://www.gov.uk/government/uploads/system/uploads/attachment_data/file/4

69213/English_Housing_Survey_Headline_Report_2013-14.pdf (Accessed: 4 January 2018).

[9] Scottish House Condition Survey team (2017) *Scottish House Condition Survey: 2016 Key Findings*. Available at:
<http://www.gov.scot/Publications/2017/12/5401/downloads> (Accessed: 4 January 2018).

[10] Revell, K. and Leather, P. (2000) *The state of UK housing: A factfile on housing conditions and housing renewal policies in the UK*. Available at:
<http://www.jrf.org.uk/sites/files/jrf/jr084-housing-conditions-policies.pdf>
(Accessed: 5 May 2015).

[11] Curtis, R. (2008) *Ventilation in traditional houses*. Available at:
<http://www.historic-scotland.gov.uk/inform-ventilation.pdf> (Accessed: 25 September 2016).

[12] Beedell, J. and Gore, S. (2009) *Energy Conservation in historic houses : A Guide for historic house owners*. Available at:
<http://www.smithsgore.co.uk/assets/x/145854>.

[13] Three regions Climate Change Group (2008) *Your home in a changing climate; Retrofitting Existing Homes for Climate Change Impacts*. Greater London Authority. Available at: http://www.ukcip.org.uk/wordpress/wp-content/PDFs/3Regions_Retrofitting.pdf (Accessed: 1 October 2014).

[14] ChangeWorks (2008) *Energy Heritage, A guide to improving energy efficiency in traditional and historic homes*. Available at:
http://www.changeworks.org.uk/uploads/83096-EnergyHeritage_online1.pdf
(Accessed: 1 October 2015).

[15] Cheltenham Township (no date o) *Historic Preservation and Sustainability*. Available at:
http://www.indy.gov/eGov/City/DMD/IHPC/Resources/Documents/Sustainability-brochure_Cheltenham.pdf (Accessed: 5 November 2014).

[16] Pickles, D., Brocklebank, I. and Chris, W. (2012) *ENERGY EFFICIENCY*

AND HISTORIC BUILDINGS; Application of part L of the Building Regulations to historic and traditionally constructed buildings. Available at:

<http://www.english-heritage.org.uk/publications/energy-efficiency-historic-buildings-ptl/eehb-partl.pdf> (Accessed: 5 July 2014).

[17] Troi, A. and Bastian, Z. (no date q) *Energy efficiency solutions for historical buildings : a handbook.*

[18] BSI (2013) *BS 7913:2013 Guide to the Conservation of Historic Buildings.*

UK. Available at:

<https://shop.bsigroup.com/ProductDetail/?pid=000000000030248522>.

[19] Utley, J. I. and Shorrocks, L. D. (2008) *Domestic energy fact file 2008.*

Watford. Available at:

http://www.bre.co.uk/filelibrary/pdf/rpts/Fact_File_2008.pdf (Accessed: 2 November 2015).

[20] Liddament, M. . and Orme, M. (1998) 'Energy and ventilation', *Applied Thermal Engineering*, 18(11), pp. 1101–1109. doi: 10.1016/S1359-4311(98)00040-4.

[21] Awbi, H. B. (1998) 'Chapter 7—Ventilation', *Renewable and Sustainable Energy Reviews*, 2(1–2), pp. 157–188. doi: 10.1016/S1364-0321(98)00015-X.

[22] Orme, M. (2001) 'Estimates of the energy impact of ventilation and associated financial expenditures', *Energy & Buildings*, 33, pp. 199–205.

Available at:

<http://www.sciencedirect.com/science/article/pii/S0378778800000827>.

[23] CIBSE (2016) *Guide B: Heating, Ventilating, Air Conditioning and Refrigeration (CIBSE Guide B).* CIBSE.

[24] *Passive Ventilation with Heat Recovery brochure-Ventive* (no date x).

Available at: <https://www.ventive.co.uk/passive-ventilation-heat-recovery/> (Accessed: 8 October 2018).

[25] Loveday, D. L. and Vadodaria, K. (no date y) *Consumer Appealing Low*

Energy technologies for Building RETrofitting Project CALEBRE. Available at: www.calebre.org.uk (Accessed: 10 October 2018).

[26] Affinity Sutton (2013) *FutureFit Final Report Pt 2: An insight into the retrofit challenge for social housing*. Available at: <http://www.affinitysutton.com/media/364646/futurefit-PDF-1.pdf> (Accessed: 1 October 2015).

[27] *EnerPHit Eco Home in North London - Enhabit - Enhabit* (no date aa). Available at: <https://www.enhabit.uk.com/case-study/enerphit-eco-home-in-north-london/> (Accessed: 10 October 2018).

[28] *Oxfordshire low energy, high comfort home off the grid - Enhabit - Enhabit* (no date ab). Available at: <https://www.enhabit.uk.com/case-study/oxfordshire-low-energy-high-comfort-home-off-the-grid/> (Accessed: 10 October 2018).

[29] *Islington high comfort low energy Victorian townhouse - Enhabit - Enhabit* (no date ac). Available at: <https://www.enhabit.uk.com/case-study/islington-high-comfort-low-energy-victorian-townhouse/> (Accessed: 10 October 2018).

[30] *Key Findings from the CALEBRE Research Project* (no date ad). Available at: www.calebre.org.uk (Accessed: 10 October 2018).

[31] Teague, A. (1995) 'Principles, methods and problems of inserting heating, ventilation and air conditioning services into heritage buildings', *Architectural Science Review*, (January 2013), pp. 37–41. Available at: <http://www.tandfonline.com/doi/pdf/10.1080/00038628.1995.9696789>.

[32] Lazzarin, R. and Gasparella, A. (1998) 'Technical and economical analysis of heat recovery in building ventilation systems', *Applied thermal engineering*, 18(97). Available at: <http://www.sciencedirect.com/science/article/pii/S1359431197000136>.

[33] El Fouih, Y., Stabat, P., Rivière, P., Hoang, P. and Archambault, V. (2012) 'Adequacy of air-to-air heat recovery ventilation system applied in low energy buildings', *Energy and Buildings*. Elsevier B.V., 54, pp. 29–39. doi: 10.1016/j.enbuild.2012.08.008.

- [34] Mardiana-Idayu, A. and Riffat, S. B. (2011) 'An experimental study on the performance of enthalpy recovery system for building applications', *Energy and Buildings*. Elsevier B.V., 43(9), pp. 2533–2538. doi: 10.1016/j.enbuild.2011.06.009.
- [35] Saadatian, O., Haw, L. C., Sopian, K. and Sulaiman, M. Y. (2012) 'Review of windcatcher technologies', *Renewable and Sustainable Energy Reviews*. Elsevier Ltd, 16(3), pp. 1477–1495. doi: 10.1016/j.rser.2011.11.037.
- [36] Montazeri, H. (2011) 'Experimental and numerical study on natural ventilation performance of various multi-opening wind catchers', *Building and Environment*. Elsevier Ltd, 46(2), pp. 370–378. doi: 10.1016/j.buildenv.2010.07.031.
- [37] Elzaidabi, A. A. M. (2008) 'Low energy, wind catcher assisted indirect- evaporative cooling system for building applications', (September), p. 232. Available at: <http://etheses.nottingham.ac.uk/703/>.
- [38] Kim, Y. S., Han, D. H., Chung, H., Jeong, H. and Choi, S. H. (2017) 'Experimental study on Venturi-type natural ventilator', *Energy and Buildings*. Elsevier, 139, pp. 232–241. doi: 10.1016/j.enbuild.2017.01.016.
- [39] Hughes, B. R., Calautit, J. K. and Ghani, S. A. (2012) 'The development of commercial wind towers for natural ventilation: A review', *Applied Energy*. Elsevier Ltd, 92, pp. 606–627. doi: 10.1016/j.apenergy.2011.11.066.
- [40] Shah, R. K. and Sekulić, D. P. (2003) 'Classification of Heat Exchangers', in *Fundamentals of Heat Exchanger Design*. John Wiley & Sons, Inc., pp. 1–77. doi: 10.1002/9780470172605.ch1.
- [41] Abu-Khader, M. M. (2012) 'Plate heat exchangers: Recent advances', *Renewable and Sustainable Energy Reviews*. Pergamon, 16(4), pp. 1883–1891. doi: 10.1016/J.RSER.2012.01.009.
- [42] Kakac, S., Shah, R. K. and Bergles, A. E. (1983) *Low reynolds number flow heat exchangers*. Hemisphere Publishing.

- [43] Jilek, J. and Young, J. H. (1993) 'Exergy efficiency of a counterflow air/air heat exchanger with vapour condensation', *Warme - und Stoffubertragung*. Springer-Verlag, 28(3), pp. 123–130. doi: 10.1007/BF01541108.
- [44] Kragh, J., Rose, J., Nielsen, T. R. and Svendsen, S. (2007) 'New counter flow heat exchanger designed for ventilation systems in cold climates', *Energy and Buildings*, 39(11), pp. 1151–1158. doi: 10.1016/j.enbuild.2006.12.008.
- [45] Nielsen, T. R., Rose, J. and Kragh, J. (2009) 'Dynamic model of counter flow air to air heat exchanger for comfort ventilation with condensation and frost formation', *Applied Thermal Engineering*. Elsevier Ltd, 29(2–3), pp. 462–468. doi: 10.1016/j.applthermaleng.2008.03.006.
- [46] Merzkirch, A., Maas, S., Scholzen, F. and Waldmann, D. (2016) 'Field tests of centralized and decentralized ventilation units in residential buildings - Specific fan power, heat recovery efficiency, shortcuts and volume flow unbalances', *Energy and Buildings*. Elsevier, 116, pp. 373–383. doi: 10.1016/j.enbuild.2015.12.008.
- [47] Drost, M. K. (1993) 'Air-to-air heat exchanger performance', *Energy and Buildings*, 19(3), pp. 215–220. doi: 10.1016/0378-7788(93)90029-T.
- [48] Rasouli, M., Ge, G., Simonson, C. J. and Besant, R. W. (2013) 'Uncertainties in energy and economic performance of HVAC systems and energy recovery ventilators due to uncertainties in building and HVAC parameters', *Applied Thermal Engineering*. Elsevier Ltd, 50(1), pp. 732–742. doi: 10.1016/j.applthermaleng.2012.08.021.
- [49] Juodis, E. (2006) 'Extracted ventilation air heat recovery efficiency as a function of a building's thermal properties', *Energy and Buildings*, 38(6), pp. 568–573. doi: 10.1016/j.enbuild.2005.07.002.
- [50] Roulet, C., Heidt, F. D., Foradini, F. and Pibiri, M. (no date ax) *Is Heat Recovery in Air Handling Units Efficient ?* Available at: <http://www.empa-ren.ch/Internet-Files/Programm/Aktuelles/aktualitaeten/Status-Seminar/pdf-files/pibiri-m-c.pdf> (Accessed: 1 October 2014).

- [51] Fisk, W. and Turiel, I. (1983) 'Residential air-to-air heat exchangers: Performance energy savings, and economics', *Energy and Buildings*, 5, pp. 197–211. Available at:
<http://www.sciencedirect.com/science/article/pii/0378778883900051>.
- [52] Calautit, J. K., O'Connor, D. and Hughes, B. R. (2016) 'A natural ventilation wind tower with heat pipe heat recovery for cold climates', *Renewable Energy*. Pergamon, 87, pp. 1088–1104. doi: 10.1016/j.renene.2015.08.026.
- [53] O'connor, D., Calautit, J. K. S., Hughes, B. R., O'Connor, D., Calautit, J. K. S. and Hughes, B. R. (2016) 'A review of heat recovery technology for passive ventilation applications', *Renewable and Sustainable Energy Reviews*. Elsevier, 54, pp. 1481–1493. doi: 10.1016/j.rser.2015.10.039.
- [54] Hedayat, Z., Belmans, B., Hossein Ayatollahi, M., Wouters, I. and Descamps, F. (2015) 'Performance Assessment of Ancient Wind Catchers - an Experimental and Analytical Study', *Energy Procedia*. Elsevier, 78, pp. 2578–2583. doi: 10.1016/J.EGYPRO.2015.11.292.
- [55] Jomehzadeh, F., Nejat, P., Calautit, J. K., Yusof, M. B. M., Zaki, S. A., Hughes, B. R. and Yazid, M. N. A. W. M. (2017) 'A review on windcatcher for passive cooling and natural ventilation in buildings, Part 1: Indoor air quality and thermal comfort assessment', *Renewable and Sustainable Energy Reviews*. Pergamon, 70, pp. 736–756. doi: 10.1016/j.rser.2016.11.254.
- [56] Nowak, T. (2007) *Energy Use in Homes 2007: A series of reports on domestic energy use in England: Energy Efficiency*. Watford. Available at:
http://www.bre.co.uk/filelibrary/pdf/rpts/Energy_Efficiency_2007.pdf (Accessed: 12 November 2014).
- [57] Nowak, T. (2007) *Energy Use in Homes 2007: A series of reports on domestic energy use in England: Thermal Insulation*. Available at:
http://www.bre.co.uk/filelibrary/pdf/rpts/Thermal_Insulation_2007.pdf (Accessed: 12 November 2014).
- [58] Nowak, T. (2007) *Energy Use in Homes 2007: A series of reports on*

domestic energy use in England: Space and Water Heating. Watford. Available at: http://www.bre.co.uk/filelibrary/pdf/rpts/Space_and_Water_Heating_2007.pdf (Accessed: 12 November 2014).

[59] Hanibuchi, H. and Hokoi, S. (1998) *Basic study of radiative and convective heat exchange in a room with floor heating*, *Ashrae Transactions*. Available at: http://www.ibpsa.org/proceedings/BS1999/BS99_C-07.pdf (Accessed: 12 November 2014).

[60] Colliver, D. (1996) 'Energy requirements for conditioning of ventilating air', *Fuel and Energy Abstracts*. Available at: <http://onlinelibrary.wiley.com/doi/10.1002/cbdv.200490137/abstract> (Accessed: 6 February 2013).

[61] Reay, D. A. (1975) 'A review of Gas-Gas Heat recovery systems', *Heat Recovery Systems*, 1, pp. 3–41. Available at: <http://www.google.com/patents?hl=en&lr=&vid=USPAT3917444&id=Jx8-AAAAEBAJ&oi=fnd&dq=Heat+Recovery+Systems&printsec=abstract>.

[62] Luo, X. J. (2017) 'Parametric study of heat transfer enhancement on cross-flow heat exchangers', *Chemical Engineering and Processing: Process Intensification*. Elsevier, 121, pp. 81–89. doi: 10.1016/J.CEP.2017.07.014.

[63] Justo Alonso, M., Liu, P., Mathisen, H. M., Ge, G. and Simonson, C. (2015) 'Review of heat/energy recovery exchangers for use in ZEBs in cold climate countries', *Building and Environment*. Pergamon, 84, pp. 228–237. doi: 10.1016/J.BUILDENV.2014.11.014.

[64] Chang, C.-C., Liang, J.-D. and Chen, S.-L. (2018) 'Performance investigation of regenerative total heat exchanger with periodic flow', *Applied Thermal Engineering*. Pergamon, 130, pp. 1319–1327. doi: 10.1016/J.APPLTHERMALENG.2017.11.024.

[65] Fernández-Seara, J., Diz, R., Uhía, F. J., Dopazo, A. and Ferro, J. M. (2011) 'Experimental analysis of an air-to-air heat recovery unit for balanced ventilation systems in residential buildings', *Energy Conversion and*

Management, 52(1), pp. 635–640. doi: 10.1016/j.enconman.2010.07.040.

[66] Chen, X., Su, Y., Reay, D. and Riffat, S. (2016) 'Recent research developments in polymer heat exchangers – A review', *Renewable and Sustainable Energy Reviews*. Pergamon, 60, pp. 1367–1386. doi: 10.1016/J.RSER.2016.03.024.

[67] T'Joen, C., Park, Y., Wang, Q., Sommers, A., Han, X. and Jacobi, A. (2009) 'A review on polymer heat exchangers for HVAC&R applications', *International Journal of Refrigeration*. Elsevier, pp. 763–779. doi: 10.1016/j.ijrefrig.2008.11.008.

[68] Seyed-Ahmadi, M., Erb, B., Simonson, C. J. and Besant, R. W. (2009) 'Transient behavior of run-around heat and moisture exchanger system. Part I: Model formulation and verification', *International Journal of Heat and Mass Transfer*. Elsevier Ltd, 52(25–26), pp. 6000–6011. doi: 10.1016/j.ijheatmasstransfer.2009.07.012.

[69] Al-Waked, R., Nasif, M. S., Morrison, G. and Behnia, M. (2013) 'CFD simulation of air to air enthalpy heat exchanger', *Energy Conversion and Management*. Elsevier Ltd, 74, pp. 377–385. doi: 10.1016/j.enconman.2013.05.038.

[70] Zhang, L.-Z. (2010) 'An analytical solution for heat mass transfer in a hollow fiber membrane based air-to-air heat mass exchanger', *Journal of Membrane Science*. Elsevier B.V., 360(1–2), pp. 217–225. doi: 10.1016/j.memsci.2010.05.015.

[71] Hwang, H. Y., Koh, H. C., Rhim, J. W. and Nam, S. Y. (2008) 'Preparation of sulfonated SEBS block copolymer membranes and their permeation properties', *Desalination*. Elsevier, 233(1–3), pp. 173–182. doi: 10.1016/J.DESAL.2007.09.040.

[72] Sabek, S., Tiss, F., Chouikh, R. and Guizani, A. (2018) 'Numerical investigation of heat and mass transfer in partially blocked membrane based heat exchanger: Effects of obstacles forms', *Applied Thermal Engineering*.

Pergamon, 130, pp. 211–220. doi:

10.1016/J.APPLTHERMALENG.2017.11.019.

[73] Liu, P., Justo Alonso, M., Mathisen, H. M. and Simonson, C. (2017) 'Energy transfer and energy saving potentials of air-to-air membrane energy exchanger for ventilation in cold climates', *Energy and Buildings*. Elsevier, 135, pp. 95–108. doi: 10.1016/J.ENBUILD.2016.11.047.

[74] Zeng, C., Liu, S. and Shukla, A. (2017) 'A review on the air-to-air heat and mass exchanger technologies for building applications', *Renewable and Sustainable Energy Reviews*. Elsevier Ltd, 75(December 2016), pp. 753–774. doi: 10.1016/j.rser.2016.11.052.

[75] Zhang, H., Xie, C., Hu, J., Liu, S., Yang, H., Wang, X. and Niu, C. (2017) 'Experimental Investigation on Heat Transfer of Carbon Nanotube Membranes', *Procedia Engineering*. Elsevier, 205, pp. 3067–3071. doi: 10.1016/J.PROENG.2017.10.283.

[76] Zhang, L. (2012) 'Progress on heat and moisture recovery with membranes: From fundamentals to engineering applications', *Energy Conversion and Management*. Elsevier Ltd, 63, pp. 173–195. doi: 10.1016/j.enconman.2011.11.033.

[77] Nasif, M., AL-Waked, R., Morrison, G. and Behnia, M. (2010) 'Membrane heat exchanger in HVAC energy recovery systems, systems energy analysis', *Energy and Buildings*. Elsevier B.V., 42(10), pp. 1833–1840. doi: 10.1016/j.enbuild.2010.05.020.

[78] Zhang, L. and Niu, J. (2001) 'Energy requirements for conditioning fresh air and the long-term savings with a membrane-based energy recovery ventilator in Hong Kong', *Energy*, 26, pp. 119–135. Available at: <http://www.sciencedirect.com/science/article/pii/S0360544200000645>.

[79] Liu, J., Li, W., Liu, J. and Wang, B. (2010) 'Efficiency of energy recovery ventilator with various weathers and its energy saving performance in a residential apartment', *Energy and Buildings*, 42(1), pp. 43–49. doi:

10.1016/j.enbuild.2009.07.009.

[80] Han, H., Choo, Y. and Kwon, Y. (2007) 'An experimental study on the effect of outdoor temperature and humidity conditions on the performance of a heat recovery ventilator', *Proceedings of Clima, Well Being Indoors*. Available at: http://www.inive.org/members_area/medias/pdf/Inive%5Cclima2007%5CA07%5CA07Q1533.pdf.

[81] Martinez, A., Urra, I., Hernandez, J., Diallo, T. and Zhao, X. (2017) 'Development of a Smart Modular Heat Recovery Unit Adaptable into a Ventilated Façade', *Procedia Environmental Sciences*. Elsevier, 38, pp. 94–101. doi: 10.1016/J.PROENV.2017.03.086.

[82] Diallo, T. M. O., Zhao, X., Dugue, A., Bonnamy, P., Javier Miguel, F., Martinez, A., Theodosiou, T., Liu, J.-S. and Brown, N. (2017) 'Numerical investigation of the energy performance of an Opaque Ventilated Façade system employing a smart modular heat recovery unit and a latent heat thermal energy system', *Applied Energy*. Elsevier, 205, pp. 130–152. doi: 10.1016/J.APENERGY.2017.07.042.

[83] Hughes, B. R., Chaudhry, H. N. and Calautit, J. K. (2014) 'Passive energy recovery from natural ventilation air streams', *Applied Energy*. Elsevier Ltd, 113, pp. 127–140. doi: 10.1016/j.apenergy.2013.07.019.

[84] O'Connor, D., Calautit, J. K. and Hughes, B. R. (2014) 'A study of passive ventilation integrated with heat recovery', *Energy and Buildings*. Elsevier, 82, pp. 799–811. doi: 10.1016/j.enbuild.2014.05.050.

[85] Calautit, J. K., Hughes, B. R., O'Connor, D., Shahzad, S. S., O'Connor, D. and Shahzad, S. S. (2017) 'Numerical and experimental analysis of a multi-directional wind tower integrated with vertically-arranged heat transfer devices (VHTD)', *Applied Energy*. Elsevier Ltd, 185, pp. 1120–1135. doi: 10.1016/j.apenergy.2016.02.025.

[86] Simonetti, M., Fracastoro, G. V., Chiesa, G. and Sola, S. (2016) 'Numerical optimization and experimental testing of a new low pressure heat exchanger

(LoPHEX) for passive ventilation of buildings', *Applied Thermal Engineering*. Elsevier Ltd, 103, pp. 720–729. doi: 10.1016/j.applthermaleng.2016.04.143.

[87] Troi, A. and Bastian, Z. (2014) 'Energy Efficiency Solutions for Historic Buildings, A Handbook'. Berlin, Boston: Birkhäuser. doi: 10.1515/9783038216506.

[88] de Dear, R. J. and Brager, G. S. (2002) 'Thermal comfort in naturally ventilated buildings: revisions to ASHRAE Standard 55', *Energy and Buildings*. Elsevier, 34(6), pp. 549–561. doi: 10.1016/S0378-7788(02)00005-1.

[89] White, J., Gillott, M. C., Wood, C. J., Loveday, D. L. and Vadodaria, K. (2016) 'Performance evaluation of a mechanically ventilated heat recovery (MVHR) system as part of a series of UK residential energy retrofit measures', *Energy and Buildings*. Elsevier, 110, pp. 220–228. doi: 10.1016/J.ENBUILD.2015.09.059.

[90] Lai, D., Qi, Y., Liu, J., Dai, X., Zhao, L. and Wei, S. (2018) 'Ventilation behavior in residential buildings with mechanical ventilation systems across different climate zones in China', *Building and Environment*. Pergamon, 143, pp. 679–690. doi: 10.1016/J.BUILDENV.2018.08.006.

[91] Schibuola, L., Scarpa, M. and Tambani, C. (2018) 'Innovative technologies for energy retrofit of historic buildings: An experimental validation', *Journal of Cultural Heritage*. Elsevier Masson, 30, pp. 147–154. doi: 10.1016/J.CULHER.2017.09.011.

[92] Sharpe, T., McGill, G., Gupta, R., Gregg, M. and Mawditt, I. (no date cn) *Characteristics and performance of MVHR systems. A meta study of MVHR systems used in the Innovate UK Building Performance Evaluation Programme*. Available at: [http://radar.gsa.ac.uk/4073/1/MVHR Meta Study Report March 2016 FINAL PUBLISHED.pdf](http://radar.gsa.ac.uk/4073/1/MVHR%20Meta%20Study%20Report%20March%202016%20FINAL%20PUBLISHED.pdf) (Accessed: 4 September 2018).

[93] McGill, G., Oyedele, L. O. and McAllister, K. (2015) 'Case study investigation of indoor air quality in mechanically ventilated and naturally ventilated UK social housing', *International Journal of Sustainable Built*

Environment. Elsevier, 4(1), pp. 58–77. doi: 10.1016/J.IJSBE.2015.03.002.

[94] Gupta, R., Kapsali, M. and Howard, A. (2018) 'Evaluating the influence of building fabric, services and occupant related factors on the actual performance of low energy social housing dwellings in UK', *Energy and Buildings*. Elsevier, 174, pp. 548–562. doi: 10.1016/J.ENBUILD.2018.06.057.

[95] Kindinis, A., Cantin, R., El Mankibi, M. and Guarracino, G. (2011) 'Thermal and Aeraulic Parametric Analysis of Historical Dwellings', *International Journal of Ventilation*, 10(2), pp. 173–183. doi: 10.1080/14733315.2011.11683946.

[96] Homod, R. Z., Sahari, K. S. M. and Almurib, H. A. F. (2014) 'Energy saving by integrated control of natural ventilation and HVAC systems using model guide for comparison', *Renewable Energy*. Pergamon, 71, pp. 639–650. doi: 10.1016/j.renene.2014.06.015.

[97] Omar, N. a. M. and Syed-Fadzil, S. F. (2011) 'Assessment of Passive Thermal Performance for a Penang Heritage Shop house', *Procedia Engineering*. Elsevier, 20, pp. 203–212. doi: 10.1016/j.proeng.2011.11.157.

[98] Rubio-Bellido, C., Pulido-Arcas, J. A. and Cabeza-Lainez, J. M. (2018) 'Understanding climatic traditions: A quantitative and qualitative analysis of historic dwellings of Cadiz', *Indoor and Built Environment*, 27(5), pp. 665–681. doi: 10.1177/1420326X16682580.

[99] Dodoo, A., Gustavsson, L. and Sathre, R. (2011) 'Primary energy implications of ventilation heat recovery in residential buildings', *Energy and Buildings*. Elsevier B.V., 43(7), pp. 1566–1572. doi: 10.1016/j.enbuild.2011.02.019.

[100] Banfill, P. F. G., Simpson, S. A., Gillott, M. C. and White, J. (2011) *Mechanical ventilation and heat recovery for low carbon retrofitting in dwellings*. Available at: http://www.ep.liu.se/ecp/057/vol3/046/ecp57vol3_046.pdf (Accessed: 2 September 2018).

[101] Simonson, C. (2005) 'Energy consumption and ventilation performance of a naturally ventilated ecological house in a cold climate', *Energy and Buildings*,

37(1), pp. 23–35. doi: 10.1016/j.enbuild.2004.04.006.

[102] Yassine, B., Ghali, K., Ghaddar, N., Srour, I. and Chehab, G. (2012) 'A numerical modeling approach to evaluate energy-efficient mechanical ventilation strategies', *Energy and Buildings*. Elsevier B.V., 55, pp. 618–630. doi: 10.1016/j.enbuild.2012.08.042.

[103] Zhou, J., Zhang, G., Lin, Y. and Li, Y. (2008) 'Coupling of thermal mass and natural ventilation in buildings', *Energy and Buildings*. Elsevier, 40(6), pp. 979–986. doi: 10.1016/j.enbuild.2007.08.001.

[104] Calebre (2013) 'Keep it Tight', *CIBSE Journal*, (September), pp. 50–52. Available at: <http://www.cibsejournal.com/archive/PDFs/CIBSE-Journal-2013-09.pdf> (Accessed: 1 October 2015).

[105] Maier, T., Krzaczek, M. and Tejchman, J. (2009) 'Comparison of physical performances of the ventilation systems in low-energy residential houses', *Energy and Buildings*, 41(3), pp. 337–353. doi: 10.1016/j.enbuild.2008.10.007.

[106] Laverge, J. and Janssens, a. (2012) 'Heat recovery ventilation operation traded off against natural and simple exhaust ventilation in Europe by primary energy factor, carbon dioxide emission, household consumer price and exergy', *Energy and Buildings*. Elsevier B.V., 50, pp. 315–323. doi: 10.1016/j.enbuild.2012.04.005.

[107] Ealiwa, M. ., Taki, A. ., Howarth, A. . and Seden, M. . (2001) 'An investigation into thermal comfort in the summer season of Ghadames, Libya', *Building and Environment*. Pergamon, 36(2), pp. 231–237. doi: 10.1016/S0360-1323(99)00071-2.

[108] Li, L. and Mak, C. M. (2007) 'The assessment of the performance of a windcatcher system using computational fluid dynamics', *Building and Environment*, 42(3), pp. 1135–1141. doi: 10.1016/j.buildenv.2005.12.015.

[109] ZEDFactory (no date de) *Load Reduction*. Available at: <http://www.zedfactory.com/loadreduction.pdf> (Accessed: 31 August 2013).

- [110] Monodraught (2013) *Windcatcher Heritage*. Available at: [http://www.monodraught.com/products/natural-ventilation/14/windcatcher-heritage/?info=67#Technical Details](http://www.monodraught.com/products/natural-ventilation/14/windcatcher-heritage/?info=67#Technical%20Details) (Accessed: 31 August 2015).
- [111] Larsen, T. S. and Heiselberg, P. (2008) 'Single-sided natural ventilation driven by wind pressure and temperature difference', *Energy and Buildings*. Elsevier, 40(6), pp. 1031–1040. doi: 10.1016/j.enbuild.2006.07.012.
- [112] Chu, C.-R., Chiu, Y.-H., Tsai, Y.-T. and Wu, S.-L. (2015) 'Wind-driven natural ventilation for buildings with two openings on the same external wall', *Energy and Buildings*. Elsevier, 108, pp. 365–372. doi: 10.1016/J.ENBUILD.2015.09.041.
- [113] Ai, Z. T. T. and Mak, C. M. M. (2014) 'Determination of single-sided ventilation rates in multistory buildings: Evaluation of methods', *Energy and Buildings*. Elsevier, 69, pp. 292–300. doi: 10.1016/j.enbuild.2013.11.014.
- [114] van Hooff, T. and Blocken, B. (2010) 'Coupled urban wind flow and indoor natural ventilation modelling on a high-resolution grid: A case study for the Amsterdam ArenA stadium', *Environmental Modelling & Software*. Elsevier, 25(1), pp. 51–65. doi: 10.1016/J.ENVSOFT.2009.07.008.
- [115] Ramponi, R. and Blocken, B. (2012) 'CFD simulation of cross-ventilation flow for different isolated building configurations: Validation with wind tunnel measurements and analysis of physical and numerical diffusion effects', *Journal of Wind Engineering and Industrial Aerodynamics*. Elsevier, 104–106, pp. 408–418. doi: 10.1016/j.jweia.2012.02.005.
- [116] van Hooff, T., Blocken, B. and Tominaga, Y. (2017) 'On the accuracy of CFD simulations of cross-ventilation flows for a generic isolated building: Comparison of RANS, LES and experiments', *Building and Environment*. Pergamon, 114, pp. 148–165. doi: 10.1016/j.buildenv.2016.12.019.
- [117] Wang, J., Wang, S., Zhang, T. and Battaglia, F. (2017) 'Assessment of single-sided natural ventilation driven by buoyancy forces through variable window configurations', *Energy and Buildings*. Elsevier, 139, pp. 762–779. doi:

10.1016/J.ENBUILD.2017.01.070.

[118] Ramponi, R. and Blocken, B. (2012) 'CFD simulation of cross-ventilation for a generic isolated building: Impact of computational parameters', *Building and Environment*. Pergamon, 53, pp. 34–48. doi:

10.1016/J.BUILDENV.2012.01.004.

[119] Foucquier, A., Robert, S., Suard, F., Stéphan, L. and Jay, A. (2013) 'State of the art in building modelling and energy performances prediction: A review', *Renewable and Sustainable Energy Reviews*, 23, pp. 272–288. doi:

10.1016/j.rser.2013.03.004.

[120] Hitchin, E. R. and Wilson, C. B. (1967) 'A review of experimental techniques for the investigation of natural ventilation in buildings', *Building Science*. Pergamon, 2(1), pp. 59–82. doi: 10.1016/0007-3628(67)90007-2.

[121] Stathopoulou, O. I., Assimakopoulos, V. D., Flocas, H. A. and Helmis, C. G. (2008) 'An experimental study of air quality inside large athletic halls', *Building and Environment*. Pergamon, 43(5), pp. 834–848. doi:

10.1016/J.BUILDENV.2007.01.026.

[122] Lee, S. C., Chan, L. Y. and Chiu, M. Y. (1999) 'Indoor and outdoor air quality investigation at 14 public places in Hong Kong', *Environment International*. Pergamon, 25(4), pp. 443–450. doi: 10.1016/S0160-4120(99)00019-7.

[123] Assimakopoulos, V. D. and Helmis, C. G. (2004) 'On the study of a sick building: the case of Athens Air Traffic Control Tower', *Energy and Buildings*. Elsevier, 36(1), pp. 15–22. doi: 10.1016/S0378-7788(03)00043-4.

[124] Zhu, Y., Hinds, W. C., Krudysz, M., Kuhn, T., Froines, J. and Sioutas, C. (2005) 'Penetration of freeway ultrafine particles into indoor environments', *Journal of Aerosol Science*. Pergamon, 36(3), pp. 303–322. doi:

10.1016/J.JAEROSCI.2004.09.007.

[125] Halios, C. H., Assimakopoulos, V. D., Helmis, C. G. and Flocas, H. A. (2005) 'Investigating cigarette-smoke indoor pollution in a controlled

environment', *Science of The Total Environment*. Elsevier, 337(1–3), pp. 183–190. doi: 10.1016/J.SCITOTENV.2004.06.014.

[126] Guo, H., Lee, S. . and Chan, L. . (2004) 'Indoor air quality investigation at air-conditioned and non-air-conditioned markets in Hong Kong', *Science of The Total Environment*. Elsevier, 323(1–3), pp. 87–98. doi: 10.1016/J.SCITOTENV.2003.09.031.

[127] Chen, Q. (2009) 'Ventilation performance prediction for buildings: A method overview and recent applications', *Building and Environment*. Pergamon, 44(4), pp. 848–858. doi: 10.1016/J.BUILDENV.2008.05.025.

[128] Calautit, J. K., Hughes, B. R., Chaudhry, H. N. and Ghani, S. A. (2013) 'CFD analysis of a heat transfer device integrated wind tower system for hot and dry climate', *Applied Energy*. Elsevier, 112, pp. 1–16. doi: 10.1016/j.apenergy.2013.01.021.

[129] James Lo, L., Banks, D. and Novoselac, A. (2013) 'Combined wind tunnel and CFD analysis for indoor airflow prediction of wind-driven cross ventilation', *Building and Environment*, 60, pp. 12–23. Available at: <http://www.sciencedirect.com/science/article/pii/S0360132312002879>.

[130] Tecele, A., Bitsuamlak, G. T. and Jiru, T. E. (2013) 'Wind-driven natural ventilation in a low-rise building: A Boundary Layer Wind Tunnel study', *Building and Environment*, 59, pp. 275–289. Available at: <http://www.sciencedirect.com/science/article/pii/S0360132312002284>.

[131] Ji, L., Tan, H., Kato, S., Bu, Z. and Takahashi, T. (2011) 'Wind tunnel investigation on influence of fluctuating wind direction on cross natural ventilation', *Building and Environment*, 46(12), pp. 2490–2499. Available at: <http://www.sciencedirect.com/science/article/pii/S0360132311001776>.

[132] Kato, S., Murakami, S., Takahashi, T. and Gyobu, T. (1997) 'Chained analysis of wind tunnel test and CFD on cross ventilation of large-scale market building', *Journal of Wind Engineering and Industrial Aerodynamics*, 67–68, pp. 573–587. doi: 10.1016/S0167-6105(97)00101-3.

- [133] Jiang, Y., Alexander, D., Jenkins, H., Arthur, R. and Chen, Q. (2003) 'Natural ventilation in buildings: measurement in a wind tunnel and numerical simulation with large-eddy simulation', *Journal of Wind Engineering and Industrial Aerodynamics*, 91(3), pp. 331–353. doi: 10.1016/S0167-6105(02)00380-X.
- [134] van Hooff, T., Blocken, B., Aanen, L. and Bronsema, B. (2011) 'A venturi-shaped roof for wind-induced natural ventilation of buildings: Wind tunnel and CFD evaluation of different design configurations', *Building and Environment*. Pergamon, 46(9), pp. 1797–1807. doi: 10.1016/J.BUILDENV.2011.02.009.
- [135] Wong, N. H. and Heryanto, S. (2004) 'The study of active stack effect to enhance natural ventilation using wind tunnel and computational fluid dynamics (CFD) simulations', *Energy and Buildings*, 36(7), pp. 668–678. doi: 10.1016/j.enbuild.2004.01.013.
- [136] Ohba, M., Irie, K. and Kurabuchi, T. (2001) 'Study on airflow characteristics inside and outside a cross-ventilation model, and ventilation flow rates using wind tunnel experiments', *Journal of Wind Engineering and Industrial Aerodynamics*, 89(14–15), pp. 1513–1524. doi: 10.1016/S0167-6105(01)00130-1.
- [137] Laurini, E., Taballione, A., Rotilio, M. and De Berardinis, P. (2017) 'Analysis and exploitation of the stack ventilation in the historic context of high architectural, environmental and landscape value', *Energy Procedia*. Elsevier, 133, pp. 268–280. doi: 10.1016/J.EGYPRO.2017.09.386.
- [138] Mardiana, A., Riffat, S. B. and Worall, M. (2013) 'Integrated heat recovery system with wind-catcher for building applications : towards energy-efficient technologies', *Materials and processes for energy: Communicating current research and technological developments*, pp. 720–727.
- [139] Shao, L. and Riffat, S. . (1997) 'Flow loss caused by heat pipes in natural ventilation stacks', *Applied Thermal Engineering*, 17(4), pp. 393–399. doi: 10.1016/S1359-4311(96)00029-4.

- [140] Qian, S., Yu, J. and Yan, G. (2017) 'A review of regenerative heat exchange methods for various cooling technologies', *Renewable and Sustainable Energy Reviews*. Pergamon, 69, pp. 535–550. doi: 10.1016/J.RSER.2016.11.180.
- [141] Mahmud, K., Mahmood, G. I., Simonson, C. J. and Besant, R. W. (2010) 'Performance testing of a counter-cross-flow run-around membrane energy exchanger (RAMEE) system for HVAC applications', *Energy and Buildings*. Elsevier B.V., 42(7), pp. 1139–1147. doi: 10.1016/j.enbuild.2010.02.005.
- [142] Hviid, C. A., Svendsen, S. and Anker, C. (2011) 'Analytical and experimental analysis of a low-pressure heat exchanger suitable for passive ventilation', *Energy and Buildings*, 43(2–3), pp. 275–284. doi: 10.1016/j.enbuild.2010.08.003.
- [143] Haghghi, A. P., Pakdel, S. H. and Jafari, A. (2016) 'A study of a wind catcher assisted adsorption cooling channel for natural cooling of a 2-storey building', *Energy*. Pergamon, 102, pp. 118–138. doi: 10.1016/J.ENERGY.2016.02.033.
- [144] O'Connor, D., Calautit, J. and Hughes, B. R. (2015) 'Effect of Rotation Speed of a Rotary Thermal Wheel on Ventilation Supply Rates of Wind Tower System', *Energy Procedia*. Elsevier, 75, pp. 1705–1710. doi: 10.1016/J.EGYPRO.2015.07.432.
- [145] Abd El-Baky, M. a. and Mohamed, M. M. (2007) 'Heat pipe heat exchanger for heat recovery in air conditioning', *Applied Thermal Engineering*, 27(4), pp. 795–801. doi: 10.1016/j.applthermaleng.2006.10.020.
- [146] Hughes, B. R., Chaudhry, H. N. and Ghani, S. A. (2011) 'A review of sustainable cooling technologies in buildings', *Renewable and Sustainable Energy Reviews*. Elsevier Ltd, 15(6), pp. 3112–3120. doi: 10.1016/j.rser.2011.03.032.
- [147] Calautit, J. K. and Hughes, B. R. (2016) 'A passive cooling wind catcher with heat pipe technology: CFD, wind tunnel and field-test analysis', *Applied*

Energy. Elsevier Ltd, 162, pp. 460–471. doi: 10.1016/j.apenergy.2015.10.045.

[148] Chaudhry, H. N. (2016) 'A study on optimising heat pipe geometrical parameters for sustainable passive cooling within the built environment', *Applied Thermal Engineering*. Pergamon, 93, pp. 486–499. doi: 10.1016/j.applthermaleng.2015.10.018.

[149] Calautit, J. K., Hughes, B. R. and Nasir, D. S. (2017) 'Climatic analysis of a passive cooling technology for the built environment in hot countries', *Applied Energy*. Elsevier, 186, pp. 321–335. doi: 10.1016/j.apenergy.2016.05.096.

[150] Chaudhry, H. N., Calautit, J. K. and Hughes, B. R. (2017) 'Optimisation and analysis of a heat pipe assisted low-energy passive cooling system', *Energy and Buildings*. Elsevier, 143, pp. 220–233. doi: 10.1016/j.enbuild.2017.02.002.

[151] Kolokotroni, M., Perera, M. D. a. E. S., Azzi, D. and Virk, G. S. (2001) 'An investigation of passive ventilation cooling and control strategies for an educational building', *Applied Thermal Engineering*, 21(2), pp. 183–199. doi: 10.1016/S1359-4311(00)00008-9.

[152] Shao, L., Riffat, S. and Gan, G. (1998) 'Heat recovery with low pressure loss for natural ventilation', *Energy and buildings*, 28(98). Available at: <http://www.sciencedirect.com/science/article/pii/S0378778898000164>.

[153] Riffat, S. and Gan, G. (1998) 'Determination of effectiveness of heat-pipe heat recovery for naturally-ventilated buildings', *Applied Thermal Engineering*, 18(97), pp. 121–130. Available at: <http://www.sciencedirect.com/science/article/pii/S1359431197000331>.

[154] Gan, G. and Riffat, S. (1998) 'A numerical study of solar chimney for natural ventilation of buildings with heat recovery', *Applied Thermal Engineering*, 18, pp. 1171–1187. Available at: <http://www.sciencedirect.com/science/article/pii/S1359431197001178>.

[155] Mahmoudi Zarandi, M. (2009) 'Analysis on Iranian Wind Catcher and Its Effect on Natural Ventilation as a Solution towards Sustainable Architecture

(Case Study: Yazd)', *International Journal of Humanities and Social Sciences*, 3(6). Available at: <https://waset.org/publications/11631/analysis-on-iranian-wind-catcher-and-its-effect-on-natural-ventilation-as-a-solution-towards-sustainable-architecture-case-study-yazd-> (Accessed: 4 September 2018).

[156] M.R.Khani, S., Bahadori, M. N. and Dehghani-Sanij, A. R. (2017) 'Experimental investigation of a modular wind tower in hot and dry regions', *Energy for Sustainable Development*. Elsevier, 39, pp. 21–28. doi: 10.1016/J.ESD.2017.03.003.

[157] Etheridge, D. W. (2000) 'Unsteady flow effects due to fluctuating wind pressures in natural ventilation design—instantaneous flow rates', *Building and Environment*. Pergamon, 35(4), pp. 321–337. doi: 10.1016/S0360-1323(99)00021-9.

[158] Sibille, E., Pfluger, R., Gritzer, F. and Happach, A. (2014) *Development of a coaxial-duct as outdoor air inlet and exhaust air outlet for ventilation units*. doi: 10.13140/2.1.1212.5448.

[159] Montazeri, H., Montazeri, F., Azizian, R. and Mostafavi, S. (2010) 'Two-sided wind catcher performance evaluation using experimental, numerical and analytical modeling', *Renewable Energy*. Elsevier Ltd, 35(7), pp. 1424–1435. doi: 10.1016/j.renene.2009.12.003.

[160] Montazeri, H. and Azizian, R. (2008) 'Experimental study on natural ventilation performance of one-sided wind catcher', *Building and Environment*, 43(12), pp. 2193–2202. doi: 10.1016/j.buildenv.2008.01.005.

[161] Dehghani-Sanij, A. R., Soltani, M. and Raahemifar, K. (2015) 'A new design of wind tower for passive ventilation in buildings to reduce energy consumption in windy regions', *Renewable and Sustainable Energy Reviews*. Elsevier, 42, pp. 182–195. doi: 10.1016/j.rser.2014.10.018.

[162] Dehghan, A. A. A., Esfeh, M. K. and Manshadi, M. D. (2013) 'Natural ventilation characteristics of one-sided wind catchers : experimental and analytical evaluation', *Energy & Buildings*. Elsevier B.V., 61, pp. 366–377. doi:

10.1016/j.enbuild.2013.02.048.

[163] Sadeghi, H., Heristchian, M., Aziminejad, A. and Nooshin, H. (2017) 'Wind effect on grooved and scallop domes', *Engineering Structures*. Elsevier, 148, pp. 436–450. doi: 10.1016/J.ENGSTRUCT.2017.07.003.

[164] Uematsu, Y., Yamada, M., Inoue, A. and Hongo, T. (1997) 'Wind loads and wind-induced dynamic behavior of a single-layer latticed dome', *Journal of Wind Engineering and Industrial Aerodynamics*. Elsevier, 66(3), pp. 227–248. doi: 10.1016/S0167-6105(97)00133-5.

[165] Cheng, C. M. and Fu, C. L. (2010) 'Characteristic of wind loads on a hemispherical dome in smooth flow and turbulent boundary layer flow', *Journal of Wind Engineering and Industrial Aerodynamics*. Elsevier, 98(6–7), pp. 328–344. doi: 10.1016/J.JWEIA.2009.12.002.

[166] Sun, Y., Qiu, Y. and Wu, Y. (2013) 'Modeling of Wind Pressure Spectra on Spherical Domes', *International Journal of Space Structures*. SAGE Publications Sage UK: London, England, 28(2), pp. 87–99. doi: 10.1260/0266-3511.28.2.87.

[167] Autodesk (2013) *Autodesk Inventor 2013*. Available at: <http://help.autodesk.com/view/INVNTOR/2013/ENU/> (Accessed: 4 January 2018).

[168] Su, Y., Riffat, S. B., Lin, Y.-L. and Khan, N. (2008) 'Experimental and CFD study of ventilation flow rate of a Monodraught™ windcatcher', *Energy and Buildings*. Elsevier, 40(6), pp. 1110–1116. doi: 10.1016/j.enbuild.2007.10.001.

[169] Montazeri, H. and Montazeri, F. (2018) 'CFD simulation of cross-ventilation in buildings using rooftop wind-catchers: Impact of outlet openings', *Renewable Energy*. Pergamon, 118, pp. 502–520. doi: 10.1016/J.RENENE.2017.11.032.

[170] Poshtiri, A. H. and Mohabbati, S. M. (2017) 'Performance analysis of wind catcher integrated with shower cooling system to meet thermal comfort conditions in buildings', *Journal of Cleaner Production*. Elsevier, 148, pp. 452–

466. doi: 10.1016/J.JCLEPRO.2017.01.160.

[171] Yaïci, W., Ghorab, M. and Entchev, E. (2013) 'Numerical analysis of heat and energy recovery ventilators performance based on CFD for detailed design', *Applied Thermal Engineering*. Elsevier Ltd, 51(1–2), pp. 770–780. doi: 10.1016/j.applthermaleng.2012.10.003.

[172] Asfour, O. and Gadi, M. (2007) 'A comparison between CFD and Network models for predicting wind-driven ventilation in buildings', *Building and Environment*, 42(12), pp. 4079–4085. doi: 10.1016/j.buildenv.2006.11.021.

[173] Madej, J. and Bedkowski, B. (2013) 'Air flow analysis for electrical motor's cooling system with Autodesk simulation CFD 2013 program', *Acta Mechanica et Automatica*, 7(2), pp. 89–92.

[174] Kietzmann, C., Chen, L. and Costa, F. (2013) 'Conformai, cooling simulation for the plastic injection molding process', in *Annual Technical Conference - ANTEC, Conference Proceedings*, pp. 1237–1242.

[175] Mashud, M. and Das, R. C. (2017) 'Effect of rear end spoiler angle of a sedan car', in *AIP Conference Proceedings*. doi: 10.1063/1.4984646.

[176] Kudriavtsev, V., Krzeminski, M., Todorcevic, S., Feeney, B., Ania, A., Balage, S., Buneta, M., Trauttmansdorff, M. and Viechweg, M. (2004) 'CFD, thermal and stress analysis for davinci X-prize manned space mission: Computational design analysis part 1 (Keynote lecture)', in *American Society of Mechanical Engineers, Pressure Vessels and Piping Division (Publication) PVP*, pp. 243–269. doi: 10.1115/PVP2004-3113.

[177] Burlacu, A., Sosoi, G., Vizitiu, R. Ștefan, Bărbuță, M., Lăzărescu, C. D., Verdeș, M. and Șerbănoiu, A. A. (2018) 'Innovative system for heat recovery from used water in the building sector', *Procedia Manufacturing*. Elsevier, 22, pp. 722–729. doi: 10.1016/J.PROMFG.2018.03.104.

[178] Burlacu, A., Lazarescu, C. D., Serbanoiu, A. A., Barbuta, M., Ciocan, V. and Verdeș, M. (2017) 'Energy efficient pipe heat exchanger for waste heat recovery from exhaust flue gases', *Environmental Engineering and*

Management Journal, 16(5), pp. 1107–1113.

[179] Nalamwar, M. R., Parbat, D. K. and Singh, D. P. (2017) 'Study of effect of windows location on ventilation by CFD simulation', *International Journal of Civil Engineering and Technology*, 8(7), pp. 521–531.

[180] Abdelhafez, M. H. H. (2018) 'Green residential districts in hot desert climate towards low energy consumption', *Journal of Engineering and Applied Science*, 65(1), pp. 1–21.

[181] Abd Elrady, A. R. and Hassan, M. H. (2015) 'Conservation of morphological characters as an approach to thermal comfort', in *Vernacular Architecture: Towards a Sustainable Future - Proceedings of the International Conference on Vernacular Heritage, Sustainability and Earthen Architecture*, pp. 15–20.

[182] Eldabosy, M. M., Farag, O. M. and Moustafa, W. S. (2015) 'Mutual passive techniques impacts on human comfort for modular Unit in Cairo desert', *Journal of Engineering and Applied Science*, 62(2), pp. 101–118.

[183] Sowgath, M. T., Rahman, M. M., Nomany, S. A., Sakib, M. N. and Junayed, M. (2015) 'CFD study of biomass cooking stove using Autodesk Simulation CFD to improve energy efficiency and emission characteristics', *Chemical Engineering Transactions*, 45, pp. 1255–1260. doi: 10.3303/CET1545210.

[184] Xie, Q., Dousti, M. J. and Pedram, M. (2015) 'Therminator: A thermal simulator for smartphones producing accurate chip and skin temperature maps', in *Proceedings of the International Symposium on Low Power Electronics and Design*, pp. 117–122. doi: 10.1145/2627369.2627641.

[185] Albatayneh, A., Alterman, D., Page, A. W. and Moghtaderi, B. (2016) 'Warming issues associated with the long term simulation of housing using CFD analysis', *Journal of Green Building*, 11(2), pp. 59–74. doi: 10.3992/jgb.11.2.57.1.

[186] Gaurav, V. R. and Laird, G. (2002) 'CFD analysis of automatic test

equipment', in *InterSociety Conference on Thermal and Thermomechanical Phenomena in Electronic Systems, IThERM*, pp. 610–617. doi: 10.1109/ITHERM.2002.1012511.

[187] Makridis, A. and Chick, J. (2013) 'Validation of a CFD model of wind turbine wakes with terrain effects', *Journal of Wind Engineering and Industrial Aerodynamics*, 123, pp. 12–29. doi: 10.1016/j.jweia.2013.08.009.

[188] Schaffrath, A., Fischer, K.-C., Hahm, T. and Wussow, S. (2007) 'Validation of the CFD code fluent by post-test calculation of a density-driven ROCOM experiment', *Nuclear Engineering and Design*, 237(15–17), pp. 1899–1908. doi: 10.1016/j.nucengdes.2007.02.029.

[189] Flaga-Maryanczyk, A., Schnotale, J., Radon, J. and Was, K. (2014) 'Experimental measurements and CFD simulation of a ground source heat exchanger operating at a cold climate for a passive house ventilation system', *Energy and Buildings*, 68, pp. 562–570. doi: 10.1016/j.enbuild.2013.09.008.

[190] Giannissi, S. G., Shentsov, V., Melideo, D., Cariteau, B., Baraldi, D., Venetsanos, A. G. and Molkov, V. (2014) 'CFD benchmark on hydrogen release and dispersion in confined, naturally ventilated space with one vent', *International Journal of Hydrogen Energy*. doi: 10.1016/j.ijhydene.2014.12.013.

[191] Xu, G., Luxbacher, K. D., Ragab, S. and Schafrik, S. (2013) 'Development of a remote analysis method for underground ventilation systems using tracer gas and CFD in a simplified laboratory apparatus', *Tunnelling and Underground Space Technology*, 33, pp. 1–11. doi: 10.1016/j.tust.2012.09.001.

[192] Rong, L., Liu, D., Pedersen, E. F. and Zhang, G. (2015) 'The effect of wind speed and direction and surrounding maize on hybrid ventilation in a dairy cow building in Denmark', *Energy and Buildings*, 86, pp. 25–34. doi: 10.1016/j.enbuild.2014.10.016.

[193] Farea, T. G., Ossen, D. R., Alkaff, S. and Kotani, H. (2015) 'CFD modeling for natural ventilation in a lightwell connected to outdoor through horizontal voids', *Energy and Buildings*, 86, pp. 502–513. doi:

10.1016/j.enbuild.2014.10.030.

[194] Perén, J. I., van Hooff, T., Leite, B. C. C., Blocken, B., Peren, J. I., van Hooff, T., Leite, B. C. C. and Blocken, B. (2014) 'CFD analysis of cross-ventilation of a generic isolated building with asymmetric opening positions: impact of roof angle and opening location', *Building and Environment*. Pergamon, 85, pp. 263–276. doi: 10.1016/j.buildenv.2014.12.007.

[195] Hall, N. and Nasa (2015) *Role of Mach Number in Compressible Flows*. Available at: <https://www.grc.nasa.gov/www/k-12/airplane/machrole.html> (Accessed: 4 January 2018).

[196] Durrani, F., Cook, M. J. and McQuirk, J. J. (2015) 'Evaluation of LES and RANS CFD modelling of multiple steady states in natural ventilation', *Building and Environment*. Pergamon, 92, pp. 167–181. doi: 10.1016/j.buildenv.2015.04.027.

[197] Tu, J., Yeoh, G.-H., Liu, C., Tu, J., Yeoh, G.-H. and Liu, C. (2018) 'Governing Equations for CFD: Fundamentals', *Computational Fluid Dynamics*. Butterworth-Heinemann, pp. 65–124. doi: 10.1016/B978-0-08-101127-0.00003-9.

[198] Maleki, S., Burton, D. and Thompson, M. C. (2017) 'Assessment of various turbulence models (ELES, SAS, URANS and RANS) for predicting the aerodynamics of freight train container wagons', *Journal of Wind Engineering and Industrial Aerodynamics*. Elsevier, 170, pp. 68–80. doi: 10.1016/J.JWEIA.2017.07.008.

[199] Lam, C. Y. (1988) 'An eddy viscosity turbulence model', *International Communications in Heat and Mass Transfer*. Pergamon, 15(3), pp. 355–363. doi: 10.1016/0735-1933(88)90036-X.

[200] Abdollahzadeh, M., Esmailpour, M., Vizinho, R., Younesi, A. and Pàscua, J. C. (2017) 'Assessment of RANS turbulence models for numerical study of laminar-turbulent transition in convection heat transfer', *International Journal of Heat and Mass Transfer*. Pergamon, 115, pp. 1288–1308. doi:

10.1016/J.IJHEATMASSTRANSFER.2017.08.114.

[201] Autodesk (2013) *Autodesk Simulation CFD 2013*. Available at: <http://help.autodesk.com/view/SCDSE/2013/ENU/> (Accessed: 4 January 2018).

[202] Nejat, P., Calautit, J. K., Majid, M. Z. A., Hughes, B. R., Zeynali, I. and Jomehzadeh, F. (2016) 'Evaluation of a two-sided windcatcher integrated with wing wall (as a new design) and comparison with a conventional windcatcher', *Energy and Buildings*. Elsevier, 126, pp. 287–300. doi: 10.1016/j.enbuild.2016.05.025.

[203] Calautit, J. K. and Hughes, B. R. (2014) 'Wind tunnel and CFD study of the natural ventilation performance of a commercial multi-directional wind tower', *Building and Environment*, 80, pp. 71–83. doi: 10.1016/j.buildenv.2014.05.022.

[204] Calautit, J. K., Hughes, B. R. and Ghani, S. A. (2013) 'A numerical investigation into the feasibility of integrating green building technologies into row houses in the Middle East', *Architectural Science Review*, 56(4), pp. 279–296. doi: 10.1080/00038628.2012.686433.

[205] Hughes, B. R. and Abdul Ghani, S. A. A. (2009) 'A numerical investigation into the effect of windvent dampers on operating conditions', *Building and Environment*, 44(2), pp. 237–248. doi: 10.1016/j.buildenv.2008.02.012.

[206] Elmualim, A. A. (2006) 'Verification of Design Calculations of a Wind Catcher/Tower Natural Ventilation System with Performance Testing in a Real Building', *International Journal of Ventilation*, 4(4), pp. 393–404. doi: 10.1080/14733315.2005.11683717.

[207] Jones, B. M. and Kirby, R. (2009) 'Quantifying the performance of a top-down natural ventilation Windcatcher™', *Building and Environment*. Elsevier Ltd, 44(9), pp. 1925–1934. doi: 10.1016/j.buildenv.2009.01.004.

[208] Liu, S., Mak, C. M. and Niu, J. (2011) 'Numerical evaluation of louver configuration and ventilation strategies for the windcatcher system', *Building and Environment*, 46(8), pp. 1600–1616. doi: 10.1016/j.buildenv.2011.01.025.

- [209] Calautit, J. K. and Hughes, B. R. (2014) 'Measurement and prediction of the indoor airflow in a room ventilated with a commercial wind tower', *Energy and Buildings*. Elsevier, 84, pp. 367–377. doi: 10.1016/J.ENBUILD.2014.08.015.
- [210] Nejat, P., Calautit, J. K., Majid, M. Z. A., Hughes, B. R. and Jomehzadeh, F. (2016) 'Anti-short-circuit device: A new solution for short-circuiting in windcatcher and improvement of natural ventilation performance', *Building and Environment*. Pergamon, 105, pp. 24–39. doi: 10.1016/J.BUILDENV.2016.05.023.
- [211] Yu, H. and Thé, J. (2016) 'Validation and optimization of SST k- ω turbulence model for pollutant dispersion within a building array', *Atmospheric Environment*. Pergamon, 145, pp. 225–238. doi: 10.1016/j.atmosenv.2016.09.043.
- [212] Iry, S. and Rafee, R. (2019) 'Transient numerical simulation of the coaxial borehole heat exchanger with the different diameters ratio', *Geothermics*. Pergamon, 77, pp. 158–165. doi: 10.1016/J.GEOTHERMICS.2018.09.009.
- [213] Batalha Leoni, G., Suaiden Klein, T. and de Andrade Medronho, R. (2017) 'Assessment with computational fluid dynamics of the effects of baffle clearances on the shell side flow in a shell and tube heat exchanger', *Applied Thermal Engineering*. Pergamon, 112, pp. 497–506. doi: 10.1016/J.APPLTHERMALENG.2016.10.097.
- [214] Kurec, K., Piechna, J. and Gumowski, K. (2017) 'Investigations on unsteady flow within a stationary passage of a pressure wave exchanger, by means of PIV measurements and CFD calculations', *Applied Thermal Engineering*. Pergamon, 112, pp. 610–620. doi: 10.1016/J.APPLTHERMALENG.2016.10.142.
- [215] Menter, F. R. (no date hg) 'AIAA 93-2906 Zonal Two Equation k-w, Turbulence Models for Aerodynamic Flows'. doi: 10.2514/6.1993-2906.
- [216] Aslam Bhutta, M. M., Hayat, N., Bashir, M. H., Khan, A. R., Ahmad, K. N.

and Khan, S. (2012) 'CFD applications in various heat exchangers design: A review', *Applied Thermal Engineering*. Pergamon, 32, pp. 1–12. doi: 10.1016/j.applthermaleng.2011.09.001.

[217] Pal, E., Kumar, I., Joshi, J. B. and Maheshwari, N. K. (2016) 'CFD simulations of shell-side flow in a shell-and-tube type heat exchanger with and without baffles', *Chemical Engineering Science*. Pergamon, 143, pp. 314–340. doi: 10.1016/J.CES.2016.01.011.

[218] Liu, S., Jin, M., Lyu, K., Zhou, T. and Zhao, Z. (2018) 'Flow and heat transfer behaviors for double-walled-straight-tube heat exchanger of HLM loop', *Annals of Nuclear Energy*. Pergamon, 120, pp. 604–610. doi: 10.1016/J.ANUCENE.2018.06.016.

[219] Sadri, R., Mallah, A. R., Hosseini, M., Ahmadi, G., Kazi, S. N., Dabbagh, A., Yeong, C. H., Ahmad, R. and Yaakup, N. A. (2018) 'CFD modeling of turbulent convection heat transfer of nanofluids containing green functionalized graphene nanoplatelets flowing in a horizontal tube: Comparison with experimental data', *Journal of Molecular Liquids*. Elsevier, 269, pp. 152–159. doi: 10.1016/J.MOLLIQ.2018.06.011.

[220] Defraeye, T., Herremans, E., Verboven, P., Carmeliet, J. and Nicolai, B. (2012) 'Convective heat and mass exchange at surfaces of horticultural products: A microscale CFD modelling approach', *Agricultural and Forest Meteorology*. Elsevier, 162–163, pp. 71–84. doi: 10.1016/J.AGRFORMET.2012.04.010.

[221] Hatami, M., Ganji, D. D. and Gorji-Bandpy, M. (2014) 'Numerical study of finned type heat exchangers for ICEs exhaust waste heat recovery', *Case Studies in Thermal Engineering*. Elsevier, 4, pp. 53–64. doi: 10.1016/J.CSITE.2014.07.002.

[222] Ocloń, P., Łopata, S. and Chłosta, K. (2016) 'Experimental and Numerical Investigation of Flow Distribution within the Heat Exchanger with Elliptical Tubes', *Procedia Engineering*. Elsevier, 157, pp. 428–435. doi: 10.1016/J.PROENG.2016.08.386.

- [223] Bae, Y.-Y., Kim, E.-S. and Kim, M. (2017) 'Assessment of low-Reynolds number k - ϵ turbulence models against highly buoyant flows', *International Journal of Heat and Mass Transfer*. Pergamon, 108, pp. 529–536. doi: 10.1016/J.IJHEATMASSTRANSFER.2016.12.039.
- [224] Ahsan, M. (2014) 'Numerical analysis of friction factor for a fully developed turbulent flow using k - ϵ turbulence model with enhanced wall treatment', *Beni-Suef University Journal of Basic and Applied Sciences*. Elsevier, 3(4), pp. 269–277. doi: 10.1016/J.BJBAS.2014.12.001.
- [225] Juretić, F. and Kozmar, H. (2013) 'Computational modeling of the neutrally stratified atmospheric boundary layer flow using the standard k - ϵ turbulence model', *Journal of Wind Engineering and Industrial Aerodynamics*. Elsevier, 115, pp. 112–120. doi: 10.1016/J.JWEIA.2013.01.011.
- [226] Lateb, M., Masson, C., Stathopoulos, T. and Bédard, C. (2013) 'Comparison of various types of k - ϵ models for pollutant emissions around a two-building configuration', *Journal of Wind Engineering and Industrial Aerodynamics*. Elsevier, 115, pp. 9–21. doi: 10.1016/J.JWEIA.2013.01.001.
- [227] Pasquali, A., Geier, M. and Krafczyk, M. (2017) 'Near-wall treatment for the simulation of turbulent flow by the cumulant lattice Boltzmann method', *Computers & Mathematics with Applications*. doi: 10.1016/j.camwa.2017.11.022.
- [228] Ai, Z. T. and Mak, C. M. (2013) 'CFD simulation of flow and dispersion around an isolated building: Effect of inhomogeneous ABL and near-wall treatment', *Atmospheric Environment*. Pergamon, 77, pp. 568–578. doi: 10.1016/J.ATMOENV.2013.05.034.
- [229] Mousa, W. A. Y., Lang, W., Auer, T. and Yousef, W. A. (2017) 'A pattern recognition approach for modeling the air change rates in naturally ventilated buildings from limited steady-state CFD simulations', *Energy and Buildings*. Elsevier, 155, pp. 54–65. doi: 10.1016/J.ENBUILD.2017.09.016.
- [230] *CFD Online - Y-Plus Wall Distance Estimation* (no date hv). Available at:

<https://www.cfd-online.com/Tools/yplus.php> (Accessed: 3 October 2018).

[231] Ali, Z., Tucker, P. G. and Shahpar, S. (2017) 'Optimal mesh topology generation for CFD', *Computer Methods in Applied Mechanics and Engineering*. North-Holland, 317, pp. 431–457. doi: 10.1016/J.CMA.2016.12.001.

[232] Shang, Z. (2014) 'Impact of mesh partitioning methods in CFD for large scale parallel computing', *Computers & Fluids*. Pergamon, 103, pp. 1–5. doi: 10.1016/J.COMPFLUID.2014.07.016.

[233] *FLUENT 6.3 User's Guide - 25.3.3 Evaluation of Gradients and Derivatives* (no date hy). Available at:

<https://www.sharcnet.ca/Software/Fluent6/html/ug/node994.htm> (Accessed: 17 September 2018).

[234] *FLUENT 6.3 User's Guide - 25.8.1 First-Order Accuracy vs. Second-Order Accuracy* (no date hz). Available at:

<https://www.sharcnet.ca/Software/Fluent6/html/ug/node1015.htm> (Accessed: 3 October 2018).

[235] RAUSCH, R., YANG, H. and BATINA, J. (1991) 'Spatial adaption procedures on unstructured meshes for accurate unsteady aerodynamic flow computation', in *32nd Structures, Structural Dynamics, and Materials Conference*. doi: 10.2514/6.1991-1106.

[236] *FLUENT 6.3 User's Guide - 25.1 Overview of Flow Solvers* (no date ib). Available at:

<https://www.sharcnet.ca/Software/Fluent6/html/ug/node986.htm#sec-uns-solve-overview> (Accessed: 18 September 2018).

[237] *Help: Automatic Convergence Assessment* (no date ic). Available at:

<http://help.autodesk.com/view/SCDSE/2015/ENU/?guid=GUID-477E1D94-2D6B-4C25-A5C6-6842532AF911> (Accessed: 17 January 2015).

[238] Elmualim, A. A. and Awbi, H. B. (2002) 'Wind Tunnel and CFD

Investigation of the Performance of "Windcatcher" Ventilation Systems',

International Journal of Ventilation. Taylor & Francis, 1(1), pp. 53–64. doi:

10.1080/14733315.2002.11683622.

[239] 'The Work at Height Regulations 2005' (no date ie). Queen's Printer of Acts of Parliament. Available at:

<http://www.legislation.gov.uk/uksi/2005/735/contents/made> (Accessed: 7 January 2018).

[240] Linden, P. (1999) 'The fluid mechanics of natural ventilation', *Annual review of fluid mechanics*. Available at:

<http://www.annualreviews.org/doi/pdf/10.1146/annurev.fluid.31.1.201>.

[241] *The Building Regulations 2010. Combustion appliances and Fuel Storage Systems. Approved Document J* (no date ig). Available at:

https://assets.publishing.service.gov.uk/government/uploads/system/uploads/attachment_data/file/468872/ADJ_LOCKED.pdf (Accessed: 3 October 2018).

[242] *Chimney Pots and Terminals* (2012). Available at: www.dunbrik.co.uk (Accessed: 3 October 2018).

[243] Straube, J. (1998) 'Moisture Control and Enclosure Wall Systems', (January 1998), p. 408. doi: 10.16953/deusbed.74839.

[244] *Technical Housing Standards-Nationally Described Space Standard. March 2015* (no date ij). Available at:

<http://forms.communities.gov.uk/orwritetousat>: (Accessed: 3 October 2018).

[245] *Housing Space Standards* (2006). Available at:

https://www.london.gov.uk/sites/default/files/hatc_housing_space_standards_report_for_gla_2006.pdf (Accessed: 3 October 2018).

[246] Franke, J., Hellsten, A., Schlünzen, H. and Carissimo, B. (2007) *Best Practice Guideline for the CFD simulation of flows in the urban environment*.

Available at: http://theairshed.com/pdf/COST_732_Best_Practice_Guideline_May_2007.pdf (Accessed: 19 September 2018).

[247] Calautit, J., Aquino, A., O'Connor, D., Cabaneros, S., Shahzad, S., Wazed, S., Garwood, T., Calautit, K. and Hughes, B. (2017) 'Indoor

environmental quality (IEQ) analysis of a low energy wind catcher with horizontally-arranged heat transfer devices', *Energy Procedia*. Elsevier, 142, pp. 2095–2101. doi: 10.1016/J.EGYPRO.2017.12.582.

[248] Calautit, J. K., Aquino, A. I., Shahzad, S., Nasir, D. S. N. M. and Hughes, B. R. (2017) 'Thermal Comfort and Indoor air Quality Analysis of a Low-energy Cooling Windcatcher', *Energy Procedia*. Elsevier, 105, pp. 2865–2870. doi: 10.1016/J.EGYPRO.2017.03.634.

[249] Bu, Z., Kato, S. and Takahashi, T. (2010) 'Wind tunnel experiments on wind-induced natural ventilation rate in residential basements with areaway space', *Building and Environment*, 45(10), pp. 2263–2272. Available at: <http://www.sciencedirect.com/science/article/pii/S0360132310001162>.

[250] Grac, G. C., Chen, Q., Glicksman, L. R. and Norford, L. K. (2002) 'Simulation of wind-driven ventilative cooling systems for an apartment building in Beijing and Shanghai', *Energy and Buildings*, 34, pp. 1–11.

[251] Shen, X., Zhang, G. and Bjerg, B. (2012) 'Comparison of different methods for estimating ventilation rates through wind driven ventilated buildings', *Energy and Buildings*. Elsevier B.V., 54, pp. 297–306. doi: 10.1016/j.enbuild.2012.07.017.

[252] Manz, H., Huber, H. and Helfenfinger, D. (2001) 'Impact of air leakages and short circuits in ventilation units with heat recovery on ventilation efficiency and energy requirements for heating', *Energy and Buildings*, 33(2), pp. 133–139. doi: 10.1016/S0378-7788(00)00077-3.

[253] Mark Kinver (2009) *BBC NEWS | Science & Environment | Study pinpoints UK wind hotspots*. Available at: <http://news.bbc.co.uk/1/hi/sci/tech/8139373.stm> (Accessed: 7 January 2018).

[254] Shah, R. K., Bergles, A. ., Mayinger, F. and Kakac, S. (1981) 'Classification of Heat Exchangers', in *Heat Exchangers*. Washington DC: Hemisphere Publishing, pp. 9–46.

[255] Jouhara, H., Chauhan, A., Nannou, T., Almahmoud, S., Delpech, B. and

- Wrobel, L. C. (2017) 'Heat pipe based systems - Advances and applications', *Energy*. Pergamon, 128, pp. 729–754. doi: 10.1016/J.ENERGY.2017.04.028.
- [256] Srimuang, W. and Amatachaya, P. (2012) 'A review of the applications of heat pipe heat exchangers for heat recovery', *Renewable and Sustainable Energy Reviews*. Pergamon, 16(6), pp. 4303–4315. doi: 10.1016/J.RSER.2012.03.030.
- [257] Shah, R. and Sekulić, D. (2003) 'Overview of Heat Exchanger Design Methodology', *Fundamentals of Heat Exchanger Design*, pp. 78–96. Available at: <http://onlinelibrary.wiley.com/doi/10.1002/9780470172605.ch2/summary> (Accessed: 12 October 2014).
- [258] Antony Aroul Raj, V. and Velraj, R. (2011) 'Heat transfer and pressure drop studies on a PCM-heat exchanger module for free cooling applications', *International Journal of Thermal Sciences*. Elsevier Masson SAS, 50(8), pp. 1573–1582. doi: 10.1016/j.ijthermalsci.2011.01.025.
- [259] Cuce, P. M. and Riffat, S. (2015) 'A comprehensive review of heat recovery systems for building applications', *Renewable and Sustainable Energy Reviews*. Elsevier, 47, pp. 665–682. doi: 10.1016/j.rser.2015.03.087.
- [260] Mardiana, a. and Riffat, S. B. (2013) 'Review on physical and performance parameters of heat recovery systems for building applications', *Renewable and Sustainable Energy Reviews*. Elsevier, 28, pp. 174–190. doi: 10.1016/j.rser.2013.07.016.
- [261] Mardiana-Idayu, a. and Riffat, S. B. (2011) 'Review on heat recovery technologies for building applications', *Renewable and Sustainable Energy Reviews*. Elsevier Ltd, 16(2), pp. 1241–1255. doi: 10.1016/j.rser.2011.09.026.
- [262] Gendebien, S., Bertagnolio, S. and Lemort, V. (2013) 'Investigation on a ventilation heat recovery exchanger: Modeling and experimental validation in dry and partially wet conditions', *Energy and Buildings*. Elsevier B.V., 62, pp. 176–189. doi: 10.1016/j.enbuild.2013.02.025.
- [263] Lienhard IV, J. H. and Lienhard V, J. H. (2008) *A Heat Transfer Textbook*.

3rd edn. Cambridge, Massachusetts: Philogiston Press.

[264] Li, Q., Flamant, G., Yuan, X., Neveu, P. and Luo, L. (2011) 'Compact heat exchangers: A review and future applications for a new generation of high temperature solar receivers', *Renewable and Sustainable Energy Reviews*. Pergamon, 15(9), pp. 4855–4875. doi: 10.1016/J.RSER.2011.07.066.

[265] Kotcioglu, I., Caliskan, S., Cansiz, A. and Baskaya, S. (2010) 'Second law analysis and heat transfer in a cross-flow heat exchanger with a new winglet-type vortex generator', *Energy*. Elsevier Ltd, 35(9), pp. 3686–3695. doi: 10.1016/j.energy.2010.05.014.

[266] Abdel-Salam, M. R. H., Besant, R. W. and Simonson, C. J. (2015) 'Sensitivity of the performance of a flat-plate liquid-to-air membrane energy exchanger (LAMEE) to the air and solution channel widths and flow maldistribution', *International Journal of Heat and Mass Transfer*, 84, pp. 1082–1100. doi: 10.1016/j.ijheatmasstransfer.2015.01.042.

[267] Manjunath, K. and Kaushik, S. C. (2014) 'Second law thermodynamic study of heat exchangers: A review', *Renewable and Sustainable Energy Reviews*. Pergamon, 40, pp. 348–374. doi: 10.1016/j.rser.2014.07.186.

[268] Khoshvaght-Aliabadi, M., Sartipzadeh, O. and Alizadeh, A. (2015) 'An experimental study on vortex-generator insert with different arrangements of delta-winglets', *Energy*. Elsevier Ltd, 82, pp. 629–639. doi: 10.1016/j.energy.2015.01.072.

[269] Al-Asadi, M. T., Alkasmoul, F. S. and Wilson, M. C. T. (2016) 'Heat transfer enhancement in a micro-channel cooling system using cylindrical vortex generators', *International Communications in Heat and Mass Transfer*. Elsevier Ltd, 74, pp. 40–47. doi: 10.1016/j.icheatmasstransfer.2016.03.002.

[270] Alam, T. and Kim, M.-H. (2018) 'A comprehensive review on single phase heat transfer enhancement techniques in heat exchanger applications', *Renewable and Sustainable Energy Reviews*. Pergamon, 81, pp. 813–839. doi: 10.1016/J.RSER.2017.08.060.

- [271] Yun, J. and Lee, K. (2000) 'Influence of design parameters on the heat transfer and flow friction characteristics of the heat exchanger with slit fins', *International Journal of Heat and Mass Transfer*, 43, pp. 2529–2539. Available at: <http://www.sciencedirect.com/science/article/pii/S0017931099003427>.
- [272] Abdollahi, A. and Shams, M. (2015) 'Optimization of shape and angle of attack of winglet vortex generator in a rectangular channel for heat transfer enhancement', *Applied Thermal Engineering*. Elsevier Ltd, 81, pp. 376–387. doi: 10.1016/j.applthermaleng.2015.01.044.
- [273] Bejan, A. (2013) 'Laminar duct flow', in *Convection Heat Transfer*. John Wiley & Sons, Inc., pp. 96–167.
- [274] Zarea, H., Moradi Kashkooli, F., Mansuri Mehryan, A., Saffarian, M. R. and Namvar Beherghani, E. (2014) 'Optimal design of plate-fin heat exchangers by a Bees Algorithm', *Applied Thermal Engineering*, 69(1–2), pp. 267–277. doi: 10.1016/j.applthermaleng.2013.11.042.
- [275] Hadidi, A. and Nazari, A. (2013) 'Design and economic optimization of shell-and-tube heat exchangers using biogeography-based (BBO) algorithm', *Applied Thermal Engineering*. Pergamon, 51(1–2), pp. 1263–1272. doi: 10.1016/J.APPLTHERMALENG.2012.12.002.
- [276] Benhammou, M. and Draoui, B. (2015) 'Parametric study on thermal performance of earth-to-air heat exchanger used for cooling of buildings', *Renewable and Sustainable Energy Reviews*. Pergamon, 44, pp. 348–355. doi: 10.1016/J.RSER.2014.12.030.
- [277] Piotrowska, E. and Chochowski, A. (2012) 'Application of parametric identification methods for the analysis of the heat exchanger dynamics', *International Journal of Heat and Mass Transfer*. Pergamon, 55(23–24), pp. 7109–7118. doi: 10.1016/J.IJHEATMASSTRANSFER.2012.07.025.
- [278] Cárdenas, B., Garvey, S., Kantharaj, B. and Simpson, M. (2017) 'Parametric investigation of a non-constant cross sectional area air to air heat exchanger', *Applied Thermal Engineering*. Pergamon, 113, pp. 278–289. doi:

10.1016/J.APPLTHERMALENG.2016.10.209.

[279] Arora, A., Subbarao, P. M. V. and Agarwal, R. S. (2016) 'Development of parametric space for the vortex generator location for improving thermal compactness of an existing inline fin and tube heat exchanger', *Applied Thermal Engineering*. Pergamon, 98, pp. 727–742. doi: 10.1016/J.APPLTHERMALENG.2015.12.117.

[280] Kim, M.-J., Lee, S.-R., Yoon, S. and Go, G.-H. (2016) 'Thermal performance evaluation and parametric study of a horizontal ground heat exchanger', *Geothermics*. Pergamon, 60, pp. 134–143. doi: 10.1016/J.GEOTHERMICS.2015.12.009.

[281] Bououd, M. and Mechaqrane, A. (2017) 'Concentration solar dryer water-to-air heat exchanger: Modeling and parametric studies', *International Journal of Hydrogen Energy*. Pergamon, 42(13), pp. 8631–8643. doi: 10.1016/J.IJHYDENE.2016.06.031.

[282] Poddar, T. K. and Polley, G. T. (1996) 'Heat Exchanger Design Through Parameter Plotting', *Chemical Engineering Research and Design*, 74(8), pp. 849–852. doi: 10.1205/026387696523139.

[283] Ye, H.-Y., Park, J.-S. and Lee, K.-S. (2014) 'Critical operating conditions for prevention of frost formation in fin-tube heat exchangers', *International Journal of Heat and Mass Transfer*, 76, pp. 279–285. doi: 10.1016/j.ijheatmasstransfer.2014.04.044.

[284] Rafati Nasr, M., Fauchoux, M., Besant, R. W. and Simonson, C. J. (2014) 'A review of frosting in air-to-air energy exchangers', *Renewable and Sustainable Energy Reviews*. Pergamon, 30, pp. 538–554. doi: 10.1016/J.RSER.2013.10.038.

[285] Krishnakumar, K., John, A. K. and Venkatarathnam, G. (2011) 'A review on transient test techniques for obtaining heat transfer design data of compact heat exchanger surfaces', *Experimental Thermal and Fluid Science*. Elsevier, 35(4), pp. 738–743. doi: 10.1016/J.EXPTHERMFLUSCI.2010.12.006.

- [286] Rattner, A. and Jonathan, B. (2006) *Nusselt Correlations List*. Available at: <http://www.seas.upenn.edu/~meam333/correlation/CorrelationsList.pdf> (Accessed: 14 October 2015).
- [287] Sheikholeslami, M., Gorji-Bandpy, M. and Ganji, D. D. (2015) 'Review of heat transfer enhancement methods: Focus on passive methods using swirl flow devices', *Renewable and Sustainable Energy Reviews*. Pergamon, 49, pp. 444–469. doi: 10.1016/J.RSER.2015.04.113.
- [288] Salviano, L. O., Dezan, D. J. and Yanagihara, J. I. (2015) 'Optimization of winglet-type vortex generator positions and angles in plate-fin compact heat exchanger: Response Surface Methodology and Direct Optimization', *International Journal of Heat and Mass Transfer*, 82, pp. 373–387. doi: 10.1016/j.ijheatmasstransfer.2014.10.072.
- [289] Boonloi, A. and Jedsadaratanachai, W. (2015) 'Turbulent forced convection in a heat exchanger square channel with wavy-ribs vortex generator', *Chinese Journal of Chemical Engineering*. Elsevier B.V., 23(8), pp. 1256–1265. doi: 10.1016/j.cjche.2015.04.001.
- [290] Yaïci, W., Ghorab, M. and Entchev, E. (2016) '3D CFD study of the effect of inlet air flow maldistribution on plate-fin-tube heat exchanger design and thermal–hydraulic performance', *International Journal of Heat and Mass Transfer*. Pergamon, 101, pp. 527–541. doi: 10.1016/J.IJHEATMASSTRANSFER.2016.05.063.
- [291] Tahseen, T. A., Ishak, M. and Rahman, M. M. (2015) 'An overview on thermal and fluid flow characteristics in a plain plate finned and un-finned tube banks heat exchanger', *Renewable and Sustainable Energy Reviews*, 43, pp. 363–380. doi: 10.1016/j.rser.2014.10.070.
- [292] Klein, S. A., Beckman, W. A. and Duffie, J. . (1994) *TRNSYS—A Transient System Simulation Program. Version 14.1*. Available at: <http://www.trnsys.com/>.
- [293] Ibáñez, M., Lázaro, A., Zalba, B. and Cabeza, L. F. (2005) 'An approach

to the simulation of PCMs in building applications using TRNSYS', *Applied Thermal Engineering*. Pergamon, 25(11–12), pp. 1796–1807. doi: 10.1016/J.APPLTHERMALENG.2004.11.001.

[294] Lu, S., Liu, S., Huang, J. and Kong, X. (2014) 'Establishment and experimental verification of PCM room's TRNSYS heat transfer model based on latent heat utilization ratio', *Energy and Buildings*, 84, pp. 287–298. doi: 10.1016/j.enbuild.2014.07.082.

[295] Chargui, R. and Sammouda, H. (2014) 'Modeling of a residential house coupled with a dual source heat pump using TRNSYS software', *Energy Conversion and Management*, 81, pp. 384–399. doi: 10.1016/j.enconman.2014.02.040.

[296] Hobbi, A. and Siddiqui, K. (2009) 'Optimal design of a forced circulation solar water heating system for a residential unit in cold climate using TRNSYS', *Solar Energy*, 83(5), pp. 700–714. doi: 10.1016/j.solener.2008.10.018.

[297] Gowreesunker, B. L., Tassou, S. A. and Kolokotroni, M. (2013) 'Coupled TRNSYS-CFD simulations evaluating the performance of PCM plate heat exchangers in an airport terminal building displacement conditioning system', *Building and Environment*, 65, pp. 132–145. doi: 10.1016/j.buildenv.2013.04.003.

[298] Eldeeb, R., Fauchoux, M. and Simonson, C. J. (2013) 'Applicability of a heat and moisture transfer panel (HAMP) for maintaining space relative humidity in an office building using TRNSYS', *Energy and Buildings*, 66, pp. 338–345. doi: 10.1016/j.enbuild.2013.07.021.

[299] Wills, A., Cruickshank, C. A. and Beausoleil-Morrison, I. (2012) 'Application of the ESP-r/TRNSYS Co-Simulator to Study Solar Heating with a Single-House Scale Seasonal Storage', *Energy Procedia*, 30, pp. 715–722. doi: 10.1016/j.egypro.2012.11.081.

[300] Sweet, M. L. and McLeskey, J. T. (2012) 'Numerical simulation of underground Seasonal Solar Thermal Energy Storage (SSTES) for a single

- family dwelling using TRNSYS', *Solar Energy*, 86(1), pp. 289–300. doi: 10.1016/j.solener.2011.10.002.
- [301] Tavoularis, S. (2005) *Measurement in Fluid Mechanics*. Cambridge University Press.
- [302] Pankhurst, R. C. and Holder, D. W. (1952) *Wind Tunnel Technique*. London: Pitman Press, Bath.
- [303] Etemad, S. G., Thibault, J. and Hashemabadi, S. H. (2003) 'Calculation of the Pitot tube correction factor for Newtonian and non-Newtonian fluids', *ISA Transactions*, 42(4), pp. 505–512. doi: 10.1016/S0019-0578(07)60001-9.
- [304] OWER, E. and PANKHURST, R. C. (1977) *The Measurement of Air Flows, The Measurement of Air Flow*. Elsevier. doi: 10.1016/B978-0-08-021281-4.50009-9.
- [305] Klopfenstein Jr, R. (1998) 'Air velocity and flow measurement using a Pitot tube', *ISA Transactions*, 37(4), pp. 257–263. doi: 10.1016/S0019-0578(98)00036-6.
- [306] Boetcher, S. K. S. and Sparrow, E. M. (2007) 'Limitations of the standard Bernoulli equation method for evaluating Pitot/impact tube data', *International Journal of Heat and Mass Transfer*, 50(3–4), pp. 782–788. doi: 10.1016/j.ijheatmasstransfer.2006.01.044.
- [307] Crowley, C., Shinder, I. I. and Moldover, M. R. (2013) 'The effect of turbulence on a multi-hole Pitot calibration', *Flow Measurement and Instrumentation*, 33, pp. 106–109. doi: 10.1016/j.flowmeasinst.2013.05.007.
- [308] Lawrie, W. R. and De La Bere, J. C. (1946) *Nomenclature for Aerodynamics (Translated DIN L100, German Standards Issued by R.L.M)*. A.R.C.
- [309] KIMO Instruments Technical Data Sheet: Pressure Transmitter CP 300 (no date kw). Available at: http://www.dixellasia.com/download/dixellasia_com/Kimo_KISTOCK/cp300.pdf

(Accessed: 7 January 2015).

[310] *FLUXUS G601 — Technical Specifications | FLEXIM* (no date kx).

Available at: <https://www.flexim.com/en/devices/portable-flowmeters-gases/fluxus-g601/downloads> (Accessed: 7 January 2018).

[311] Hughes, B. and Ghani, S. (2008) 'Investigation of a windvent passive ventilation device against current fresh air supply recommendations', *Energy and Buildings*, 40(9), pp. 1651–1659. doi: 10.1016/j.enbuild.2008.02.024.

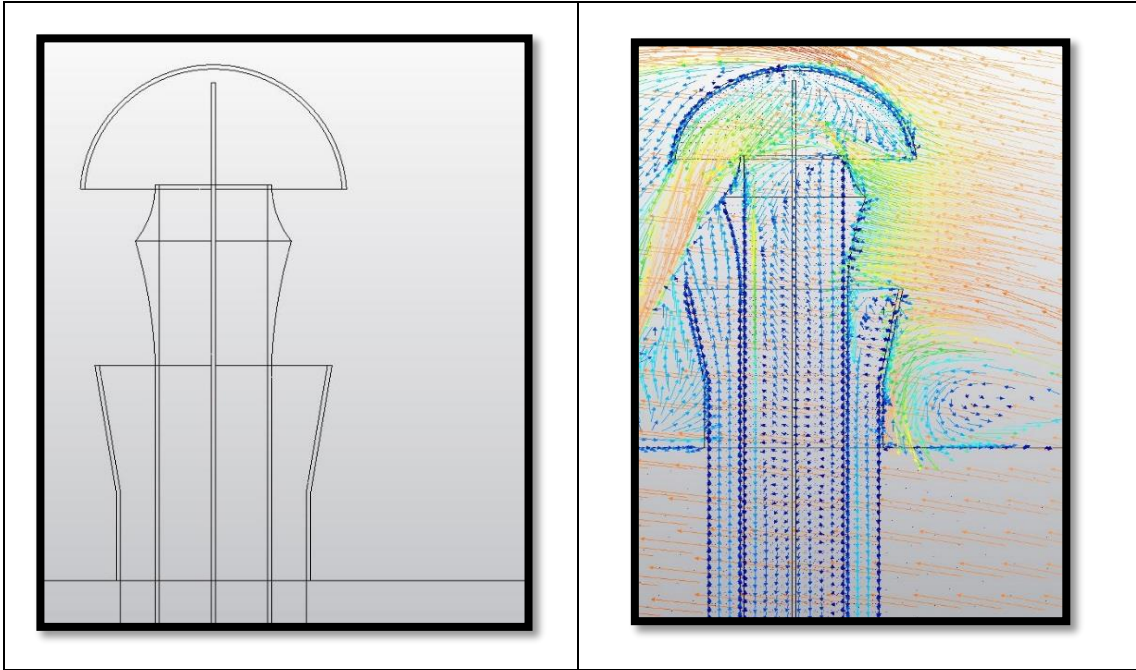
APPENDICES

Appendix A Windcatcher Initial Concepts

The initial windcatcher concepts are shown below with their velocity vectors at 2.5m/s incident wind speed simulated using Autodesk CFD.



Figure_Apx A-1: Initial Concept 1



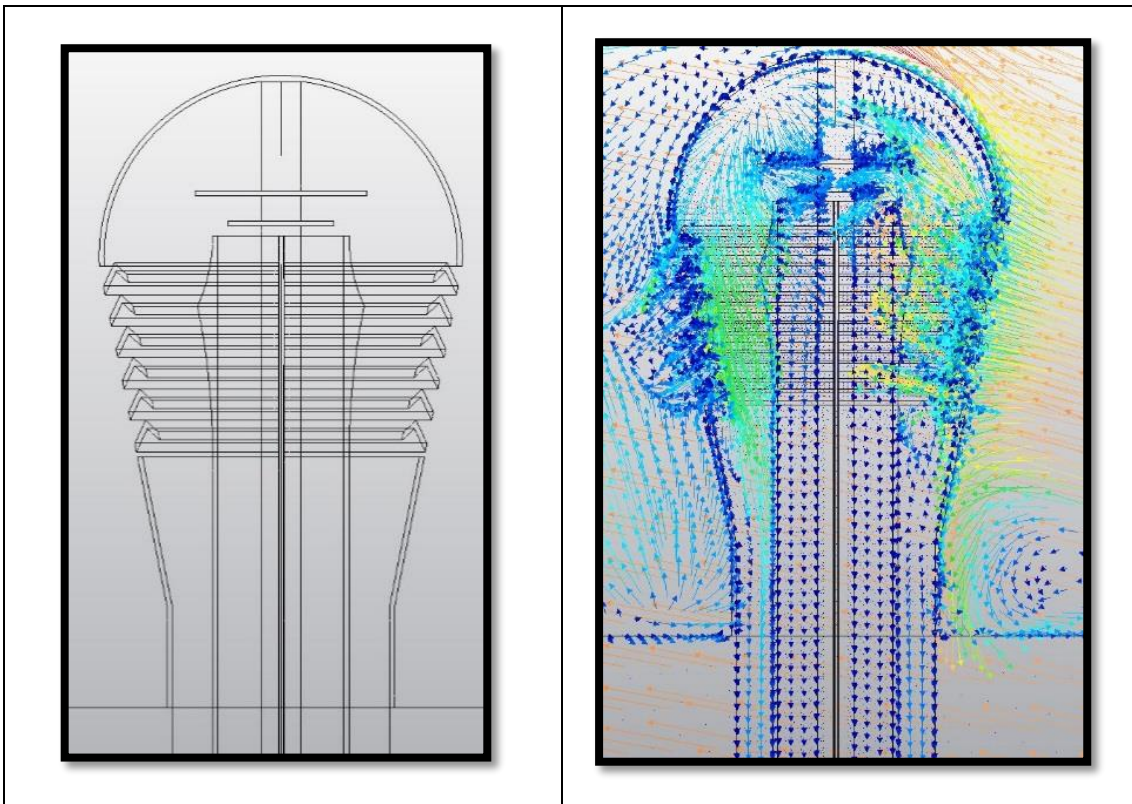
Figure_Apx A-2: Initial Concept 2



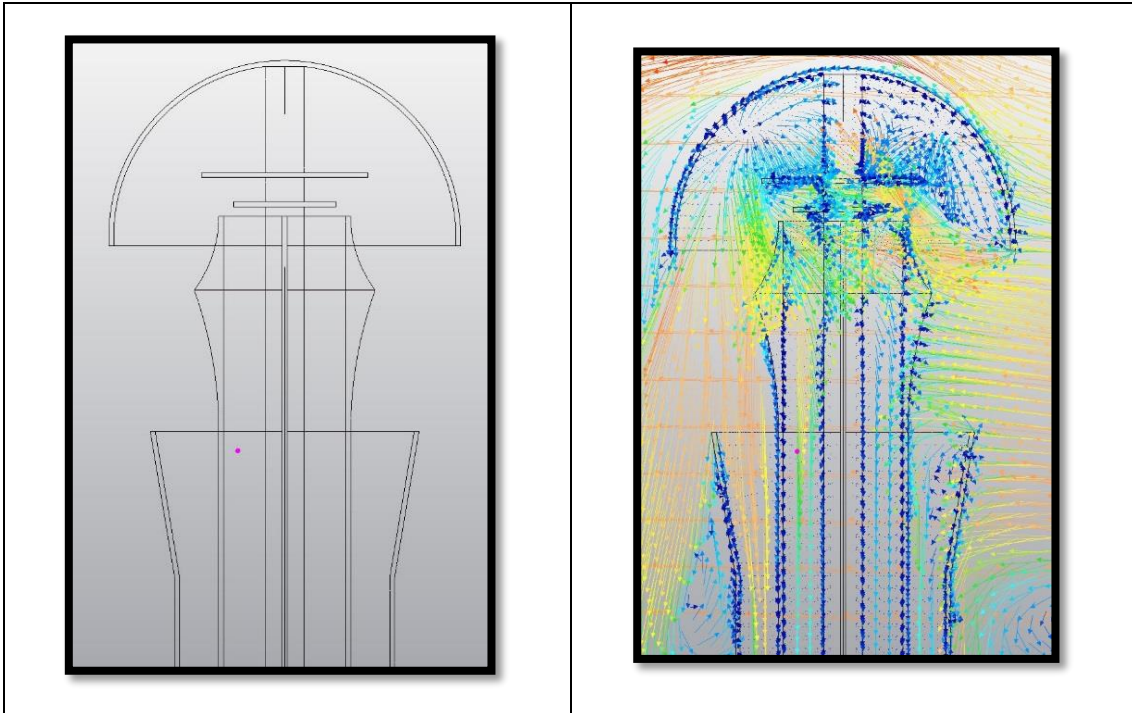
Figure_Apx A-3: Initial Concept 3



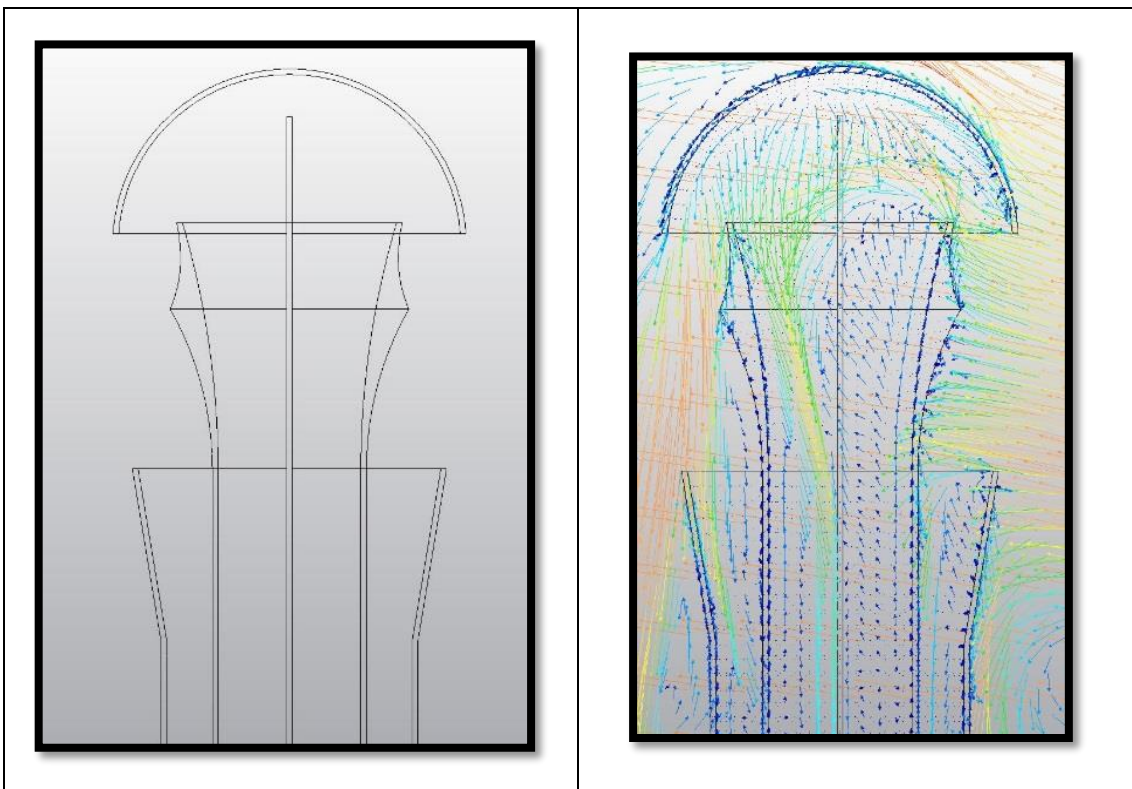
Figure_Apx A-4: Initial Concept 4



Figure_Apx A-5: Initial Concept 5



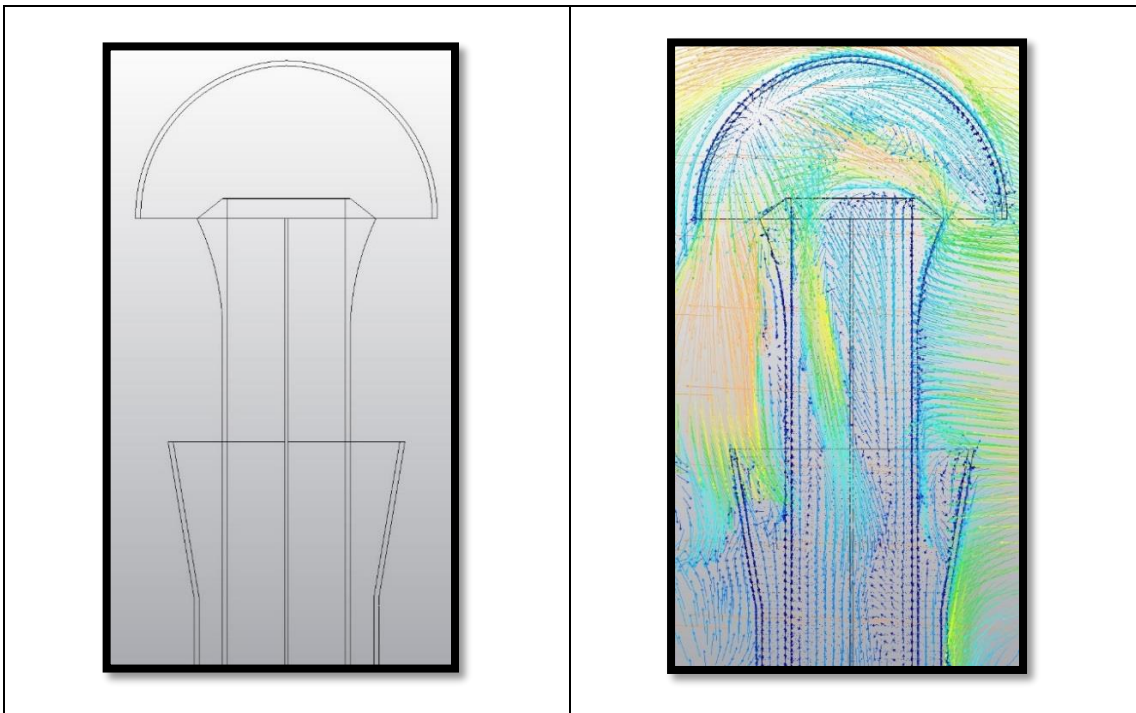
Figure_Apx A-6: Initial Concept 6



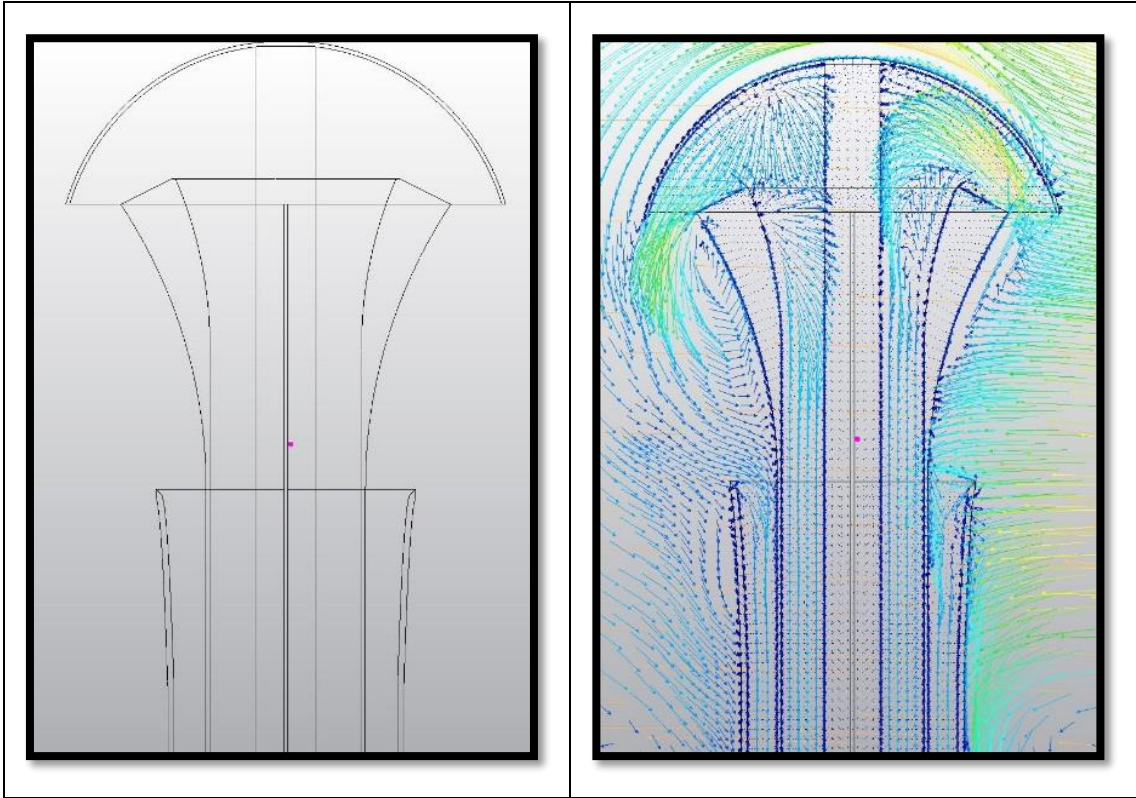
Figure_Apx A-7: Initial Concept 7



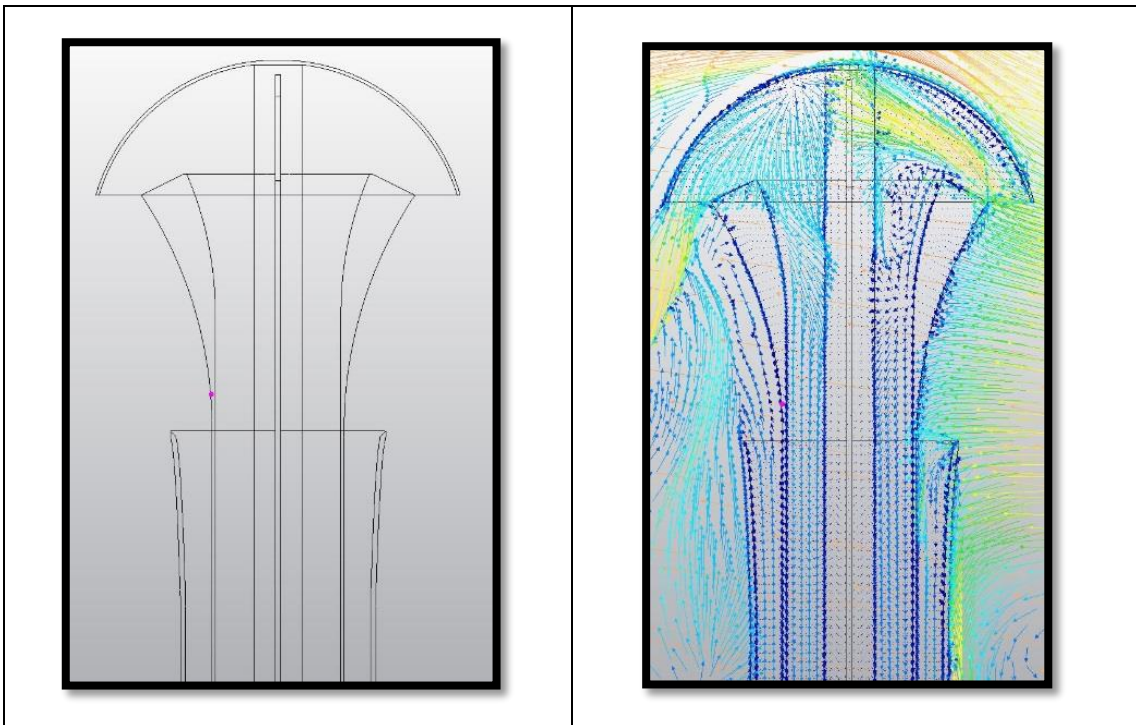
Figure_Apx A-8: Initial Concept 8



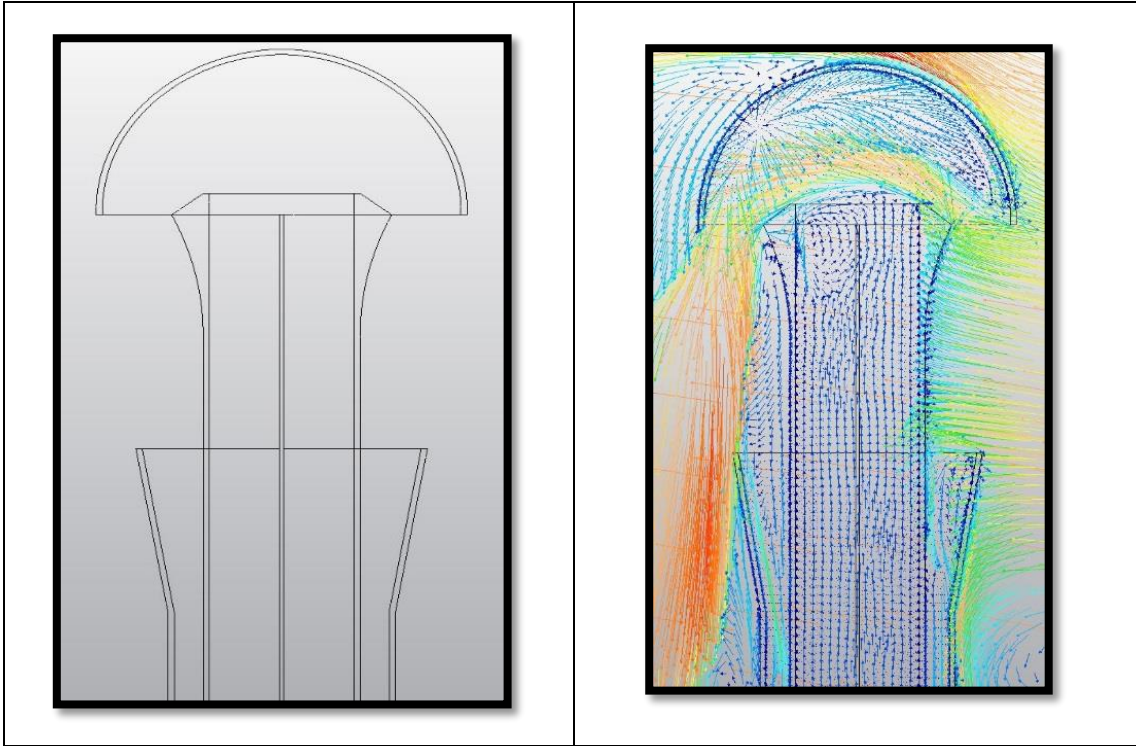
Figure_Apx A-9: Initial Concept 9



Figure_Apx A-10: Initial Concept 10



Figure_Apx A-11: Initial Concept 11



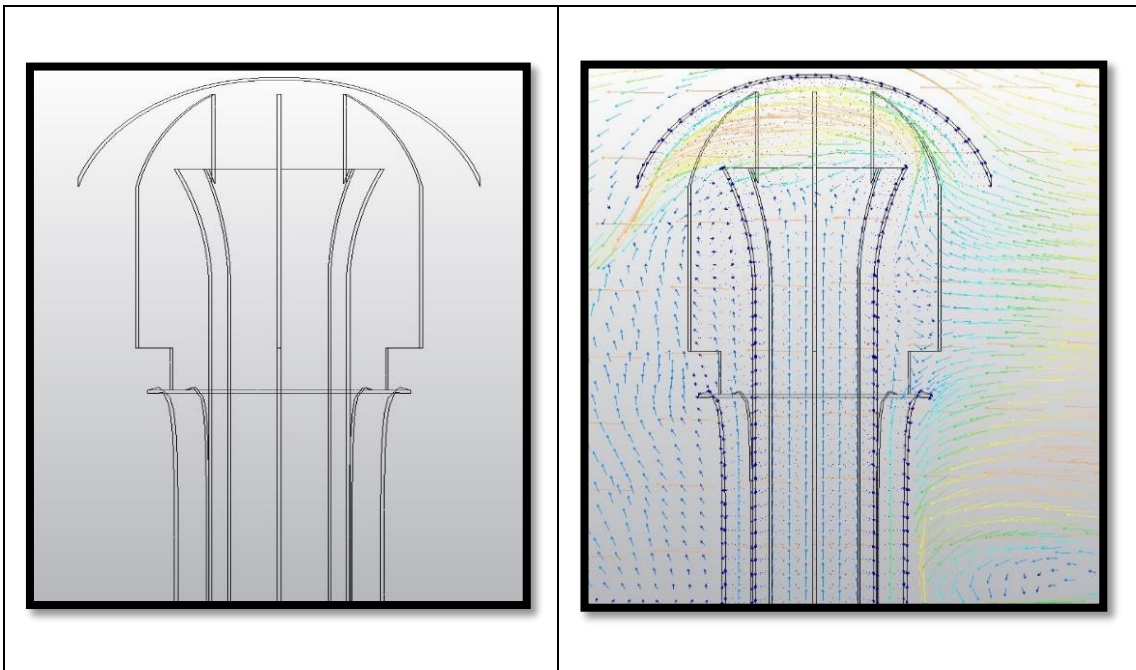
Figure_Apx A-12: Initial Concept 12



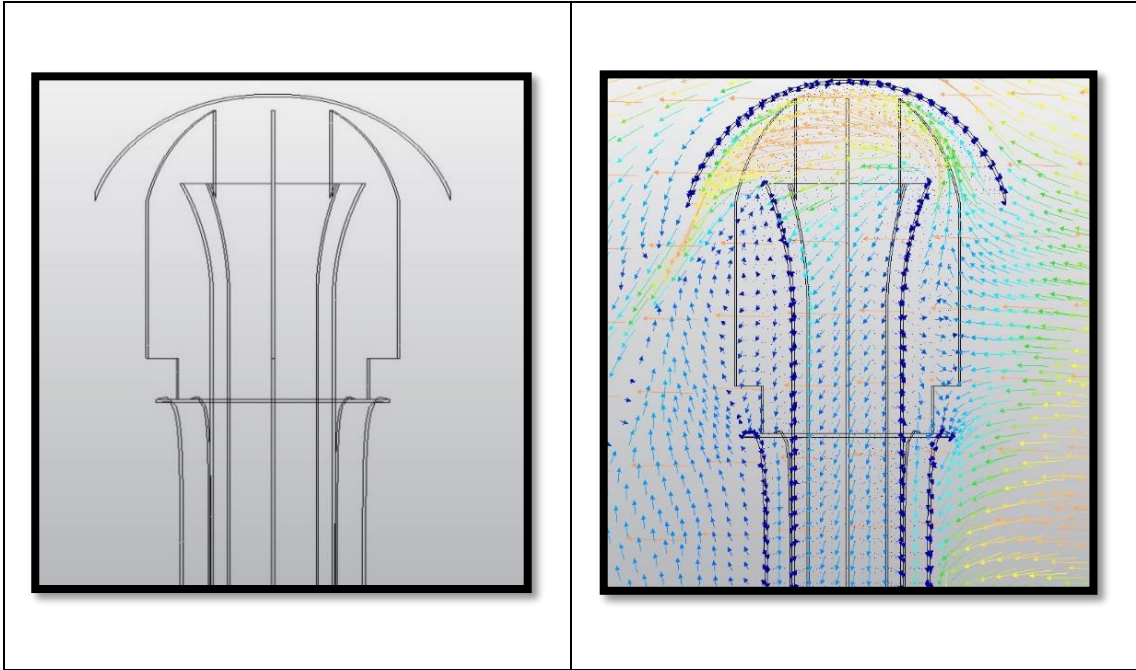
Figure_Apx A-13: Initial Concept 13



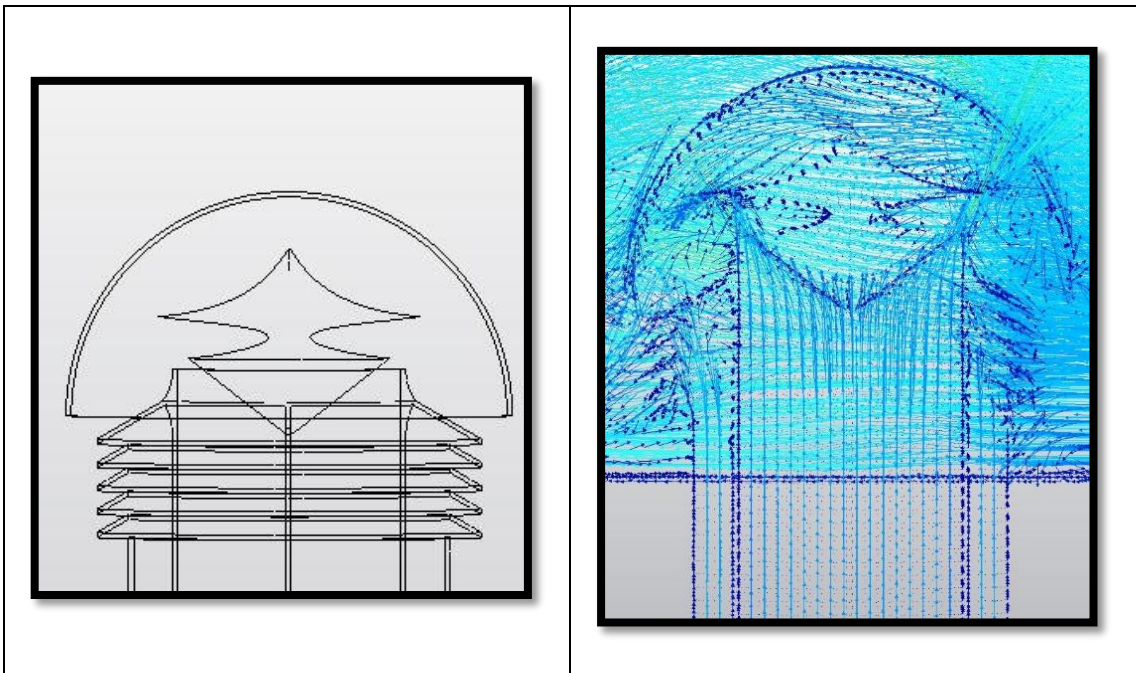
Figure_Apx A-14: Initial Concept 14



Figure_Apx A-15: Initial Concept 15



Figure_Apx A-16: Initial Concept 16



Figure_Apx A-17: Initial Concept 17